Dissecting the interplay of cardiomyocytes and cardiac fibroblasts using human stem cell models of disease

by
Caitlin Hall



UNIVERSITY OF BIRMINGHAM

A thesis submitted to the University of Birmingham for the degree

of Doctor of Philosophy

Institute of Cardiovascular Sciences
College of Medical and Dental Sciences
University of Birmingham
December 2023

UNIVERSITY OF
BIRMINGHAM

University of Birmingham Research Archive

e-theses repository

This unpublished thesis/dissertation is copyright of the author and/or third parties. The intellectual property rights of the author or third parties in respect of this work are as defined by The Copyright Designs and Patents Act 1988 or as modified by any successor legislation.

Any use made of information contained in this thesis/dissertation must be in accordance with that legislation and must be properly acknowledged. Further distribution or reproduction in any format is prohibited without the permission of the copyright holder.

Abstract

The cardiac fibroblast is an important cardiac cell type whose main role is to maintain the extracellular matrix of the heart and provide structural support for cardiomyocytes. During disease, cardiac fibroblasts become activated to myofibroblasts. This process is a key hallmark of the pathological remodelling known as cardiac fibrosis - resulting from persistent myofibroblasts and excessive deposition of matrix proteins. Cardiac fibrosis is associated with a majority of cardiovascular diseases as well as increased mortality and morbidity. Reversing the myofibroblast phenotype provides an avenue to reduce cardiac fibrosis and restore normal cardiac function. This has been explored to a certain degree using rodent models but has yet to be fully explored using human cells.

The primary activator of myofibroblasts is TGF-β, however, mechanical stress has also been linked to this process. In this work, we investigated whether inhibition of TGF-β receptor 1 or decreasing tensile strength *in vitro* could reverse activated myofibroblasts back to a quiescent cardiac fibroblast phenotype. This was explored using both primary human cells and human induced pluripotent stem cells (iPSC).

Cardiac fibroblasts and myofibroblasts have also been investigated for both their direct and indirect effects on cardiomyocytes. Again, this has been explored predominantly using animal models. Optical mapping is a method often utilised in the study of arrhythmogenesis to interrogate the disruption of electrical wave propagation in the heart. Recently, it has been advanced to map human iPSC derived cardiomyocyte (hiPSC-CM) monolayers enabling study of disease phenotypes and drug testing *in vitro* using human models. The work presented here aimed to investigate the effects of quiescent cardiac fibroblasts and activated myofibroblasts on cardiomyocyte electrophysiology and contraction using human iPSC-derived cells and optical mapping.

Declaration

I hereby declare that the work presented here in this thesis titled, “Dissecting the interplay of cardiomyocytes and cardiac fibroblasts using human stem cell models of disease” is the work of my own, unless otherwise stated. The work here was written and submitted by me to the College of Medical and Dental Sciences, University of Birmingham, United Kingdom as fulfilment of the degree of Doctor of Philosophy. I further declare that this work has not been submitted to any other university for the award of any other degree, diploma or equivalent course.

Caitlin Hall

Acknowledgements

I would like to express my gratitude to all those who have contributed to the completion of this thesis. This journey has been challenging, in part due to COVID-19, and could not have been endured without the help and support of my family, friends and colleagues.

I would first like to acknowledge my funding body, the MRC, without which I would not have been able to do this Ph.D. My Ph.D. program MRC IMPACT provided invaluable support and guidance, especially in the first few months, for which I am immensely grateful.

Thank you to my primary supervisor Davor Pavlovic, I am indebted to you. Without their unwavering assistance, encouragement, and expertise, none of this would have been possible. Thank you also to my secondary supervisor Professor Chris Denning. The help provided by them and their team for the iPSC work was indispensable. I wish I had been able to join them in Nottingham but the challenges of the work and COVID meant this was not to be. Finally, thanks to Katja and the rest of the Gehmlich group who also provided valuable insight and assistance into the challenges of iPSC differentiations.

Special shout-out to Chris O'shea without whom the optical mapping work would not have been possible. I will be forever grateful to you for everything you have done. Thank you for all your help both in and out of the lab as a friend, sounding board, and optical mapping expert. None of this would have been possible without you.

I have met so many amazing people thanks to this Ph.D., friends that I hope to have for life. Special thanks to Amar Azad and Jonathan Law. We started at or around the same time and they both helped and taught me so much. Thank you to Leena Patel, Aleen baber, Jonas Euchner, Stanimir Tashev and Dylan Marques for putting up with me, for helping me, and for making me laugh every day. You guys are the best. To everybody else in the ICVS, I also say thank you.

To my family, my Mum, Dad, and sister, thank you for everything, without your support, this thesis would never have been finished. Thank you for putting up with me while I finished writing and allowing me the time and space to finish at my own speed.

Project Outcomes

Publications:

Hall C, Gehmlich K, Denning C, Pavlovic D. Complex Relationship Between Cardiac Fibroblasts and Cardiomyocytes in Health and Disease. J Am Heart Assoc. 2021 Feb 15:e019338. doi: 10.1161/JAHA.120.019338. PMID: 33586463

Hall C, Law JP, Reyat JS, Cumberland MJ, Hang S, Vo NTN, Raniga K, Weston CJ, O'Shea C, Townend JN, Gehmlich K, Ferro CJ, Denning C, Pavlovic D. Chronic activation of human cardiac fibroblasts in vitro attenuates the reversibility of the myofibroblast phenotype. Sci Rep. 2023 Jul 26;13(1):12137. doi: 10.1038/s41598-023-39369-y. PMID: 37495732; PMCID: PMC10372150

Abstracts:

Hall C, Law JP, Reyat JS, Fabritz L, Kirchhof P, Gehmlich K, Weston C, Townend JN, Ferro CJ, Denning C, Pavlovic D, Investigating the potential for reversal of myofibroblast activation in human cardiac fibroblasts in 2D culture, EP Europace, May 2021, doi.org/10.1093/europace/euab116.568

Hall C, Law JP, Reyat JS, Cumberland MJ, Weston C, Townend JN, Ferro CJ, Gehmlich K, Denning C, Pavlovic D, Long term activation of human cardiac fibroblasts in 2D culture is irreversible, Journal of Molecular and Cellular Cardiology, 2022, https://doi.org/10.1016/j.yjmcc.2022.08.073

Posters presented at European Heart Rhythm Association 2021 (EHRA) online congress, joint BAS/BSCR meeting 2022, and XXIV World Congress ISHR 2022
Talk presented at The Physiological Society 'Cross-Talk of Cells in the Heart: Novel Mechanisms of Disease and Arrhythmias' September 2023

Contents

1 Introduction **1**

1.1 The Heart 1

1.2 Cardiac Fibrosis 2

1.2.1 The Cardiac Fibroblast 3

1.2.2 Myofibroblast activation 4

1.3 Cardiac fibroblast-cardiomyocyte interactions 6

1.3.1 Interaction via gap junctions 7

1.3.2 Paracrine interactions 8

1.3.3 The role of mechanical stimuli 11

1.4 Reversing the MyoFb phenotype 13

1.5 Models of cardiac disease 15

1.5.1 Animal models of cardiac fibrosis 15

1.5.2 iPSC models of cardiac disease 17

1.6 Thesis motivation and aims 23

1.7 Published literature review 24

2 Materials and Methods **40**

2.1 Fibroblast cell culture 40

2.2 Soft substrates 40
2.3 Proliferation assay 41
2.4 Seeding density assay 42
2.5 Immunocytochemistry protocol 1 42
2.6 Immunocytochemistry protocol 2 43
2.7 Image analysis 44
2.8 RT-qPCR 44
2.9 iPSC culture 45
2.10 iPSC derivation of cardiac fibroblasts 46
2.11 iPSC derivation of cardiomyocytes 47
2.12 Optical mapping system 48
2.13 Optical mapping of iPSC-CMs 49
2.14 Cardiac fibroblast-cardiomyocyte co-culture 49
2.15 Statistical methods 50

3 Reversing the myofibroblast phenotype in chronically activated human cardiac fibroblasts 51

3.1 Computational modeling of cardiac fibroblast activation 51
3.2 Primary cardiac fibroblasts activate to myofibroblasts following long term culture in 2D 54
3.3 Myofibroblasts cannot reverse to a quiescent phenotype using biochemical and mechanical inputs either alone or in combination . . 58
3.3.1 Unresponsiveness to TGF-beta activation and inhibition is maintained in HCFs cultured on stiff plastic 64

3.4 Chronically activated human iPSC derived cardiac fibroblasts cannot be reversed to a quiescent phenotype 66
3.4.1 Differentiation of human iPSC derived cardiac fibroblasts . 66
3.4.2 Chronic activation of hiPSC-cFbs renders them unresponsive to TGF-beta stimulation or inhibition 68
3.5 Discussion 75
3.5.1 Mechanical stiffness and myofibroblast activation 76
3.5.2 Myofibroblast reversal and TGF-β receptor inhibition 77
3.5.3 Proliferation of the myofibroblast 78
3.5.4 Conclusion 79

4 Optimisation of optical mapping for 2D monolayers of iPSC-cardiomyocytes 80

4.1 Optimisation of and confirmation of cardiomyocyte differentiation . 82
4.2 iPSC-CMs remain stable during optical mapping 85
4.3 Use of different imaging parameters doesn't affect calcium transient duration measurements 88
4.4 Use of different imaging parameters doesn't affect action potential duration measurements 92
4.5 Blebbistatin does not affect the electrophysiology of iPSC-CMs . . 97
4.6 Isoprenaline induces the expected changes in calcium transient and action potential duration 100
4.7 Discussion 104
4.7.1 Selecting the appropriate imaging parameters 104
4.7.2 Blebbistatin 105

4.7.3 Pacing 106
4.7.4 Conclusion 107

5 Effects of co-culture with cardiac fibroblasts on electrophysiology and contraction of iPSC-cardiomyocytes 109

5.1 Culture of iPSC-CMs with SB431542 for 2 days has no effect on contraction or electrophysiology 109
5.2 Co-culture of cardiomyocytes with cardiac fibroblasts for 2 days has no effect on contraction or electrophysiology 113
5.3 Co-culture of cardiomyocytes with cardiac fibroblasts for 5 days has no effect on contraction and electrophysiology 119
5.4 Discussion 127
5.4.1 Conclusion 131

6 Conclusions 132

6.1 Thesis outcomes 132
6.2 Discussion 133
6.2.1 Stiffness and tissue culture surfaces 133
6.2.2 Multicellular models 134
6.2.3 2D versus 3D 135
6.2.4 Future work 136
6.3 Conclusions 138

Chapter 1

Introduction

1.1 The Heart

The heart is a muscular organ whose main purpose is to pump blood around the body. The heart consists of four chambers, the right and left atria and the right and left ventricles. The right atrium collects deoxygenated blood from the body which moves into the right ventricle before being pumped towards the lungs for oxygenation. Blood flows back to the heart via the pulmonary veins where it collects in the left atrium before moving to the left ventricle to be pumped around the rest of the body [1].

Cardiac function is primarily regulated by an electrical conduction system that stimulates contraction. Electrical stimuli originate from the sinus node initiating a wave of depolarisation across the right atrium, followed by the left. Electrical conduction converges on the atrioventricular node before passing to the bundle of His and Purkinje fibres which then stimulate ventricular depolarisation [1, 2].

The human heart is comprised of 4 major cell types that help it carry out its specialised function. The primary cell type is that of the cardiomyocyte. Cardiomyocytes are the contractile cells of the heart and make up the majority of the

heart by volume (roughly 70%) and 30-40% by number [3, 4]. Cardiac fibroblasts, endothelial cells and immune cells make up the majority of the non-myocyte population in the human heart. The cardiac fibroblast has an important structural role while also aiding in wound healing and repair (see section 1.2.1) [4, 5, 6]. Endothelial cells comprise the inner walls of the cardiac chambers and the linings of blood vessels. Their main role is to control blood flow [3, 4]. Lastly, we have the immune cells which include macrophages, T cells and B cells. These cells are involved in inflammation and are important regulators in cardiac disease [3, 7].

1.2 Cardiac Fibrosis

Cardiovascular disease (CVD) is the leading cause of death globally and includes diseases such as stroke, hypertension, ischaemia, and heart failure. The number of people affected by CVDs is increasing due to ageing populations and an increase in comorbidities including obesity and chronic kidney disease [8, 9]. CVDs cause millions of deaths worldwide every year with further losses attributed to disability-adjusted life years [9]. Cardiac fibrosis is associated with many of these CVDs and is often associated with a worse prognosis due to impaired cardiac function [10, 11].

Despite the fibrotic process being an initially reparative and healing process, cardiac fibrosis develops from pathological deposition of extracellular matrices (ECM). As part of the wound healing stage, following a cardiac injury such as myocardial infarction, there is a reparative stage of fibrosis known as replacement

fibrosis. This acts to replace dead cardiomyocytes with a fibrotic scar and maintain some cardiac function [12, 13]. However, signalling cues from fibroblasts and the dying cardiomyocytes also leads to cardiac fibrosis in the interstitial regions and away from the infarct zone. This interstitial fibrosis also occurs during more chronic and inflammatory conditions such as hypertensive cardiac disease. If this is left untreated it will ultimately become irreversible replacement fibrosis [13, 14]. Cardiac fibrosis leads to electrical and structural remodelling that results in cardiac dysfunction and can act as a substrate for arrhythmias by creating conduction blocks [15, 16]. There are currently no approved therapies for the treatment of cardiac fibrosis so there is understandably a great interest in dissecting the underlying mechanisms in the hopes of uncovering new therapeutic targets.

1.2.1 The Cardiac Fibroblast

The main process of cardiac fibrosis is driven by the activation of the cardiac fibroblast to the myofibroblast (MyoFb) [17]. The cardiac fibroblast is one of the main cell types in the heart with an important role in maintaining the ECM, providing structural support for the cardiomyocytes, and in wound healing and repair [5]. The exact numbers of fibroblasts in the heart differ according to different sources but most recent research suggests that they make up roughly 30-40$\%$ of the heart by cell number [4, 6, 18]. The proportion of cardiac fibroblasts also increases with age and in the presence of cardiac disease such as in heart failure and following myocardial infarction [19, 20, 21].

Single-cell sequencing data has also demonstrated the existence of multiple sub-

populations of cardiac fibroblasts within the heart. These subpopulations not only differ by activation state but suggest differing roles within the different regions of the heart [4, 6, 18]. It may also be indicative of the various possible lineages that can give rise to cardiac fibroblasts.

In the myocardium, cardiac fibroblasts predominantly originate from the pro-epicardium but can also stem from epithelial- and endothelial-to-mesenchymal transition [5, 22]. However, this heterogeneity means that there are no cellular markers exclusive to the cardiac fibroblast. Colloquial markers used and described in the literature are DDR2, vimentin, tcf21, and collagens 1 and 3 [5]. Regardless of origin, upon stimulation by disease or injury, cardiac fibroblasts will activate to MyoFbs [23, 24].

1.2.2 Myofibroblast activation

When activated to MyoFbs, these cells become less proliferative, increase their deposition of collagens and increase production of α-SMA stress fibres that provide them with contractile properties [24, 25, 26]. The main purpose of the MyoFb is to repair the myocardium following injury through the regulation of metalloproteinases (MMPs) and tissue inhibitors of metalloproteinases (TIMPs) [27]. In the context of myocardial infarction, MyoFbs increase the deposition of collagen to replace the necrotic tissue, forming a fibrotic scar [13, 17, 28]. Despite being necessary to prevent rupture of the myocardium, the presence of fibrosis ultimately leads to increased stiffness in the myocardium that decreases cardiac function and acts as a substrate for arrhythmogenesis [10, 29].

The cardiac fibroblast to MyoFb activation process is multi-faceted and mediated by many different factors [12, 30] (Figure 1.1). The main instigator of MyoFb activation is transforming growth factor-beta (TGF-β), with several independent studies demonstrating direct involvement [31, 32, 33]. Other paracrine factors have also been implicated, such as Angiotensin II (Ang II) and Interleukin-6 (IL-6) [34, 35]. A more novel activating factor is mechanical stress or tension, with multiple studies observing that the use of stiff culture surfaces leads to the expression of α-SMA in cardiac fibroblasts [26, 36]. Many of these activating factors are also involved in modulating communications between cardiac fibroblasts and cardiomyocytes.

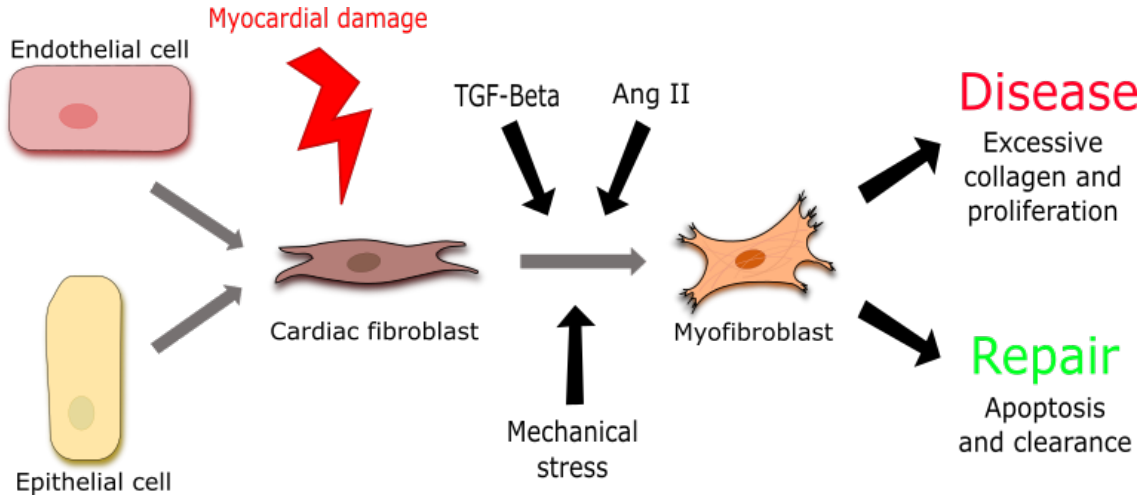


Figure 1.1: Resident cardiac fibroblasts derive from endothelial- or epithelial-to-mesenchymal transition. Injury to the myocardium initiates signalling pathways that trigger the activation of cFbs to MyoFbs. Loss of structural integrity via CM death also creates mechanical stress that mediates cFb to MyoFb activation. Consequences of MyoFb activation vary between repair and disease processes. There are multiple mechanisms for activation including mechanical stimuli and paracrine factors from a variety of different sources such as CMs and the cFbs themselves. Image taken from my literature review (see end of chapter)[12].

1.3 Cardiac fibroblast-cardiomyocyte interactions

Over the past few decades, more and more research has shown the importance of non-excitatory cells in maintaining normal electrical function in the heart [37, 38, 39]. More specifically, cardiac fibroblasts have been observed to have effects on cardiomyocyte electrophysiology - both through direct contacts, i.e. gap junctions, and paracrine effects, i.e. TGF-β and Ang II [40, 41, 42] (Figure 1.2).

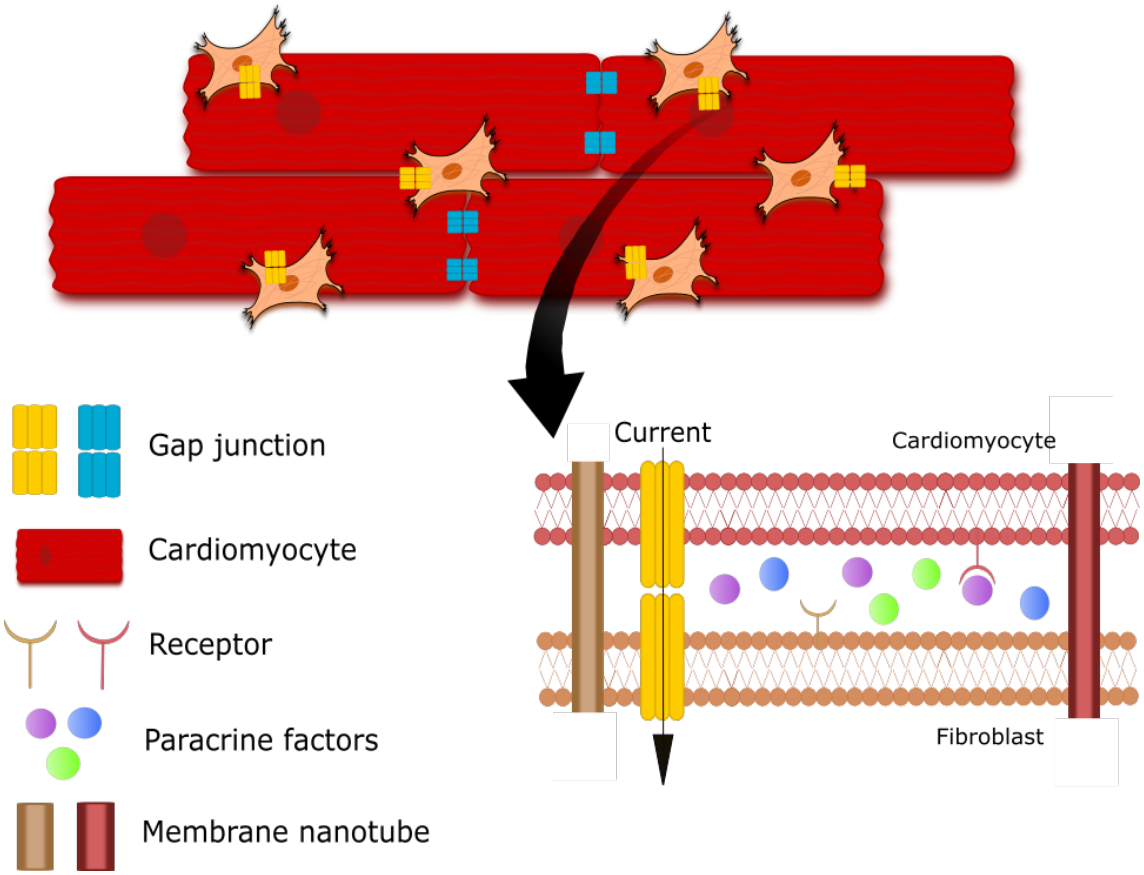


Figure 1.2: Figure depicting cardiomyocyte-MyoFb communcations. Gap junctions present at distal junctions between CMs as well as elsewhere between CMs and MyoFbs. Gap junctions and membrane nanotubes allow exchange of molecules between the cytoplasms of cells. Paracrine factors secreted by cells bind receptors on neighbouring membranes initiating signalling pathways. Image taken from my review (see end of chapter) [12].

1.3.1 Interaction via gap junctions

Gap junctions are believed to be the main mechanism for electrotonic coupling within the human heart [43]. These ion channels connect neighbouring cells allowing the propagation of electrical signals between them [44]. Different combinations of connexin proteins produce varying levels of channel permeability [45]. The main subtypes found in the heart are Cx40, Cx43 and Cx45. In cardiac fibroblasts and ventricular cardiomyocytes, the most commonly expressed connexin is Cx43 [43, 44].

Changes in the expression of connexin proteins have been observed in ageing and following cardiac injury. These changes that often lead to conduction slowing and increased risk of arrhythmias can be observed in both cardiomyocytes and cardiac fibroblasts [46, 47, 48]. In models of cardiac injury, both Vasquez *et al* (2010) and Zhang *et al* (2010) observed an increase in Cx43 expression in cardiac fibroblasts which led to an increase in functional coupling with cardiomyocytes [48, 49]. Zhang *et al* (2010) also observed a decrease in Cx43 expression in cardiomyocytes from these same models. Nagaraju *et al* (2019) built on this work demonstrating that MyoFbs had an increased expression of Cx43 and an increase in functional coupling with cardiomyocytes when compared to cardiac fibroblasts [42]. This suggests that cardiac fibroblasts and MyoFbs may be compensating for the loss to conserve cardiac function [49]. Whether this phenomenon occurs in humans still needs to be investigated.

1.3.2 Paracrine interactions

Evidence also exists for the interaction of cardiomyocytes and cardiac fibroblasts indirectly using paracrine signalling [12]. *In vitro* studies have investigated this using multiple methods including separated co-culture methods and conditioned medium collected from the culture of cardiac fibroblasts. These have indicated a role for paracrine mediators on the electrophysiology of cardiomyocytes [48, 50, 51]. LaFramboise *et al* (2007) observed cardiomyocyte hypertrophy and reduced spontaneous contractions in the presence of cardiac fibroblast conditioned medium [52]. Vasquez *et al* (2010) expanded on this work comparing conditioned medium of fibroblasts from healthy and diseased hearts. They demonstrated slower conduction velocities and shortened action potential durations using MyoFb conditioned medium when compared to the healthy cardiac fibroblasts [48].

When delving into the paracrine factors that cause these changes, several stand out from the literature, TGF-β, Ang II and IL-6.

TGF-β

TGF-β is a cytokine involved in a multitude of processes, not limited to proliferation, differentiation and migration [53]. TGF-β binds to TGF-β receptors to stimulate multiple downstream pathways via either Smad- or non-Smad-mediated transcription [12]. It has been an important area of cardiac fibrosis research as the main driver for MyoFb activation [31, 32]. Several studies have also reported

increased levels of TGF-β in models of hypertrophy and heart failure suggesting additional roles outside of fibrosis [54, 55]. These effects have been described to be more potent in the atria compared to the ventricles perhaps contributing to the prevalence of atrial fibrillation [56, 57]. Because of this important role in cardiac disease, multiple groups have investigated the TGF-β signalling pathway to identify potential anti-fibrotic therapeutics. Both Kuwahara *et al* (2002) and Khalil *et al* (2017) demonstrated a reduction of fibrosis by reducing TGF-β signalling [31, 58]. Suppression or reversal of the MyoFb phenotype has been also demonstrated using TGF-β receptor inhibition [20, 59, 60]. However, due to the widespread use of TGF-β throughout the body, increased mortality has been observed in TGF-β knockdown models and following chronic pharmacological inhibition [20, 31].

The direct impact of TGF-β on electrical activity in the heart is less well described. Cartledge *et al* (2015) demonstrated that co-culture with MyoFbs alters calcium transients when compared to co-culture with cardiac fibroblasts and that these effects were blocked in the presence of a TGF-β receptor inhibitor. However, treatment with TGF-β alone could not recapitulate these changes, suggesting the MyoFbs themselves were driving these changes and not the increased expression of TGF-β associated with activation [12, 50]. A study conducted by Kaur *et al* (2013) demonstrated a significant increase in peak Na^+ current when exposed to TGF-β which was reversed in the presence of a TGF-β neutralising antibody. It remains unclear whether these effects would have any impact on action potential morphology or induce any changes in intracellular Na^+ concentration [51].

The involvement of TGF-β in cardiac fibrosis and hypertrophy is well-documented. Its precise role in the activation of MyoFbs and cardiomyocyte-fibroblast communications is becoming more evident. Modern -omics studies and the use of computer modelling are providing more in-depth analysis of the TGF-β signalosome that will aid in the identification of novel downstream anti-fibrotic targets [12, 60, 61, 62].

Angiotensin II

Ang II is a hormone within the renin-angiotensin system that is involved in the regulation of blood pressure and sodium homeostasis [63, 64]. The use of ACE inhibitors (angiotensin-converting enzyme) has long been an established treatment of hypertension [65]. However, ACE inhibition has also been observed to reduce ventricular remodelling through the reduction of cardiac hypertrophy and fibrosis [66, 67].

Ang II is secreted by cardiac fibroblasts and MyoFbs and has been implicated as a potent pro-fibrotic factor [67, 68, 69]. Cao *et al* (2018) demonstrated significant upregulation of α-SMA in response to Ang II and a correlated increase in Cx43 expression, both indicative of MyoFb activation [34]. Exposure of Ang II to cardiac fibroblasts also stimulates the release of TGF-β and IL-6 further promoting fibrosis [69]. Together, this data suggests a greater role for Ang II in the heart, and more specifically, in cardiac fibrosis. The use of ACE inhibitors in patients with hypertensive heart disease has been shown to reduce cardiac fibrosis further suggesting this pathway may be of interest in identifying anti-fibrotic therapies

[70].

Interleukin-6

Like TGF-β, IL-6 is a cytokine involved in multiple processes of differentiation, growth and survival [71]. Although IL-6 has a prominent role in inflammation, the IL-6 signalling pathway is also involved in cardiac function with an important role in cardio-protection following acute injury. However, perpetuated stimulation is observed to cause cardiomyocyte hypertrophy and fibrosis [71, 72, 73, 74]. Ma *et al* (2012) demonstrated that cardiac fibroblasts were the main source of IL-6 in the heart following stimulation by Ang II. They also observed that this was reliant on the presence of macrophages and that the presence of macrophages led to activation of MyoFbs in an IL-6 dependent manner [35]. Other research has demonstrated that cardiomyocytes themselves are also a source of IL-6 in the heart and that following injury, cardiomyocyte secretion of IL-6 is increased thus creating a feedback loop in cardiac fibroblasts that perpetuates cardiac hypertrophy and fibrosis [69, 75, 76]. Mechanisms driving this sustained IL-6 response in cardiac disease are unclear and require further investigation.

1.3.3 The role of mechanical stimuli

Young's modulus describes the ability of a substance to stretch and deform, i.e. how elastic a material is [77]. There are disputing values for Young's modulus of the human heart due to the difficulty in obtaining healthy material. However, it is estimated to be between 10-30 kPa [78, 79, 80]. During disease, the presence of

fibrosis leads to a much stiffer substrate of 100+ kPa [29, 79]. It is now recognised that the use of standard tissue culture plastic, due to the higher tensile strengths ($\sim$3 GPa), leads to MyoFb activation. This has been demonstrated by several studies where α-SMA expression was increased after only a few hours of culture [26, 79, 81]. Other experiments have shown that mimicking healthy (10-30 kPa) substrates leads to decreased expression of collagen and α-SMA while mimicking diseased substrates (100+ kPa) leads to increased expression of collagen and α-SMA expression [79, 80, 81, 82]. With this in mind, it is likely that many existing studies that utilise standard stiff plastic culture conditions are therefore working with activated MyoFbs. Future research should aim to consider the stiffness of the substrate in order to align more closely with physiological conditions.

The impact of mechanical forces has not only been implicated in MyoFb activation but in cardiomyocyte-cardiac fibroblast communications through a process known as mechano-electric feedback [83, 84]. Zhuang *et al* (2000) demonstrated *in vitro* that the application of pulsatile stretch, induced expression of proteins involved in mechanical and electrical coupling. The observed increase in the expression of Cx43 corresponded to a rapid increase in conduction velocity [84]. This work was built upon by Nguyen *et al* (2018) who demonstrated that the use of softer substrates not only promoted stronger contractions and transmission of mechanical signals by cardiomyocytes but that the attenuation of signal propagation in the presence of MyoFbs occurred in a stiffness-dependent manner [29]. Mechanosensitive channel blockers have also been shown to improve electrical

conduction in the presence of MyoFbs [85]. This data is evidence of the importance of environmental stiffness in regulating cardiomyocyte electrophysiology. Reversing MyoFb activation and reducing the stiffness of the heart may provide important avenues for decreasing the burden of cardiac fibrosis on the heart.

For more information regarding MyoFb activation and the effects of cardiac fibroblasts on cardiomyocytes, please see my published literature review at the end of this chapter (Section 1.7).

1.4 Reversing the MyoFb phenotype

With such a commanding presence in cardiac disease, there is understandably great interest in reducing or reversing the burden of cardiac fibrosis in the human heart. Recent research has suggested this may be achievable through reversal of the MyoFb phenotype [20, 59, 86].

TGF-β, as the main activator of MyoFbs, has been a predominant target of interest in MyoFb reversal. Multiple studies have demonstrated that the use of a TGF-β receptor inhibitor has either prevented expression of α-SMA fibres in quiescent cells or decreased expression in already activated cells [20, 59, 60, 86]. There have also been preclinical studies demonstrating the effectiveness of TGF-β receptor inhibition as an effective anti-fibrotic treatment.

Despite global Smad2/3 knockouts being embryonic lethal, Khalil *et al* (2017) demonstrated that knockout of fibroblast-specific TGF-β signalling components, such as the TGF-β receptor 1, led to cardio-protective effects against fibrosis [31].

Other *in vivo* studies have reported significant reductions in cardiac fibrosis when using neutralising monocloncal antibodies or small molecule inhibitors of TGF-β or TGF-β receptor 1 [54, 58, 87]. Although there are complications targeting TGF-β due to its ubiquitous nature throughout the human body, these results suggest that targeting specific aspects of the TGF-β signalling pathway within fibroblasts may hold promise for anti-fibrotic therapies.

The use of softer substrates has also been investigated for MyoFb reversal. The presence of fibrosis within the heart leads to a stiffening that both decreases cardiac function and perpetuates MyoFb activation. Therefore, by decreasing the stiffness of the heart, it may be possible to prevent further MyoFb activation and progression to pathological fibrosis. Several studies have demonstrated that culture on stiff substrates leads to the activation of MyoFbs and that use of softer substrates can prevent activation of MyoFbs [36, 82]. However, few have investigated whether soft substrates can reverse the MyoFb phenotype.

Wang *et al* (2012) demonstrated using valvular MyoFbs and tunable substrates that softening culture surfaces from 32 to 7 kPa led to a down-regulation of activation markers such as α-SMA and CTGF. These cells also maintained their ability to re-activate to MyoFbs in the presence of TGF-β [80]. Similarly, when Giles *et al* (2020) cultured primary mouse fibroblasts on stiff plastic followed by soft hydrogels, they also observed a decrease in activation markers such as CTGF, Periostin and collagens 1 and 3 [88]. Whether these results can be replicated using human cells is yet to be investigated.

1.5 Models of cardiac disease

With cardiovascular disease as the leading cause of mortality for decades, it is important to be able to model the disease in the lab. Historically, animal models such as rats or mice have been favoured when it comes to modelling cardiac disease. These animals have a high reproductive capacity and are relatively low cost allowing larger numbers to be used thereby increasing the statistical power of such studies [89, 90]. Bigger animals such as rabbits, dogs or pigs have also been utilised [89]. *In vivo* studies allow better examination of whole organism physiology and toxicity effects of drugs than *in vitro* studies, but they can be laborious and costly, especially when using larger organisms [89, 91]. Another issue is that there are often species differences, limiting the extrapolation of results to humans. For example, mice have a higher heart rate and differential expression of proteins and ion channels. These differences may in part explain some of the high failure rates of cardiac drugs in human clinical trials [89, 91].

1.5.1 Animal models of cardiac fibrosis

Cardiac fibrosis is present in many CVDs and establishing an appropriate model is important to properly investigate the pathophysiological mechanisms of the disease. Rodent models are the preferred model for investigating cardiac disease and can be created using a variety of different techniques: surgery, pharmacology and genetic modification [90]. The method used will depend on the aspect of fibrosis being investigated. For example, the fibrosis formed following myocardial infarction is more specific and localised and is often replicated using surgery by

left coronary artery ligation. On the other hand, the more diffuse fibrosis formed during inflammatory or chronic diseases such as hypertension, can be recreated using a high-salt diet, genetic modification (as with the spontaneously hypertensive rat) or exposure to Ang II [92]. Each of these methods comes with its own set of advantages and limitations. The use of the high salt diet creates a progressive disease that mimics human fibrosis, however, it only creates a relatively low level of fibrosis [92]. The use of surgical models is invasive, requires a lot of training, and has an associated mortality that increases costs. The benefits are that it creates a robust model of reparative cardiac fibrosis and the associated cardiac dysfunction [92]. Using pharmacological methods such as Ang II exposure tends to induce a much faster onset of fibrosis than seen in humans but provides a high degree of fibrosis in a shorter period of time [92].

It is also important to consider that outside of the inflicted cardiac injury, the hearts in these models are otherwise healthy often without any co-morbidities [92, 93]. Furthermore, fibrosis is known to be a substrate for arrhythmias due to both structural and electrical remodelling [15, 16]. This is difficult to investigate using rodent models as they have an inherent invulnerability to arrhythmia induction when compared to larger animals such as dogs or pigs. It has also been found that when these arrhythmias do occur, they are more easily reversed in murine models [93]. There is a nuance involved in selecting the right model for investigating cardiac fibrosis and discovering potential anti-fibrotic therapeutics. Each has different features that can help us to understand the pathological mechanisms of cardiac fibrosis. Many of the models used also exhibit multi-organ damage that would not

necessarily be observed in clinical settings. This demonstrates the need for the development of more representative human models.

1.5.2 iPSC models of cardiac disease

Developments in the world of induced pluripotent stem cell (iPSC) research have led to the increased use of iPSC models which may provide a better representation of human biology [94, 95, 96]. Over the last 20 years, the ability to differentiate pluripotent stem cells (PSCs) has become more efficient and reliable. Despite differentiation being a relatively length process (10-15 days), several established protocols provide comparative success and efficiency [97, 98, 99].

iPSC-cardiomyocytes (iPSC-CMs) provide reasonable benefits compared to traditional models of disease. These models can be higher throughput due to the proliferative capacity of iPSCs which means experiments can be conducted more easily and in higher numbers giving greater statistical power. iPSC-CM models are also ethically unbiased and provide the opportunity to work with patient-specific cells and mutations [97, 100]. By deriving iPSCs directly from patient cells, first-hand examination of disease-causing mutations can be conducted and exact disease mechanisms can be elucidated [94, 97]. This has been applied to channelopathies, such as long QT syndrome, as well as to hypertrophic and dilated cardiomyopathies [97]. Moretti *et al* (2010) was the first to generate iPSCs from patients with LQT1 syndrome which demonstrated the symptomatic prolonged action potential duration compared to controls [97, 101]. Since then further models have been created that have been successfully used to help us

better understand disease mechanisms and improve drug testing [97, 102].

There is also emerging evidence that iPSC-CM models may be better predictors of drug toxicity than the current predominantly used mouse models [103]. More than a quarter of phase 2 clinical trials fail due to safety concerns, cardiotoxicity being amongst the leading causes [97]. iPSC-CMs provide a human-relevant tool to study adverse drug responses. Pointin *et al* (2017) demonstrated that 3D cardiac microtissues, derived using iPSCs, were capable of correctly predicting the contractile consequences of specific drugs [104]. Similarly, Saleem *et al* (2020) tested a variety of drugs in iPSC-CMs, in both 2D and 3D formats, and demonstrated high predictive accuracy, 85 $\%$ and 93 $\%$, respectively [103].

iPSC-CM models not only have the ability to aid in cardiotoxicity studies, but they also have the potential to improve personalised medicine. Patient-derived iPSC-CMs were obtained from breast cancer patients following treatment with doxorubicin and used to correctly recapitulate doxorubicin-induced toxicity [105]. Stillitano *et al* (2017) further illustrated that iPSC-CMs could replicate the propensity to exhibit an arrhythmogenic drug response using patients with LQT syndrome [106].

Outside of disease modelling, iPSC-CM models provide significant promise as potential sources for cardiac cell therapy. Adult human cardiomyocytes have minimal regenerative or proliferative capacity. iPSC-CMs, partly due to their foetal

phenotype, show the ability to proliferate to some degree [97]. Research has therefore begun using iPSC-derived CMs for engraftments and cell-based therapies to repair injured hearts. Several studies have demonstrated that injecting iPSC-CMs into damaged hearts can contribute to contraction and restore cardiac function to some extent [97, 107, 108]. However, both Chong *et al* (2014) and Shiba *et al* (2016) observed increased arrhythmias in the host animals a few days after injection that were often fatal [107, 108]. Being able to reduce, control or completely remove these arrhythmogenic side effects will dictate the future of these therapies for use in human patients.

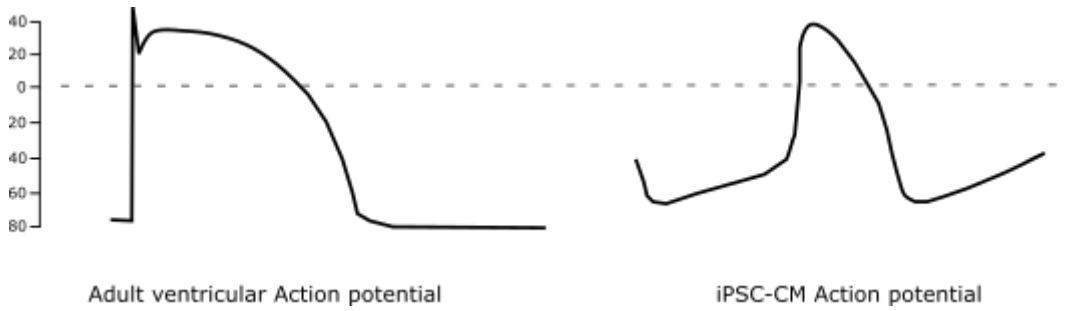


Figure 1.3: Schematic demonstrating the differences between a human adult ventricular action potential and a human iPSC-derived cardiomyocyte action potential. Adapted from Goverson *et al* (2018) [109].

Despite all of these many beneficial uses, iPSC-CMs still have an immature phenotype and cannot reflect whole organ systems. Compared to adult CMs, iPSC-CMs are rounder, smaller, not rod-shaped, and spontaneously contract [109, 110]. A differential expression of ion channels such as the I_{K1} leads to a different action potential waveform as seen in Figure 1.3 including a slower upstroke and a lack of a notch during the plateau phase [109]. This means certain aspects of cardiomyocyte electrophysiology cannot be studied using iPSC-CMs

without employing some method of maturation.

Fatty acid maturation

A distinctive characteristic of cardiomyocyte maturation is the switch from glucose metabolism to fatty acid metabolism. Typical cell culture generally uses glucose as an energy source, therefore, supplementation of fatty acids has since been explored for the maturation of iPSC-CMs in culture [111]. Several independent studies have demonstrated that the addition of fatty acids to culture media leads to longer and more structured sarcomeres, significant increases in contractile force and improved calcium transient and action potential dynamics [111, 112, 113]. However, despite these benefits, no study has yet shown the complete maturation of iPSC-CMs using these methods.

Ageing in culture

Another aspect used for maturation is ageing or extended time in culture. Lundy *et al* (2013) compared ESC-CM and iPSC-CMs grown in short term (30 days) versus long-term culture (100 days). They observed significant increases in sarcomere length and size, as well as, a decrease in circularity. Faster calcium kinetics and more mature action potential morphology were also exhibited following long-term culture [114]. Sartiani *et al* (2007) similarly found that maintaining cells in culture for up to 3 months led to a more adult phenotype. With a focus on ion channel expression, they observed increased expression of I_{to1} and I_{K1} in later-stage ESC-CMs, which led to more mature action potential characteristics [115].

Micropatterning

Under standard culture conditions, iPSC-CMs do not have the typical rod-shape and lack myofibril alignment along a dominant axis. Micropatterning has therefore been utilised to aid in the alignment and maturation of iPSC-CMs [116, 117]. Feaster *et al* (2015) demonstrated that the use of a ”matrigel mattress” produced iPSC-CMs with contractile properties more similar to rabbit-CMs. These iPSC-CMs also acquired morphological features associated with maturity such as elongation, decreased circularity and increased sarcomere length compared to control iPSC-CMs [116]. Other studies have demonstrated that plating neonatal rat cells on micropatterned laminin led to better organisation and alignment of cardiomyocytes mimicking the adult rat myocardium. These aligned neonatal cells also exhibited increased expression of N-cadherin and the intercalated disks resembled those found *in vivo* [118, 119].

Use of 3D culture

One final method of maturation amassing popularity is that of 3D cultures such as engineered heart tissues (EHTs) and cardiac organoids [120, 121, 122]. Correia *et al* (2018) observed an upregulation in genes related to fatty acid metabolism in 3D aggregates when compared to 2D iPSC-CMs, as well as, a downregulation in genes related to glycolysis. They also detected a significant increase in action potential duration in 3D aggregates [120]. When Lemoine *et al* (2017) compared EHTs with 2D monolayers of iPSC-CMs they discovered an increased density of I_{Na}, similar to that reported for adult cardiomyocytes. They also observed,

using microelectrode techniques, upstroke velocities comparable to human left ventricular tissue [121]. Other models have also shown that the inclusion of other cardiac cell types, such as cardiac fibroblasts and/or endothelial cells can not only improve maturity but provide insight into important cell-cell interactions [123, 124].

Regardless of the maturation method used, iPSC-CMs still do not represent the full mature phenotype as expected in adult ventricular cardiomyocytes. Despite the numerous benefits of using these cells a precise method of maturation should still be investigated to further improve the application of these cells in clinical medicine.

Over the past couple of decades, studies have been exploring the intricate and complex nature of cell-cell interactions in the heart, such as between the cardiac fibroblast and cardiomyocyte. Nonetheless, there exists only one study that has demonstrated direct contacts between these two cell types *in vivo* and whether this phenomena exists in humans is yet to be confirmed [125]. Due to the difficulties in obtaining human cardiac tissue, cellular systems are crucial to advancing our understanding of cardiac disease. However, there are challenges with *in situ* experiments and culturing cFbs in vitro, mainly due to their tendency to turn into myofibroblasts. Coupled with the immaturity of iPSC-CMs, it's crucial to find methods to improve and develop tissue culture models to allow more representative human research to be conducted. With the complex nature of fibrosis, the development of appropriate co-culture models may help to unravel the pathogenicity of

the disease. Given the conservation of many of these processes across various organs, identifying shared mechanisms could yield substantial clinical benefits for a spectrum of diseases entailing fibrosis.

1.6 Thesis motivation and aims

Cardiac fibroblasts are integral to the proper function of the myocardium. However, due to the stiffness of tissue culture plastic, research is often done using activated MyoFbs as opposed to quiescent cardiac fibroblasts. Reversing the MyoFb phenotype could also provide an interesting avenue for fibrotic therapies. We hypothesised that the culture of cardiac fibroblasts in 2D culture on stiff plastic leads to myofibroblast activation. The aim of this work was therefore to investigate the activation of human cardiac fibroblasts in culture and the potential for reversibility of the activated MyoFb phenotype in 2D culture.

Much of the current published *in vitro* work has been conducted using animal models. The question remains as to whether this translates to human biology. Therefore we also aimed to investigate whether activated MyoFbs and quiescent cardiac fibroblasts have differential effects on cardiac electrophysiology and contraction when using human iPSC models. Here, we hypothesise that MyoFbs will have a greater and more detrimental effect on cardiomyocyte electrophysiology - prolonging APD and CTD, and increasing heterogeneity, providing an arrhythmogenic substrate.

1.7 Published literature review

During my first year, I wrote a literature review that was successfully published in the Journal of the American Heart Association. A significant amount of this work was conducted during the COVID-19 isolation period. The manuscript was reviewed and edited by the co-authors.

Hall C, Gehmlich K, Denning C, Pavlovic D. Complex Relationship Between Cardiac Fibroblasts and Cardiomyocytes in Health and Disease. J Am Heart Assoc. 2021 Feb 15:e019338. doi: 10.1161/JAHA.120.019338. PMID: 33586463

Journal of the American Heart Association

CONTEMPORARY REVIEW

Complex Relationship Between Cardiac Fibroblasts and Cardiomyocytes in Health and Disease

Caitlin Hall, MSci; Katja Gehmlich, PhD; Chris Denning, PhD*; Davor Pavlovic, PhD*

ABSTRACT: Cardiac fibroblasts are the primary cell type responsible for deposition of extracellular matrix in the heart, providing support to the contracting myocardium and contributing to a myriad of physiological signaling processes. Despite the importance of fibrosis in processes of wound healing, excessive fibroblast proliferation and activation can lead to pathological remodeling, driving heart failure and the onset of arrhythmias. Our understanding of the mechanisms driving the cardiac fibroblast activation and proliferation is expanding, and evidence for their direct and indirect effects on cardiac myocyte function is accumulating. In this review, we focus on the importance of the fibroblast-to-myofibroblast transition and the cross talk of cardiac fibroblasts with cardiac myocytes. We also consider the current use of models used to explore these questions.

Key Words: arrhythmias ■ cardiac fibroblasts ■ cardiomyocytes ■ fibrosis ■ heart failure ■ myofibroblast

Downloaded from http://ahajournals.org by on February 15, 2021

Because of aging populations and lifestyle changes, the total number of deaths caused by cardiovascular diseases (CVDs) is increasing, by ≈21% from 2007 to 2017.[1] High mortality rates as well as a high level of morbidity contribute to the high economic burden of CVDs.[2] Many of these deadly and debilitating CVDs are associated with cardiac fibrosis, which can be classified as either diffuse interstitial or replacement fibrosis.[3] Replacement fibrosis occurs immediately following cardiac injury, such as myocardial infarction (MI), to form a fibrotic scar preventing rupture of the myocardium.[3,4] Interstitial fibrosis is associated with inflammation and more chronic conditions, such as cardiomyopathies or hypertension, and if the underlying condition is left untreated, results in irreversible replacement fibrosis.[3–5] Cardiac fibrosis contributes to both electrical and structural remodeling of the heart, which ultimately leads to decreased cardiac function, heart failure, and arrhythmias.[4,6–8] The relationship between fibrosis and CVDs has been the subject of multiple studies. However, with no efficient treatments directly targeting cardiac fibrosis, it presents an ever-growing clinical challenge.[9,10] The fibrotic process is mediated by activation of cardiac fibroblasts (cFbs), an important nonexcitatory cell population in the heart, responsible for deposition of extracellular matrix (ECM) in health and disease. cFbs can influence cardiac function through direct and indirect effects on cardiomyocytes.[11–13] In this review, we summarize the current understanding of the interactions between cFbs and cardiomyocytes and discuss the key questions remaining.

CARDIAC FIBROBLASTS

The human heart is composed of 5 major cell types: cardiomyocytes, fibroblasts, endothelial cells, macrophages, and smooth muscle cells.[14–16] Cardiomyocytes contribute roughly 30% to 40% by number and roughly 65% to 80% by volume in the adult mammalian heart.[16–21] Recent single-cell sequencing studies highlight considerable heterogeneity between the different regions of the human heart, with ventricles

Correspondence to: Davor Pavlovic, PhD, Institute of Cardiovascular Sciences, University of Birmingham, Birmingham B15 2TT, United Kingdom. E-mail: d.pavlovic@bham.ac.uk and Chris Denning, PhD, Biodiscovery Institute, University of Nottingham, University Park, Nottingham NG7 2RD, United Kingdom. E-mail: chris.denning@nottingham.ac.uk

*Dr Denning and Dr Pavlovic are co–senior authors.

For Sources of Funding and Disclosures, see page 11.

© 2021 The Authors. Published on behalf of the American Heart Association, Inc., by Wiley. This is an open access article under the terms of the Creative Commons Attribution License, which permits use, distribution and reproduction in any medium, provided the original work is properly cited.

JAHA is available at: www.ahajournals.org/journal/jaha

Nonstandard Abbreviations and Acronyms

Ang II	angiotensin II
cFb	cardiac fibroblast
Cx43	connexin 43
ECM	extracellular matrix
FSP1	fibroblast-specific protein 1
hiPSC	human induced pluripotent stem cell
SMAD	small mothers against decapentaplegic
TGF-β	transforming growth factor-β
α-SMA	α-smooth muscle actin

having distinct cellular signatures compared with atria (47.1% cardiomyocytes compared with 31.1%, respectively).[16,20] Reports on proportion of cFbs in heart differ, from circa 20% to 60% in rats and humans.[6,15,16,19] cFb numbers increase with development, aging, and disease. Banerjee et al showed that, in both rats and mice, the number of fibroblasts increases postnatally until adulthood is reached (≈30% to ≈64% in rat and ≈10% to ≈25% in mouse).[15] An increase in cFbs has also been demonstrated in heart failure and following MI.[14,22,23]

Comparison of transcriptomes has revealed more similarities between cFbs and cardiomyocytes than between other fibroblast cell types.[24,25] In addition, use of single-cell RNA sequencing has identified several subpopulations of cFbs within the heart, displaying distinct genetic signatures.[16] As mesenchymal cells present in every tissue in our body, these subpopulations may be indicative of the various possible cFb lineages.[6,16] In the heart, cFbs are primarily derived from the proepicardium, but can also arise by epithelial-to-mesenchymal and endothelial-to-mesenchymal transition.[6,26] Because of this heterogeneity and their ubiquitous nature, markers specific to cFbs are still lacking. Vimentin is often used alongside specific morphological properties of cFbs, such as the lack of a basement membrane. Some reports have used FSP1 (fibroblast-specific protein 1) and discoidin domain receptor to identify cFbs, but these are also found in leukocytes and fibrocytes, respectively.[6,27]

Regardless of origin, resident cFbs are dispersed throughout the heart as strands and sheets that sit between cardiac muscle fibers acting as a scaffold.[28,29] Their main function is to maintain the ECM through regulation of matrix metalloproteinases and tissue inhibitors of metalloproteinases, and therefore mediate secretion and degradation of collagen.[30] During disease or injury (eg, following MI), cFbs undergo a transition from fibroblast to myofibroblast.[6,31] This activated phenotype is described as having a spindle shape, increased proliferation, expression of α-smooth muscle actin (α-SMA), and increased production of collagen.[32,33] Single-cell sequencing in mouse hearts further defined these differences between the activated myofibroblast and nonactivated cFb. They found ≈30 genes differentially expressed between the 2 cell types, including periostin and collagens 1 and 3, all known to be associated with the myofibroblast.[34]

The main role of this cell type is wound healing and repair. Following MI, formation of a fibrotic scar, in place of necrotic tissue, prevents rupture of the myocardium.[4,22] The expression of α-SMA stress fibers provides these cells with the ability to contract. This causes shrinkage of the fibrotic scar and produces tension, which, in turn, increases the stiffness of the myocardium.[32,35–37] Although initially beneficial for maintenance of cardiac function and prevention of heart rupture, long-term effects of excessive fibrosis are detrimental (see section on Cross Talk Between the Myofibroblast and the Cardiomyocyte below).

Structural and electrical remodeling of the myocardium, attributed to chronic and proinflammatory conditions, such as hypertension, is commonly associated with cardiac fibrosis.[28,38,39] Inflammation has been demonstrated to lead to cardiac fibrosis via activation of profibrotic signaling cascades via interleukin 6 (IL-6) (see section on Interleukin 6 below).[40] Stiffness itself can activate cFbs, leading to transition to myofibroblasts (Figure 1). Myofibroblasts themselves can secrete further profibrotic factors, driving progression to the kind of fibrosis seen following MI.[28,32,41,42] Alongside increased stiffness, fibrosis has also been observed to slow conduction and disrupt electrical wave propagation. Ultimately, these factors contribute to decreased cardiac function and increased susceptibility to arrhythmias.[43]

The transition from cFb to myofibroblast is a multifactorial process mediated by several factors (Figure 1).[28,37] Transforming growth factor-β (TGF-β) has been shown in several independent studies to be directly involved in this transition process.[44–46] Myofibroblasts, once activated, can themselves secrete TGF-β, thus creating a detrimental positive feedback loop leading to sustained fibrosis.[47–49] The importance of tensile strength and mechanical stress in the activation of myofibroblasts has also been demonstrated (see section on Cross Talk Between the Myofibroblast and the Cardiomyocyte for more detail).[32,48,50] Perhaps not surprisingly, cFb activation can modulate cardiomyocyte function, and several modes of cFb-cardiomyocyte communication have been uncovered.

MECHANISMS OF CFB-CARDIOMYOCYTE COMMUNICATION

In the 1980s, multiple studies demonstrated cell-cell interactions between excitatory and nonexcitatory cells

Downloaded from http://ahajournals.org by on February 15, 2021

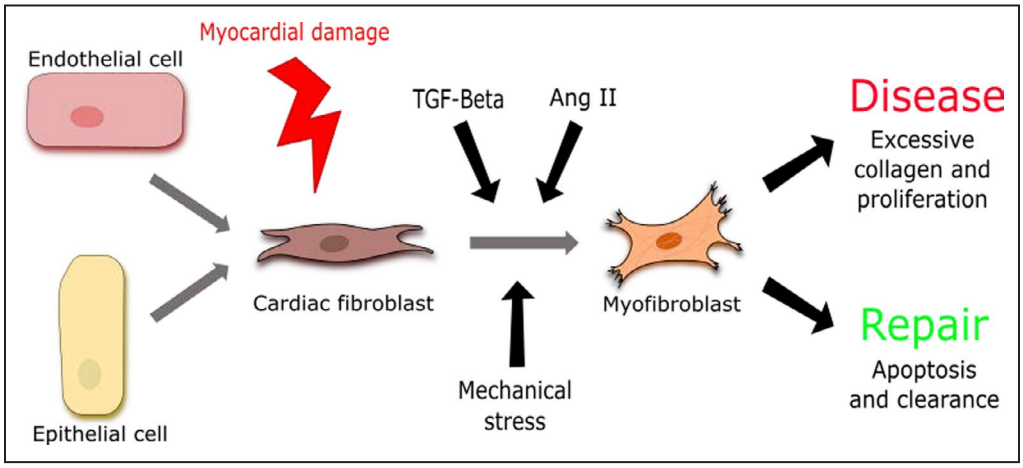


Figure 1. Resident cardiac fibroblasts (cFbs) derive from endothelial-to-mesenchymal or epithelial-to-mesenchymal transition.
Injury to the myocardium initiates signaling pathways that trigger the activation of cFbs to myofibroblasts (MyoFbs). Loss of structural integrity via cardiomyocyte (CM) death also creates mechanical stress that mediates cFb to MyoFb activation. Consequences of MyoFb activation vary between repair and disease processes. There are multiple mechanisms for activation, including mechanical stimuli and paracrine factors, such as transforming growth factor-β (TGF-β) and angiotensin II (Ang II), from a variety of different sources, such as CMs and the cFbs themselves.[28,43]

in the heart. These were shown to be mediated via paracrine signaling and/or direct contacts between the cells.[51,52] From the mid-2000s, there has been more focus on the effects of the nonexcitatory stromal cells on the electrophysiological features of the heart, with changes to conduction velocity and membrane depolarization observed during coculture.[53] This is perhaps not surprising considering that they make up a significant proportion of the total cell count.[54] More recently, multiple studies have identified that electrotonic communication occurs between cFbs and cardiomyocytes. This was demonstrated using cultured as well as freshly isolated cFbs in vitro, and in animal disease models in vivo.[13,53,55,56] The interaction and communication between cardiomyocytes and cFbs was shown to occur through several different modes (Figure 2). These include heterologous coupling through the formation of gap junctions or membrane nanotubes, and via mechanical forces and paracrine signaling.[13,53,57,58] However, the question still remains as to whether these coupling events occur in vivo in humans.

COMMUNICATION VIA GAP JUNCTIONS

Gap junctions are considered the main mechanism for electrotonic coupling in the heart.[59] They are ion channels that allow propagation of electrical signals between neighboring cells. Gap junctions are formed through the combination of 2 hemichannels, which are either homomeric or heteromeric. Depending on the composition of the 2 hemichannels, the junction will be either homotypic or heterotypic.[60] The combination of different connexins has demonstrated varying levels of channel permeability.[61,62] Connexin 40, connexin 43 (Cx43), and connexin 45 are the 3 main connexin subtypes found in the heart. Cx43 is the most widely expressed across the atrial and ventricular myocardium in both cardiomyocytes and cFbs.[59,60]

Changes in the expression of Cx43, and in some cases connexin 45, have been observed to affect cardiac function. Studies have shown that the aging heart is accompanied by abnormalities in expression and distribution of Cx43.[63,64] When 10-week-old rat hearts were compared with those from 2-year-old rats, a decreased intensity of Cx43 expression was seen in the left ventricles.[64] Similar results were also seen in the atria of guinea pig hearts, accompanied by deterioration of adhesive junctions as well as gap junctions.[63] Furthermore, this age-related decrease in Cx43 has been linked to slowed conduction velocity.[65] Together, these results show that through mediating expression of Cx43, aging can lead to conduction slowing and increased risk of arrhythmias.

These changes have also been observed following cardiac injury. Vasquez et al[13] revealed that Cx43 and connexin 45 are present at cardiomyocyte-fibroblast contact points in neonatal rat cells. In a model of cardiac injury, an increase in expression of Cx43 in cFbs, along with an observed increase in functional coupling between cardiomyocytes and cFbs, was detected. The same study also identified that myofibroblasts isolated from infarcted hearts, when cocultured with

Downloaded from http://ahajournals.org by on February 15, 2021

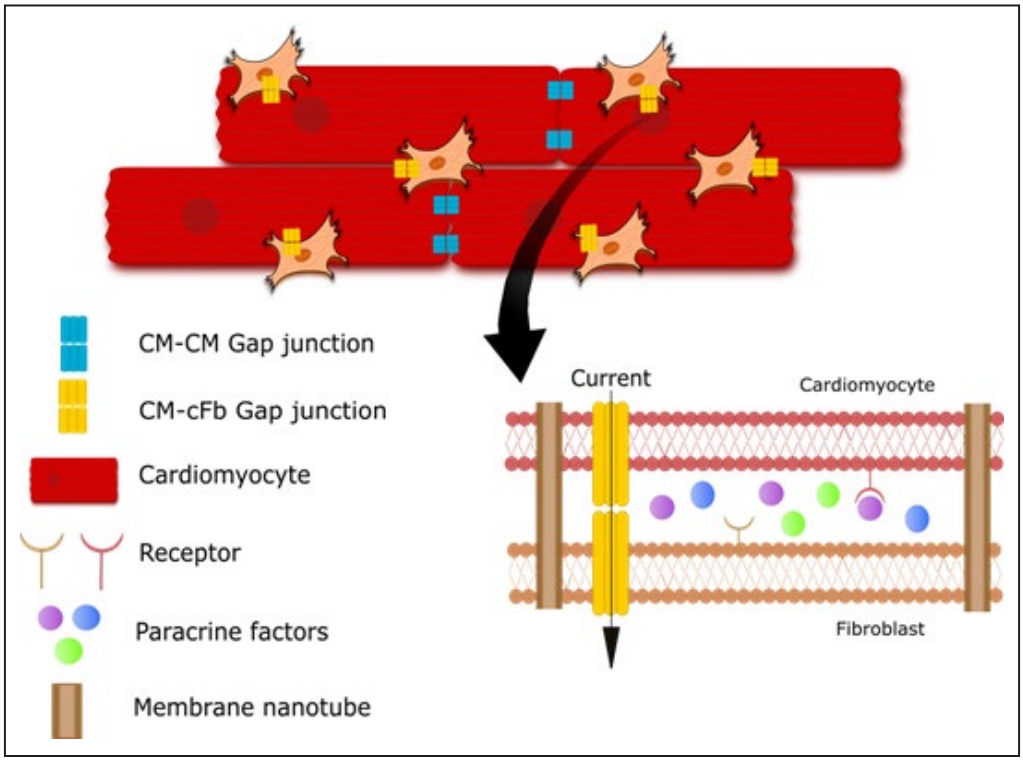


Figure 2. Figure depicting cardiomyocyte (CM)–myofibroblast (MyoFb) communcations. Gap junctions are present at distal junctions between CMs as well as elsewhere between CMs and MyoFbs. Gap junctions and membrane nanotubes allow exchange of molecules between the cytoplasms of cells. Paracrine factors secreted by cells bind receptors on neighbouring membranes, initiating signaling pathways. cFb indicates cardiac fibroblast.

cardiomyocytes, decreased conduction velocities of the action potential and reduced action potential duration at 70% repolarization. More important, the authors showed that the effects on conduction and action potential duration were cFb density dependent, thus pointing toward a potential role in driving electrophysiological heterogeneity across the heart and thus contributing to increase in arrhythmias.[13] This cFb density dependency on cardiomyocyte electrophysiological features was also shown in modeling studies by Sanchez et al, with effects being most prominent in the left atrial pulmonary vein myocardium, a common site of atrial ectopy.[66]

Zhang et al demonstrated in a mouse model that cFbs are activated following MI. Interestingly, these observations were apparent even in remote regions, away from the site of injury.[67] This implicates myofibroblasts in the postinfarct remodeling process, as established by other groups.[67,68] More important, Zhang et al demonstrated that cFbs from infarcted hearts displayed increased expression of Cx43 and intercellular cardiomyocyte coupling. However, in contrast, cardiomyocytes from these models exhibited downregulation and redistribution of Cx43 following MI. Decreased expression of Cx43 in cardiomyocytes has been shown to lead to increased propensity for abnormal conduction and susceptibility to arrhythmias.[67,69] These data together suggest that cFbs may be maintaining electrical coupling, to some extent, to preserve cardiac function.[67] Whether this adaptive process is ultimately detrimental to the heart requires further confirmation. With the availability of human induced pluripotent stem cell–derived cFbs and cardiomyocytes, there is an opportunity, and a clear need, for further studies robustly examining the interaction and effects of nonactivated and activated cFbs on cardiomyocyte electrophysiological features in human cell lines.[70]

COMMUNICATION VIA MEMBRANE NANOTUBES

Another mechanism that facilitates cFb-cardiomyocyte communication is that of membrane nanotubes. This was established as a novel interaction by He et al, who demonstrated that membrane nanotubes, through the exchange of Ca^{2+}, could facilitate both long- and short-range connectivity between cardiomyocytes and cFbs and therefore regulate cardiac contractility.[57] Membrane nanotubes are long, thin, membrane-bound connections that consist of F-actin and, in some cells, microtubules.[71,72] They are

Downloaded from http://ahajournals.org by on February 15, 2021

suggested to help to control structural connectivity between cardiomyocytes and cFbs but also allow direct communication via the exchange of organelles, vesicles, and ions, such as Ca^{2+}, across distances of up to several micrometers. In theory, membrane nanotubes have the advantage over gap junctions, which are limited to transfer of molecules of <1.2 kDa and only where cells are in close proximity.[57] Although membrane nanotubes have been identified in both cardiomyocytes and cFbs in vivo,[57,72] the proposed effects on contractility have not, and more research is required to identify their role and contributions to mediating electrical signals in the heart.

COMMUNICATION VIA PARACRINE SIGNALING

Cardiomyocytes and cFbs can also interact indirectly via paracrine signaling.[73] Considering that fibrosis is also demonstrated in areas remote to the injured myocardium, it is perhaps not surprising that paracrine factors may be involved in this process.[74] To further investigate this concept, several groups have used separated coculture methods, using physical inserts to separate the 2 cell types within the same well or cFb conditioned medium harvested from cultured cFbs.[13,75,76] These have demonstrated the involvement of paracrine mediators independently and alongside that of mechanical stress or physical coupling on electrophysiological activity.[13,75] LaFramboise et al showed that, following the addition of cFb conditioned medium, cardiomyocyte hypertrophy as well as reduction of spontaneous contractions were observed in neonatal cardiomyocytes.[75] Vasquez et al[13] built on this work by comparing effects of conditioned media obtained from normal hearts and hearts with MI. They showed that conditioned medium from cFbs isolated from rat hearts with MI leads to slowed conduction velocities and a shortened action potential duration when compared with normal cFbs.[13]

There is growing evidence in support of cFb-produced paracrine factors playing a role in modulation of cardiac function and arrhythmogenesis. Many of these paracrine factors involved are known, however, mechanisms driving the observed changes in cardiac function and are under investigation. These will be discussed in the next section.

CROSS TALK BETWEEN THE MYOFIBROBLAST AND THE CARDIOMYOCYTE

Following identification of such communications between cFbs-cardiomyocytes, the importance of defining the consequences of these mechanisms became apparent. The primary focus to date has been on TGF-β. An important mediator in the differentiation of cFb to myofibroblast, it has also been shown to have direct effects on cardiomyocyte function.[47,72,77] However, there is also evidence for the involvement of angiotensin II (Ang II), IL-6, and mechanical stimuli in the communication processes.[72,73]

ROLE OF TGF-β

TGF-β is an important cytokine involved in many different cellular processes, including proliferation, differentiation, and migration.[77] Its expression is altered by several stimuli, such as mechanical stretch, hormones, and cytokines. In the heart, it is the driving force for myofibroblast activation and is therefore crucial during injury and wound healing.[44,78] TGF-β receptor stimulation activates multiple downstream pathways, via both small mothers against decapentaplegic (Smad)– (Figure 3) and non–Smad-mediated transcription (Figure 4), to induce cFb proliferation, collagen synthesis, and myofibroblast activation.[4,47,79] Multiple studies have shown that TGF-β activates cFbs, at least to some extent, demonstrated by the expression of α-SMA fibers and a contractile phenotype.[4,25,47]

In 1988, Thompson et al reported the importance of TGF-β in cardiac disease in rats. They showed a marked increase in TGF-β in cardiomyocytes following MI with increased localization to the border zone.[80] Several studies since then have reported TGF-β contributing to both fibrotic and hypertrophic effects in the myocardium, both in vitro and in vivo.[4,73,77] Furthermore, higher levels of TGF-β are detected in hypertrophic hearts and in heart failure models.[22,81] These effects have been identified in direct coculture with cFbs and myofibroblasts and through the use of cFb/myofibroblast conditioned medium. In the presence of a TGF-β receptor inhibitor, these effects were reduced or even reversed. These studies clearly highlight the role of TGF-β in profibrotic and prohypertrophic processes.[73,82]

Nakajima et al also observed the effects of TGF-β to be more prominent in the atria compared with the ventricles. Through use of models with constitutive TGF-β activity, they concluded that TGF-β alone was not sufficient in promoting ventricular fibrosis in their mouse model.[77] Rahmutula et al later built on this work using a similar model. They observed an increased expression in TGF-β signaling proteins in both atria and ventricles, although expression of fibrotic genes was only increased in the atria. This expression was associated with an increased atrial susceptibility to fibrosis and arrhythmia. Similar observations were made in human

Downloaded from http://ahajournals.org by on February 15, 2021

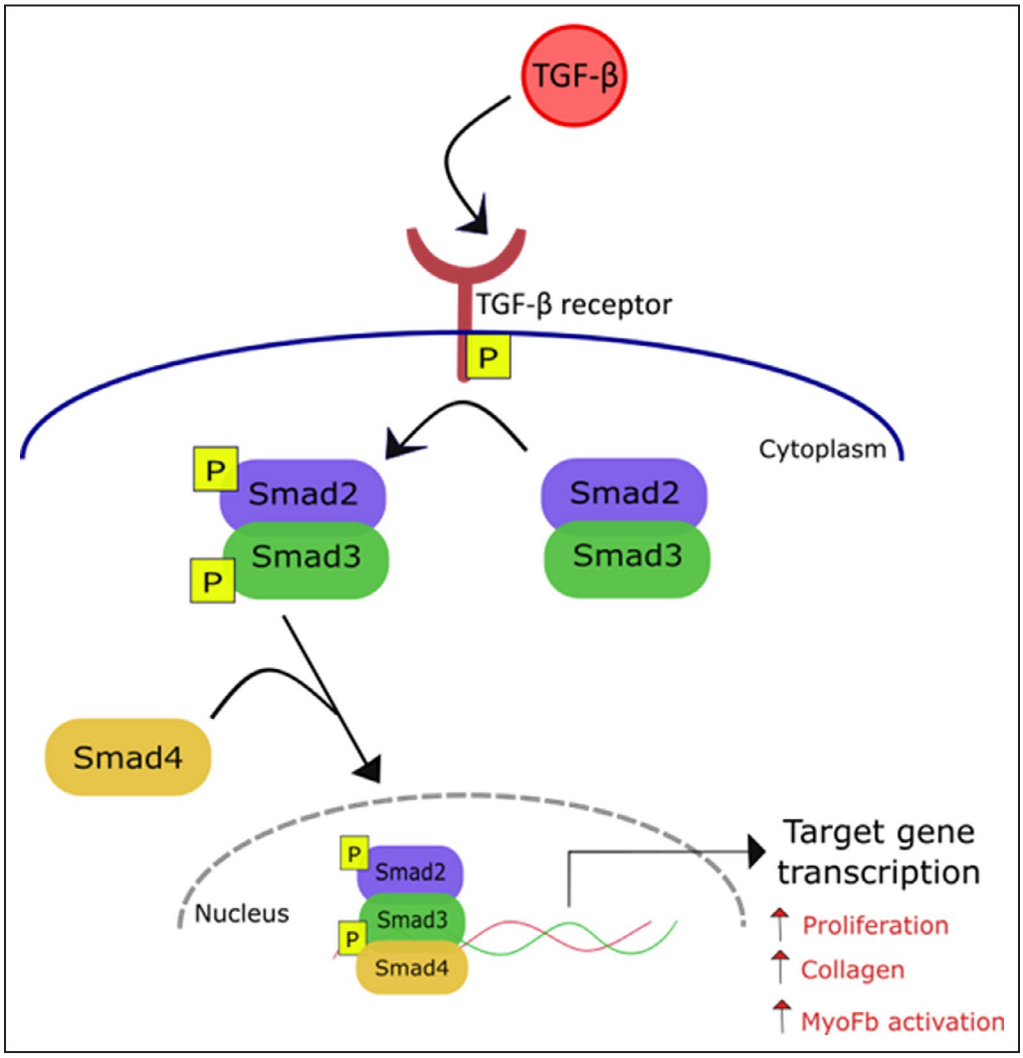


Figure 3. Schematic of transforming growth factor-β (TGF-β) activation via small mothers against decapentaplegic (Smad) signaling.
TGF-β binds its receptor, initiating phosphorylation (p) of Smad2/3. This complex then binds Smad4 and translocates to the nucleus to induce transcription of target genes involved in proliferation, collagen production, and activation of cardiac fibroblasts to myofibroblasts (MyoFbs).[42,75]

atrial tissue.[83] Interestingly, it has also been demonstrated that TGF-β maintains a positive feedback loop by acting on cardiomyocytes to sustain its own expression and maintain myofibroblast proliferation.[73,84] Competitive inhibition of TGF-β receptors can prevent the cFb activation process.[22] Several independent studies have explored targeting TGF-β signaling as a potential antifibrotic therapeutic strategy. Kuwahara et al observed, in pressure overloaded mouse hearts, that fibrosis could be decreased using an anti–TGF-β neutralizing antibody.[49] Similarly, Khalil et al demonstrated that deletion of *Smad2/3* attenuated the fibrotic response in pressure overloaded mouse hearts. However, increased mortality in TGF-β receptor knockdown models and following long-term pharmacological inhibition after MI limits its therapeutic use.[22,44]

Despite this, a study by Davies et al further implicated non-Smad signaling in atrial remodeling and arrhythmogenesis, specifically with age. Through use of a conditional mouse knockdown of *Mkk4*, they demonstrated MKK4 as a negative regulator of TGF-β signaling through activation of the JNK pathway. They showed that, with age and with *Mkk4* deletion, there were significantly greater levels of fibrotic tissue, TGF-β1 expression, TGF-β receptor expression, and effects on matrix metalloproteinase and tissue inhibitor of metalloproteinase expression levels, providing a substrate for arrhythmogenesis. Furthermore, they discovered that, in patients with atrial fibrillation, there were decreased levels of MKK4.[85]

More recently, TGF-β has also been linked to the WNT signaling pathway in the context of fibrosis and

Downloaded from http://ahajournals.org by on February 15, 2021

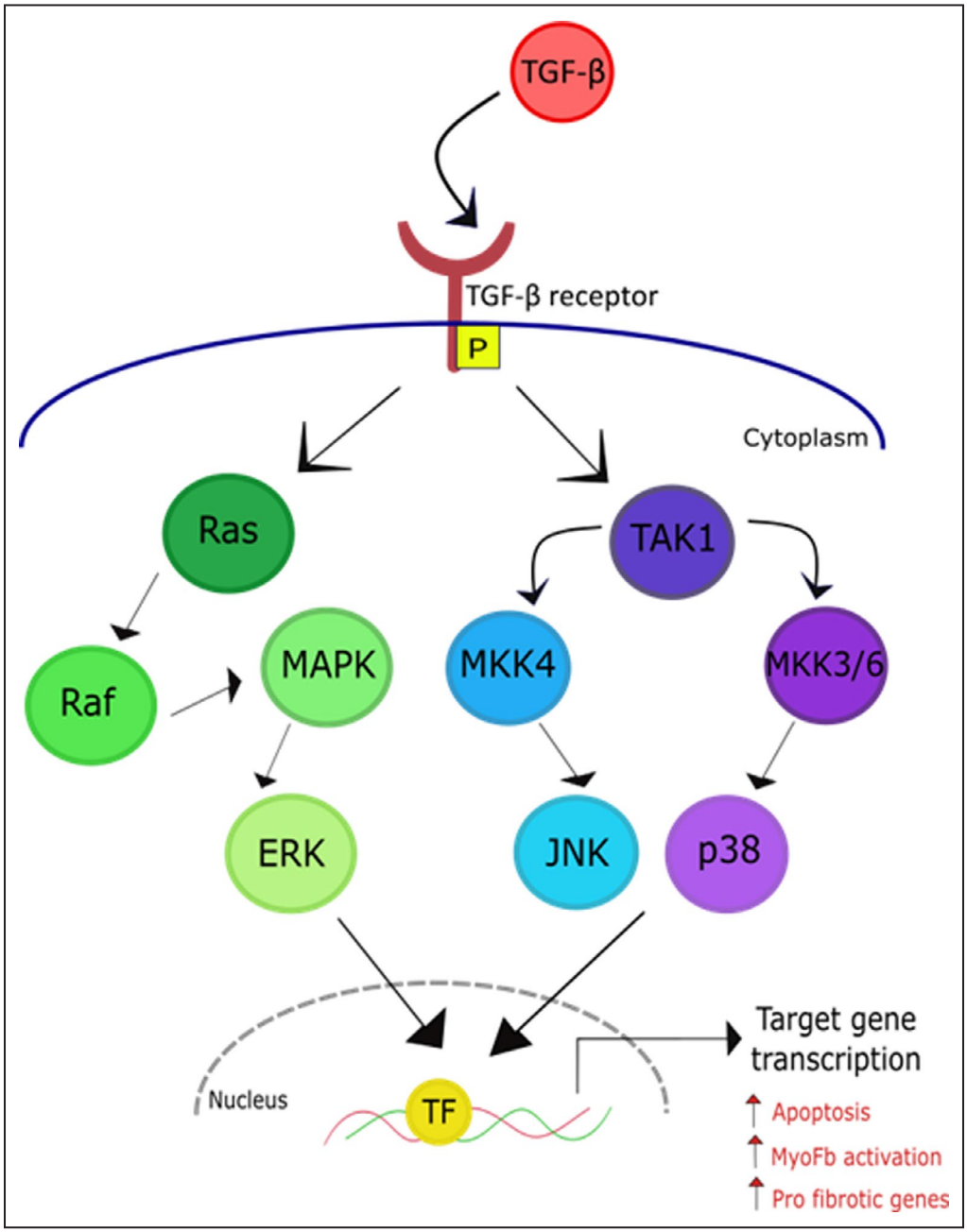


Figure 4. Schematic of transforming growth factor-β (TGF-β) activation via noncanonical (small mothers against decapentaplegic–independent) signaling.
TGF-β binds its receptor, initiating activation of Ras or TAK1 and further downsteam activation of extracellular signal-regulated kinase (ERK), JNK, or p38. This leads to promotion of transcription factors (TFs) and the transcription of target genes involved in myofibroblast (MyoFb) activation, fibrosis, and cardiomyocyte apoptosis.[79] MAPK indicates mitogen-activated protein kinase.

cardiac tissue remodeling.[86] Several groups have observed a role for WNT proteins in the activation of myofibroblasts. Blyszczuk et al demonstrated this through the suppression of TGF-β–mediated myofibroblast activation by blocking WNT signaling.[87] Others have observed stimulation of proliferation and upregulation of profibrotic genes through activation of the WNT pathway.[86,88,89] These data, together with those of Davies et al,[85] suggest that although TGF-β itself may not be an appropriate target for pharmacological intervention, deciphering downstream targets could in fact provide new avenues for treatment.

The influence of TGF-β on ionic handling in the heart is less well defined. In coculture with cardiomyocytes, both cFbs (defined as α-SMA–negative Fbs) and myofibroblasts have been reported to alter Ca^{2+}

Downloaded from http://ahajournals.org by on February 15, 2021

transients. Myofibroblasts decreased Ca^{2+} transient amplitudes, whereas surprisingly, cFbs increased them. This effect was blocked by a TGF-β receptor inhibitor. TGF-β treatment of cardiomyocytes alone was not able to recapitulate the effects seen in co-culture systems, indicating that TGF-β itself does not drive these Ca^{2+} transient alterations.[73] Kaur et al observed a peak Na^+ current increase of ≈40% following exposure to TGF-β. TGF-β effects on the current magnitude were voltage independent, and these effects were reversed in presence of a TGF-β neutralizing antibody.[76] Whether these effects alter action potential morphological features and conduction or whether TGF-β leads to changes in intracellular Na^+ concentrations is unclear.

The effects of TGF-β on cardiac pathogenesis have been recognized for many years through promotion of fibrosis and cardiomyocyte hypertrophy.[49,81,85] The precise role of TGF-β in cardiac disease is only now becoming more evident. Numerous studies and the modern -omics approaches have highlighted TGF-β involvement in the modulation of multiple signaling pathways, important in activating the myofibroblast.[44,90,91] Novel use of computer modeling has enabled generation of in silico fibrosis models,[92] allowing dissection of the TGF-β signalosome and potentially identification of novel downstream targets for antifibrotic therapy.

ANGIOTENSIN II

Ang II is a hormone that acts as part of the renin-angiotensin system and is involved in regulating blood pressure and sodium homeostasis.[93,94] Inhibition of Ang II signaling through use of angiotensin-converting enzyme inhibitors has long been used to treat hypertension.[95] However, evidence over the years has also suggested an important role for Ang II in ventricular remodeling following cardiac injury.[96,97] Schieffer et al showed that, by blocking angiotensin receptors and by angiotensin-converting enzyme inhibition, ventricular remodeling was attenuated through reduction of cardiac hypertrophy and fibrosis.[96]

Recent evidence implicates Ang II as a powerful profibrotic factor, as secreted by cFbs/myofibroblasts.[98,99] Indeed, several independent studies demonstrate that exposure to Ang II stimulates cFb proliferation and, ultimately, fibrotic processes.[97,99,100] Cao et al observed that Ang II significantly upregulated α-SMA in neonatal rat cFbs and that this correlated with an initial increase in Cx43 expression, indicative of myofibroblast activation.[90] In the heart, myofibroblasts have been identified as a significant source of Ang II, implying the existence of a positive-feedback mechanism.[100] Ang II also stimulates the release of TGF-β and IL-6 from cFbs, which has been shown to further escalate the fibrotic process and the hypertrophic response seen in cardiomyocytes.[99,101] In patients with hypertensive heart disease, the angiotensin-converting enzyme inhibitor, lisinopril, reduced myocardial fibrosis, irrespective of its effects on left ventricular hypertrophy.[102] These clinical findings validate some of the preclinical evidence in favor of Ang II being a major driver of cardiac fibrosis.

INTERLEUKIN 6

IL-6 is a cytokine involved in processes of differentiation, growth, and survival.[103] Studies show that the IL-6 signaling pathway is crucial to cardiac function and cardioprotection following acute injury. However, continuous activation has been associated with attenuated cardiac function attributable to processes including cardiomyocyte hypertrophy and fibrosis.[104,105] IL-6 is secreted by both cardiomyocytes and cFbs, with increased expression seen in myocardial hypertrophy.[106,107] Although cardiomyocytes and cFbs lack IL-6 receptors, local IL-6 secretion is likely to promote recruitment of the inflammatory cells to myocardium. Indeed, IL-6 has clearly been demonstrated to play a prominent role in inflammation.[40,103]

A study conducted by Ma et al used a macrophage/cFb coculture model to observe the effects of Ang II and IL-6 on the activation of cFbs. They observed that cFbs were the main source of IL-6 following stimulation of Ang II and that this was reliant on the presence of macrophages. It was also determined that the presence of macrophages stimulated α-SMA expression and collagen synthesis, and therefore activation of myofibroblasts, in an IL-6–dependent manner.[108] These results dictate in part a role for IL-6 in cardiac fibrosis through inflammatory processes. However, it was subsequently demonstrated that following cardiac injury, cardiomyocytes are stimulated to produce IL-6, in turn thus stimulating proliferation of cFbs and further IL-6 secretion. This feedback loop fuels cardiac fibrosis and hypertrophy, leading to decreased cardiac function.[99,106,107] Furthermore, Meléndez et al demonstrated that elevations in IL-6 resulted in cardiac fibrosis and a large degree of ventricular stiffness.[40]

The role of IL-6 has also been investigated using complete genetic knockouts. These mice displayed significant differences when compared with wild type. The hearts were larger while also having thinner chamber walls. Echocardiographic analysis showed cardiac dilation, implying decreased cardiac function. Increased collagen deposition was also observed in knockout mice, along with a higher percentage of cFbs. However, interestingly, abrogation

Downloaded from http://ahajournals.org by on February 15, 2021

of IL-6 led to decreased cellular interactions between cardiomyocytes-cFbs because of a loss of cellular adhesion.[104] Remarkably, a more recent study, performed by McArthur et al, observed an upregulation of Cx43 expression following stimulation with IL-6. Although this was only significant when in combination with the soluble IL-6 receptor, it does point to a greater involvement in these cellular interactions.[109] This evidence supports the involvement of inflammation, and specifically IL-6, in myocardial disorder through cardiomyocyte hypertrophy, fibrosis, and a loss of cardiomyocyte-cFb interactions. However, mechanisms driving the sustained IL-6 response that leads to these pathogenic transitions are unclear and require further investigation.

ROLE OF MECHANICAL STIMULI

The Young modulus is a mechanical property that describes the elasticity of a material.[110] The healthy myocardium has a Young modulus ranging from 10 to 30 kPa.[48,111,112] However, following disease or injury, the development of a collagenous fibrotic scar increases the Young modulus to ≥100 kPa.[35,113] The protein α-SMA is associated with an increase in contractile force, which is needed for wound contraction following collagen deposition and is therefore used as an activation marker for myofibroblasts.[41,42]

It is now commonly accepted that, under standard tissue culture conditions, because of the stiffer plastic surfaces (≈3 GPa), cFbs undergo activation to myofibroblasts. Several independent studies demonstrated increased expression of α-SMA after only a few hours of culture in rat cFbs.[13,41,112] Further evidence for the role of mechanical signals in the cFb-to-myofibroblast activation process has been demonstrated through the use of multiple substrates of varying Young moduli to mimic healthy and pathological cardiac environments. Use of higher Young moduli substrates (≥100 kPa) leads to increased proliferation of cFbs, higher levels of α-SMA, and increased deposition of collagen.[41,112] How these mechanical signals drive the conversion to myofibroblast phenotype is unclear.[41] Despite this, most studies to date use culture conditions with stiffer surfaces, thus presumably working with activated cFbs. Future studies should take into account substrate stiffness when designing experiments using cFbs to better match physiological conditions (see section on Cardiomyocyte and Cardiac Fibroblast In Vitro Culture Models). Some groups have begun to experiment with polyacrylamide- or poly(ethylene glycol)-based hydrogels, and others are using silicone.[48,114] In addition, with several commercially sourced culture dishes with softer Young moduli available, these experiments are now more achievable.

As well as acting as a stimulus for activation, mechanical forces have also been implicated in communicative processes in a phenomenon known as mechanoelectric feedback. The effect of mechanical forces on cardiomyocyte-cardiomyocyte communications is relatively well investigated[115,116]; however, the role of mechanical signal transmission between cardiomyocytes and cFbs is yet to be elucidated. Intercalated discs are structures found at the distal ends of cardiomyocytes, mediating the mechanoelectric feedback between cardiomyocytes.[117–119] They consist of the fascia adherens, desmosomes, and gap junctions.[117] Fascia adherens junctions are constructed from adhesion proteins, known as cadherins, that link the intercalated discs to the actin cytoskeleton within the cardiomyocytes.[118,119] Mutations in cadherins, as well as plakoglobin and desmoplakin, have significantly affected electrical coupling.

Normal electrical coupling of cardiomyocytes has some dependence on normal mechanical coupling, and thus it is reasonable to assume that the mechanoelectric phenomenon also mediates heterocellular coupling of cFbs and cardiomyocytes.[119,120] This has been evidenced in part through the application of pulsatile stretch, which induced higher expression of proteins involved in both mechanical and electrical coupling in neonatal rat cardiomyocytes.[116] Zhuang et al used a custom-made stretch apparatus to apply 10% pulsatile stretch to cells for either 6 or 72 hours. They observed an increase in Cx43 expression, which corresponded to a relatively rapid increase in conduction velocity. This increase in electrical coupling could contribute to the formation of arrhythmia through dysregulated conduction in heterogeneously contracting cardiac tissue.[116] Conversely, Thompson et al showed that inhibiting myofibroblast contraction and blocking mechanosensitive channels in monolayers of cocultured myofibroblasts and neonatal rat ventricular cardiomyocytes lead to a minimal increase in myofibroblast membraneous expression of Cx43, a significant increase in cadherin expression, and an increase in conduction velocity.[84] It is difficult to reconcile these divergent findings. Pulsatile stretch and reduced cellular tension are both likely to play a role in disease progression; however, the pathophysiological relevance of these studies remains to be confirmed.

Multiple studies have also shown that growing cFbs or cardiomyocytes on stiffer substrates causes an increase in expression of proteins mediating cell-cell contact.[84,119] N-cadherin is most commonly found between myofibroblasts and cardiomyocytes. By applying pulsatile stretch to cultures of cardiomyocytes and/or myofibroblasts, there was an upregulation in expression of adhesion proteins, such as N-cadherin, in both cardiomyocytes and myofibroblasts.[116,119]

Downloaded from http://ahajournals.org by on February 15, 2021

Thompson et al have also demonstrated that reduced expression of N-cadherin, via short-interfering RNA, reversed conduction slowing by myofibroblasts.[121]

Multiple lines of evidence confirm that environmental stiffness affects structural and functional properties of the myocardium. Increased mechanical forces can lead to altered cardiomyocyte electrophysiological features and pathological fibrosis.[32,112] Better understanding of the mechanisms and key players driving cardiac fibrosis is necessary if we are to develop targeted therapeutic agents.

CARDIOMYOCYTE AND CFB IN VITRO CULTURE MODELS

Current in vitro cell culture models do not recapitulate the stiffness characteristics of healthy or diseased myocardium, nor do they regularly consider multiple cells types that exist in the heart and their interplay. Considering that standard plastic dishes, because of high tensile strength, can lead to fibroblast activation, some previous work may require validation.[13,72] Indeed, activation state of the cFb can significantly modulate structural and functional myocardial properties.[13,73] cFbs and myofibroblasts (TGF-β–treated or α-SMA–positive cells) have differential effects on electrophysiological features in cardiomyocytes. More important, in coculture with cardiomyocytes, myofibroblasts often cause a slowing of conduction.[73,84,121] However, defining what is the tensile strength of healthy human myocardium is not straightforward. Tensile strengths in the range of 5 to 50 kPa have been reported.[36,41,111,112] Determination of the Young modulus in healthy and diseased human myocardial tissue can be compromised by handling after surgery but equally by different stages of disease. Furthermore, whether the Young modulus varies between the different chambers of the heart is yet to be investigated and should be considered moving forward.

Most experiments are conducted using murine cardiomyocytes and cFbs, despite significant differences in electrophysiological features when compared with humans, which have been reviewed extensively elsewhere.[122,123] These species differences are thought to contribute to high failure rates of cardiac drugs in clinical trials.[124] The use of human induced pluripotent stem cell–derived cardiomyocytes (hiPSC-CMs) may circumvent these problems to some extent. However, hiPSC-CMs show an immature phenotype, including spontaneous beating, reduced expression of the potassium channels, and a more depolarized resting membrane potential.[124] The cardiac differentiation process is also a relatively lengthy one.[125] Methods aimed at improving differentiation efficiency and hiPSC-CM yield are becoming routine, whereas many groups have shown tangible improvements in maturity.[126–128] Yang et al treated hiPSC-CMs for 2 weeks with fatty acids and observed a more mature phenotype. This included larger and less circular cell size and a significant increase in sarcomere length. Also observed were increases in calcium transient amplitude and twitch force.[129] A slightly more established method is the use of mechanical forces during the differentiation process. Through increased substrate stiffness or application of stretch, several independent studies have demonstrated more mature characteristics.[130–132]

Cellular interactions are of course also to be considered when developing a culture model for experimentation. Novel methods, allowing differentiation of human induced pluripotent stem cell–derived cFbs, have been developed, opening up opportunities for much needed human coculture experiments.[133,134] Furthermore, the roles of other cell types are also beginning to be explored.[20] Hulsmans et al observed the presence of Cx43 at cell-cell contacts between cardiomyocytes and macrophages. They also demonstrated that, in the presence of macrophages, cardiomyocytes had a more depolarized resting membrane potential and decreased action potential duration.[135] Use of endothelial and fibroblast coculture methods has also been reported to aid in induced pluripotent stem cell–derived cardiomyocyte maturation.[136–139]

Consideration of the effects of ECM on cardiomyocyte and cFb structure and function is also necessary. The varying composition of the ECM can alter its properties, such as stiffness, and consequently exert differential effects on cardiomyocytes and cFbs.[28,35] It is therefore important to replicate the ECM cellular environment as closely as possible in vitro to create representative culture models. Research groups often use collagen coatings during cell culture as collagen is highly expressed in the myocardium.[112] However, following injury, it has been demonstrated that the collagen composition of the ECM changes to express more collagen 1 than collagen 3.[42,140] Equally, ECM protein fibronectin was shown to be required for TGF-β–induced myofibroblast differentiation.[48] ECM also has positive effects on cardiomyocyte organization in culture, aiding in cellular alignment, similar to that seen in vivo. This has been demonstrated through use of ridged collagen plates, where cardiomyocytes are allowed to connect to the ECM, forming laminae.[141]

More frequently, hiPSC-CMs are being used in a 3-dimensional context to mimic the more complex tissue environment that exists in vivo. This concept of cardiac tissue engineering allows interrogation of both cell-ECM and cell-cell interactions, not only between

Downloaded from http://ahajournals.org by on February 15, 2021

cardiomyocytes but also between other cardiac cell types.[72,142] A recent study by Lee et al established a 3-dimensional microtissue, using both cardiomyocytes and cFbs, to develop a novel model of cardiac fibrosis.[143] Research such as this allows more accurate interrogation of cardiac disease and creates new platforms for discovery of more tailored medicine through use of patient-derived models.

IS THE MYOFIBROBLAST PHENOTYPE REVERSIBLE?

Previously, it was thought that the myofibroblast was a terminally differentiated phenotype. The only method of reestablishing tissue homeostasis was that of apoptotic clearance after wound healing. However, more recent studies suggest that dedifferentiation or phenotype reversibility is possible and could hold the answer to identifying new therapeutic targets.[47]

Several pathways have been identified in the cFb-myofibroblast activation process, with TGF-β being the main target of interest. Indeed, competitive inhibition of TGF-β receptors leads to a decrease in expression of α-SMA fibers, a marker for myofibroblast activation.[47,48] Other research has shown that softer substrates, around or just below what would be expected of the healthy myocardium, also lead to a decrease in expression of α-SMA fibers.[37,48] α-SMA expression levels in these studies did not return to those of quiescent cFbs, suggesting that there may be an intermediate stage, termed the protomyofibroblast,[42,144] as observed in a liver fibrosis study.[145] This cFb plasticity was only demonstrated in freshly isolated cells, so the myofibroblast reversibility in long-term culture on harder substrates needs to be investigated.[22,32,48] Interestingly, a study by Nagaraju et al observed that myofibroblasts obtained from patients with heart failure had less α-SMA expression following treatment with a TGF-β receptor inhibitor. Whether this was dedifferentiation or simply a loss of α-SMA fibers is unclear.[22]

Prolonged activation of myofibroblasts leads to sustained fibrotic processes within the myocardium, leading to deterioration of heart function. Fibrosis, although ultimately detrimental, is necessary immediately following the myocardial injury, and myofibroblasts are a crucial part of this process. Inhibition of TGF-β following myocardial injury has led to increased mortality in a mouse model.[22] Full genetic knockouts of TGF-β or certain signaling components (ie, Smad2) have embryonic lethality.[44,146] Therefore, reversal of the cFb-to-myofibroblast transition may not be an appropriate therapeutic approach for myocardial injury, although it may be more useful for treatment of chronic CVD, thus preventing the progression toward heart failure.[22]

CONCLUSIONS

Studies over the past 20 years have started to unveil the complexity of the cell-cell interactions within the myocardium. In this article, we focus on the role of the cFb and the activated myofibroblast in altering the structure and function of the myocardium. Yet, there are still conflicting views as to the effects of these 2 cell types on cardiac electrophysiological features and whether these phenomena occur in humans. To advance the work further, we will require use of the full range of cellular and animal model systems available, while acknowledging the particular strengths and weaknesses each possesses.

There are difficulties involved with in situ experimentation; there are also limitations involved with culturing cFbs in vitro, in particular their propensity for differentiation/activation to myofibroblasts. In addition, considering the immaturity of hiPSC-CM models, the importance of developing better, more representative fibrosis models is necessary.

Another issue that cannot be avoided is the immense complexity of the pathogenesis of fibrosis. With multiple different and often intersecting pathways, it will be difficult to identify a single valid target to reduce or revert the process. However, only by integrating existing biological and computational platforms with systems biology approaches will further progress be made. Many of these processes are conserved across organs and, therefore, identifying common mechanisms could have huge clinical benefit for many different diseases involving fibrosis.

ARTICLE INFORMATION

Affiliations

From the Institute of Cardiovascular Sciences, University of Birmingham, United Kingdom (C.H., K.G., D.P.); Division of Cardiovascular Medicine, Radcliffe Department of Medicine and British Heart Foundation Centre of Research Excellence Oxford, University of Oxford, United Kingdom (K.G.); and Biodiscovery Institute, University of Nottingham, United Kingdom (C.D.).

Sources of Funding

This work was supported by the British Heart Foundation grants (PG/17/55/33087, RG/17/15/33106, FS/19/12/34204, and FS/19/16/34169 to Dr Pavlovic; SP/15/9/31605, PG/14/59/31000, RG/14/1/30588, RM/13/30157, and P47352/CRM to Dr Denning; and FS/12/40/29712 to Dr Gehmlich); the Wellcome Trust Grants (109604/Z/15/Z to Dr Pavlovic and 201543/B/16/Z to Dr Gehmlich); Animal Free Research UK (AFR19-20293 to Drs Pavlovic and Denning); National Centre for the Replacement, Refinement, and Reduction of Animals in Research (CRACK-IT:35911-259146 and NC/K000225/1 to Dr Denning and NC/T001747/1 to Dr Gehmlich); Accelerator Award (AA/18/2/34218) to Institute of Cardiovascular Sciences at Birmingham; and Oxford British Heart Foundation Centre of Research Excellence (RE/13/1/30181).

Disclosures

None.

Downloaded from http://ahajournals.org by on February 15, 2021

REFERENCES

1. GBD 2017 Causes of Death Collaborators. Global, regional, and national age-sex-specific mortality for 282 causes of death in 195 countries and territories, 1980–2017: a systematic analysis for the Global Burden of Disease Study 2017. *Lancet*. 2018;392:1736–1788. DOI: 10.1016/S0140-6736(18)32203-7.
2. Gheorghe A, Griffiths U, Murphy A, Legido-Quigley H, Lamptey P, Perel P. The economic burden of cardiovascular disease and hypertension in low- and middle-income countries: a systematic review. *BMC Public Health*. 2018;18:975. DOI: 10.1186/s12889-018-5806-x.
3. Mewton N, Liu CY, Croisille P, Bluemke D, Lima JA. Assessment of myocardial fibrosis with cardiovascular magnetic resonance. *J Am Coll Cardiol*. 2011;57:891–903. DOI: 10.1016/j.jacc.2010.11.013.
4. Li J, Philip JL, Xu X, Theccanat T, Razzaque MA, Akhter SA. β-arrestins regulate human cardiac fibroblast transformation and collagen synthesis in adverse ventricular remodeling. *J Mol Cell Cardiol*. 2014;76:73–83. DOI: 10.1016/j.yjmcc.2014.08.006.
5. Eijgenraam TR, Sillje HHW, de Boer RA. Current understanding of fibrosis in genetic cardiomyopathies. *Trends Cardiovasc Med*. 2020;30:353–361. DOI: 10.1016/j.tcm.2019.09.003.
6. Ongstad E, Kohl P. Fibroblast-myocyte coupling in the heart: potential relevance for therapeutic interventions. *J Mol Cell Cardiol*. 2016;91:238–246. DOI: 10.1016/j.yjmcc.2016.01.010.
7. Wu T-J, Ong JJC, Hwang C, Lee JJ, Fishbein MC, Czer L, Trento A, Blanche C, Kass RM, Mandel WJ, et al. Characteristics of wave fronts during ventricular fibrillation in human hearts with dilated cardiomyopathy: role of increased fibrosis in the generation of reentry. *J Am Coll Cardiol*. 1998;32:187–196. DOI: 10.1016/S0735-1097(98)00184-3.
8. Azevedo PS, Polegato BF, Minicucci MF, Paiva SA, Zornoff LA. Cardiac remodeling: concepts, clinical impact, pathophysiological mechanisms and pharmacologic treatment. *Arq Bras Cardiol*. 2016;106:62–69. DOI: 10.5935/abc.20160005.
9. Swaney JS, Roth DM, Olson ER, Naugle JE, Meszaros JG, Insel PA. Inhibition of cardiac myofibroblast formation and collagen synthesis by activation and overexpression of adenylyl cyclase. *Proc Natl Acad Sci USA*. 2005;102:437–442. DOI: 10.1073/pnas.0408704102.
10. Nguyen TP, Xie Y, Garfinkel A, Qu Z, Weiss JN. Arrhythmogenic consequences of myofibroblast-myocyte coupling. *Cardiovasc Res*. 2012;93:242–251. DOI: 10.1093/cvr/cvr292.
11. Beltrami CA, Finato N, Rocco M, Feruglio GA, Puricelli C, Cigola E, Quaini F, Sonnenblick EH, Olivetti G, Anversa P. Structural basis of end-stage failure in ischemic cardiomyopathy in humans. *Circulation*. 1994;89:151–163. DOI: 10.1161/01.CIR.89.1.151.
12. Pick R, Janicki JS, Weber KT. Myocardial fibrosis in nonhuman primate with pressure overload hypertrophy. *Am J Pathol*. 1989;135:771–781.
13. Vasquez C, Mohandas P, Louie KL, Benamer N, Bapat AC, Morley GE. Enhanced fibroblast-myocyte interactions in response to cardiac injury. *Circ Res*. 2010;107:1011–1020. DOI: 10.1161/CIRCRESAHA.110.227421.
14. Wang LI, Yu P, Zhou B, Song J, Li Z, Zhang M, Guo G, Wang Y, Chen X, Han L, et al. Single-cell reconstruction of the adult human heart during heart failure and recovery reveals the cellular landscape underlying cardiac function. *Nat Cell Biol*. 2020;22:108–119. DOI: 10.1038/s41556-019-0446-7.
15. Banerjee I, Fuseler JW, Price RL, Borg TK, Baudino TA. Determination of cell types and numbers during cardiac development in the neonatal and adult rat and mouse. *Am J Physiol Heart Circ Physiol*. 2007;293:H1883–H1891. DOI: 10.1152/ajpheart.00514.2007.
16. Tucker NR, Chaffin M, Fleming SJ, Hall AW, Parsons VA, Bedi KC Jr, Akkad AD, Herndon CN, Arduini A, Papangeli I, et al. Transcriptional and cellular diversity of the human heart. *Circulation*. 2020;142:466–482.
17. Zhou P, Pu WT. Recounting cardiac cellular composition. *Circ Res*. 2016;118:368–370. DOI: 10.1161/CIRCRESAHA.116.308139.
18. Nag AC. Study of non-muscle cells of the adult mammalian heart: a fine structural analysis and distribution. *Cytobios*. 1980;28:41–61.
19. Vliegen HW, van der Laarse A, Cornelisse CJ, Eulderink F. Myocardial changes in pressure overload-induced left ventricular hypertrophy: a study on tissue composition, polyploidization and multinucleation. *Eur Heart J*. 1991;12:488–494. DOI: 10.1093/oxfordjournals.eurheartj.a059928.
20. Bergmann O, Zdunek S, Felker A, Salehpour M, Alkass K, Bernard S, Sjostrom S, Szewczykowska M, Jackowska T, dos Remedios C, et al. Dynamics of cell generation and turnover in the human heart. *Cell*. 2015;161:1566–1575. DOI: 10.1016/j.cell.2015.05.026.
21. Litviňuková M, Talavera-López C, Maatz H, Reichart D, Worth CL, Lindberg EL, Kanda M, Polanski K, Heinig M, Lee M, et al. Cells of the adult human heart. *Nature*. 2020;588:466–472. DOI: 10.1038/s41586-020-2797-4.
22. Nagaraju CK, Robinson EL, Abdesselem M, Trenson S, Dries E, Gilbert G, Janssens S, Van Cleemput J, Rega F, Meyns B, et al. Myofibroblast phenotype and reverisbility of fibrosis in patients with end-stage heart failure. *J Am Coll Cardiol*. 2019;73:2267–2282.
23. Sridhar S, Vandersickel N, Panfilov AV. Effect of myocyte-fibroblast coupling on the onset of pathological dynamics in a model of ventricular tissue. *Sci Rep*. 2017;7:40985. DOI: 10.1038/srep40985.
24. Furtado MB, Nim HT, Boyd SE, Rosenthal NA. View from the heart: cardiac fibroblasts in development, scarring and regeneration. *Development*. 2016;143:387–397. DOI: 10.1242/dev.120576.
25. Ackers-Johnson M, Li PY, Holmes AP, O'Brien SM, Pavlovic D, Foo RS. A simplified, langendorff-free method for concomitant isolation of viable cardiac myocytes and nonmyocytes from the adult mouse heart. *Circ Res*. 2016;119:909–920. DOI: 10.1161/CIRCRESAHA.116.309202.
26. Kohl P, Gourdie RG. Fibroblast-myocyte electrotonic coupling: does it occur in native cardiac tissue? *J Mol Cell Cardiol*. 2014;70:37–46. DOI: 10.1016/j.yjmcc.2013.12.024.
27. Fan D, Takawale A, Lee J, Kassiri Z. Cardiac fibroblasts, fibrosis and extracellular matrix remodeling in heart disease. *Fibrogenesis Tissue Repair*. 2012;5:15. DOI: 10.1186/1755-1536-5-15.
28. Talman V, Ruskoaho H. Cardiac fibrosis in myocardial infarction-from repair and remodeling to regeneration. *Cell Tissue Res*. 2016;365:563–581. DOI: 10.1007/s00441-016-2431-9.
29. Ruiz-Villalba A, Simon AM, Pogontke C, Castillo MI, Abizanda G, Pelacho B, Sanchez-Dominguez R, Segovia JC, Prosper F, Perez-Pomares JM. Interacting resident epicardium-derived fibroblasts and recruited bone marrow cells form myocardial infarction scar. *J Am Coll Cardiol*. 2015;65:2057–2066. DOI: 10.1016/j.jacc.2015.03.520.
30. Eghbali M, Czaja MJ, Zeydel M, Weiner FR, Zern MA, Seifter S, Blumenfeld OO. Collagen chain mRNAs in isolated heart cells from young and adult rats. *J Mol Cell Cardiol*. 1988;20:267–276. DOI: 10.1016/S0022-2828(88)80059-2.
31. Banerjee I, Yekkala K, Borg TK, Baudino TA. Dynamic interactions between myocytes, fibroblasts, and extracellular matrix. *Ann N Y Acad Sci*. 2006;1080:76–84. DOI: 10.1196/annals.1380.007.
32. Herum KM, Choppe J, Kumar A, Engler AJ, McCulloch AD. Mechanical regulation of cardiac fibroblast profibrotic phenotypes. *Mol Biol Cell*. 2017;28:1871–1882. DOI: 10.1091/mbc.e17-01-0014.
33. Nagaraju CK, Dries E, Gilbert G, Abdesselem M, Wang N, Amoni M, Driesen RB, Sipido KR. Myofibroblast modulation of cardiac myocyte structure and function. *Sci Rep*. 2019;9:8879. DOI: 10.1038/s41598-019-45078-2.
34. Gladka MM, Molenaar B, de Ruiter H, van der Elst S, Tsui H, Versteeg D, Lacraz GPA, Huibers MMH, van Oudenaarden A, van Rooij E. Single-cell sequencing of the healthy and diseased heart reveals cytoskeleton-associated protein 4 as a new modulator of fibroblasts activation. *Circulation*. 2018;138:166–180. DOI: 10.1161/CIRCULATIONAHA.117.030742.
35. Nguyen DT, Nagarajan N, Zorlutuna P. Effect of substrate stiffness on mechanical coupling and force propagation at the infarct boundary. *Biophys J*. 2018;115:1966–1980. DOI: 10.1016/j.bpj.2018.08.050.
36. Emig R, Zgierski-Johnston CM, Beyersdorf F, Rylski B, Ravens U, Weber W, Kohl P, Horner M, Peyronnet R. Human atrial fibroblast adaptation to heterogeneities in substrate stiffness. *Front Physiol*. 2019;10:1526. DOI: 10.3389/fphys.2019.01526.
37. Kollmannsberger P, Bidan CM, Dunlop JWC, Fratzl P, Vogel V. Tensile forces drive a reversible fibroblast-to-myofibroblast transition during tissue growth in engineered clefts. *Sci Adv*. 2018;4:eaao4881. DOI: 10.1126/sciadv.aao4881.
38. Ren J, Yang M, Qi G, Zheng J, Jia L, Cheng J, Tian C, Li H, Lin X, Du J. Proinflammatory protein CARD9 is essential for infiltration of monocytic fibroblast precursors and cardiac fibrosis caused by angiotensin II infusion. *Am J Hypertens*. 2011;24:701–707. DOI: 10.1038/ajh.2011.42.
39. Van Linthout S, Miteva K, Tschope C. Crosstalk between fibroblasts and inflammatory cells. *Cardiovasc Res*. 2014;102:258–269. DOI: 10.1093/cvr/cvu062.
40. Melendez GC, McLarty JL, Levick SP, Du Y, Janicki JS, Brower GL. Interleukin 6 mediates myocardial fibrosis, concentric hypertrophy,

Downloaded from http://ahajournals.org by on February 15, 2021

and diastolic dysfunction in rats. *Hypertension*. 2010;56:225–231. DOI: 10.1161/HYPERTENSIONAHA.109.148635.
41. Wang J, Chen H, Seth A, McCulloch CA. Mechanical force regulation of myofibroblast differentiation in cardiac fibroblasts. *Am J Physiol Heart Circ Physiol*. 2003;285:H1871–H1881. DOI: 10.1152/ajphe art.00387.2003.
42. Penke LR, Peters-Golden M. Molecular determinants of mesenchymal cell activation in fibroproliferative diseases. *Cell Mol Life Sci*. 2019;76:4179–4201. DOI: 10.1007/s00018-019-03212-3.
43. Ten Tusscher KH, Panfilov AV. Influence of diffuse fibrosis on wave propagation in human ventricular tissue. *Europace*. 2007;9(suppl 6):vi38–vi45. DOI: 10.1093/europace/eum206.
44. Khalil H, Kanisicak O, Prasad V, Correll RN, Fu X, Schips T, Vagnozzi RJ, Liu R, Huynh T, Lee SJ, et al. Fibroblast-specific TGF-beta-Smad2/3 signaling underlies cardiac fibrosis. *J Clin Invest*. 2017;127:3770–3783.
45. Vaughan MB, Howard EW, Tomasek JJ. Transforming growth factor-beta1 promotes the morphological and functional differentiation of the myofibroblast. *Exp Cell Res*. 2000;257:180–189.
46. Scharenberg MA, Pippenger BE, Sack R, Zingg D, Ferralli J, Schenk S, Martin I, Chiquet-Ehrismann R. TGF-beta-induced differentiation into myofibroblasts involves specific regulation of two MKL1 isoforms. *J Cell Sci*. 2014;127:1079–1091.
47. Hecker L, Jagirdar R, Jin T, Thannickal VJ. Reversible differentiation of myofibroblasts by MyoD. *Exp Cell Res*. 2011;317:1914–1921. DOI: 10.1016/j.yexcr.2011.03.016.
48. Wang H, Haeger SM, Kloxin AM, Leinwand LA, Anseth KS. Redirecting valvular myofibroblasts into dormant fibroblasts through light-mediated reduction in substrate modulus. *PLoS One*. 2012;7:e39969. DOI: 10.1371/journal.pone.0039969.
49. Kuwahara F, Kai H, Tokuda K, Kai M, Takeshita A, Egashira K, Imaizumi T. Transforming growth factor-beta function blocking prevents myocardial fibrosis and diastolic dysfunction in pressure-overloaded rats. *Circulation*. 2002;106:130–135.
50. Arora PD, Narani N, McCulloch CA. The compliance of collagen gels regulates transforming growth factor-beta induction of alpha-smooth muscle actin in fibroblasts. *Am J Pathol*. 1999;154:871–882.
51. Schroedl NA, Hartzell CR. Myocytes and fibroblasts exhibit functional synergism in mixed cultures of neonatal rat heart cells. *J Cell Physiol*. 1983;117:326–332. DOI: 10.1002/jcp.1041170307.
52. Suzuki T, Tsuruda A, Katoh S, Kubodera A, Mitsui Y. Purification of endothelin from a conditioned medium of cardiac fibroblastic cells using beating rate assay of myocytes cultured in a serum-free medium. *J Mol Cell Cardiol*. 1997;29:2087–2093. DOI: 10.1006/jmcc.1997.0443.
53. Miragoli M, Gaudesius G, Rohr S. Electrotonic modulation of cardiac impulse conduction by myofibroblasts. *Circ Res*. 2006;98:801–810. DOI: 10.1161/01.RES.0000214537.44195.a3.
54. Grove D, Zak R, Nair KG, Aschenbrenner V. Biochemical correlates of cardiac hypertrophy, IV: observations on the cellular organization of growth during myocardial hypertrophy in the rat. *Circ Res*. 1969;25:473–485. DOI: 10.1161/01.RES.25.4.473.
55. Quinn TA, Camelliti P, Rog-Zielinska EA, Siedlecka U, Poggioli T, O'Toole ET, Knopfel T, Kohl P. Electrotonic coupling of excitable and nonexcitable cells in the heart revealed by optogenetics. *Proc Natl Acad Sci USA*. 2016;113:14852–14857. DOI: 10.1073/pnas.1611184114.
56. Camelliti P, Green CR, LeGrice I, Kohl P. Fibroblast network in rabbit sinoatrial node: structural and functional identification of homogeneous and heterogeneous cell coupling. *Circ Res*. 2004;94:828–835. DOI: 10.1161/01.RES.0000122382.19400.14.
57. He K, Shi X, Zhang X, Dang S, Ma X, Liu F, Xu M, Lv Z, Han D, Fang X, et al. Long-distance intercellular connectivity between cardiomyocytes and cardiofibroblasts mediated by membrane nanotubes. *Cardiovasc Res*. 2011;92:39–47. DOI: 10.1093/cvr/cvr189.
58. Guo Y, Zeng Q-C, Zhang C-Q, Zhang X-Z, Li R-X, Wu J-M, Guan J, Liu LU, Zhang X-C, Li J-Y, et al. Extracellular matrix of mechanically stretched cardiac fibroblasts improves viability and metabolic activity of ventricular cells. *Int J Med Sci*. 2013;10:1837–1845. DOI: 10.7150/ijms.6786.
59. Vozzi C, Dupont E, Coppen SR, Yeh HI, Severs NJ. Chamber-related differences in connexin expression in the human heart. *J Mol Cell Cardiol*. 1999;31:991–1003. DOI: 10.1006/jmcc.1999.0937.
60. McArthur L, Chilton L, Smith GL, Nicklin SA. Electrical consequences of cardiac myocyte: fibroblast coupling. *Biochem Soc Trans*. 2015;43:513–518. DOI: 10.1042/BST20150035.
61. Rackauskas M, Verselis VK, Bukauskas FF. Permeability of homotypic and heterotypic gap junction channels formed of cardiac connexins mCx30.2, Cx40, Cx43, and Cx45. *Am J Physiol Heart Circ Physiol*. 2007;293:H1729–H1736. DOI: 10.1152/ajpheart.00234.2007.
62. Rackauskas M, Kreuzberg MM, Pranevicius M, Willecke K, Verselis VK, Bukauskas FF. Gating properties of heterotypic gap junction channels formed of connexins 40, 43, and 45. *Biophys J*. 2007;92:1952–1965. DOI: 10.1529/biophysj.106.099358.
63. Nagibin V, Egan Benova T, Viczenczova C, Szeiffova Bacova B, Dovinova I, Barancik M, Tribulova N. Ageing related down-regulation of myocardial connexin-43 and up-regulation of MMP-2 may predict propensity to atrial fibrillation in experimental animals. *Physiol Res*. 2016;65(suppl 1):S91–S100. DOI: 10.33549/physiolres.933389.
64. Watanabe M, Ichinose S, Sunamori M. Age-related changes in gap junctional protein of the rat heart. *Exp Clin Cardiol*. 2004;9:130–132.
65. Yan J, Thomson JK, Zhao W, Wu X, Gao X, DeMarco D, Kong W, Tong M, Sun J, Bakhos M, et al. The stress kinase JNK regulates gap junction Cx43 gene expression and promotes atrial fibrillation in the aged heart. *J Mol Cell Cardiol*. 2018;114:105–115. DOI: 10.1016/j.yjmcc.2017.11.006.
66. Sanchez J, Gomez JF, Martinez-Mateu L, Romero L, Saiz J, Trenor B. Heterogeneous effects of fibroblast-myocyte coupling in different regions of the human atria under conditions of atrial fibrillation. *Front Physiol*. 2019;10:847. DOI: 10.3389/fphys.2019.00847.
67. Zhang Y, Kanter EM, Yamada KA. Remodeling of cardiac fibroblasts following myocardial infarction results in increased gap junction intercellular communication. *Cardiovasc Pathol*. 2010;19:e233–e240. DOI: 10.1016/j.carpath.2009.12.002.
68. Squires CE, Escobar GP, Payne JF, Leonardi RA, Goshorn DK, Sheats NJ, Mains IM, Mingoia JT, Flack EC, Lindsey ML. Altered fibroblast function following myocardial infarction. *J Mol Cell Cardiol*. 2005;39:699–707. DOI: 10.1016/j.yjmcc.2005.07.008.
69. Peters NS, Green CR, Poole-Wilson PA, Severs NJ. Reduced content of connexin43 gap junctions in ventricular myocardium from hypertrophied and ischemic human hearts. *Circulation*. 1993;88:864–875. DOI: 10.1161/01.CIR.88.3.864.
70. Blyszczuk P, Zuppinger C, Costa A, Nurzynska D, Di Meglio FD, Stellato M, Agarkova I, Smith GL, Distler O, Kania G. Activated cardiac fibroblasts control contraction of human fibrotic cardiac microtissues by a beta-adrenoreceptor-dependent mechanism. *Cells*. 2020;9:1270.
71. Gerdes HH, Carvalho RN. Intercellular transfer mediated by tunneling nanotubes. *Curr Opin Cell Biol*. 2008;20:470–475. DOI: 10.1016/j.ceb.2008.03.005.
72. Pellman J, Zhang J, Sheikh F. Myocyte-fibroblast communication in cardiac fibrosis and arrhythmias: mechanisms and model systems. *J Mol Cell Cardiol*. 2016;94:22–31. DOI: 10.1016/j.yjmcc.2016.03.005.
73. Cartledge JE, Kane C, Dias P, Tesfom M, Clarke L, Mckee B, Al Ayoubi S, Chester A, Yacoub MH, Camelliti P, et al. Functional crosstalk between cardiac fibroblasts and adult cardiomyocytes by soluble mediators. *Cardiovasc Res*. 2015;105:260–270. DOI: 10.1093/cvr/cvu264.
74. Weber KT, Brilla CG. Pathological hypertrophy and cardiac interstitium: fibrosis and renin-angiotensin-aldosterone system. *Circulation*. 1991;83:1849–1865. DOI: 10.1161/01.CIR.83.6.1849.
75. LaFramboise WA, Scalise D, Stoodley P, Graner SR, Guthrie RD, Magovern JA, Becich MJ. Cardiac fibroblasts influence cardiomyocyte phenotype in vitro. *Am J Physiol Cell Physiol*. 2007;292:C1799–C1808. DOI: 10.1152/ajpcell.00166.2006.
76. Kaur K, Zarzoso M, Ponce-Balbuena D, Guerrero-Serna G, Hou L, Musa H, Jalife J. TGF-beta1, released by myofibroblasts, differentially regulates transcription and function of sodium and potassium channels in adult rat ventricular myocytes. *PLoS One*. 2013;8:e55391.
77. Nakajima H, Nakajima HO, Salcher O, Dittie AS, Dembowsky K, Jing S, Field LJ. Atrial but not ventricular fibrosis in mice expressing a mutant transforming growth factor-beta(1) transgene in the heart. *Circ Res*. 2000;86:571–579.
78. Lijnen P, Petrov V, Rumilla K, Fagard R. Transforming growth factor-beta 1 promotes contraction of collagen gel by cardiac fibroblasts through their differentiation into myofibroblasts. *Methods Find Exp Clin Pharmacol*. 2003;25:79–86. DOI: 10.1358/mf.2003.25.2.723680.
79. Parichatikanond W, Luangmonkong T, Mangmool S, Kurose H. Therapeutic targets for the treatment of cardiac fibrosis and cancer: focusing on TGF-beta signaling. *Front Cardiovasc Med*. 2020;7:34.

Downloaded from http://ahajournals.org by on February 15, 2021

80. Thompson NL, Bazoberry F, Speir EH, Casscells W, Ferrans VJ, Flanders KC, Kondaiah P, Geiser AG, Sporn MB. Transforming growth factor beta-1 in acute myocardial infarction in rats. *Growth Factors*. 1988;1:91–99. DOI: 10.3109/08977198809000251.
81. Teekakirikul P, Eminaga S, Toka O, Alcalai R, Wang L, Wakimoto H, Nayor M, Konno T, Gorham JM, Wolf CM, et al. Cardiac fibrosis in mice with hypertrophic cardiomyopathy is mediated by non-myocyte proliferation and requires Tgf-beta. *J Clin Invest*. 2010;120:3520–3529.
82. Gray MO, Long CS, Kalinyak JE, Li HT, Karliner JS. Angiotensin II stimulates cardiac myocyte hypertrophy via paracrine release of TGF-beta 1 and endothelin-1 from fibroblasts. *Cardiovasc Res*. 1998;40:352–363.
83. Rahmutula D, Marcus GM, Wilson EE, Ding CH, Xiao Y, Paquet AC, Barbeau R, Barczak AJ, Erle DJ, Olgin JE. Molecular basis of selective atrial fibrosis due to overexpression of transforming growth factor-beta1. *Cardiovasc Res*. 2013;99:769–779.
84. Thompson SA, Copeland CR, Reich DH, Tung L. Mechanical coupling between myofibroblasts and cardiomyocytes slows electric conduction in fibrotic cell monolayers. *Circulation*. 2011;123:2083–2093. DOI: 10.1161/CIRCULATIONAHA.110.015057.
85. Davies L, Jin J, Shen W, Tsui H, Shi Y, Wang Y, Zhang Y, Hao G, Wu J, Chen SI, et al. Mkk4 is a negative regulator of the transforming growth factor beta 1 signaling associated with atrial remodeling and arrhythmogenesis with age. *J Am Heart Assoc*. 2014;3:e000340. DOI: 10.1161/JAHA.113.000340 10.1161/JAHA.113.000340.
86. Dzialo E, Tkacz K, Blyszczuk P. Crosstalk between the TGF-beta and WNT signalling pathways during cardiac fibrogenesis. *Acta Biochim Pol*. 2018;65:341–349.
87. Blyszczuk P, Muller-Edenborn B, Valenta T, Osto E, Stellato M, Behnke S, Glatz K, Basler K, Luscher TF, Distler O, et al. Transforming growth factor-beta-dependent Wnt secretion controls myofibroblast formation and myocardial fibrosis progression in experimental autoimmune myocarditis. *Eur Heart J*. 2017;38:1413–1425.
88. Duan J, Gherghe C, Liu D, Hamlett E, Srikantha L, Rodgers L, Regan JN, Rojas M, Willis M, Leask A, et al. Wnt1/betacatenin injury response activates the epicardium and cardiac fibroblasts to promote cardiac repair. *EMBO J*. 2012;31:429–442.
89. Lal H, Ahmad F, Zhou J, Yu JE, Vagnozzi RJ, Guo Y, Yu D, Tsai EJ, Woodgett J, Gao E, et al. Cardiac fibroblast glycogen synthase kinase-3beta regulates ventricular remodeling and dysfunction in ischemic heart. *Circulation*. 2014;130:419–430.
90. Cao L, Chen Y, Lu L, Liu Y, Wang Y, Fan J, Yin Y. Angiotensin II upregulates fibroblast-myofibroblast transition through Cx43-dependent CaMKII and TGF-beta1 signaling in neonatal rat cardiac fibroblasts. *Acta Biochim Biophys Sin (Shanghai)*. 2018;50:843–852.
91. Ceccato TL, Starbuck RB, Hall JK, Walker CJ, Brown TE, Killgore JP, Anseth KS, Leinwand LA. Defining the cardiac fibroblast secretome in a fibrotic microenvironment. *J Am Heart Assoc*. 2020;9:e017025. DOI: 10.1161/JAHA.120.017025.
92. Rikard SM, Athey TL, Nelson AR, Christiansen SLM, Lee JJ, Holmes JW, Peirce SM, Saucerman JJ. Multiscale coupling of an agent-based model of tissue fibrosis and a logic-based model of intracellular signaling. *Front Physiol*. 2019;10:1481. DOI: 10.3389/fphys.2019.01481.
93. Fukamizu A, Takahashi S, Seo MS, Tada M, Tanimoto K, Uehara S, Murakami K. Structure and expression of the human angiotensinogen gene: identification of a unique and highly active promoter. *J Biol Chem*. 1990;265:7576–7582.
94. Yang G, Merrill DC, Thompson MW, Robillard JE, Sigmund CD. Functional expression of the human angiotensinogen gene in transgenic mice. *J Biol Chem*. 1994;269:32497–32502.
95. Toto RD, Rinner S, Ram CV. ACE inhibitors and target organ protection: an expanded role for these antihypertensive agents? *Postgrad Med*. 2004;116:11–16, 19–22, 48.
96. Schieffer B, Wirger A, Meybrunn M, Seitz S, Holtz J, Riede UN, Drexler H. Comparative effects of chronic angiotensin-converting enzyme inhibition and angiotensin II type 1 receptor blockade on cardiac remodeling after myocardial infarction in the rat. *Circulation*. 1994;89:2273–2282. DOI: 10.1161/01.CIR.89.5.2273.
97. Sun Y, Zhang JQ, Zhang J, Ramires FJ. Angiotensin II, transforming growth factor-beta1 and repair in the infarcted heart. *J Mol Cell Cardiol*. 1998;30:1559–1569.
98. Sopel MJ, Rosin NL, Lee TD, Legare JF. Myocardial fibrosis in response to angiotensin II is preceded by the recruitment of mesenchymal progenitor cells. *Lab Invest*. 2011;91:565–578. DOI: 10.1038/labinvest.2010.190.
99. Fredj S, Bescond J, Louault C, Delwail A, Lecron JC, Potreau D. Role of interleukin-6 in cardiomyocyte/cardiac fibroblast interactions during myocyte hypertrophy and fibroblast proliferation. *J Cell Physiol*. 2005;204:428–436. DOI: 10.1002/jcp.20307.
100. Sadoshima J, Izumo S. Molecular characterization of angiotensin II–induced hypertrophy of cardiac myocytes and hyperplasia of cardiac fibroblasts: critical role of the AT1 receptor subtype. *Circ Res*. 1993;73:413–423. DOI: 10.1161/01.RES.73.3.413.
101. Sano M, Fukuda K, Kodama H, Pan J, Saito M, Matsuzaki J, Takahashi T, Makino S, Kato T, Ogawa S. Interleukin-6 family of cytokines mediate angiotensin II-induced cardiac hypertrophy in rodent cardiomyocytes. *J Biol Chem*. 2000;275:29717–29723. DOI: 10.1074/jbc.M003128200.
102. Brilla CG, Funck RC, Rupp H. Lisinopril-mediated regression of myocardial fibrosis in patients with hypertensive heart disease. *Circulation*. 2000;102:1388–1393. DOI: 10.1161/01.CIR.102.12.1388.
103. Arcone R, Pucci P, Zappacosta F, Fontaine V, Malorni A, Marino G, Ciliberto G. Single-step purification and structural characterization of human interleukin-6 produced in *Escherichia coli* from a T7 RNA polymerase expression vector. *Eur J Biochem*. 1991;198:541–547.
104. Banerjee I, Fuseler JW, Intwala AR, Baudino TA. IL-6 loss causes ventricular dysfunction, fibrosis, reduced capillary density, and dramatically alters the cell populations of the developing and adult heart. *Am J Physiol Heart Circ Physiol*. 2009;296:H1694–H1704. DOI: 10.1152/ajpheart.00908.2008.
105. Fontes JA, Rose NR, Cihakova D. The varying faces of IL-6: from cardiac protection to cardiac failure. *Cytokine*. 2015;74:62–68. DOI: 10.1016/j.cyto.2014.12.024.
106. Hirota H, Yoshida K, Kishimoto T, Taga T. Continuous activation of gp130, a signal-transducing receptor component for interleukin 6-related cytokines, causes myocardial hypertrophy in mice. *Proc Natl Acad Sci USA*. 1995;92:4862–4866. DOI: 10.1073/pnas.92.11.4862.
107. Ancey C, Corbi P, Froger J, Delwail A, Wijdenes J, Gascan H, Potreau D, Lecron JC. Secretion of IL-6, IL-11 and LIF by human cardiomyocytes in primary culture. *Cytokine*. 2002;18:199–205. DOI: 10.1006/cyto.2002.1033.
108. Ma F, Li Y, Jia L, Han Y, Cheng J, Li H, Qi Y, Du J. Macrophage-stimulated cardiac fibroblast production of IL-6 is essential for TGF beta/Smad activation and cardiac fibrosis induced by angiotensin II. *PLoS One*. 2012;7:e35144.
109. McArthur L, Riddell A, Chilton L, Smith GL, Nicklin SA. Regulation of connexin 43 by interleukin 1beta in adult rat cardiac fibroblasts and effects in an adult rat cardiac myocyte: fibroblast co-culture model. *Heliyon*. 2020;6:e03031.
110. Akhtar R, Sherratt MJ, Cruickshank JK, Derby B. Characterizing the elastic properties of tissues. *Mater Today (Kidlington)*. 2011;14:96–105. DOI: 10.1016/S1369-7021(11)70059-1.
111. Hinz B. Matrix mechanics and regulation of the fibroblast phenotype. *Periodontol 2000*. 2013;63:14–28. DOI: 10.1111/prd.12030.
112. Bhana B, Iyer RK, Chen WL, Zhao R, Sider KL, Likhitpanichkul M, Simmons CA, Radisic M. Influence of substrate stiffness on the phenotype of heart cells. *Biotechnol Bioeng*. 2010;105:1148–1160. DOI: 10.1002/bit.22647.
113. Fomovsky GM, Holmes JW. Evolution of scar structure, mechanics, and ventricular function after myocardial infarction in the rat. *Am J Physiol Heart Circ Physiol*. 2010;298:H221–H228. DOI: 10.1152/ajpheart.00495.2009.
114. Wilson CL, Hayward SL, Kidambi S. Astrogliosis in a dish: substrate stiffness induces astrogliosis in primary rat astrocytes. *RSC Adv*. 2016;6:34447–34457. DOI: 10.1039/C5RA25916A.
115. Kamkin A, Kiseleva I, Wagner KD, Scholz H. Mechano-electric feedback in the heart: evidence from intracellular microelectrode recordings on multicellular preparations and single cells from healthy and diseased tissue. In: Kamkin A, Kiseleva I, eds. *Mechanosensitivity in Cells and Tissues*. Moscow, Russia: Academia; 2005.
116. Zhuang J, Yamada KA, Saffitz JE, Kleber AG. Pulsatile stretch remodels cell-to-cell communication in cultured myocytes. *Circ Res*. 2000;87:316–322. DOI: 10.1161/01.RES.87.4.316.
117. Estigoy CB, Ponten F, Odeberg J, Herbert B, Guilhaus M, Charleston M, Ho JWK, Cameron D, Dos Remedios CG. Intercalated discs: multiple proteins perform multiple functions in non-failing and failing human hearts. *Biophys Rev*. 2009;1:43. DOI: 10.1007/s12551-008-0007-y.
118. Gutstein DE, Liu FY, Meyers MB, Choo A, Fishman GI. The organization of adherens junctions and desmosomes at the cardiac intercalated

Downloaded from http://ahajournals.org by on February 15, 2021

disc is independent of gap junctions. *J Cell Sci*. 2003;116:875–885. DOI: 10.1242/jcs.00258.
119. Yamada K, Green KG, Samarel AM, Saffitz JE. Distinct pathways regulate expression of cardiac electrical and mechanical junction proteins in response to stretch. *Circ Res*. 2005;97:346–353. DOI: 10.1161/01.RES.0000178788.76568.8a.
120. Engler AJ, Carag-Krieger C, Johnson CP, Raab M, Tang HY, Speicher DW, Sanger JW, Sanger JM, Discher DE. Embryonic cardiomyocytes beat best on a matrix with heart-like elasticity: scar-like rigidity inhibits beating. *J Cell Sci*. 2008;121:3794–3802. DOI: 10.1242/jcs.029678.
121. Thompson SA, Blazeski A, Copeland CR, Cohen DM, Chen CS, Reich DM, Tung L. Acute slowing of cardiac conduction in response to myofibroblast coupling to cardiomyocytes through N-cadherin. *J Mol Cell Cardiol*. 2014;68:29–37. DOI: 10.1016/j.yjmcc.2013.12.025.
122. Wessels A, Sedmera D. Developmental anatomy of the heart: a tale of mice and man. *Physiol Genomics*. 2003;15:165–176. DOI: 10.1152/physiolgenomics.00033.2003.
123. Camacho P, Fan H, Liu Z, He JQ. Small mammalian animal models of heart disease. *Am J Cardiovasc Dis*. 2016;6:70–80.
124. Goversen B, van der Heyden MAG, van Veen TAB, de Boer TP. The immature electrophysiological phenotype of iPSC-CMs still hampers in vitro drug screening: special focus on IK1. *Pharmacol Ther*. 2018;183:127–136. DOI: 10.1016/j.pharmthera.2017.10.001.
125. Burridge PW, Matsa E, Shukla P, Lin ZC, Churko JM, Ebert AD, Lan F, Diecke S, Huber B, Mordwinkin NM, et al. Chemically defined generation of human cardiomyocytes. *Nat Methods*. 2014;11:855–860. DOI: 10.1038/nmeth.2999.
126. Machiraju P, Greenway SC. Current methods for the maturation of induced pluripotent stem cell-derived cardiomyocytes. *World J Stem Cells*. 2019;11:33–43. DOI: 10.4252/wjsc.v11.i1.33.
127. Mosqueira D, Mannhardt I, Bhagwan JR, Lis-Slimak K, Katili P, Scott E, Hassan M, Prondzynski M, Harmer SC, Tinker A, et al. CRISPR/Cas9 editing in human pluripotent stem cell-cardiomyocytes highlights arrhythmias, hypocontractility, and energy depletion as potential therapeutic targets for hypertrophic cardiomyopathy. *Eur Heart J*. 2018;39:3879–3892. DOI: 10.1093/eurheartj/ehy249.
128. Buikema JW, Lee S, Goodyer WR, Maas RG, Chirikian O, Li G, Miao YI, Paige SL, Lee D, Wu H, et al. Wnt activation and reduced cell-cell contact synergistically induce massive expansion of functional human iPSC-derived cardiomyocytes. *Cell Stem Cell*. 2020;27:50–63.e5. DOI: 10.1016/j.stem.2020.06.001.
129. Yang X, Rodriguez ML, Leonard A, Sun L, Fischer KA, Wang Y, Ritterhoff J, Zhao L, Kolwicz SC, Pabon L, et al. Fatty acids enhance the maturation of cardiomyocytes derived from human pluripotent stem cells. *Stem Cell Rep*. 2019;13:657–668. DOI: 10.1016/j.stemcr.2019.08.013.
130. Abilez OJ, Tzatzalos E, Yang H, Zhao M-T, Jung G, Zöllner AM, Tiburcy M, Riegler J, Matsa E, Shukla P, et al. Passive stretch induces structural and functional maturation of engineered heart muscle as predicted by computational modeling. *Stem Cells*. 2018;36:265–277. DOI: 10.1002/stem.2732.
131. Rodriguez AG, Han SJ, Regnier M, Sniadecki NJ. Substrate stiffness increases twitch power of neonatal cardiomyocytes in correlation with changes in myofibril structure and intracellular calcium. *Biophys J*. 2011;101:2455–2464. DOI: 10.1016/j.bpj.2011.09.057.
132. Mihic A, Li J, Miyagi Y, Gagliardi M, Li SH, Zu J, Weisel RD, Keller G, Li RK. The effect of cyclic stretch on maturation and 3D tissue formation of human embryonic stem cell-derived cardiomyocytes. *Biomaterials*. 2014;35:2798–2808. DOI: 10.1016/j.biomaterials.2013.12.052.
133. Zhang H, Tian L, Shen M, Tu C, Wu H, Gu M, Paik DT, Wu JC. Generation of quiescent cardiac fibroblasts from human induced pluripotent stem cells for in vitro modeling of cardiac fibrosis. *Circ Res*. 2019;125:552–566. DOI: 10.1161/CIRCRESAHA.119.315491.
134. Zhang J, Tao R, Campbell KF, Carvalho JL, Ruiz EC, Kim GC, Schmuck EG, Raval AN, da Rocha AM, Herron TJ, et al. Functional cardiac fibroblasts derived from human pluripotent stem cells via second heart field progenitors. *Nat Commun*. 2019;10:2238. DOI: 10.1038/s41467-019-09831-5.
135. Hulsmans M, Clauss S, Xiao L, Aguirre AD, King KR, Hanley A, Hucker WJ, Wülfers EM, Seemann G, Courties G, et al. Macrophages facilitate electrical conduction in the heart. *Cell*. 2017;169:510–522.e20. DOI: 10.1016/j.cell.2017.03.050.
136. Chen K, Bai H, Arzigian M, Gao YX, Bao J, Wu WS, Shen WF, Wu L, Wang ZZ. Endothelial cells regulate cardiomyocyte development from embryonic stem cells. *J Cell Biochem*. 2010;111:29–39. DOI: 10.1002/jcb.22680.
137. Yoshida S, Miyagawa S, Fukushima S, Kawamura T, Kashiyama N, Ohashi F, Toyofuku T, Toda K, Sawa Y. Maturation of human induced pluripotent stem cell-derived cardiomyocytes by soluble factors from human mesenchymal stem cells. *Mol Ther.* 2018;26:2681–2695. DOI: 10.1016/j.ymthe.2018.08.012.
138. Giacomelli E, Bellin M, Sala L, van Meer BJ, Tertoolen LG, Orlova VV, Mummery CL. Three-dimensional cardiac microtissues composed of cardiomyocytes and endothelial cells co-differentiated from human pluripotent stem cells. *Development*. 2017;144:1008–1017. DOI: 10.1242/dev.143438.
139. Giacomelli E, Meraviglia V, Campostrini G, Cochrane A, Cao XU, van Helden RWJ, Krotenberg Garcia A, Mircea M, Kostidis S, Davis RP, et al. Human-iPSC-derived cardiac stromal cells enhance maturation in 3D cardiac microtissues and reveal non-cardiomyocyte contributions to heart disease. *Cell Stem Cell*. 2020;26:862–879.e11. DOI: 10.1016/j.stem.2020.05.004.
140. Gluck JM, Herren AW, Yechikov S, Kao HKJ, Khan A, Phinney BS, Chiamvimonvat N, Chan JW, Lieu DK. Biochemical and biomechanical properties of the pacemaking sinoatrial node extracellular matrix are distinct from contractile left ventricular matrix. *PLoS One*. 2017;12:e0185125. DOI: 10.1371/journal.pone.0185125.
141. Baudino TA, McFadden A, Fix C, Hastings J, Price R, Borg TK. Cell patterning: interaction of cardiac myocytes and fibroblasts in three-dimensional culture. *Microsc Microanal*. 2008;14:117–125. DOI: 10.1017/S1431927608080021.
142. Ronaldson-Bouchard K, Yeager K, Teles D, Chen T, Ma S, Song L, Morikawa K, Wobma HM, Vasciaveo A, Ruiz EC, et al. Engineering of human cardiac muscle electromechanically matured to an adult-like phenotype. *Nat Protoc*. 2019;14:2781–2817. DOI: 10.1038/s41596-019-0189-8.
143. Lee MO, Jung KB, Jo SJ, Hyun SA, Moon KS, Seo JW, Kim SH, Son MY. Modelling cardiac fibrosis using three-dimensional cardiac microtissues derived from human embryonic stem cells. *J Biol Eng*. 2019;13:15. DOI: 10.1186/s13036-019-0139-6.
144. Hinz B. Formation and function of the myofibroblast during tissue repair. *J Invest Dermatol*. 2007;127:526–537. DOI: 10.1038/sj.jid.5700613.
145. Kisseleva T, Cong M, Paik Y, Scholten D, Jiang C, Benner C, Iwaisako K, Moore-Morris T, Scott B, Tsukamoto H, et al. Myofibroblasts revert to an inactive phenotype during regression of liver fibrosis. *Proc Natl Acad Sci USA*. 2012;109:9448–9453. DOI: 10.1073/pnas.1201840109.
146. Kulkarni AB, Karlsson S. Transforming growth factor-beta 1 knockout mice: a mutation in one cytokine gene causes a dramatic inflammatory disease. *Am J Pathol*. 1993;143:3–9.

Downloaded from http://ahajournals.org by on February 15, 2021

Chapter 2

Materials and Methods

2.1 Fibroblast cell culture

Cryopreserved human cardiac fibroblasts (HCF) were obtained from PromoCell®. Cells were thawed using Fibroblast Growth Medium 3 (PromoCell®, C23025/C23130) into T75cm^2 corning flasks. Cells were kept at 37^{o}C and 5$\%$ CO_2 in a humidified incubator. Every 4-7 days cells were passaged using 0.05$\%$ Trypsin-EDTA (Gibco®, 25300054). Cells were incubated for 5 mins at 37^{o}C before being collected using fresh media and centrifuged at 1200 g for 4 mins. The supernatant was then aspirated, cells resuspended in fresh media and split 1:4-1:8 into new flasks. For experimental purposes all tissue culture plastic was coated with 10 μg/ml Fibronectin (Sigma-Aldrich, F1141-5MG) for at least 45 mins at room temperature (RT) before use.

2.2 Soft substrates

Soft substrate plates were obtained from Cell Guidance Systems Ltd. Softwell® Easy Coat™ plates were used for 6 well experiments at 2 and 25 kPa. Softwell

G™ 96 Glass Bottom Plate, Easy Coat™ were used for 96 well experiments at 2 and 25 kPa. Plates were coated with 10 μg/ml Fibronectin (Sigma-Aldrich, F1141-5MG) for at least 45 mins at RT before use. Once plated, cells were incubated at 37^{o}C and 5$\%$ CO_2 for 2-4 days before being stained for immunocytochemistry or used with CyQUANT® (Invitrogen™, C35006) or RT-qPCR.

2.3 Proliferation assay

To quantify proliferation rates the CyQUANT® NF proliferation assay kit (Invitrogen™, C35006) was used. Cells were collected and counted using Trypan blue stain 0.4$\%$ (Invitrogen™ T10282) and the Countess™ automated cell counter. Cells were then seeded at the desired concentration into 96 well black plates (Perkin Elmer®, 6005182) or Softwell G™ 96 Glass Bottom Plates. The first column of each plate (8 wells) had media only to act as blanks. Cells were left to adhere at 37^{o}C and 5$\%$ CO_2 for 3-4 hours. Experimental conditions were added as required – varying concentrations of TGF-β (Bio-techne®, 240-B-010) or SD-208 (Bio-techne®, 3269/10) – to the Day 1 and 2 plates. The CyQUANT® (Invitrogen™, C35006) dye binding solution was prepared by adding CyQUANT® NF dye and equal amounts of the dye delivery reagent to 1X HBSS buffer. 100 μL was added to all wells except the negative control on the Day 0 plates following adhesion of cells (3-4 hours after plating) and to the Day 1 and 2 plate 24 and 48 hours later, respectively. All experiments were done in duplicate or triplicate. The plates containing dye solution were incubated for 1 hour at 37 ^{o}C. Fluorescence intensity from each well was then quantified using with a FlexStation® 3

microplate reader (Molecular Devices) using the SoftMax Pro software. Excitation wavelength was set at 485 nm and emission detection at 530 nm. The plates were read from the bottom.

2.4 Seeding density assay

To identify the optimal cell density and TGF-β concentration for future experiments, a seeding density assay was conducted. Cells were seeded into 96 well black plates at varying cell number: 1,750, 3,500, 7000, 14000, 28000, and 56000 cells/cm^2. The PromoCell® recommended seed is 7,000 cells/cm^2. Day 0, 1 and 2 plates were prepared with or without serum. Cells were left to adhere for 3-4 hours at 37^{o}C and 5$\%$ CO_2. At this time, CyQUANT® dye was added to the Day 0 plate as described above (Section 2.3) and varying concentrations of TGF-β were added to the appropriate wells (1.25, 2.5, 5, 10, 20 and 40 ng/ml) of the Day 1 and Day 2 plates. These were then left for 24 and 48 hrs before CyQUANT® was added and fluorescence intensity quantified. Data was normalised to the blanks and then corrected against the negative controls. Data was then analysed for significance using a Two-way ANOVA.

2.5 Immunocytochemistry protocol 1

At the desired end point cells were washed with sterile Dulbecco's Phosphate-Bufffered Saline (DPBS) (Sigma-Aldrich, D8662) and fixed using 4$\%$ paraformaldehyde for 90 mins at RT. Stored cells were kept at 4^{o}C in sterile DPBS for up to 1 month. Cells were permeabilised with 0.1$\%$ Triton™X-100 (Sigma-Aldrich,T8787)

in DPBS for 5 mins at RT and then blocked with 5% Bovine Serum Albumin (BSA) (Sigma-Aldrich, A1933) in DPBS for 1 hour at RT. Incubation with primary antibodies followed overnight at 4^{o}C. Vimentin (abcam®, ab45939) was used at a concentration of 0.25 μg/ml and α-SMA (Sigma-Aldrich, A2547) at a dilution of 1:1000. Both primary and secondary antibodies were made up in 1% BSA in DPBS. The cells were then blocked for a second time with 5% BSA in DPBS for 30 mins at RT before being incubated with secondary antibodies (abcam, Alexa Fluor® 488, ab150077) (Thermofisher Scientific, Alexa Fluor® 647, A21235) at 1:1000 dilution for 90 mins at RT. Cells were kept in the dark and were further incubated with DAPI (Thermofisher Scientific, 62248) at a concentration of 1:1000 in DPBS. Finally, cells were mounted onto glass slides using Histomount (Scientific Laboratory Supplies, NAT1038). Cells were visualised using the Zeica LSM780 Confocal laser scanning microscope equipped with the objective C-Apochromat 40x/1.20 W. Images were acquired using the Zen Black software.

2.6 Immunocytochemistry protocol 2

At the desired end point cells were fixed using 4% paraformaldehyde for 10 mins at RT followed by one wash with DPBS. Cells were stored in DPBS at 4^{o}C for a maximum of 1 month. Samples were blocked and permeabilised with blocking buffer (1% BSA in DPBS with 5% FBS and 0.5% Triton™X-100) for 30 mins at RT. Cells were subsequently incubated with primary antibodies in blocking buffer for 60 mins at RT. Vimentin was used at a concentration of 0.25 μg/ml and α-SMA at a dilution of 1:500. Cells were then washed with blocking buffer twice for 3 mins.

Following this, cells were kept in the dark and incubated with secondary antibodies in blocking buffer minus Triton™X-100 for 60 mins at RT. Both secondary antibodies were used at a dilution of 1:500 (Thermofisher Scientific, Alexa Fluor® 647, A-21246, and Alexa Fluor® 488, A-11029). Cells were then washed twice with blocking buffer minus Triton™X-100 for 3 mins. Cells were further incubated with a concentration of 1:1000 in DPBS. Finally, cells were mounted onto glass slides using Histomount. Cells were visualised using the Zeica LSM780 Confocal laser scanning microscope equipped with the objective C-Apochromat 40x/1.20 W. Images were acquired using the Zen Black software.

2.7 Image analysis

Individual cells were identified within the confocal images. The area of each cell was selected within ImageJ. The raw integrated density for α-SMA was obtained for each cell and normalised to the area of the cell. Percentage of cells positive for α-SMA fibres was calculated using cellpose.

2.8 RT-qPCR

RNA was extracted using an RNeasy mini kit (QIAGEN, 74106) and quantified using a nanodrop spectrophotometer (Thermofisher Scientific, ND-2000). RNA was then converted to cDNA using the High-capacity cDNA reverse transcription kit (Thermofisher Scientific, 4368814) within 24 hours. cDNA was diluted with nuclease free water to 5 ng/μl before use. Master mixes were prepared for each primer (Table 2.1) and 10ng of cDNA was used per reaction. The master mix

kit used was TaqMan™ Fast Advanced Master Mix for qPCR (Thermofisher Scientific,4444556). Primers were used at a 1x final concentration. *GAPDH* was used as a loading control. The PCR parameters used are shown in Table 2.2. RT-qPCR reactions were run on the 7500 Fast Real-Time PCR system (Applied Biosystems). Relative quantification of genes was conducted using the 2(-Delta Delta C(T)) method.

Gene	Protein	Assay ID
ACTA2	α-smooth muscle actin	Hs00426835_g1
COL1A1	Collagen type 1	Hs00164004_m1
COL3A1	Collagen type 3	Hs00943809_m1
GAPDH	Glyceraldehyde 3-phosphate dehydrogenase	Hs02786624_g1

Table 2.1: Taqman gene expression assays

Parameter	UNG incubation	Polymerase activation	PCR (40 cycles)	
	Hold	Hold	Denature	Anneal/extend
Temperature	50^{o}C	95^{o}C	95^{o}C	60^{o}C
Time [mm:ss]	2:00	10:00	00:15	1:00

Table 2.2: PCR parameters used for RT-PCR. 96 well plates were used with 20μl per reaction

2.9 iPSC culture

The hiPSC lines Kolf2-C1 and ReBL-PAT, were used for differentiation of cardiomyocytes and cardiac fibroblasts. Both Kolf2-C1 and ReBL-PAT were derived from white males. hiPSCs were cultured on 1:100-1:200 dilution of Matrigel®

(Corning 356231) with daily media changes using Essential 8™ medium (ThermoFisher Scientific A1517001). hiPSCs were split approximately once a week using 0.5 mM EDTA in PBS at a ratio of 1:7 or 1:15.

2.10 iPSC derivation of cardiac fibroblasts

hiPSCs were seeded at 2 x10^4/cm^2 on Matrigel® coated 6 well plates on day -2. On day 0 media was replaced with RPMI-1640 with 2% B-27™ supplement, minus insulin supplemented with 6 μM CHIR99021 (Tocris Bioscience, 4424). On day 2 CHIR99021 was removed and media was replaced with RPMI-1640+B-27™ minus insulin. On day 3 media was replaced with RPMI-1640+B-27™ minus insulin supplemented with 5 μM IWR-1-endo (Sigma, I0161). On day 6 re-plate hiPSC derived cardiac progenitor cells at a density of 2 x10^4/cm^2 in advanced DMEM supplemented with 5 μM CHIR99021 and 2 μM Retinoic acid (Sigma-Aldrich, R2625) for 3 days. On day 8 change media to advanced DMEM alone for 4 days. On day 12 re-plate hiPSC-epicardial cells in FGM3 supplemented with 10 ng/ml FGF 2 (Peprotech 100-18B) and 10 μM SB431542 (Selleck S1067). Media was changed every 2 days. From day 18 cells were assessed for fibroblast purity [126]

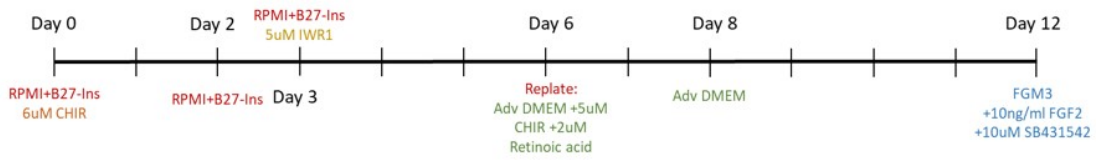


Figure 2.1: **Protocol for the differentiation of cardiac fibroblasts from iPSCs** [126]

2.11 iPSC derivation of cardiomyocytes

hiPSCs were seeded at 7x10^5 on Matrigel® coated 25 cm^2 tissue culture flasks on day -3. On day -1 cells were treated with StemPro™-34 (ThermoFisher Scientific 10639011) supplemented with 1% L-Glutamine, 1ng/mL BMP-4 (R&D systems 314-BP-010) and 1:100 dilution of Matrigel®. 12-16 hours later (day 0) media was replaced with StemPro™-34 supplemented with 1% L-Glutamine, 10 ng/mL BMP-4 and 8 ng/mL Activin A (Lifetech PHC9561). On day 2 media was replaced with RPMI-1640 (ThermoFisher Scientific 11875085) supplemented with 2% B-27™ supplement, minus insulin (ThermoFisher Scientific A1895601), 10 μM KY02111 (R&D systems 4731) and 10 μM XAV939 (R&D systems 3748). On day 4 media was replaced with RPMI-1640 supplemented with 2% B-27™ supplement (ThermoFisher Scientific 17504044), 10 μM KY02111 and 10 μM XAV939. On day 6 media was changed to RPMI-1640+B-27™ and cultured with this media every other day until use. Cells began beating around day 12. Once beating iPSC derived cardiomyocytes (iPSC-CMs) were dissociated using TrypLE™ Select Enzyme (10X) (ThermoFisher Scientific A1217701) and plated using plating media, which consisted of RPMI-1640 supplemented with 10% Knock Out Serum Replacement (ThermoFisher Scientific 10828010) and 2 μM Thiazovivin (Selleck S1459). Media was changed to RPMI-1640+B-27 24 hours after passaging [99]. iPSC-CMs were seeded between 1.75-2 x10^6 in 35mm dishes for use with optical mapping and 1-2 x10^5 on coverslips for immunocytochemistry.

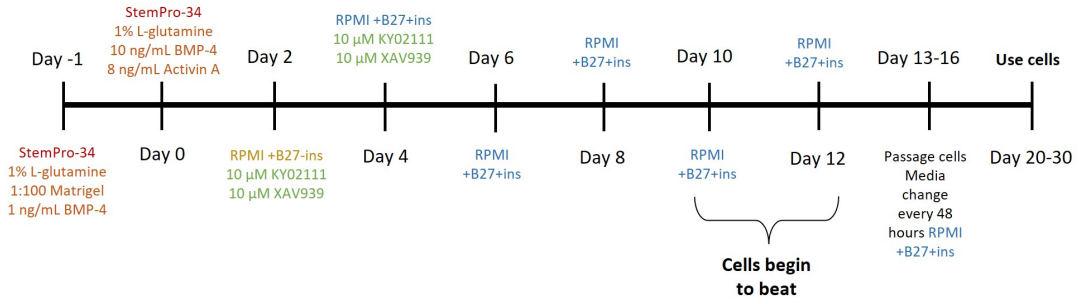


Figure 2.2: **Protocol for the differentiation of cardiomyocytes from iPSCs** [99]

2.12 Optical mapping system

The optical mapping system used for the work presented here was re-purposed and optimised for use with iPSC-CM monolayers and can be seen in Figure 2.3. The optimisation process is elaborated on in Chapter 4. Cells were kept at 37^{o}C using a H-401 temperature pad (Okolab). A 10x objective was used to visualise cells. To visualise Fluovolt loaded cells, a 470nm LED was used in conjunction with a 520/50nm filter. To visualise Fura-2,AM loaded cells, a 380nm LED was used with a T470nm dichromatic mirror and a 510nm long pass filter.

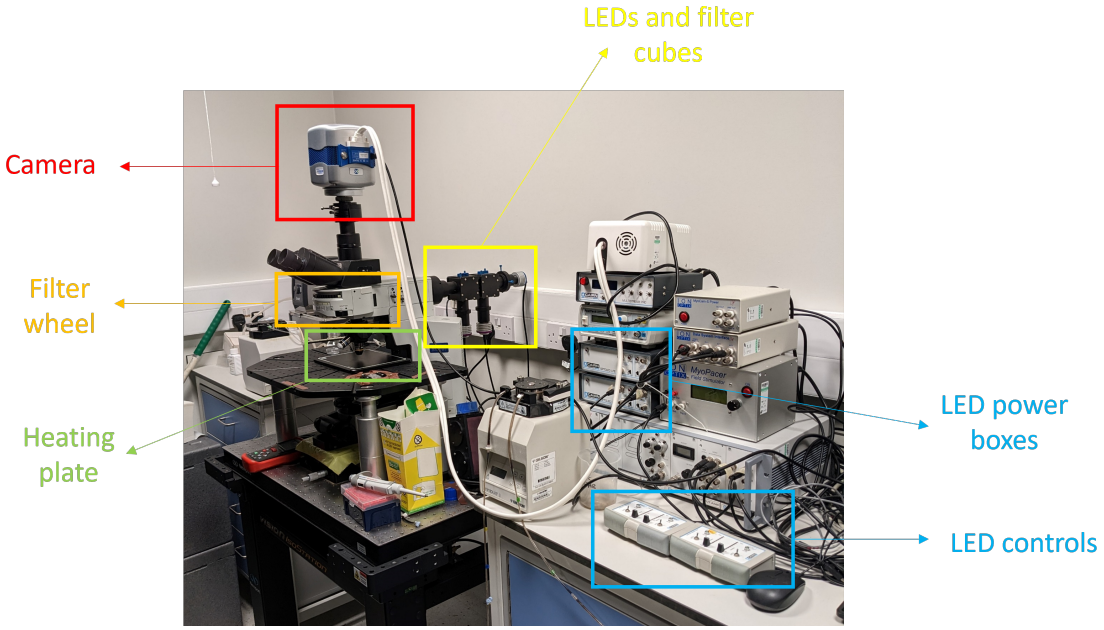


Figure 2.3: **Visual representation of the optical mapping setup used in this thesis**

2.13 Optical mapping of iPSC-CMs

iPSC-CMs were plated at a density of 2x10^6 per 35mm dish for a dense monolayer. iPSC-CMs were used between day 20 and 30. For interrogation of calcium transients, cells were incubated with 10 μM Fura-2, AM (Invitrogen™, F1221) in 1 mL RPMI+B27+ins for 20 mins at 37^{o}C. Cells were then incubated with Tyrode's solution for a further 20 mins at 37^{o}C to allow the dye to de-esterify and the cells to acclimatise to the Tyrode's solution. Fura-2, AM dye was excited at 380 nM with fluorescence passing through a 510 +/-40 nm emission filter. For action potential recordings, iPSC-CMs were incubated with 1 mL 0.5x concentration of FluoVolt™ (Invitrogen™, F10488) in Tyrode's solution for 15 minutes at 37^{o}C followed by Tyrode's solution alone for a further 15 mins at 37^{o}C. FluoVolt™ dye was excited at 470 nM with fluorescence passing through a 525 +/-25 nM emission filter. Spontaneous calcium transients and action potentials were recorded using an Evolve delta 512x512 EMCCD camera and the WinFluor software. Data was analysed using Electromap.

2.14 Cardiac fibroblast-cardiomyocyte co-culture

Dense monolayers of iPSC-CMs were obtained by seeding 2x10^6 per 30cm dish. iPSC-cFbs were plated on top of the iPSC-CMs at varying densities of 2:1 (CM:cFb), 5:1 or 10:1 for 2 days and evaluated using MUSCLEMOTION (contraction analysis) and optical mapping. iPSC-cFbs were plated on top of the iPSC-CMs at a density of 10:1 (CM:cFb) for 5 days in the presence or absence of 10 μM SB541342 or 10 ng/mL TGF-β and evaluated using MUSCLEMOTION (contrac-

tion analysis) and optical mapping.

2.15 Statistical methods

Data are presented as mean $\pm$ standard error of the mean. Differences between group means were examined using nested or ordinary one-way analysis of variance (ANOVA) and were considered statistically significant when $P < 0.05$. Statistical analysis was conducted using GraphPad Prism 9.

Chapter 3

Reversing the myofibroblast phenotype in chronically activated human cardiac fibroblasts

Activation of cardiac fibroblasts to MyoFbs underlies the development of pathological cardiac fibrosis [24, 28]. The ability to reverse MyoFbs back to their quiescent phenotype offers a mechanism to reduce the burden of cardiac fibrosis and reduce cardiac dysfunction. Existing research has shown to some extent that this is possible using freshly isolated cells and short-term culture [20, 59, 80]. In this chapter, chronic activation of human MyoFbs is investigated using primary human cardiac fibroblasts and human iPSC-derived cells. The possibility of reversing human MyoFbs to their quiescent phenotype is also explored.

3.1 Computational modeling of cardiac fibroblast activation

The work done in this section was conducted by Mukti Chowkwale from the Jeff Saucerman lab. A computational model was created from experimental data in the published literature with the aim of identifying context-dependent drivers of MyoFb activation [60]. 177 papers were used for model development to define the network structure and 41 papers were used for validation of the model and

its predictions. Through the integration of multiple signalling pathways, the model can be used to predict changes in gene expression and protein activity related to MyoFb activation. All pathways and biochemical and mechanical inputs have been previously shown to regulate cardiac fibroblast activation and are altered during cardiac injury and heart failure. The mechanical stimulus input within the model stems from the application of various stretch apparatus. Each interaction within the model is supported by two independent studies, most of which were conducted in cardiac fibroblasts [60].

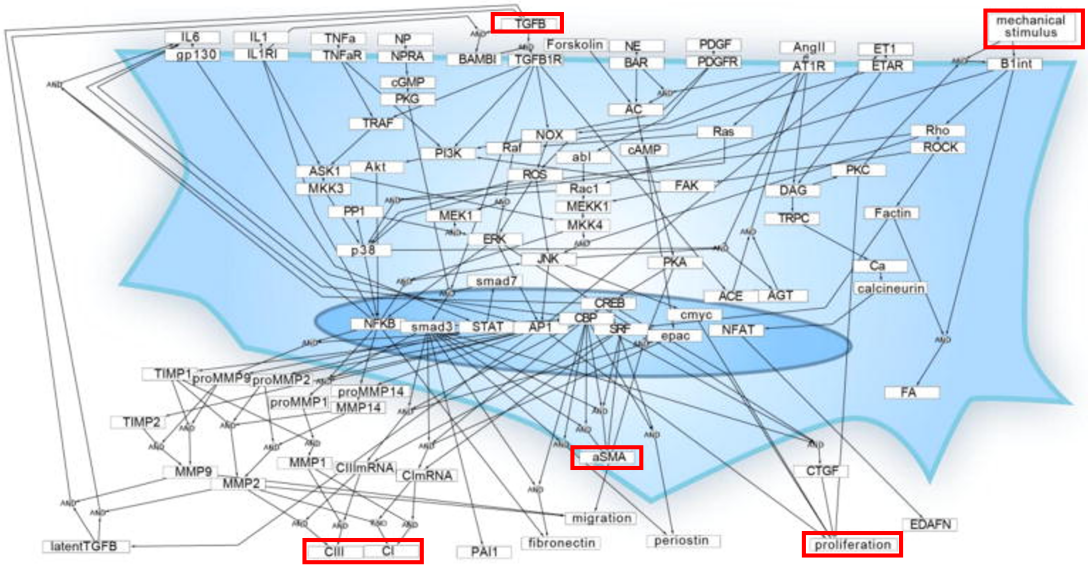


Figure 3.1: **Fibroblast signalling network as created by Saucerman et al ([60]).** 91 nodes representing gene products or cell processes. Each node is connected by an arrow or arrows representing a reaction described by published experimental data. Red boxes dictate the inputs and output used for this work. (Adapted from [60])

The model was used here to simulate the response of cardiac fibroblasts to the stiff and soft substrates used experimentally (3 GPa, 25 kPa and 2 kPa) and in the presence of 10 ng/mL TGF-β. Baseline condition was defined as 25% signalling activity for all untested inputs. Figure 3.2 shows that modelled cardiac fibroblasts cultured at 3 GPa show no to little change in expression of α-SMA,

collagen 1 and collagen 3 but an increase in expression of TGF-β receptor 1 and proliferation rates (Figure 3.2 A). When cultured on 25 or 2 kPa the modelled cardiac fibroblasts show increases in all outputs measured (Figure 3.2 B and C). When the expression of activation markers is compared across the 3 substrates, there is a consistent increase seen on 3 GPa when compared to 25 and 2 kPa (Figure 3.2 D-F). However, expression of TGF-β receptor 1 is the same across the three substrates and is only increased by the presence of TGF-β (3.2 H). Proliferation shows the same pattern (3.2 G).

The experimental data used for both creation and validation of the model was predominantly conducted in mouse and neonatal rat cardiac fibroblasts. The subsequent sections investigate whether these results will be recapitulated using human cells.

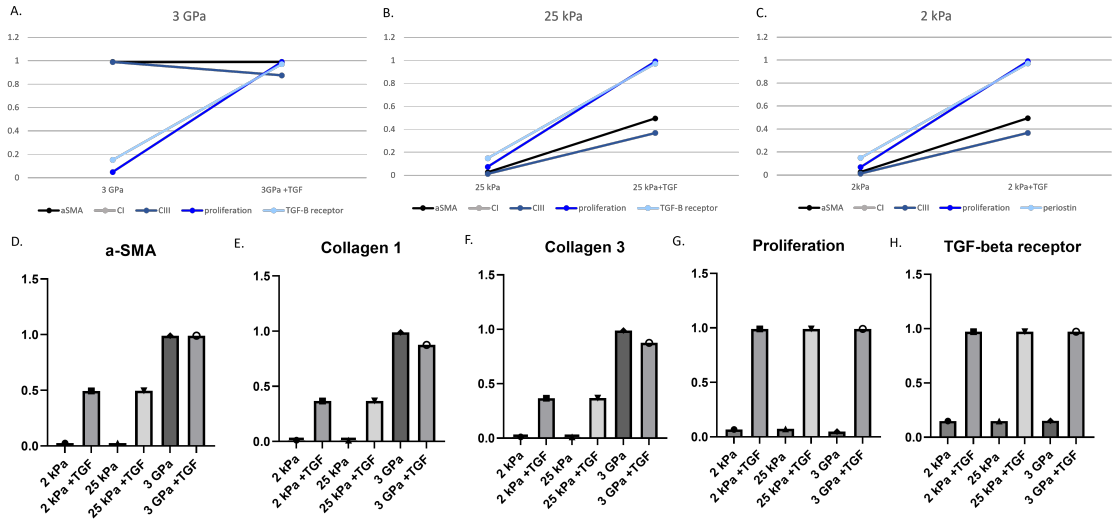


Figure 3.2: **Model predictions for cardiac fibroblasts grown on stiff and soft substrates.** Effects of TGF-β on expression of α-SMA, collagen 1 and 3, and TGF-β receptor 1 was assessed for cardiac fibroblasts grown on 3 GPa, 25 kPa and 2 kPa substrates. Effects of TGF-β on proliferation were also studied. A-C Modelled response of cardiac fibroblasts to TGF-β on different substrates (3 GPa, 25 kPa and 2 kPa). D-H Comparison of modelled response of cardiac fibroblasts across the three different substrates

3.2 Primary cardiac fibroblasts activate to myofibroblasts following long term culture in 2D

Standard tissue culture methods include the use of stiff plastic (E=3 GPa) that does not reflect that of the human myocardium (10-30 kPa). Research has shown that culture of murine cardiac fibroblasts on stiff plastic induces MyoFb activation as demonstrated by an increase in expression of α-SMA and collagen [82]. To investigate the effects of long-term culture on human cardiac fibroblasts (2-4 weeks), human primary cardiac fibroblasts (HCF) were obtained from "healthy" regions of explanted hearts and cultured in stiff polystyrene tissue culture flasks for up to 10 passages. These cells were also exposed to 10 ng/mL TGF-β to determine if already activated, could these cells activate further.

Cell culture media often contains serum which includes TGF-β, a known activator of cardiac fibroblasts. To ensure the addition of serum in the cell culture media was not dampening the effects of the added TGF-β, HCFs were grown in the presence and absence of serum and then exposed to TGF-β (Figure 3.3). In the presence of serum, there is a roughly 2-fold increase in the amount of HCFs after 24 hours and then again after 48 hours (Figure 3.3 A). In the absence of serum, there is almost no increase in HCFs after 48 hours (Figure 3.3 B). The addition of TGF-β up to 40 ng/mL had no affect on proliferation in the presence or absence of serum (Figure 3.3 A and B). Expression of α-SMA protein, as assessed by immunofluorescence staining, was unchanged in the absence of serum in the presence of 10 ng/mL TGF-β. For this reason, serum was used for subsequent experiments.

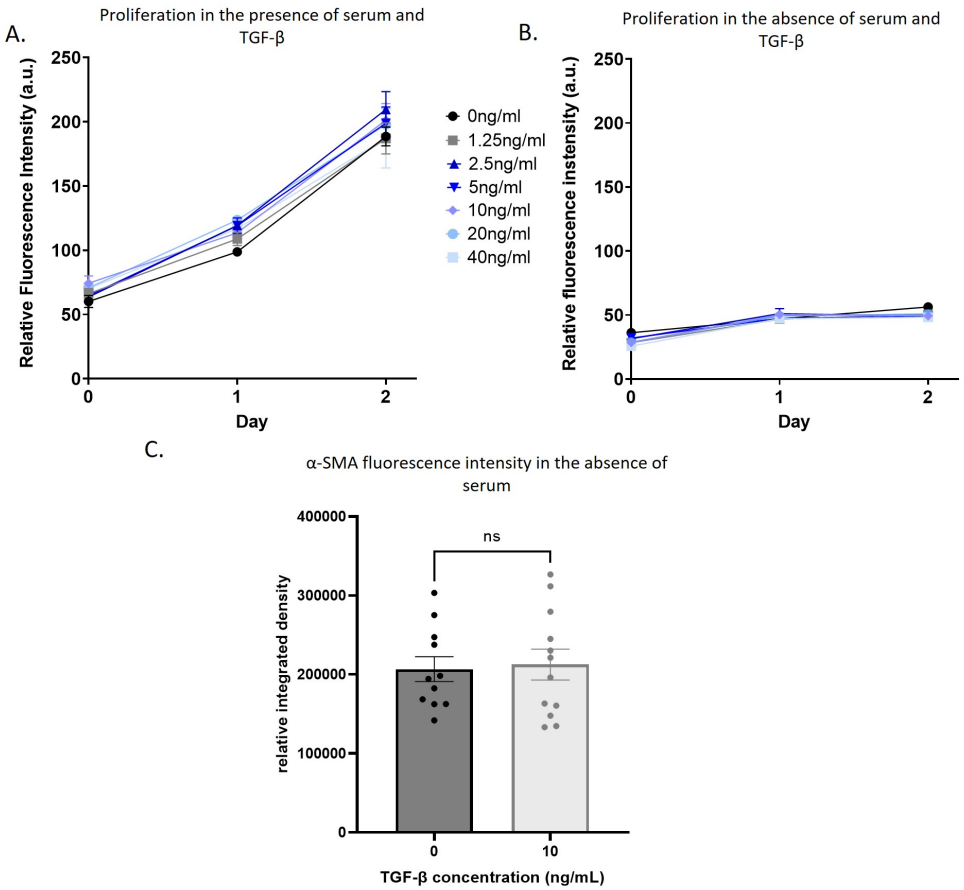


Figure 3.3: **Response of human cardiac fibroblasts to TGF-β in the presence or absence of 10$\%$ serum.** A - Proliferation over 48 hours was assessed using the CyQUANT assay in the presence of 10$\%$ serum and varying concentrations of TGF-β (0, 1.25, 2.5, 5, 10, 20, and 40 ng/mL). B - Proliferation over 48 hours in the absence of serum and varying concentrations of TGF-β. C - Quantification of immunofluorescence staining for α-SMA protein in the absence of serum with or without exposure to 10 ng/mL TGF-β. Data presented as mean $\pm$ S.E.M. N = 14 wells per plate, 3 plates (A, B); 1 experiment, 3 images per condition

Following culture on 3 GPa stiff plastic, α-SMA was detected in HCFs demonstrating MyoFb activation at baseline (Figure 3.3 and 3.4). To further assess their activation potential, these cells were then exposed to 10 ng/mL TGF-β for 2 days for immunofluorescence and proliferation (to avoid high confluency) and 4 days for RT-qPCR experiments. Expression of activation markers α-SMA, collagen 1 and 3 were assessed. Vimentin was used as a marker for cardiac fibroblasts.

Addition of TGF-β for 2 days had no significant effect on α-SMA as measured by relative fluorescence or percentage of cells positive for α-SMA staining (Figure 3.4 A and B). Cell size was also unaffected by the addition of TGF-β (Figure 3.4 C). Proliferation was measured after 48 hours as a percentage change in fluorescence from baseline (Day 0). Treatment with TGF-β had no discernible effect on proliferation (Figure 3.4). There was also no significant effect on mRNA expression levels for any of the 3 activation markers investigated (α-SMA, Collagen 1 and 3) following treatment with TGF-β for 4 days.

These results indicate that primary human cardiac fibroblasts are activated following 2-4 weeks of culture on standard tissue culture plastic (3 GPa) and are unresponsive to further TGF-β stimulation.

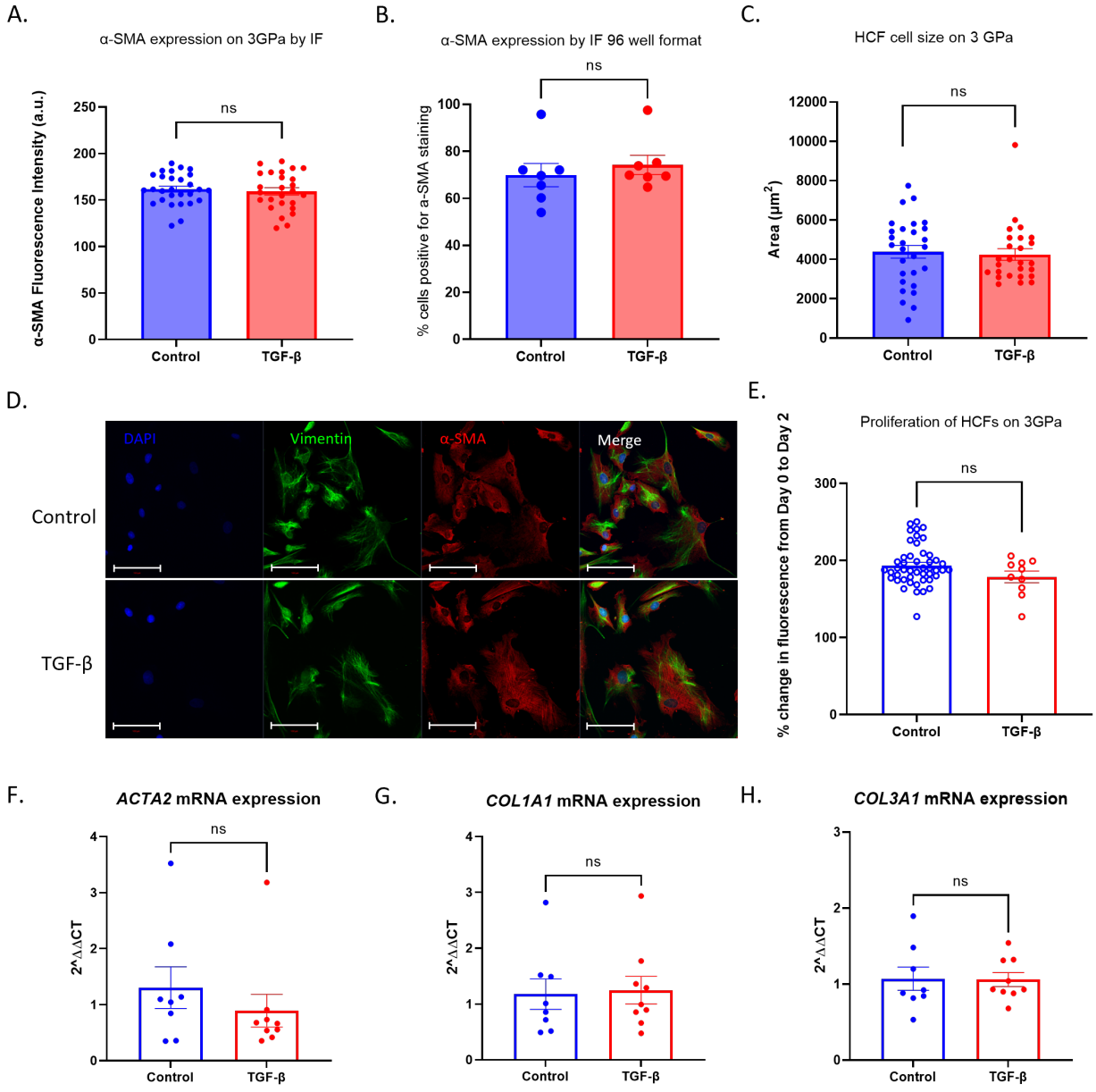


Figure 3.4: **Activation status and proliferation of HCFs on 3 GPa tissue culture plastic**. Cells were grown in the presence or absence of TGF-β for 2 days (proliferation and immunofluorescence) or 4 days (RT-qPCR). DAPI is in blue, vimentin in green and α-SMA in red. A - Quantification of α-SMA protein expression by immunofluorescence. B - $\%$ cells positive for α-SMA staining in 96 well format using Operetta CLS system. C - Comparison of cell size using cell area. D - Representative images for immunofluorescence staining in panel A and C. Scale bar 100 μm. E - Proliferation over 48 hours was assessed as a $\%$ change in fluorescence from Day 0 by CyQUANT assay. F-H - mRNA expression of activation markers ACTA2, COL1A1 and COL3A1 as measured by RT-qPCR. Data presented as mean $\pm$ S.E.M. N = 3 experiments, 3 images per condition (A, C), 3 plates, 18 wells (B), 4 plates, 6+ wells per plate (E), 8-9 (F-H).

3.3 Myofibroblasts cannot reverse to a quiescent phenotype using biochemical and mechanical inputs either alone or in combination

To investigate whether this activated MyoFb phenotype could be reversed, HCFs were exposed to TGF-β receptor inhibitor SD208 (30 nM) (Figure 3.5) and sub-cultured on softer substrates of 25 and 2 kPa for 2-4 days (Figure 3.6). α-SMA expression was unchanged as measured by immunofluorescence both in terms of relative fluorescence and percentage of cells positive for α-SMA staining (Figure 3.5 A and B). Cell size was similarly unaffected by the addition of SD208, as was proliferation (Figure 3.5 C and E). Despite a trend towards decreased α-SMA and collagen 1 mRNA expression levels in the presence of SD208, this was non-significant (Figure 3.5 F and G). There was also no significant change in the expression of Collagen 3 mRNA following the addition of SD208 (Figure 3.5 H).

2 days of sub-culture on softer substrates of 25 or 2 kPa had no significant effect on the expression of α-SMA as assessed by immunofluorescence (Figure 3.6 A and D). A significant decrease in cell size was seen on 2 kPa when compared with 3 GPa control (Figure 3.6 B). Similarly, a trend towards decreased cell size was seen on 25 kPa however this was non-significant (Figure 3.6 B). Proliferation across the 3 substrates was not significantly changed although there was a trend towards decreased proliferation on 2 kPa (Figure 3.6 C).

It was then investigated whether sub-culture on soft substrates in combination with TGF-β receptor inhibition could reverse the activated MyoFb phenotype (Fig-

ures 3.7 and 3.8). Neither addition of TGF-β nor SD208 had any significant effect on α-SMA in cells sub-cultured on 25 kPa as assessed by immunofluorescence (Figure 3.7 A). mRNA expression levels of α-SMA, collagen 1 and collagen 3 were also unchanged when compared to the undrugged control and to HCFs grown on 3 GPa (Figure 3.7 D-F). Furthermore, proliferation of HCFs on 25 kPa in the presence or absence of TGF-β or SD208 was not significantly different (Figure 3.7 B). Sub-culture on 2 kPa comparably had no significant effects on proliferation or expression of α-SMA (Figure 3.8 A and B). mRNA expression levels of activation markers α-SMA, collagen 1 and 3 were also indistinguishable from the undrugged control or cells grown on 3 GPa (Figures 3.8 D-F).

These results demonstrate that HCFs cultured on stiff 3 GPa plastic are unresponsive to TGF-β receptor inhibition. The data further indicates that HCFs are unable to transition back to their quiescent phenotype using culture on soft substrates alone or in combination with TGF-β receptor inhibition.

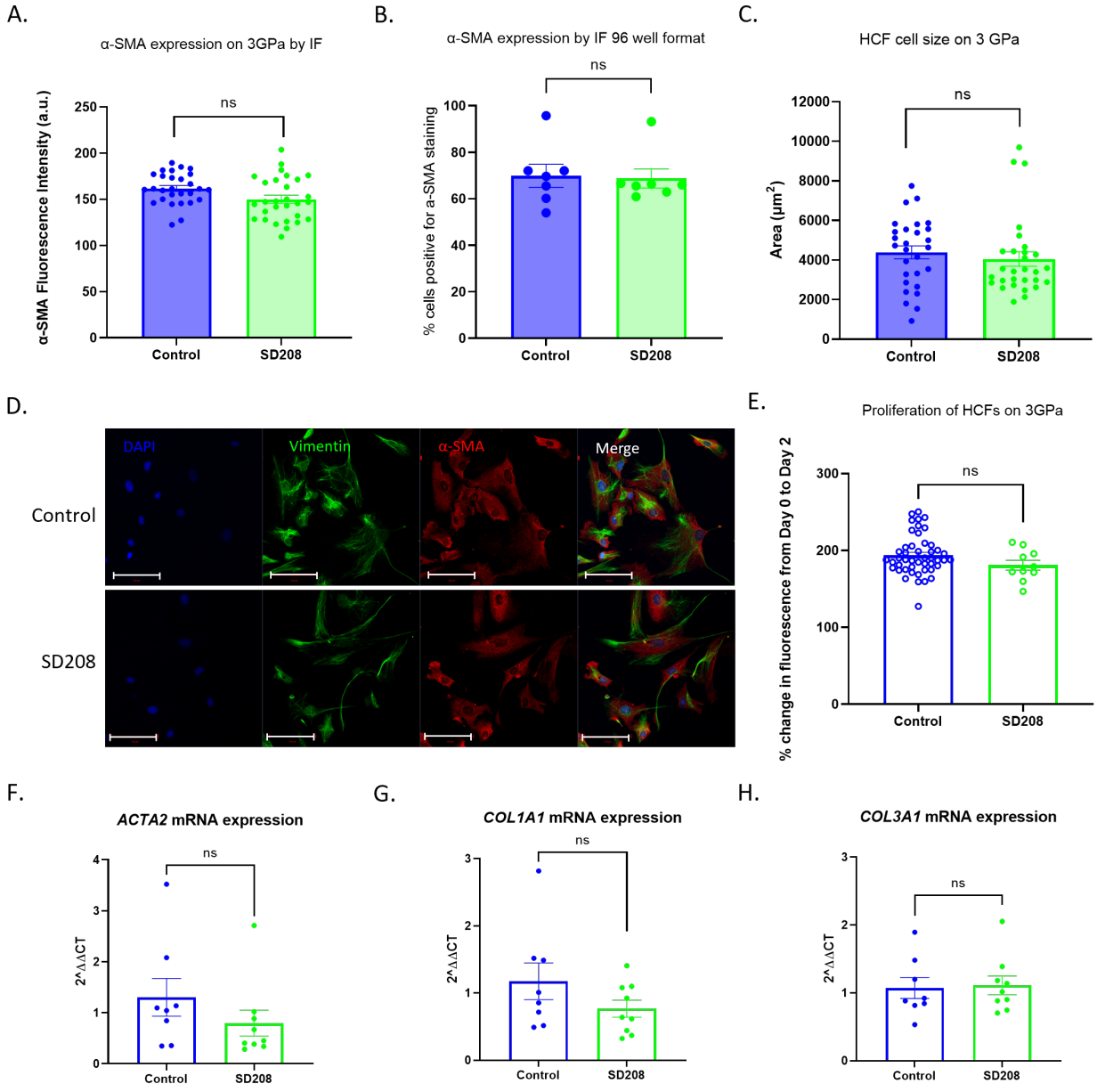


Figure 3.5: **Reversal of HCFs on 3 GPa tissue culture plastic using 30 nM SD208.** Cells were grown on 3 GPa plastic in the presence or absence of 30 nM SD208 for 2 days (proliferation and immunofluorescence) or 4 days (RT-qPCR). A - Quantification of α-SMA protein expression by immunofluorescence. B - $\%$ cells positive for α-SMA staining in 96 well format using Operetta CLS system. C - Comparison of cell size using cell area. D - Representative images for immunofluorescence staining in panel A and C. Scale bar 100 μm. E - Proliferation over 48 hours was assessed as a $\%$ change in fluorescence from Day 0 by CyQUANT assay. F-H - mRNA expression of activation markers ACTA2, COL1A1 and COL3A1 as measured by RT-qPCR. Data presented as mean $\pm$ S.E.M. N = 3 experiments, 3 images per condition (A, C), 3 plates, 18 wells (B), 4 plates, 6+ wells per plate (E), 8-9 (F-H).

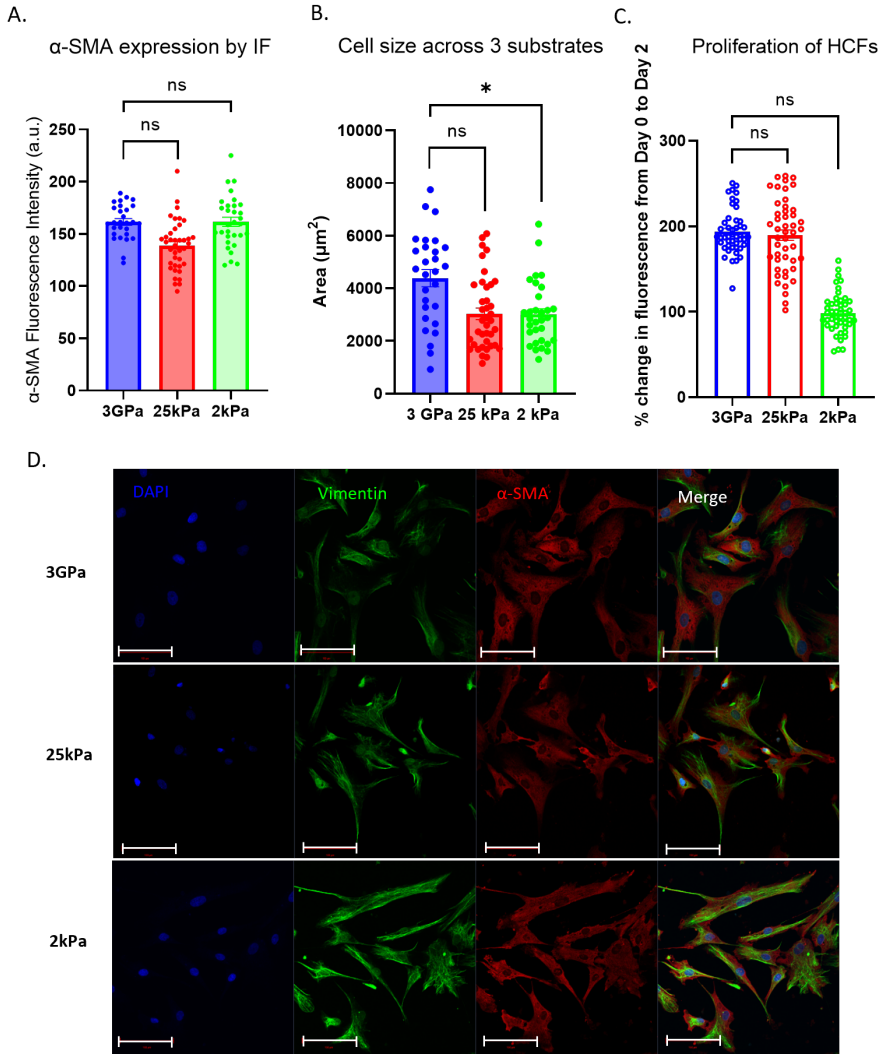


Figure 3.6: **Activation status of HCFs sub-cultured on 25 and 2 kPa soft substrates.** Cells were grown on 3 GPa and then subculture on 25 or 2 kPa soft substrates for 2 days. A - Quantification of α-SMA protein expression by immunofluorescence. B - Comparison of cell size using cell area. C - Proliferation over 48 hours was assessed as a $\%$ change in fluorescence from Day 0 by CyQUANT assay. D - Representative images for immunofluorescence staining in panel A and B. Scale bar 100 μm. Data presented as mean $\pm$ S.E.M. N = 3 experiments, 3 images per condition (A, B), 4 plates, 6+ wells per plate (C).

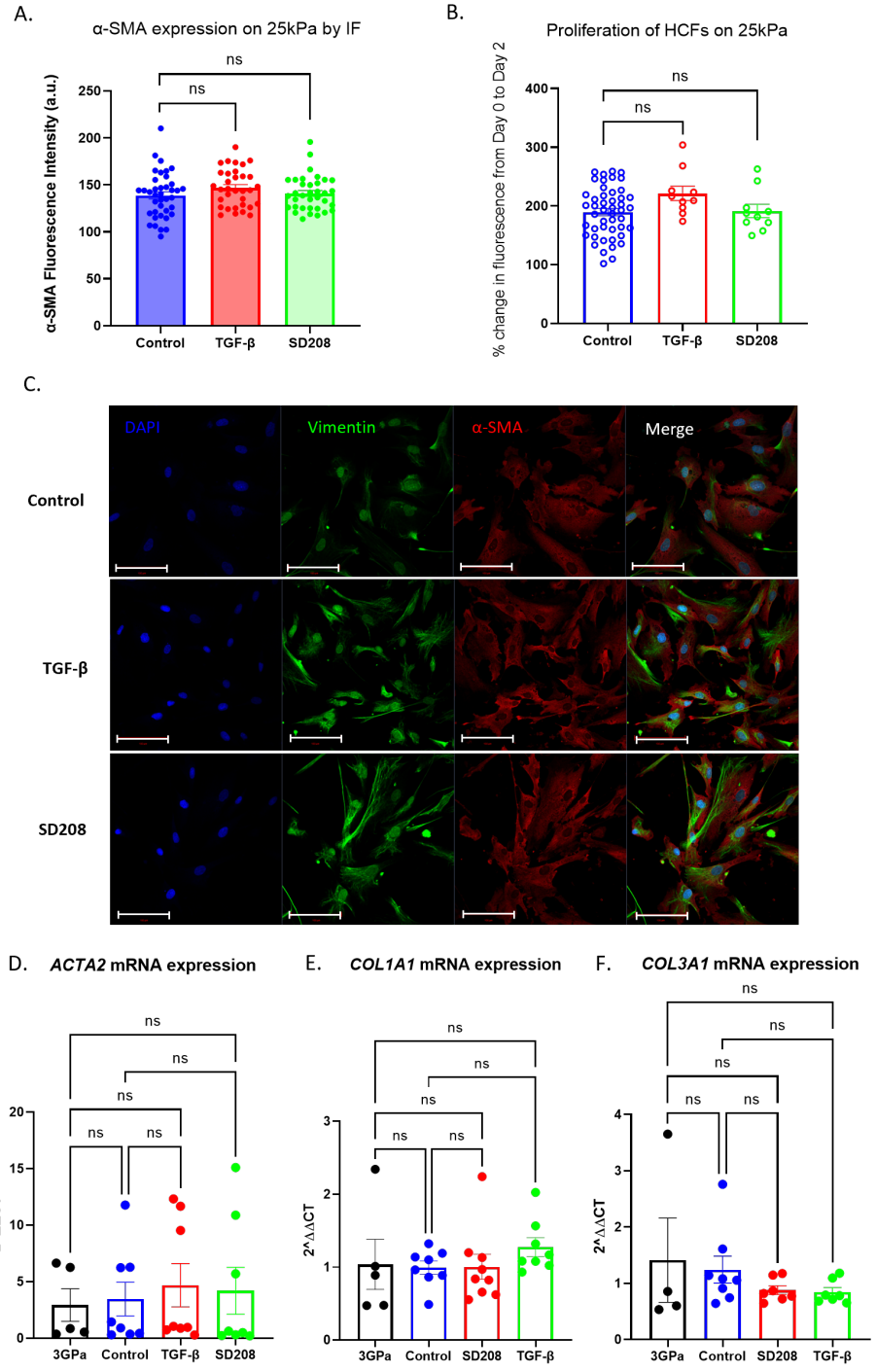


Figure 3.7: **Activation status and proliferation of HCFs sub-cultured on 25 kPa.** Cells were grown in the presence or absence of TGF-β or SD208 for 2-4 days. A - Quantification of α-SMA protein expression by immunofluorescence. B - Proliferation over 48 hours was assessed as a $\%$ change in fluorescence from Day 0 by CyQUANT assay. C - Representative images for immunofluorescence staining in panel A and B. Scale bar 100 μm. D-F - mRNA expression of activation markers ACTA2, COL1A1 and COL3A1 as measured by RT-qPCR. Data presented as mean $\pm$ S.E.M. N = 3 experiments, 3 images per condition (A, C), 4 plates, 6+ wells per plate (B), 5-8 (D-F)

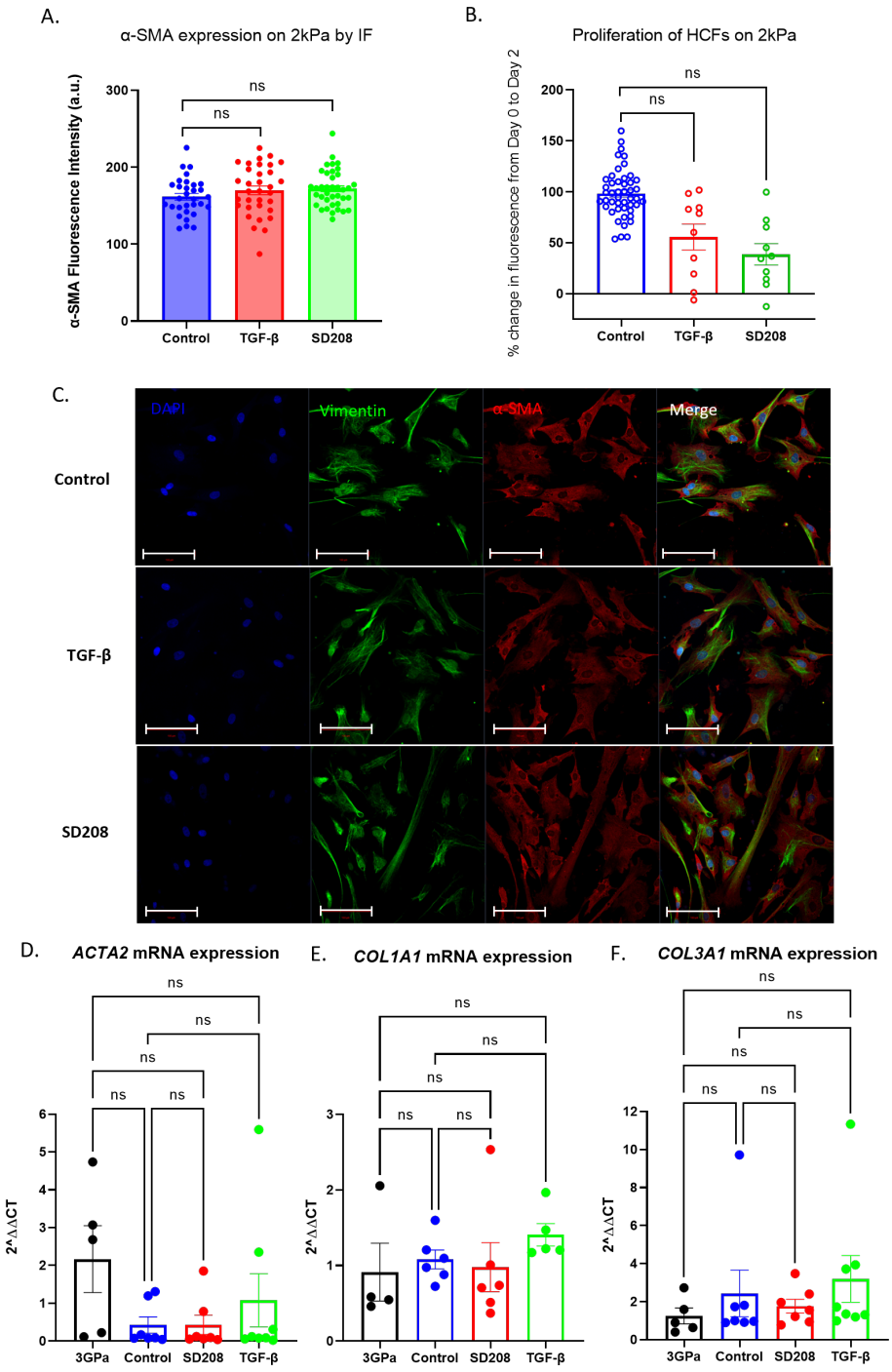


Figure 3.8: **Activation status and proliferation of HCFs sub-cultured on 2 kPa.** Cells were grown in the presence or absence of TGF-β or SD208 for 2-4 days. A - Quantification of α-SMA protein expression by immunofluorescence. B - Proliferation over 48 hours was assessed as a $\%$ change in fluorescence from Day 0 by CyQUANT assay. C - Representative images for immunofluorescence staining in panel A and B. Scale bar 100 μm. D-F - mRNA expression of activation markers ACTA2, COL1A1 and COL3A1 as measured by RT-qPCR. Data presented as mean $\pm$ S.E.M. N = 3 experiments, 3 images per condition (A, C), 4 plates, 6+ wells per plate (B), 5-8 (D-F)

3.3.1 Unresponsiveness to TGF-beta activation and inhibition is maintained in HCFs cultured on stiff plastic

To further assess reversibility, HCF were thawed from passage 5 (p5) and cultured in the presence or absence of TGF-β receptor inhibitor SB431542 (SB). SB is used in the literature to maintain iPSC-derived cFbs as quiescent. Having seen no effect using SD208 and to have a more direct comparison to later iPSC-cFb experiments (Section 3.4), the switch was made to SB. At each passage post-thaw up to p9, α-SMA expression was assessed by immunofluorescence. These experiments allowed us to examine whether long-term TGF-β receptor inhibition can indeed reverse chronically activated HCF. Total α-SMA expression as measured by relative integrated density does not significantly change from passage 6 to 9 (Figure 3.9 A). Similarly, $\%$ cells positive for α-SMA fibres does not significantly change during long-term culture in the presence or absence of SB (Figure 3.9 B). Interestingly, $\%$ of α-SMA positive cells decreased (p = $>$0.05) with long term culture suggesting de-differentiation of HCF. Our data also demonstrate that HCF are unresponsive to TGF-β at each passage tested (p6-p9) regardless of whether they are cultured in the presence or absence of SB (Figure 3.9 C).

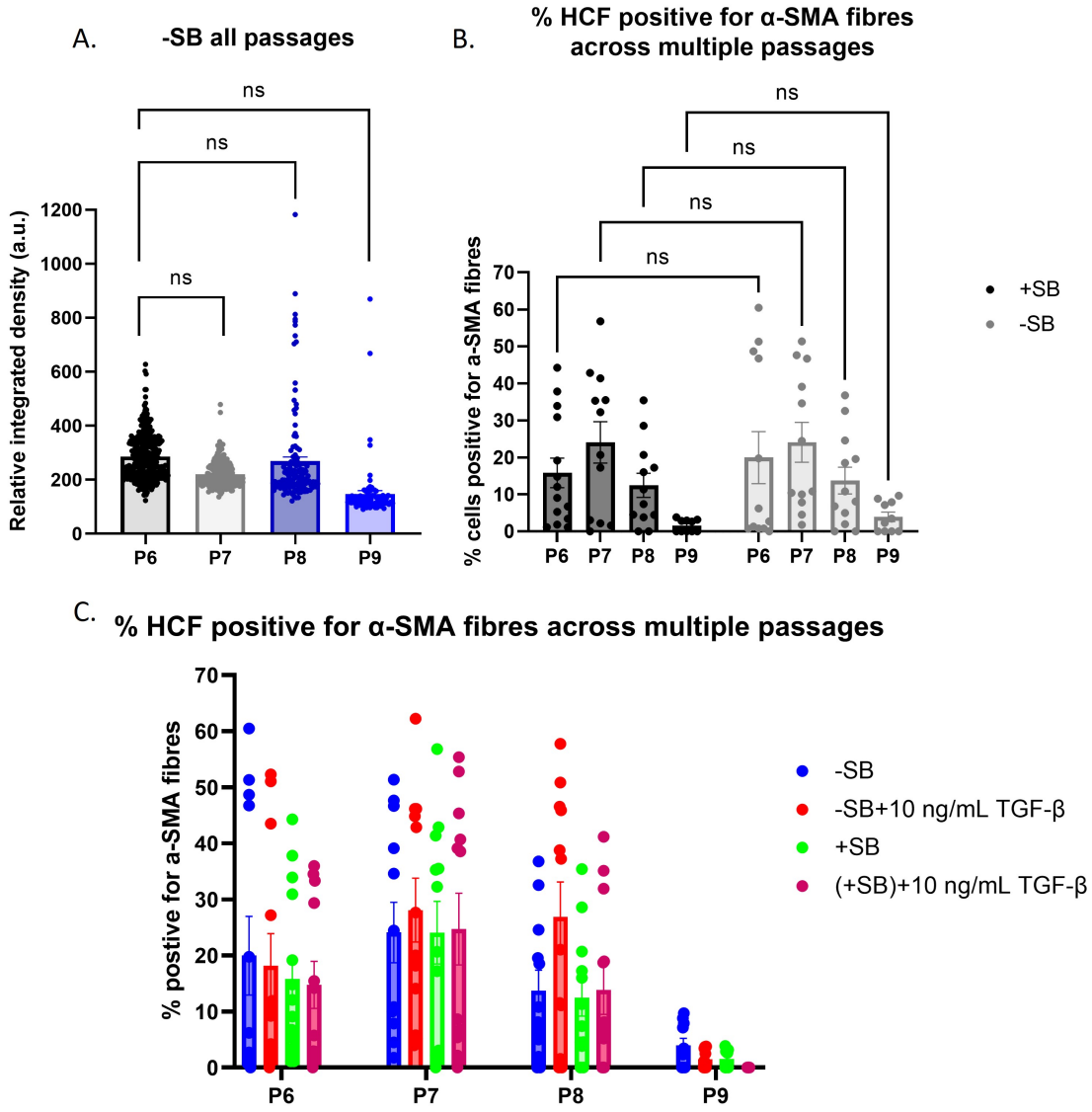


Figure 3.9: **Activation status of human cardiac fibroblasts on stiff plastic across multiple passages.** HCF were thawed on 3 GPa plastic with and without TGF-β receptor inhibitor SB431542 (SB). At each passage post thaw up to P9 cells were plated and exposed to 10 ng/mL TGF-β for 2 days. A – relative fluorescence staining of α-SMA in individual cells at P6-9. B – percentage of HCF positive for α-SMA fibrous staining at P6-9 cultured in the presence and absence of SB. C – percentage of HCF positive for α-SMA fibrous staining at P6-9 cultured with and without SB followed by exposure to 10 ng/mL TGF-β for 2 days. Data presented as mean $\pm$ S.E.M N = 2 cryovials, N = 6 wells, 2 images per well, A = individual cells, B and C = $\%$ cells per image

3.4 Chronically activated human iPSC derived cardiac fibroblasts cannot be reversed to a quiescent phenotype

3.4.1 Differentiation of human iPSC derived cardiac fibroblasts

Through the work detailed in sections 3.1 and 3.2, it has been shown that human primary HCFs activate to MyoFbs when kept in culture. An alternative method is therefore required to obtain healthy quiescent cardiac fibroblasts for better representation of the human myocardium for research purposes. It has been detailed in Wu *et al* (2020) [126] that iPSC-derived cardiac fibroblasts (hiPSC-cFbs) can be maintained as quiescent using TGF-β receptor inhibitor SB431542 (SB). This section details the investigation into chronic activation and reversibility of hiPSC-cFbs.

As mentioned, in section 1.2.1, cardiac fibroblasts have no markers specific to themselves alone. Therefore, multiple markers are required to guarantee successful differentiation from iPSCs. These include DDR2, vimentin, and collagen 1, with the absence of α-SMA as a marker for quiescence and prescence of α-SMA as a marker for activation. Figure 3.10 shows successful differentiation of cardiac fibroblasts by the presence of vimentin, DDR2 and collagen 1 and an absence of α-SMA staining. Figure 3.11 shows that when maintained in the presence of SB the cells show little to no staining for fibrous α-SMA. However, when exposed to TGF-β iPSC-cFbs activate to MyoFbs as demonstrated by the increase in size and the presence of α-SMA fibrous staining (Figure 3.11).

These results indicate successful differentiation of iPSCs to cardiac fibrob-

lasts. They also demonstrate that these cells maintain quiescence in culture with the ability to activate to MyoFbs when exposed to TGF-β.

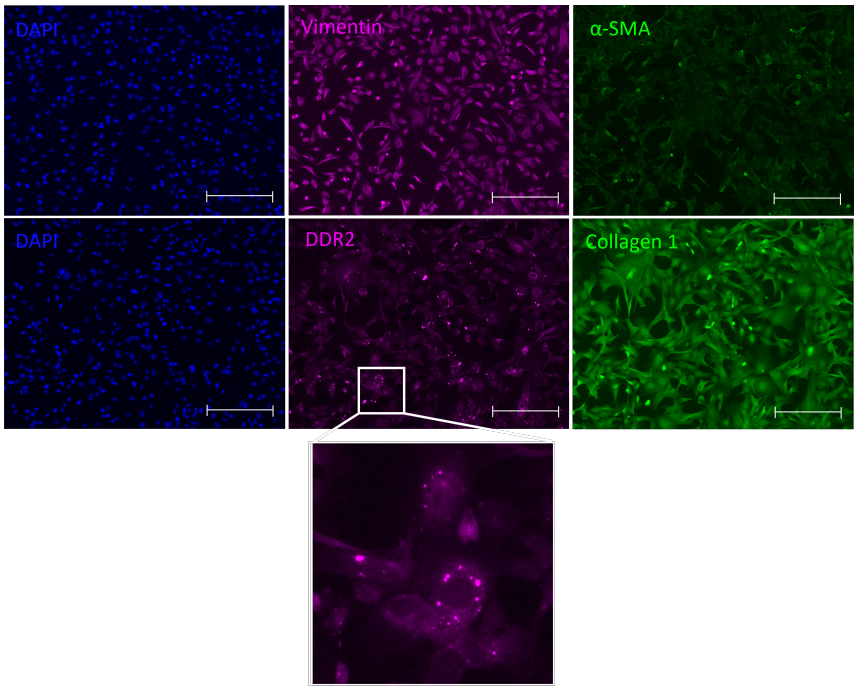


Figure 3.10: **Immunofluorescence staining confirming differentiation of iPSCs to cardiac fibroblasts.** DAPI is stained in blue, vimentin and DDR2 in purple and α-SMA and collagen 1 in green. Scale bar is 300 μm.

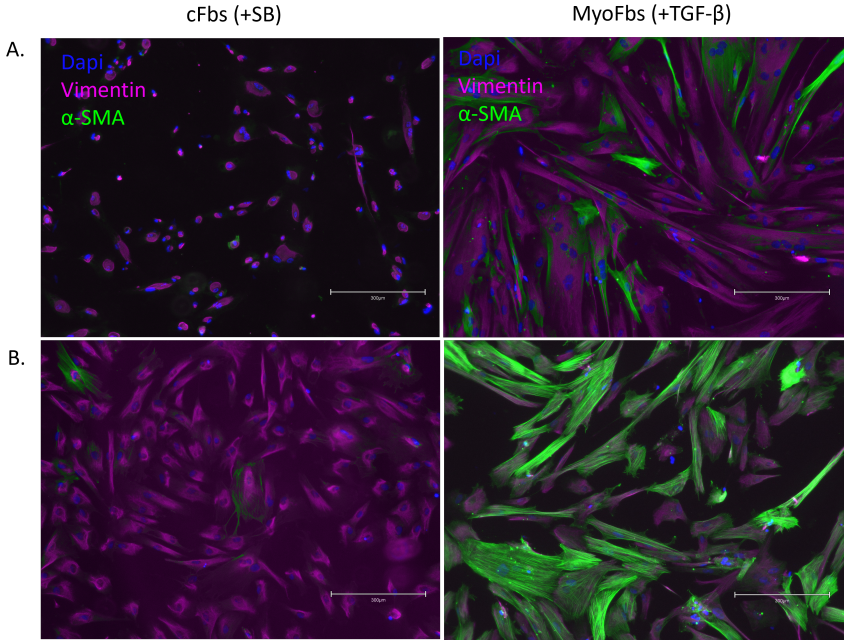


Figure 3.11: **Activation of iPSC-cFbs using TGF-β.** iPSC-cFbs in the presence of SB or TGF-β. DAPI is in blue, vimentin in purple and α-SMA in green. A and B are different batches of differentiations. Scale bar is 300 μm.

3.4.2 Chronic activation of hiPSC-cFbs renders them unresponsive to TGF-beta stimulation or inhibition

Having established that hiPSC-cFbs can be maintained as quiescent in culture on 3 GPa plastic, these cells were used to further investigate whether chronic activation leads to an irreversible MyoFb phenotype. To do this, hiPSC-cFbs were cultured in the absence of SB for 2 weeks to generate an activated MyoFb phenotype (see figure 3.12).

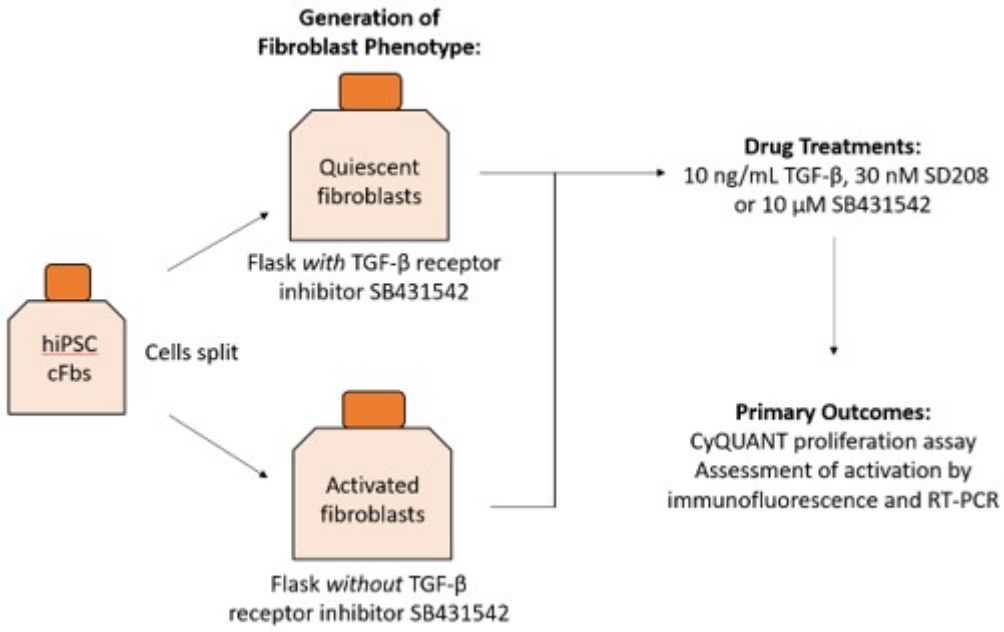


Figure 3.12: **Protocol schematic describing the experimental design for hiPSC-cFbs.** Cells were grown in the presence or absence of 10 μM SB431542 followed by exposure to 10 ng/mL TGF-β or 30 nM SD208 for 2-4 days. These cells were then used for immunofluorescence staining, the CyQUANT assay or RT-qPCR

Quiescent iPSC-cFbs show a significant increase in α-SMA staining following exposure to TGF-β (Figure 3.13 A). Removal of SB for only 2 days shows a two-fold increase in the percentage of cells showing positive staining of α-SMA, though non-significant (Figure 3.13 A). This suggests culture on 3 GPa stiff plas-

tic alone activates iPSC-cFbs. In contrast, chronically activated hiPSC-cFbs - those grown without SB for 2 weeks - showed no change in α-SMA staining when exposed to TGF-β (Figure 3.13 B). Nor did they show any response to TGF-β receptor inhibition when exposed to SD208 or SB (Figure 3.13 B).

This closely reflects that seen with primary HCFs (section 3.1, 3.2 and 3.3) confirming standard tissue culture practices (3 GPa stiff plastic) do in fact activate cFbs to MyoFbs. Also in line with the primary HCFs was the observation that chronic activation leads to a loss of fibrous α-SMA staining (Figure 3.13).

To investigate this phenomenon further, we explored the effect of culture on stiff 3 GPa substrates and the addition of TGF-β on the activation state of quiescent hiPSC-cFbs over time. A qualitative assessment of α-SMA expression was conducted over the period of 1 week using immunofluorescence. hiPSC-cFbs were cultured in the absence of a TGF-β receptor inhibitor. α-SMA fibres began to appear at the 24-hour mark (Figure 3.14 and 3.15) both in the absence and presence of TGF-β. In the presence of TGF-β, an increased proportion of cells stained with α-SMA up to 96 hours (Figure 3.14, 50-80$\%$ of cells and figure 3.15). Culture on 3 GPa alone also resulted in an increase in α-SMA fibrous staining but to a lesser degree than with TGF-β at each of the time points investigated (Figure 3.14, 5-20$\%$ and figure 3.15). In both conditions, the percentage of cells expressing α-SMA began to decrease between 96 hours and 1 week (168 hours). This is in line with our previous observations (Figure 3.13 B) where a loss of fibrous staining was seen in activated hiPSC-cFbs following long term (over two weeks) culture on stiff substrates in the absence of a TGF-β receptor inhibitor.

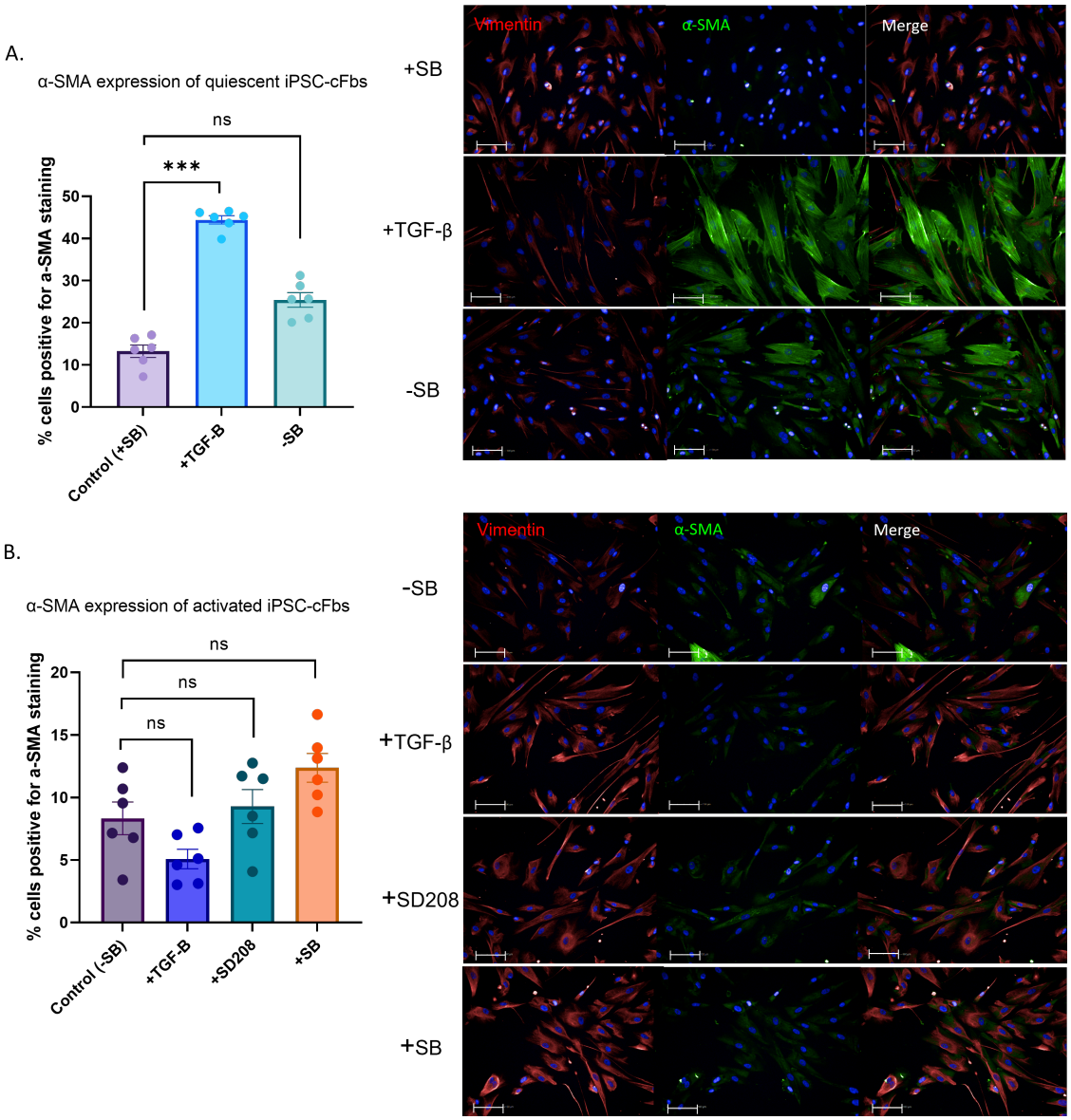
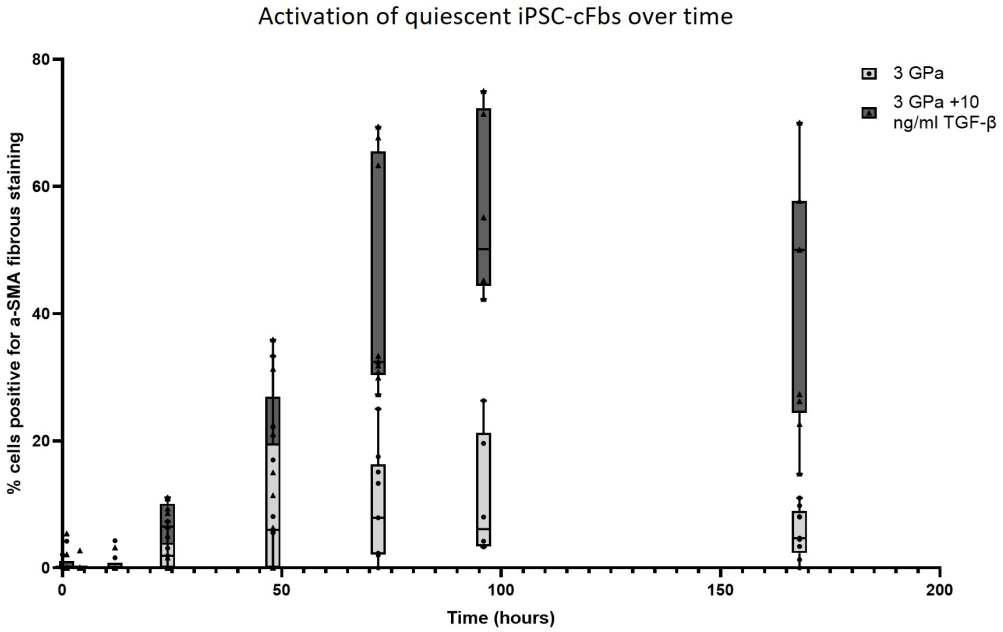


Figure 3.13: **Immunofluorescence staining of quiescent and activated hiPSC-cFbs.** Quiescent and activated hiPSC-cFbs generated as per figure 3.12 were assessed for α-SMA staining. DAPI is in blue, vimentin in red and α-SMA in green. A - Quiescent hiPSC-cFbs were exposed to 10 ng/mL TGF-β for 2 days. Withdrawal of SB for 2 days was also assessed. B - Activated hiPSC-cFbs were exposed to 10 ng/mL TGF-β, 30 nM SD208 or 10 μM SB for 2 days. Data presented as percentage of cells displaying α-SMA expression by immunofluorescence. Scale bar 100 µm. Data presented as mean $\pm$ S.E.M. N = 3 plates, 18 wells, nested one-way ANOVA compared with control.

A.



B.

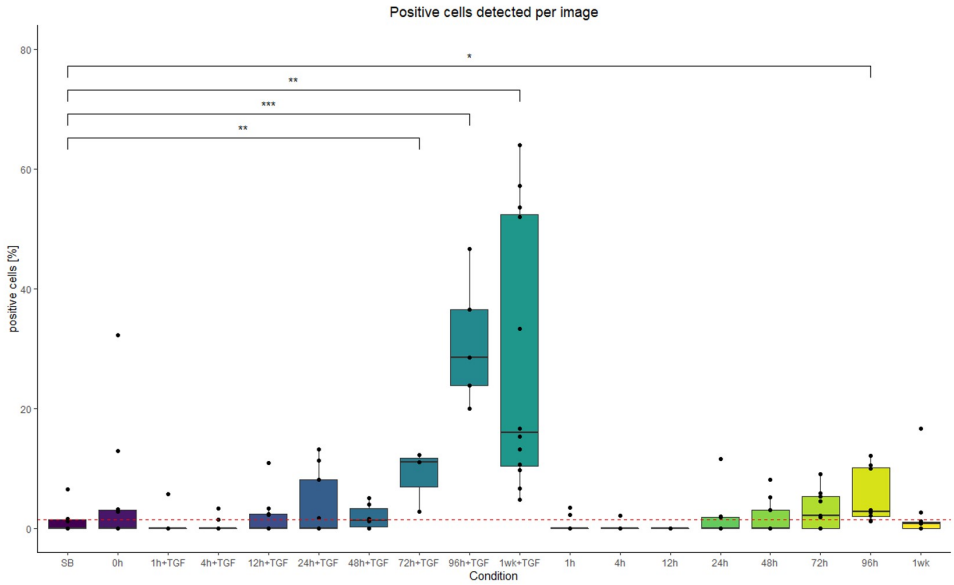


Figure 3.14: **Activation of hiPSC-cFbs over time on stiff 3 GPa stiff plastic**. SB was removed from the culture of quiescent hiPSC-cFbs for 7 days and α-SMA was assessed in the presence and absence of TGF-β at 1, 4, 12, 24, 48, 72, 96 and 168 hours. 2 methods of analysis were performed. A - Percentage of cells positive for α-SMA fibrous staining was assessed manually. B - Percentage of cells positive for fibrous staining was assessed using CellPose. Representative images shown in figure 3.15. Data presented as minimum to maximum. N = 3 wells, 3 images per well.

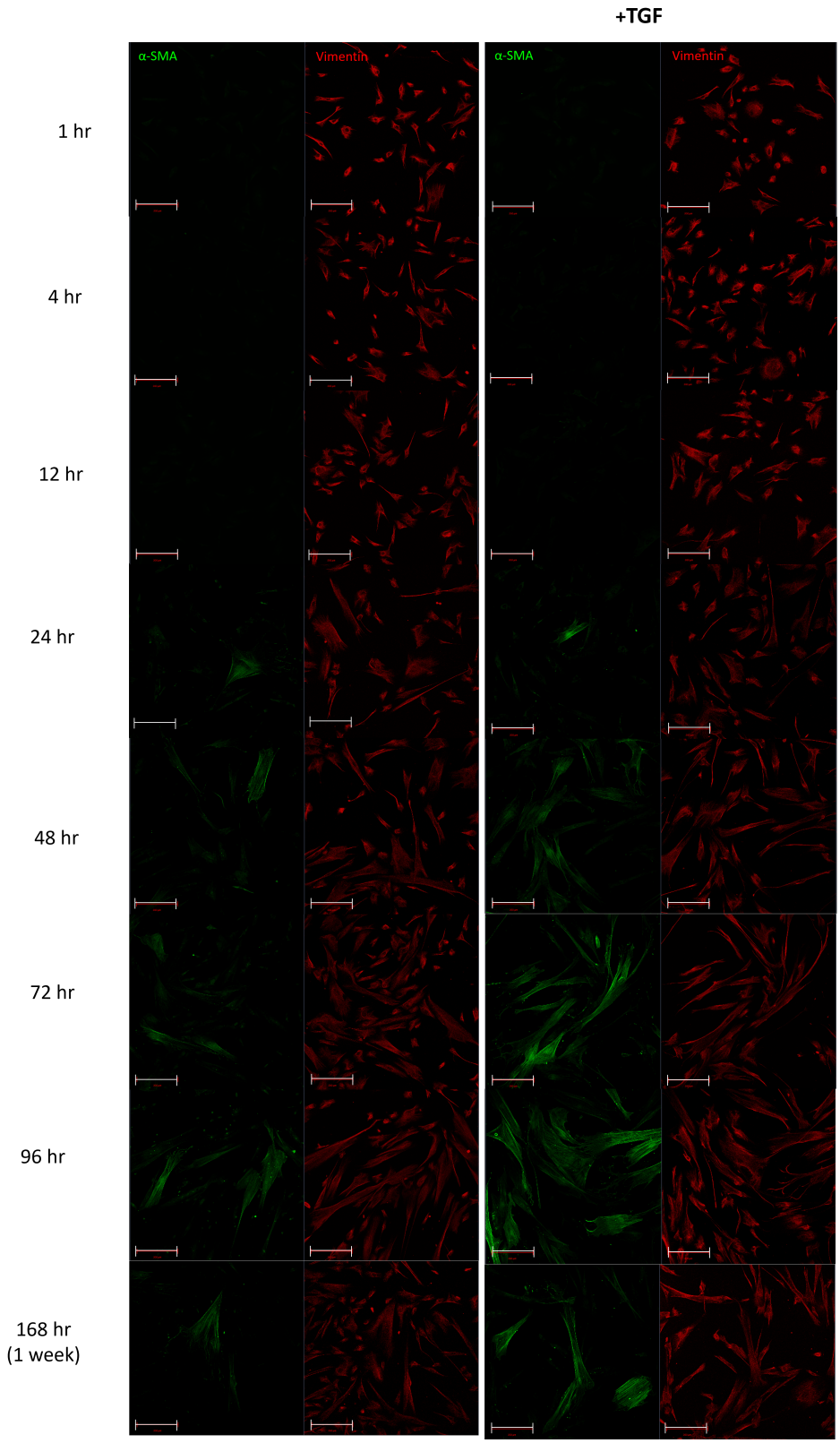


Figure 3.15: **Representative immunofluorescence images for figure 3.14.** α-SMA staining in iPSC-cFbs over a 1 week time period on 3 GPa plastic in the presence and absence of 10 ng/mL TGF-β. On the left are cells grown without TGF-β and on the right are cells grown with 10 ng/mL TGF-β. α-SMA in green and vimentin, as a marker for cardiac fibroblasts, is in red. Scale bar is 200 µm.

Proliferation was also assessed using quiescent and activated hiPSC-cFbs. Activated hiPSC-cFbs show significantly decreased proliferation rates when compared to quiescent cells (Figure 3.16 A). Similarly, acute activation of quiescent hiPSC-cFbs with TGF-β also caused a significant decrease in proliferation rates when compared to the undrugged control. Removal of SB for 2 days led to a small but non-significant decrease in proliferation (Figure 3.16 B). Chronically activated hiPSC-cFbs - generated from removal of SB from culture for 2 weeks - showed no response to TGF-β or SD208, nor re-addition of SB (Figure 3.16 C).

Investigation of mRNA changes in activated and quiescent hiPSC-cFbs showed robust increases in both α-SMA and collagen 1 in response to TGF-β compared to undrugged controls. Neither quiescent nor activated hiPSC-cFbs showed any significant changes in mRNA expression in response to SB. mRNA expression levels of TGF-β receptor 1 were unchanged in response to both TGF-β and SB.

Taken together, these results predominantly mirror those seen with the primary HCFs. Although changes in mRNA expression of activation markers were seen, there was no response to SB at the protein level (Figure 3.13) or in terms of proliferation. These results indicate that chronically activated MyoFbs cannot be reversed to their quiescent phenotype using TGF-β receptor inhibition.

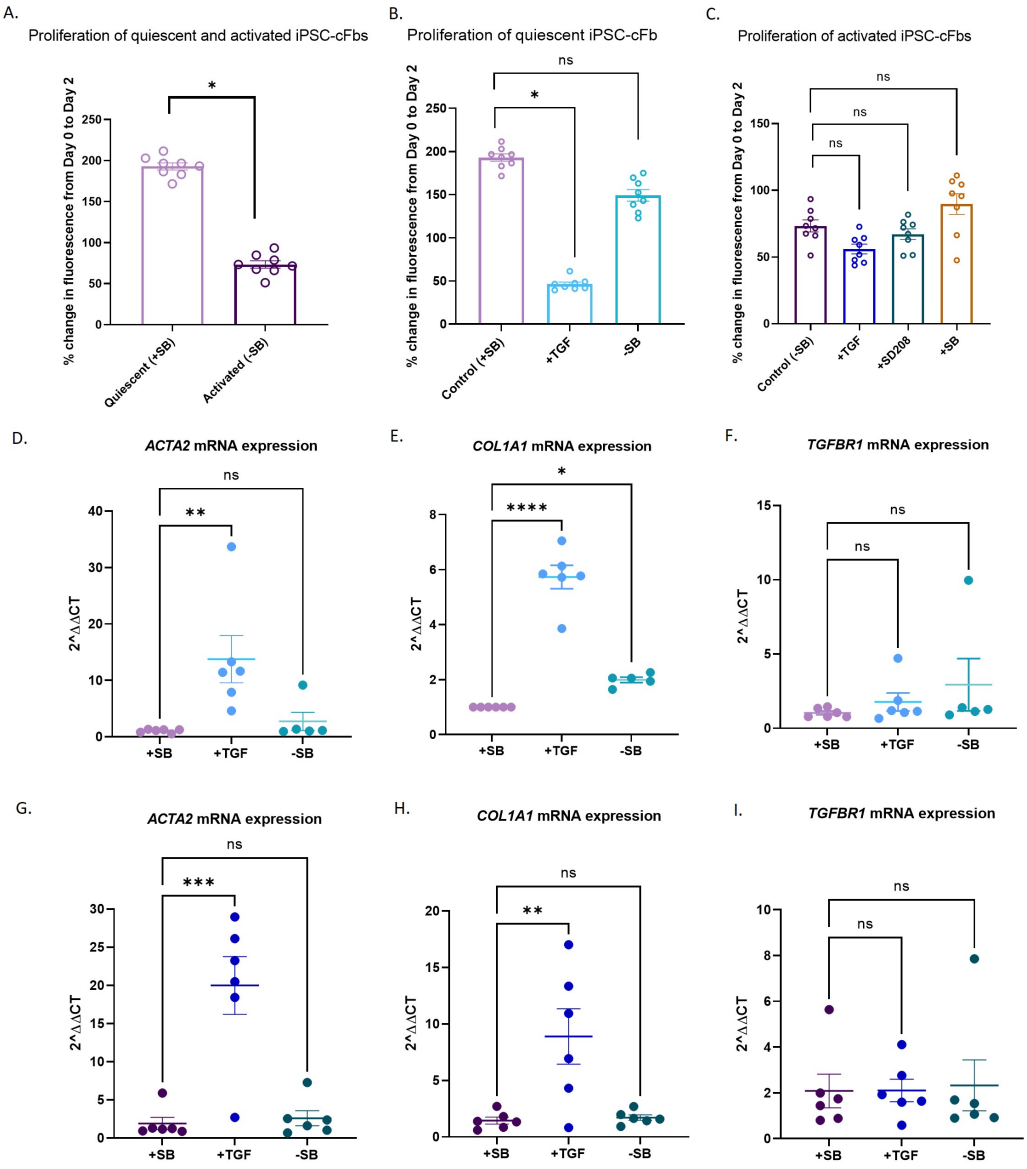


Figure 3.16: **Activation status and proliferation of quiescent and activated hiPSC-cFbs.** A-C Proliferation was assessed over 48 hours as a percentage change from baseline (Day 0). A - Proliferation of quiescent and activated hiPSC-cFbs. B - Proliferation of quiescent hiPSC-cFbs following exposure to 10 ng/mL TGF-β or removal of SB. C - Proliferation of activated hiPSC-cFbs following exposure to 10 ng/mL TGF-β, 30 nM SD208 or 10 μM SB. D-I RT-qPCR for activation markers *ACTA2*, *COL1A1* and *TGFβR1* following 4 days of culture. D-F mRNA expression of hiPSC-cFbs grown in the presence of SB. G-I mRNA expression of hiPSC-cFbs grown in the absence of SB for 2 weeks. Data presented as mean $\pm$ S.E.M. N = 3 plates, 24 wells (A-C), 5-6 (D-I). nested one-way ANOVA compared with control (A-C), one-way ANOVA compared with control (D-I).

3.5 Discussion

The presence of cardiac fibrosis is associated with many CVDs and is associated with increased mortality and morbidity. There is, therefore, a great interest in identifying anti-fibrotic therapies especially as none currently exist. As an important driver of cardiac fibrosis, the MyoFb has understandably been the subject of many studies. The potential to reverse MyoFb activation and reduce the perpetual cycle of pathological cardiac fibrosis could provide new avenues for therapy. In this chapter, primary human and human iPSC-derived cardiac fibroblasts are used to investigate the reversal of the MyoFb phenotype. The results in this chapter demonstrate that standard plastic, due to high tensile strength, leads to chronic MyoFb activation and that this leads to a diminished response to TGF-β. It is also shown that neither short-term culture on soft substrates, nor inhibition of TGF-β receptors are able to reverse this chronic MyoFb phenotype.

The results of this chapter differ when compared to most of the published literature. This is also demonstrated when comparing the experimental results to the modelling results in section 3.1. The model predicted (Figure 3.2) that both TGF-β or the culture of cells on lower substrate materials would lead to changes in expression of activation markers and proliferation, however when using human cardiac fibroblasts we found no significant changes in expression or proliferation. This is most likely because the model is built on predominantly mouse and rat data and not human data. It has also been built using freshly isolated cells and not those cultured for several weeks as in this chapter. Whether the differences

seen here are solely due to species differences or down to the ”chronic” activation of long-term culture is yet unknown.

Another interesting observation is that in much of the immunofluorescence data captured in this chapter, both the primary HCFs and iPSC-cFbs display an unusual α-SMA staining pattern. Rather than the typical fibrous staining of an activated MyoFb (Figure 3.11), a diffuse staining throughout the cytoplasm was observed in our chronically activated cells (Figure 3.4 3.5, 3.7, 3.8). The exact explanation for this is unclear. However, it may be that chronic exposure to such a high stiffness (3 GPa plastic) may result in the disassembly of the α-SMA fibres. This is supported by the observational loss of fibres over time in culture as seen in figure 3.14. Perhaps the localisation of α-SMA within the MyoFb could be used as a marker for irreversible chronic activation and late-stage fibrosis. Alternatively, it might be that some level of de-differentiation may be occurring due to the high level of stress exerted on these cells from the high substrate stiffness.

3.5.1 Mechanical stiffness and myofibroblast activation

Several studies have shown that primary cells begin to express α-SMA fibres after several hours in culture on stiff plastic substrates supporting the hypothesis that stiff substrates activate cardiac fibroblasts to MyoFbs [81, 82, 127]. It has also been demonstrated that using softer, but still stiff substrates, that more closely reflect that of the diseased myocardium (30-100 kPa) also leads to MyoFb activation as demonstrated by an increase in expression of activation markers such

as α-SMA, collagen 1 and 3, and periostin [36, 82, 80]. This data supports the idea that increased stiffness in the myocardium during CVD leads to perpetuated MyoFb activation. The work conducted here also suggests we need to rethink our tissue culture practices in regards to working with cardiac fibroblasts due to the high tensile strengths involved.

Several studies have also shown that softer substrates can prevent the activation of MyoFbs, however, reversal has been less well explored [81, 82, 88]. Wang *et al* (2012) explored this possibility with some success using valvular cells [80]. The data presented in this chapter suggests soft substrates are not sufficient to reverse the MyoFb phenotype, although it is possible that our use of soft substrates for only 2-4 days may not have been long enough when using a chronically activated cell type. Regardless of whether longer culture on soft substrates can reverse the MyoFb phenotype or not, use of soft substrates should provide a more physiological surface to work with and may be able to maintain quiescence in the absence of a pharmcological inhibitor (SB).

3.5.2 Myofibroblast reversal and TGF-β receptor inhibition

In this work, TGF-β receptor inhibition was also investigated with the potential to reverse the MyoFb phenotype. There have been reports of TGF-β inhibition decreasing the expression of MyoFb activation markers using both murine and human cells [20, 60, 88]. In contrast, we found that the use of neither SD208 nor SB431542 had any effect on α-SMA or collagen expression. It must be noted that in existing research, experiments utilised freshly isolated cells cultured for shorter

periods suggesting they may not have been fully activated. Our cells were purposefully kept for 2-4 weeks to induce a chronically activated phenotype. Also, our use of 30 nM SD208, though used in other cardiac fibroblast studies [60] was much lower than that used in the study performed using human cells (3 μM) [20]. Tomosek and Gabbiani previously suggested that there may be an intermediate "protomyofibroblast" phenotype that bridges the differentiation of fibroblasts to MyoFbs [128]. Identification of more than 2 populations of fibroblasts in the healthy and diseased hearts in sequencing studies may also support this theory [4, 6]. Taken together, the results in this chapter suggest there may be the presence of a threshold of activation after which MyoFbs become unresponsive to any method of de-activation.

3.5.3 Proliferation of the myofibroblast

Previously, it has been assumed that MyoFbs have an increased proliferative capacity when compared to quiescent cardiac fibroblasts in order to fulfill their role in wound healing and repair [17, 23]. However, more recently it has been demonstrated that this might not be the case. Hecker *et al* (2011) demonstrated that lung MyoFbs were less proliferative than their quiescent counterparts [86]. Using a cardiac mouse model of myocardial infarction, Bugg *et al* (2022) demonstrated that cardiac fibroblasts also had a reduced proliferative capacity following injury [25]. Furthermore, a study using human fibroblasts from failing hearts showed a significant decrease in the proliferative marker Ki-67 [20]. However, in these patients, there was also an increase in vimentin in these hearts suggesting an

increase in cardiac fibroblasts [20]. The results in this chapter demonstrate that, whether through acute (TGF-β stimulation) or chronic (long-term culture on stiff substrates) activation, MyoFbs have a reduced proliferative capacity when compared to their quiescent counterparts. It may be that injury stimulates cardiac fibroblast proliferation prior to differentiation into MyoFbs in order to fulfill their role in healing but this remains to be studied.

3.5.4 Conclusion

The lack of effective treatments for reversing cardiac fibrosis demonstrates how important reversing the MyoFb phenotype could be to decreasing mortality and morbidity. Although the reversal methods explored in this chapter show no avail, other methods of reversal may still be possible (See section 6.2.4). The activation process is complex and multifactorial and by fully dissecting the cardiac to MyoFb transition other therapeutic targets may be discovered. The increasing ease and use of large-scale sequencing studies are supplying a wealth of information to contribute to this goal. Fibrotic processes are generally conserved across the different organ systems, identifying new targets to reverse MyoFb activation would not only benefit the treatment of CVDs but would have massive clinical benefit for multiple different diseases.

Chapter 4

Optimisation of optical mapping for 2D monolayers of iPSC-cardiomyocytes

Optical mapping is a technique used to study the electrophysiology of the heart in health and disease. Through excitation of voltage and/or calcium dyes, optical mapping allows us to obtain recordings with higher spatial resolution than standard electrode-based mapping techniques [129, 130]. Electrical activity and calcium handling are recorded from the surface of the heart using specialised cameras, such as CCD (charged coupled device) or CMOS (complementary metal oxide semiconductor) sensors [131]. While voltage-sensitive dyes localise in cell membranes and exhibit a fluorescence output that is changed rapidly in response to changes in the membrane potential, calcium-sensitive dyes bind directly to calcium in the cell with a fluorescence output that changes in relation to the movement of calcium, into and out of the cytosol from the extracellular space and sarcoplasmic reticulum [129, 131]. Using optical filters, dye-loaded cells are excited at specifc wavelengths and emitted fluorescent photons imaged by the detector [129].

Often, the contraction of cardiomyocytes or cardiac tissues while mapping dis-

torts the signals. Therefore, contraction uncouplers, such as blebbistatin or BDM (2,3-butanedione monoxime), may be utilised to suppress contraction and prevent motion artefacts [129, 130]. However, there are contradicting reports as to the electrophysiological side effects of using blebbistatin [132, 133]. Both Brack *et al* (2013) and Kappadan *et al* (2020) showed prolongation of the action potential using rabbit hearts [132, 133]. In contrast, Fedorov *et al* (2006) found no effects of blebbistatin on either calcium transient morphology or action potential duration, up to a concentration of 10 μM [134]. Similarly, there are also studies in zebrafish and mouse hearts that also show no significant effects of blebbistatin on cardiac electrophysiology [135, 136].

Because of this, many have found technical or computational approaches as an alternative to motion-contraction uncouplers. One such example is excitation or emmission ratiometry. Ratiometric dyes allow excitation or emission spectra to be recorded at two different wavelengths [137]. It has been demonstrated *in vivo* and *ex vivo* to reduce drift and motion artefacts without effecting electrophysiology [138, 139].

Optical mapping is often utilised in the study of arrhythmogenesis to interrogate the disruption of electrical wave propagation in the heart with the aim of informing more effective treatment therapies [131]. Since its development in 1976, optical mapping systems have become vital in electrophysiological research [140]. Recently, they have been advanced to map human iPSC-CM monolayers enabling the study of disease phenotypes and drug testing *in vitro* using human models

[129, 141]. However, optical mapping of iPSC-CM monolayers presents unique challenges due to poor signal quality compared to whole tissues (which produce higher fluorescent signals), and susceptibility to phototoxicity and photobleaching. Equally, as mentioned in section 1.2.1, iPSC-CMs have inherent limitations such as a lack of maturity, a more positive diastolic membrane potential and decreased inwardly rectifying potassium current (I_{K1}) density. However, further development of these models has shown increased accuracy for cardiotoxicity prediction using *in vitro* drug screening [142].

In this chapter, I discuss the differentiation of human iPSCs to cardiomyocytes and the optimisation of an existing optical mapping rig for use with iPSC-CM monolayers to study calcium handling and action potential morphology.

4.1 Optimisation of and confirmation of cardiomyocyte differentiation

Differentiation of cardiomyocytes involves the use of small molecule inhibitors to drive cells towards the mesoderm, cardiac mesoderm, cardiac progenitors, and then finally beating cardiomyocytes (Figure 4.1). α-actinin is used as a marker for cardiomyocytes. Prior to differentiation, the optimum seeding density for differentiation can be identified to obtain optimal differentiation efficiency. This was conducted using two different parental iPSC lines, Kolf-C2 and Rebl-Pat (Figure 4.2). Figure 4.2 demonstrates that regardless of seeding density, cardiomyocyte differentiation provides 60-80$\%$ purity by α-actinin staining. In the Rebl-Pat line, significant differences were not observed between the densities. However, there may be a trend toward a higher percentage of cardiomyocytes being produced

by the lower seeding density of 7x10^5 so this was used moving forward. In figure 4.3, α-actinin staining elucidates clear evidence of sarcomeres, further indicating successful differentiation to cardiomyocytes. However, these images also demonstrate the immaturity of iPSC-CMs showing a spherical shape and disorganised sarcomeric structures.

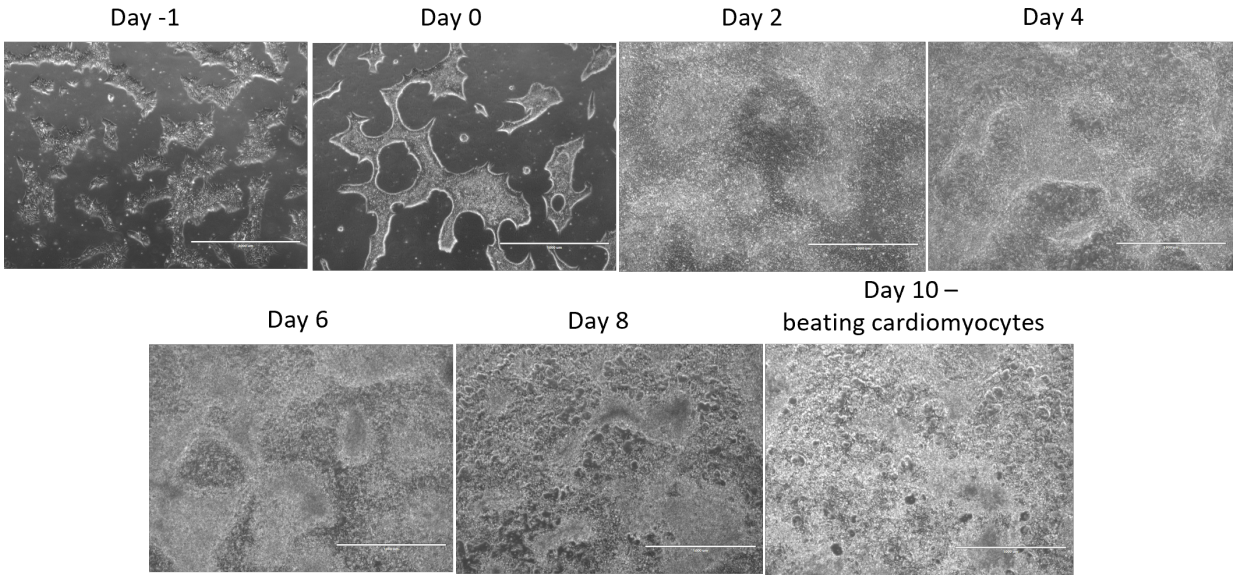


Figure 4.1: **Images of the differentiation process for cardiomyocytes from hiPSCs.** Cardiomyocyte differentiation begins at day -1. Photos were taken at every media change through the differentiation protocol up to day 10 when cells begin to beat.

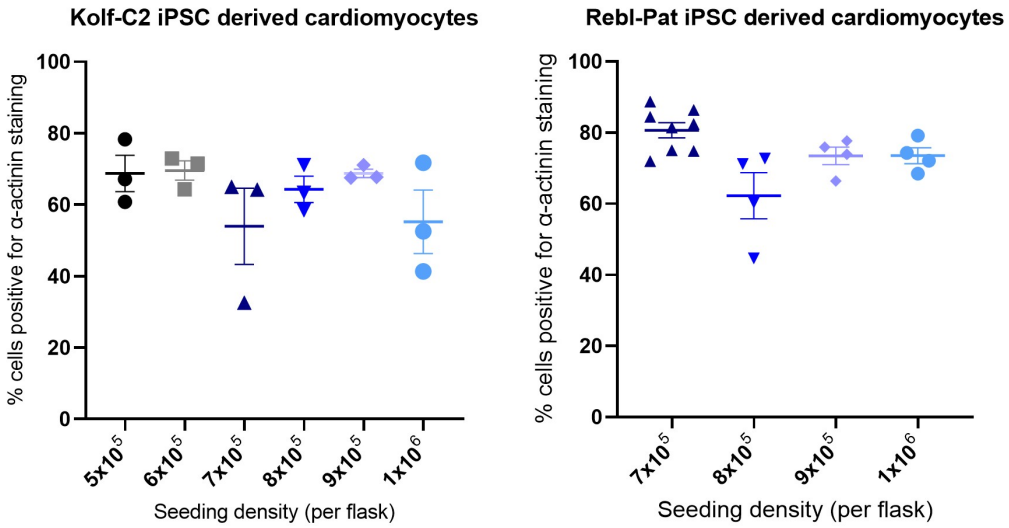


Figure 4.2: **Percentage of cells staining positive for α-actinin following iPSC-CM differentiation.** iPSC-CMs generated from 2 parental cell lines from multiple different seeding densities (5, 6, 7, 8, 9 x10^5 and 1x10^6) were assessed for α-actinin staining using immunofluorescence. Kolf-c2 staining was assessed using the Operetta platform. Data was non-significant as assessed using one-way ANOVA. Rebl-Pat staining was assessed using confocal microscopy. Data was non-significant as assessed using a nested one-way ANOVA. Data presented as mean $\pm$ S.E.M. N = 3 batches of differentiations

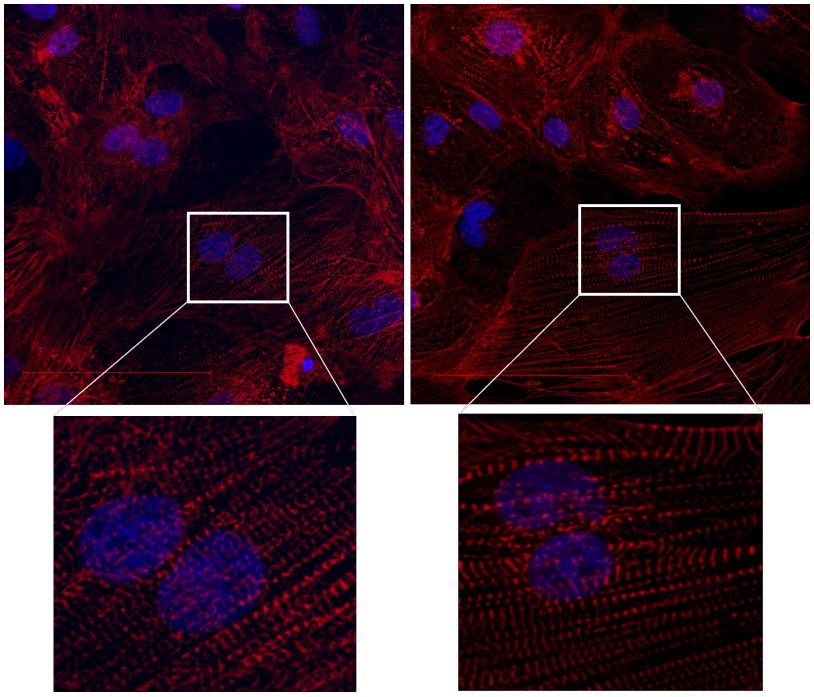


Figure 4.3: **Representative images for Rebl-Pat iPSC-CM differentiations in Figure 4.2.** DAPI is in blue, α-actinin in red. White boxes show zoomed in sections of the red α-actinin stained sarcomeres. Scale bar is 100 μm.

To assess how maintenance in culture affects iPSC-CMs, and to determine the

optimal day to optically map the cells, beat rate was compared across different ages (Figure 4.4). iPSC-CMs were assessed between days 20 and 36. Figure 4.4 shows a significant decrease in beat rate from days 32-36 when compared to day 20. Cells at these later time points were also less likely to survive the dye loading process and were thereby deemed less healthy. Therefore, cells were only used for optical mapping between days 20 and 30.

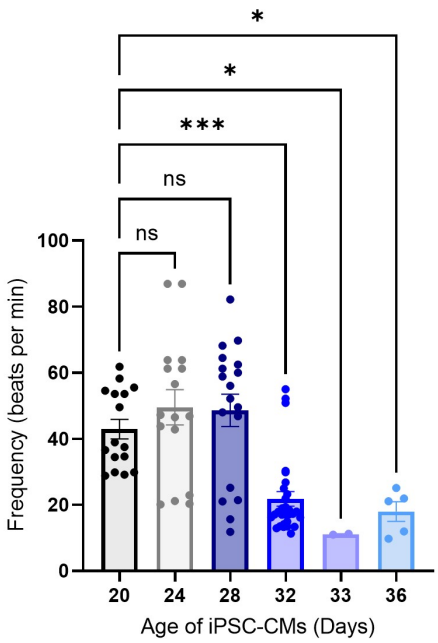


Figure 4.4: **Comparison of beat rate across different ages of iPSC-CMs.** iPSC-CMs were loaded with Fura-2, AM and optically mapped at different ages. Data presented as the mean ± S.E.M. N = 6 batches of differentiations

4.2 iPSC-CMs remain stable during optical mapping

To interrogate calcium handling in iPSC-CMs, cells were loaded with 10 µM Fura-2, AM. Calcium transients were recorded every 5 minutes for 30 minutes. Studies were conducted at room temperature and at 37^{o}C. (Figure 4.5 and 4.6). To assess changes in calcium influx, via sarcoplasmic extrusion and reuptake, duration measurements were taken at 50% relaxation from two different points – the

maximum rise upstroke and the peak amplitude. Additionally, to assess the physiological state of the cells and experimental quality, we measured beat rate and fluorescence amplitude. Figure 4.5 A shows that repeatedly exposing the same area to light does not affect the fluorescence amplitude of the calcium transience over the course of 30 minutes. This demonstrates that any changes seen over time are not due to photobleaching. At 37 degrees both cycle length and beat rate remained the same from 0 to 30 minutes (Figure 4.5 B and C). Calcium transient duration decreased insignificantly over the course of the 30 minutes for both peak and maximum rise upstroke measurements (Figure 4.5 C and D). Taken together, these results suggest that optical mapping for 30mins at 37^{o}C is a stable method to assess calcium handling properties of the iPSC-CMs. Figure 4.6 shows a comparison of the cells when measured at room temperature versus 37^{o}C. At room temperature, iPSC-CMs show an initial decrease in beat rate between 0 and 5 minutes before stabilising over the next 20 minutes (Figure 4.6 B). This change is obviously mirrored in the cycle length measurements. There is an initial increase from 0 to 5 minutes before stabilising around 6000 ms (Figure 4.6 A). Understandably, at room temperature calcium transient durations are much longer than typically expected of iPSC-derived cardiomyocytes, when taken from both measurements (Figure 4.6 C) [143].

These data demonstrate that optically mapping iPSC-CMs for 30 minutes does not affect their electrophysiology, however mapping at room temperature may induce calcium handling changes at baseline (prolonged CTD_{50}) and reduce exper-

imental stability. For these reasons, investigations were performed at 37^{o}C here on in.

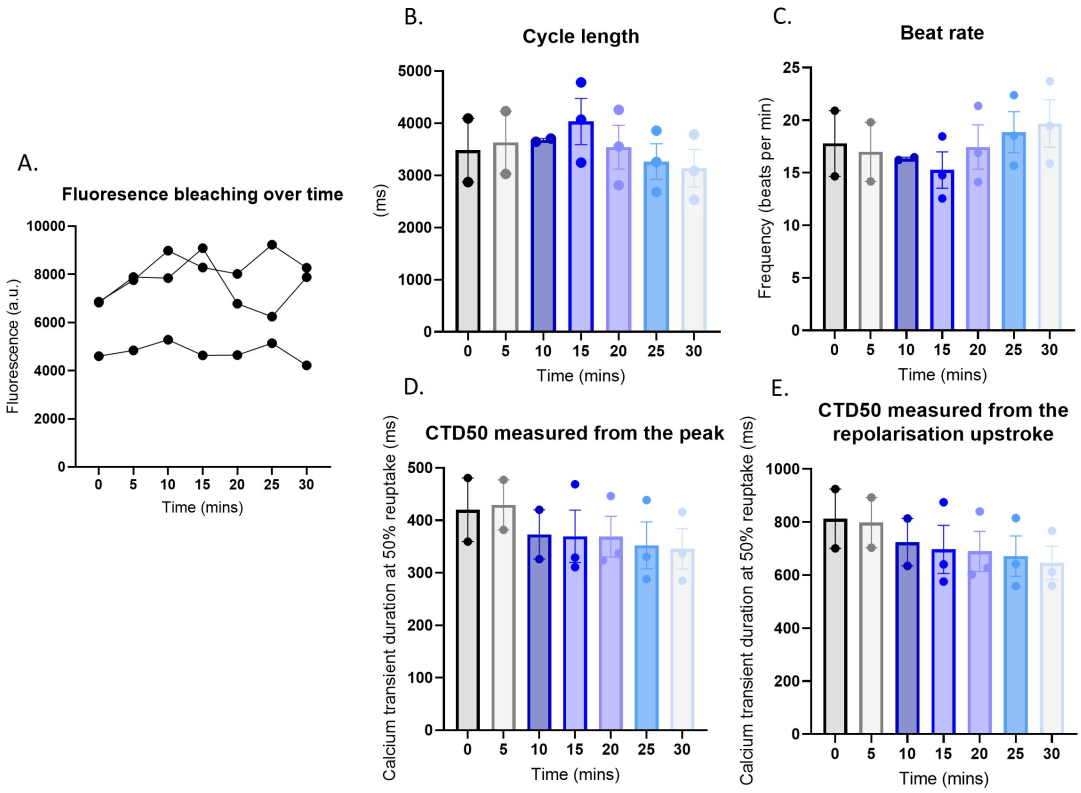


Figure 4.5: **iPSC-CMs were loaded with 10 μM Fura-2,AM and calcium transients were recorded at 37^{o}C over the course of 30 minutes** A - Fluorescence of 3 dishes over the course of 30 minutes. B-C - Cycle length and beat rate over the course of 30 minutes. D-E - Calcium transient duration measurements for maximum rise upstroke and peak at 50% decay over the course of 30 minutes. B-E - Data was non-significant when compared to 0 minutes using one-way ANOVA. Data presented as mean $\pm$ S.E.M. N = 2/3

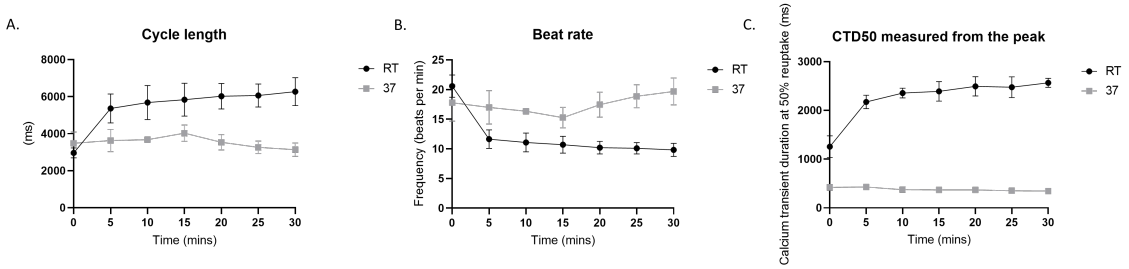


Figure 4.6: **iPSC-CMs were loaded with 10 μM Fura and calcium transients were recorded at room temperature or 37^o from the same area every 5 minutes for 30 minutes.** A-B - Cycle length and beat rate over the course of 30 minutes at room temperature and 37^o. C - Calcium transient duration measurements for peak at 50% decay over the course of 30 minutes at room temperature and 37^o. N=2/3

4.3 Use of different imaging parameters doesn't affect calcium transient duration measurements

Different optical mapping parameters were investigated to optimise our existing setup for iPSC-CM monolayers. Spatial binning is the method of combining adjacent pixels on the camera detector to sum their values and reduce background noise. The rationale here is that 'signal' photons are constructively summed, and so the signal is amplified, while the random nature of noise means there will be destructive summation, and so noise is reduced. Due to the short exposure times required to accurately capture signal morphology of electrophysiological signals, such as the calcium transient or action potential, spatial binning is often required as raw single detector pixel signal can be extremely noisy. However, spatial binning reduces the effective spatial resolution, and so may mask the utility of optical mapping to study regional variations, conduction dynamics, etc. [144]. We therefore sought to test signal quality and accuracy at various levels of spatial binning to find the least binning we could apply (to maximise spatial resolution) while accurately measuring the calcium transients of the iPSC-CMs.

We selected bin sizes of 5, 10, 20 and 64 detector pixels, which resulted in pixel sizes for the imaged sample of 4, 8, 16 and 51.2 μm respectively (using a 10x objective). As expected, cycle length and beat rate were unchanged by the change in pixel size (Figure 4.7 A, B, E and F). However, CTD_{50} values were decreased by using a pixel size of 51.2 μm (Figure 4.7 C, D, G and H), and activation maps were significantly distorted (Figure 4.7 I). iPSC-CMs are roughly 100 μm in size,

therefore averaging too large an area may lead to the integration of signals from cells that are asynchronous, distorting the recorded signal which will change the measured CTD_{50} values and activation as observed. Furthermore, as outlined, large pixel sizes reduce spatial resolution, explaining the changes in activation maps at 51.2 μm pixel size.

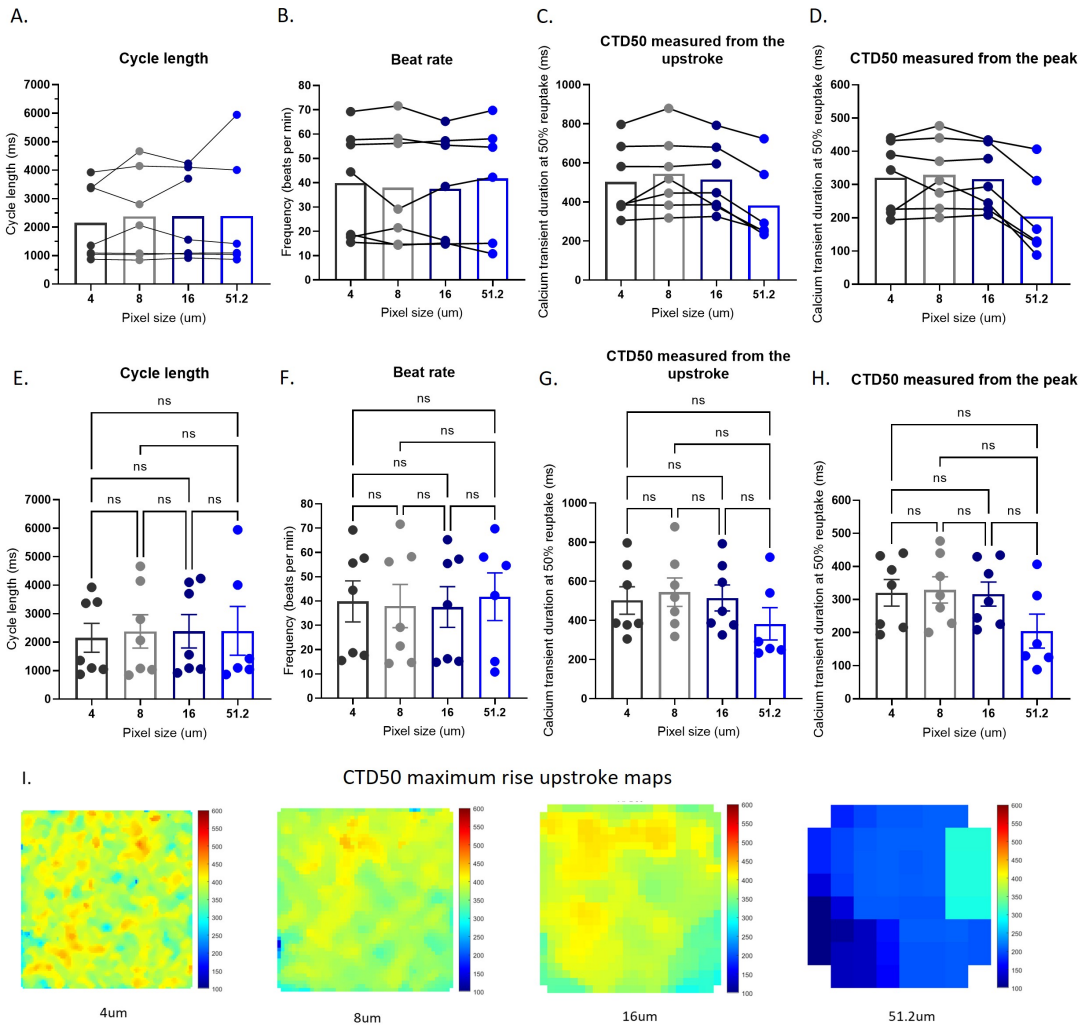


Figure 4.7: **Calcium transient recordings were measured in iPSC-CMs at increasing pixel size, 4, 8, 16 and 51.2 μm representative of pixel binning for 5, 10, 20 and 64 pixels.** A and E - Cycle length at increasing pixel sizes. B and F - Beat rate of iPSC-CMs at increasing pixel size. C and G - CTD_{50} maximum rise upstroke measurements at different pixel sizes. D and H - CTD_{50} peak measurements at different pixel sizes. A-D show consecutive measurements from one area within one dish connected by a line whereas E-H show the same data represented as mean $\pm$ S.E.M. with pairwise comparisons from a one-way ANOVA. I - Representative CTD_{50} maps for maximum rise upstroke measurements at pixel size 4, 8, 16 and 51.2 μm. N = 6/7 dishes

Another important aspect to consider is frame rate (inversely proportional to exposure time). Longer exposure times, in theory, will lead to higher quality signals due to an increase in the number of photons collected per frame. However, too long an exposure time can distort the recorded signal morphology [144]. This is a result of the millisecond scale phenomena inherent in cardiac electrophysiology. Again therefore, a balance needs to be found to optimise exposure time. Figure 4.8 shows that calcium transient measurements are unchanged by the change in length of exposure. Cycle length is observed to be between 1000-2000 ms (Figure 4.8 A) and beat rate between 40 and 60 beats per minute (Figure 4.8 B). CTD_{50} values also remain statistically unchanged, however there is a trend for shorter CTD_{50} values at the shortest exposure time (Figure 4.8 C and D).

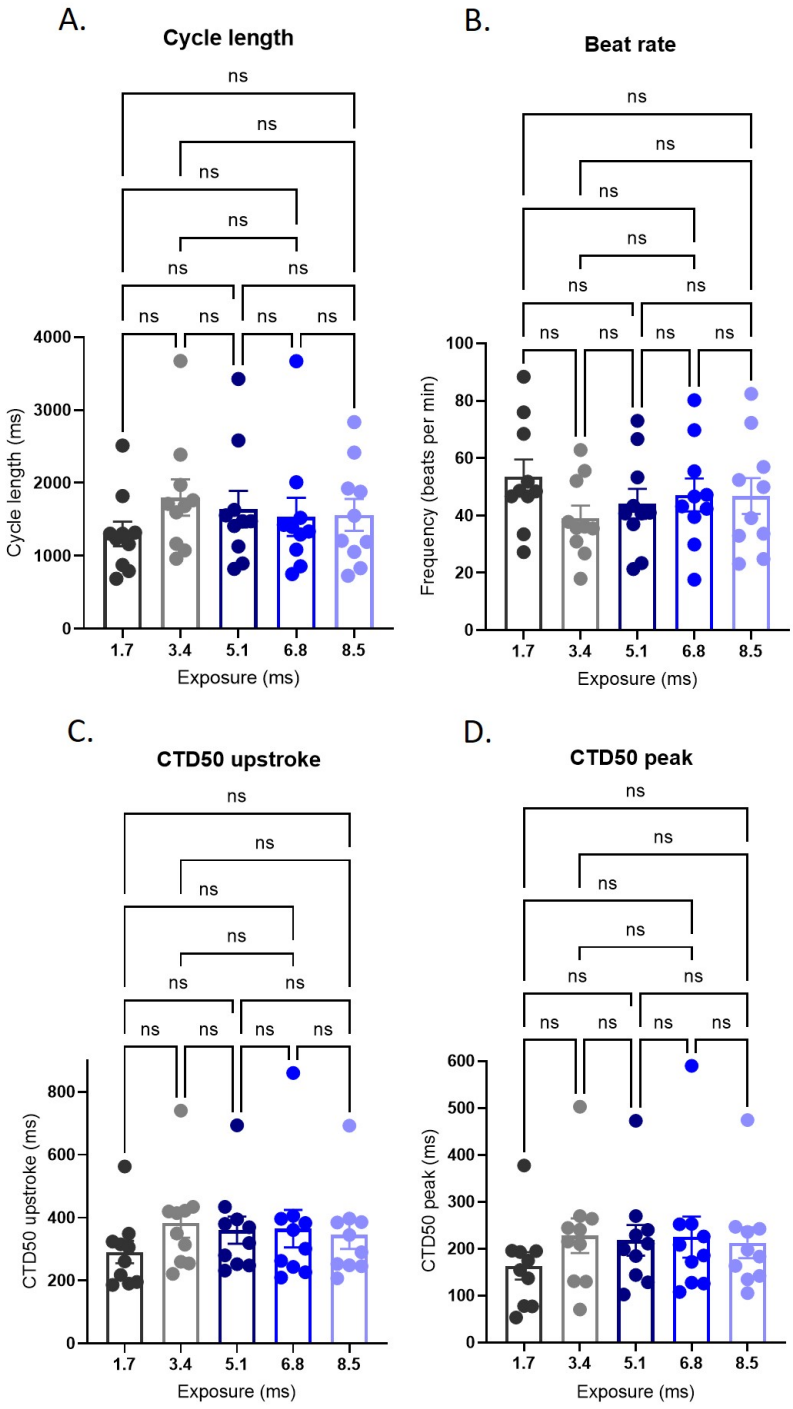


Figure 4.8: **Calcium transient recordings were measured at different exposure times of 1.7, 3.4, 5.1, 6.8 or 8.5 milliseconds (ms).** A - Cycle length at different exposure times. B - Beat rate at different exposure times. C - CTD_{50} maximum rise upstroke measurements at different exposure times. D - CTD_{50} peak measurements at different exposure times. Data presented as mean ± S.E.M. N = 10 dishes.

4.4 Use of different imaging parameters doesn't affect action potential duration measurements

As mentioned previously, optical mapping parameters needed to be optimised for iPSC-CM monolayers. The previous experiments (section 4.3) were therefore repeated using Fluovolt to measure the action potential of the iPSC-CMs. As expected, cycle length and beat rate were unchanged by the change in pixel size (Figure 4.9 A-D). As seen with CTD_{50} in section 4.3, APD50 was decreased slightly by using a pixel size of 51.2 μm and activation maps were distorted - though to a lesser extent than that seen with calcium loading (Figure 4.9 E, H and K). APD70 and APD90 were less affected and all effects were non-significant (Figure 4.9 F, G, I and J). This data confirms that use of 51.2 μm is unsuitable, likely due to the reduction in spatial resolution and an averaging of too many asynchronous signals.

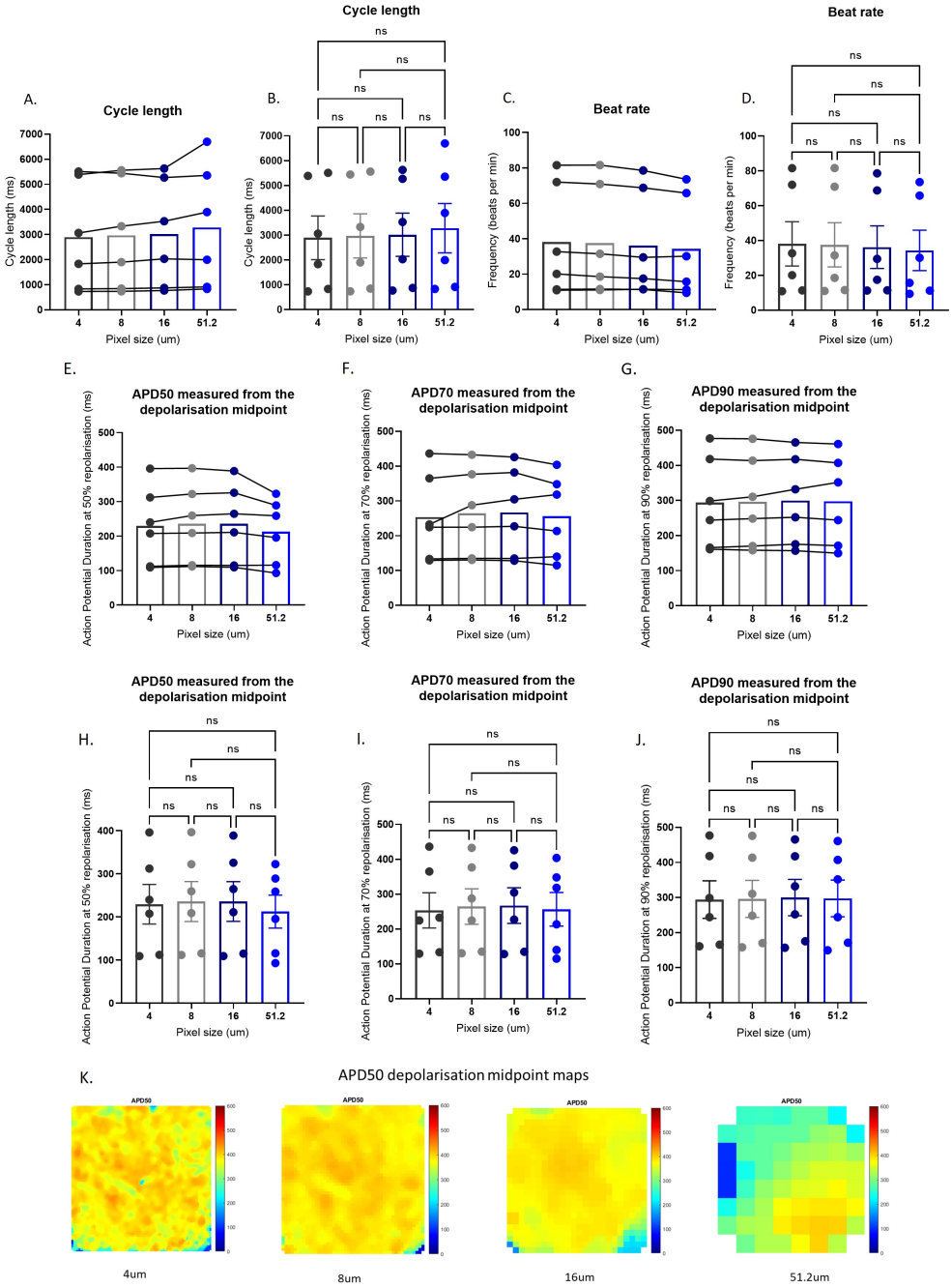


Figure 4.9: **Action potential recordings were measured in iPSC-CMs at increasing pixel size, 4, 8, 16 and 51.2 μm representative of pixel binning for 5, 10, 20 and 64 pixels.** A-B - Cycle length at increasing pixel sizes. C-D - Beat rate of iPSC-CMs at increasing pixel size. E and H - APD50 depolarisation midpoint measurements at different pixel sizes. F and I - APD70 depolarisation midpoint measurements at different pixel sizes. G and J - APD90 depolarisation midpoint measurements at different pixel sizes. A, C, and E-G show consecutive measurements from one area within one dish connected by a line whereas B, D, and H-J show the same data represented as mean $\pm$ S.E.M. with pairwise comparisons from a one-way ANOVA. K - Representative APD50 maps for depolarisation midpoint measurements at pixel size 4, 8, 16 and 51.2 μm. N = 6 dishes.

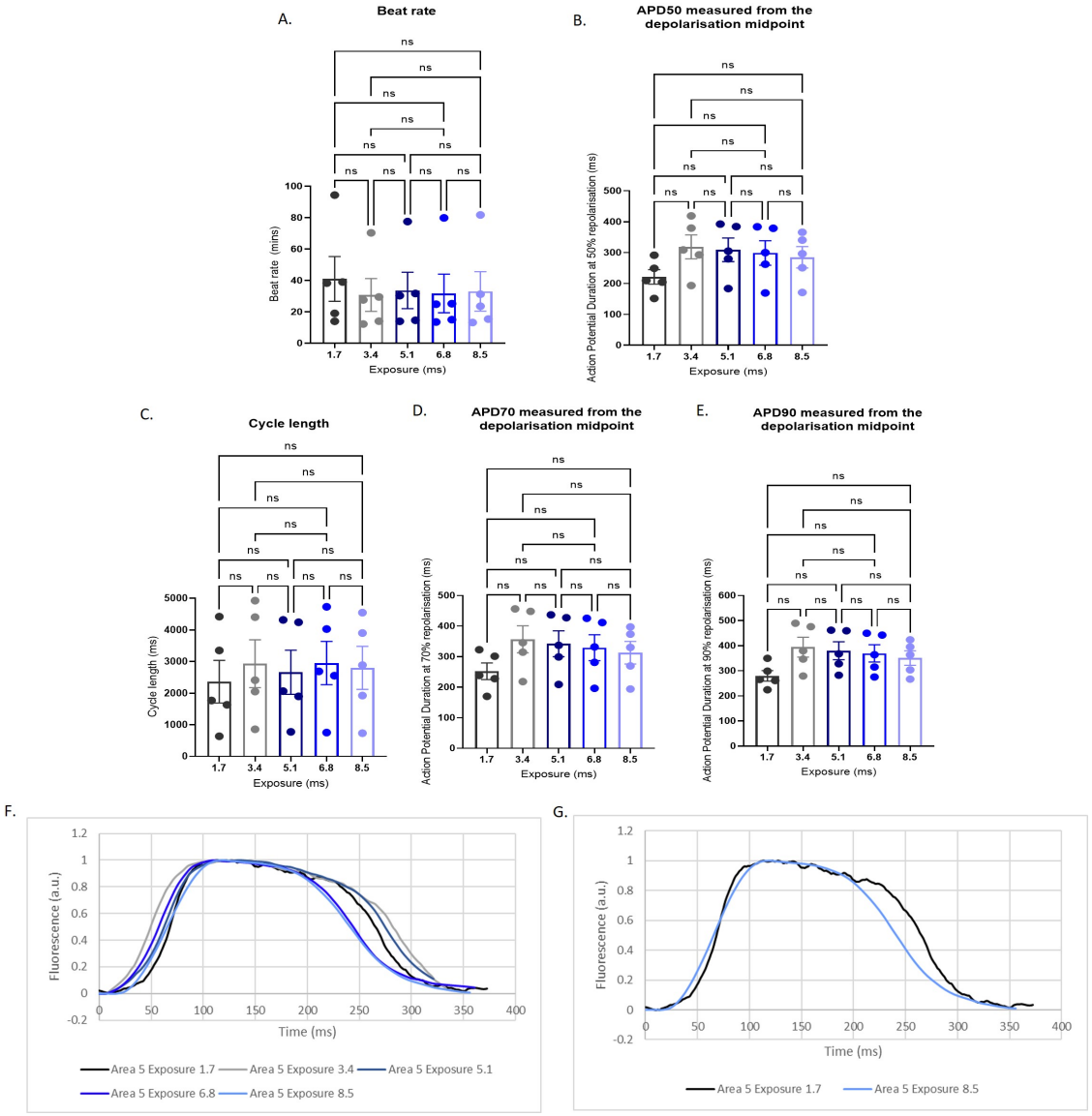


Figure 4.10: **Action potential recordings were measured at different exposure times of 1.7, 3.4, 5.1, 6.8 or 8.5 milliseconds (ms).** A - Cycle length at different exposure times. B - Beat rate at different exposure times. C-E - APD50, 70, and 90 depolarisation midpoint measurements at different exposure times. F-G - Representative example of AP measures. Data presented as mean ± S.E.M. N = 5 dishes (A-E), 1 (F-G).

Change of exposure times on voltage measurements was also investigated. Cycle length and beat rate were unaffected by a change in exposure times (Figure 4.10 A and B). As with the CTD_{50} values (Figure 4.8), there is a trend for a reduced APD value at 1.7 ms exposure (Figure 4.10 C-E). Compared to the CTD_{50} measurements, APD is reduced to a greater extent at the shorter expo-

sure times. The upstroke of an action potential is very rapid ($<$2-3ms). Therefore, the lower exposure times are better able to capture the action potential depolarisation dynamics and so more accurately quantify the activation time (either maximum upstroke velocity or peak) [131]. Hence, as observed by others, short exposure times are required to accurately measure the action potential morphology. This is demonstrated in figure 4.10 F and G where the morphology at 1.7 ms appears shows clear action potential characteristics (rapid upstroke, prolonged plateau phase followed by more rapid repolarisation). At 8.5 ms, these details appear to be 'smoothed out' (Figure 4.10 G).

Additionally, to take into account that these are freely beating cells - and without pacing - APD and CTD as a function of beat rate was investigated. This also enables examination of restitution effects. Figure 4.11 A and B show a slight negative correlation, as would be expected. However, due to the normal range of beat rate (i.e. less than 100 beats per minute), significant restitution dynamics were not observed as might be observed at faster rates where the restitution slope steepens [145, 146].

Finally, we and others have observed that dye loading can alter inherent physiology of iPSC-CMs and can detrimentally alter cells (e.g. stop them beating). We therefore sought to test whether the loading of the voltage and calcium indicators differentially affected the cells. A comparison of beat rate in Fura-2 AM and Fluovolt loaded cells shows that there is no significant effect of each dye on the beat rate (Figure 4.11 C). This shows that both dyes are tolerated to the same degree

by these cells.

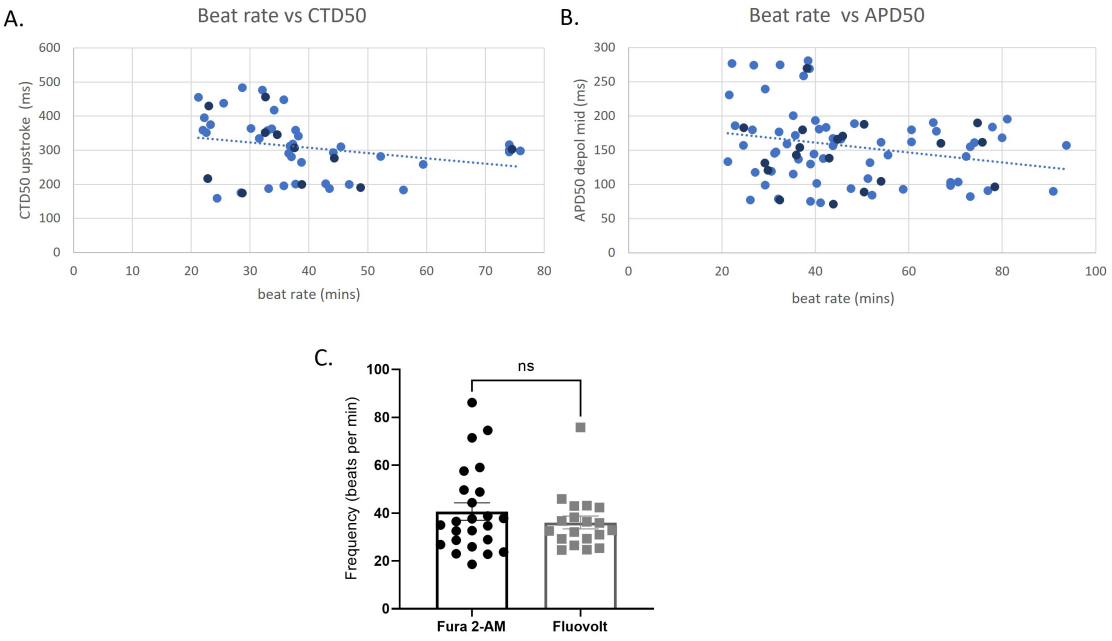


Figure 4.11: A - Correlation of beat rate with CTD_{50}. B - Correlation of beat rate with APD50. Dark blue dots represents averaged areas. C - Comparison of beat rate in Fura-2 AM and Fluovolt loaded cells. N = 41 (A), 65 (B), 19-24 (C)

Together these data indicate that the change in imaging parameters has no significant effect on calcium or voltage measurements. In general, to obtain the highest spatial and temporal resolution, this requires the smallest pixel size and the shortest exposure time, respectively. However, at these settings, the data becomes a lot larger which makes data handling more difficult. Despite this, morphologically, the action potentials look more physiological at the lower exposure time of 1.7 ms (Figure 4.10). In terms of pixel size, we observed no significant changes except at that of 51.2 μm, so 8 μm was selected (to enable the highest spatial resolution). Moving forward all optical mapping measurements will be obtained using 1.7 ms exposure time and 8 μm pixel size.

4.5 Blebbistatin does not affect the electrophysiology of iPSC-CMs

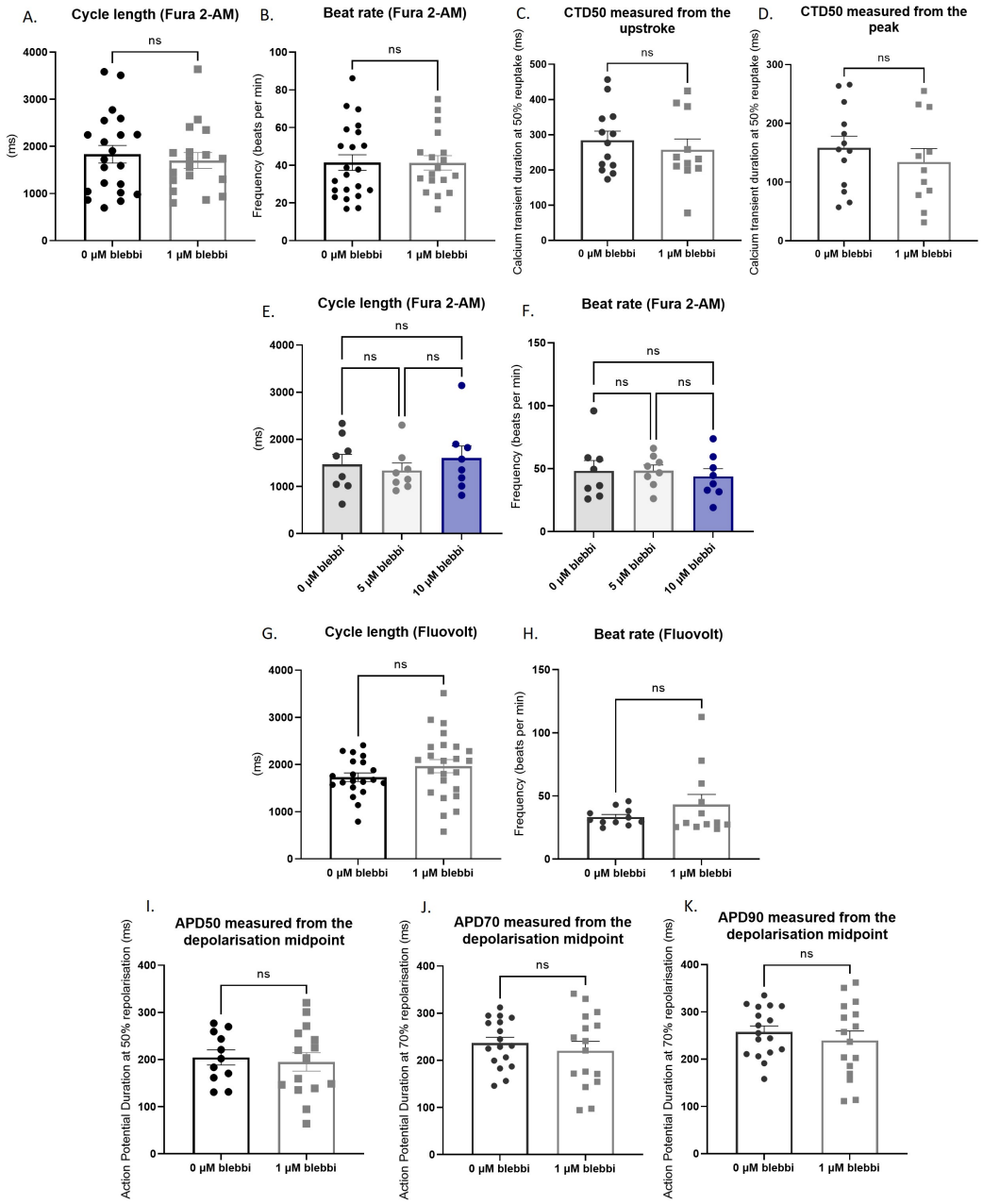


Figure 4.12: **Effect of blebbistatin on the electrophysiology of iPSC-CMs.** iPSC-CMs were loaded with 10 μM Fura 2-AM and calcium transient durations were measured in the presence or absence of blebbistatin. A-B. Cycle length and beat rate were recorded with and without 1 μM blebbistatin. C-D. CTD50 was measured from the upstroke or from the peak with or without 1 μM blebbistatin. E-F. Cycle length and beat rate were then recorded with or without 5 or 10 μM blebbistatin. iPSC-CMs were loaded with 0.5x Fluovolt dye and action potential measurements were taken at 50, 70 and 90% repolarisation. G-H. Cycle length and beat rate were also recorded with and without 1 μM blebbistatin. I-K. APD50, 70 and 90 for depolarisation midpoint measurements with and without blebbistatin. Data presented as mean $\pm$ S.E.M. N = 18-25 (A, B), 11-13 (C, D), 8 (E, F), 20-24 (G), 11-17 (H-K)

The contraction of cardiomyocytes or heart tissue while mapping distorts the recorded signals. Therefore, excitation-contraction uncouplers such as, blebbistatin or BDM (2,3-butanedione monoxime), must be utilised to suppress contraction and prevent motion artefacts [129, 130]. Existing studies have suggested that blebbistatin may have concomitant effects on cardiac electrophysiology [132]. For example, Kappadan *et al* (2020) demonstrated prolongation of the action potential in the presence of blebbistain (from 0.7 up to 2.8 μM) [133]. Therefore, the effects of blebbistatin on iPSC-CM electrophysiology was assessed.

Use of 1 μM blebbistatin had no significant effect on cycle length and beat rate of Fura-2, AM loaded iPSC-CMs, or on CTD_{50} measurements (Figure 4.12 A-D). However, it was observed, using a light microscope, that these cells continued to contract. Increased concentrations of 5 and 10 μM blebbistatin were then used and despite no significant effects on cycle length and beat rate, contraction was still observed.

When used in conjunction with Fluovolt, 1 μM blebbistatin showed no significant effects on cycle length or beat rate (Figure 4.12 G and H). There were also no effects seen on APD50, 70 or 90 (Figure 4.12 I-K). Similarly to Fura-2, AM loaded cells, Fluovolt loaded iPSC-CMs continued to contract in the presence of blebbistatin. Despite this, no contraction artefacts were seen so blebbistatin was not used moving forward for latter optical mapping experiments. The difference in signals when motion artefacts are present is displayed in figure 4.13. A possible explanation for this is that at the confluency used, each cell in the iPSC-CM is

attached directly to the plastic-ware used monolayer and thereby doesn't have the room to contract as forcefully as with whole tissues which tend to move in and out of the background.

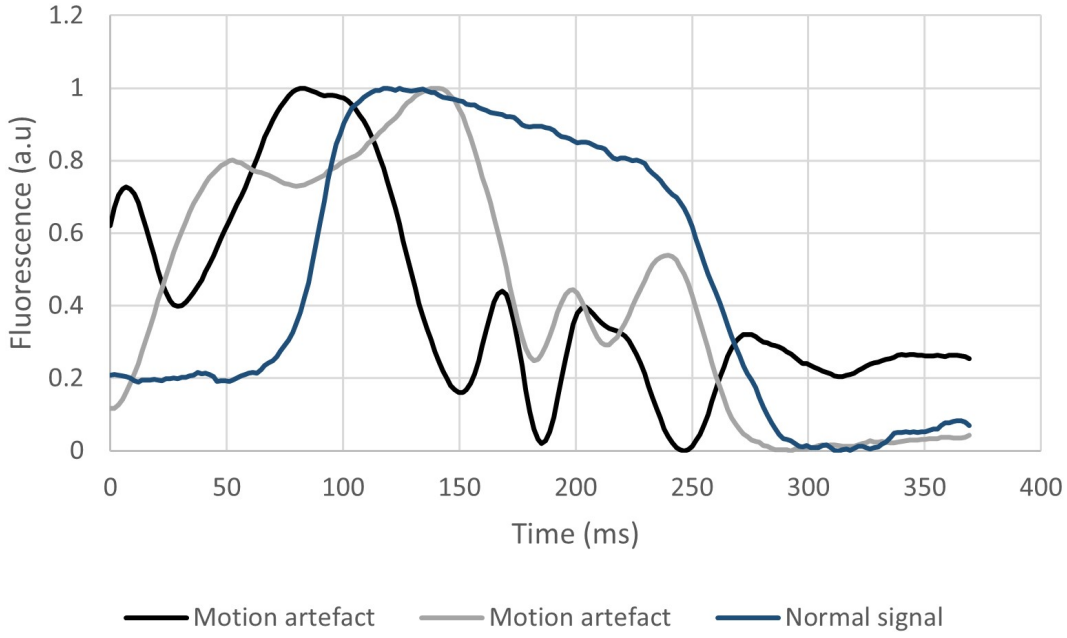


Figure 4.13: **Representation of motion artefacts recorded by optical mapping compared to a normal AP measure**

4.6 Isoprenaline induces the expected changes in calcium transient and action potential duration

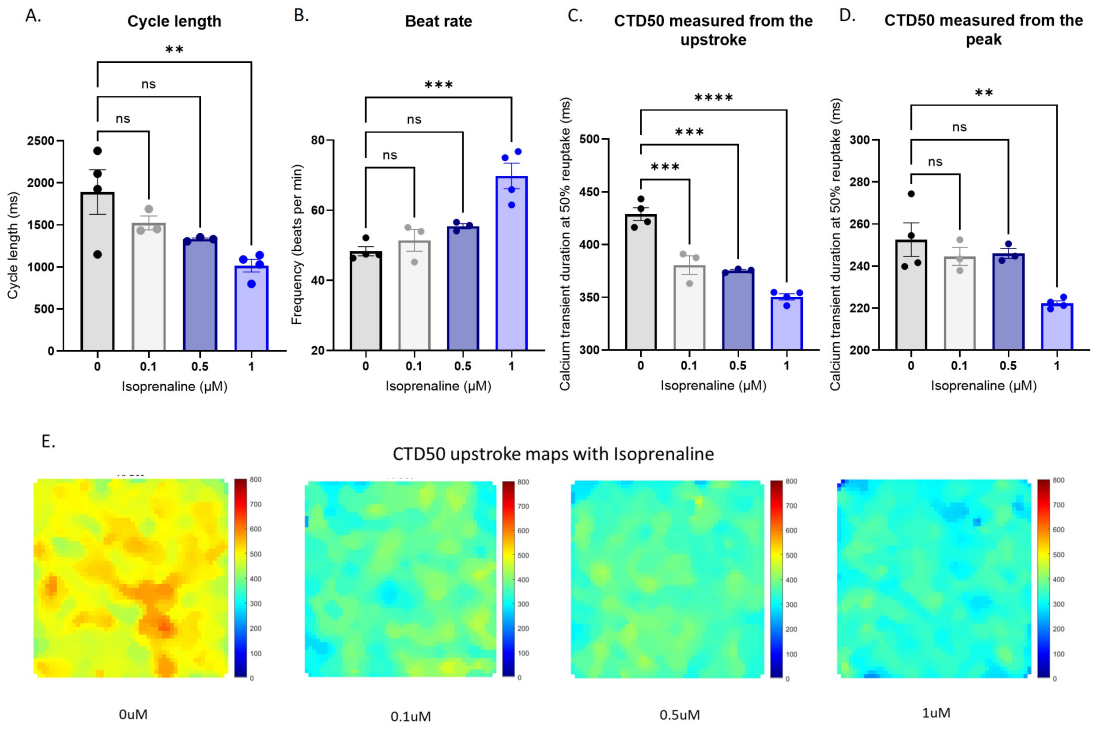


Figure 4.14: **iPSC-CMs were incubated with 0.1, 0.5 and 1 μM isoprenaline for 5 minutes before calcium transient duration measurements were recorded.** A-B - Cycle length and beat rate at different isoprenaline concentrations. C-D - CTD_{50} peak and maximum rise upstroke measurements at different isoprenaline concentrations. E - Representative CTD_{50} maximum rise upstroke maps at different concentrations of isoprenaline. Data presented as mean ± S.E.M. N = 2-5

As a final validation of our new system, we sought to investigate the response of the iPSC-CMs to pharmacological stimuli. Isoprenaline is a non-selective β adrenoceptor agonist that acts to increase beat rate and shorten APD and CTD_{50} in cardiomyocytes [147]. It was used here to validate our optical mapping system. iPSC-CMs demonstrated a dose-response relationship in the presence of increasing concentrations of isoprenaline in terms of calcium handling (Figure 4.14). There was a trend toward decreasing cycle length and increasing beat rate with increasing concentrations of isoprenaline. Significance was only seen at the highest concentration of 1 μM isoprenaline (Figure 4.14 A and B). There was a significant decrease in CTD_{50} when measured from the maximum rise upstroke at all concentrations of isoprenaline from 0.1 to 1 μM (Figure 4.14 C). When CTD_{50} was measured from the peak there was still a trend towards decreasing CTD_{50} but significance was only seen at 1 μM (Figure 4.14D). Representative maps demonstrate well the decrease in CTD_{50} when in the presence of isoprenaline from roughly 500 ms to 350 ms (Figure 4.14 E).

Voltage dynamics responded similarly to isoprenaline (Figure 4.15). Cycle length decreased in the presence of 0.1 and 0.5 μM isoprenaline while beat rate, inversely proportional to cycle length, increased (Figure 4.15 A and B). APD50, 70, and 90 all decrease stepwise from 0 to 0.5 µM isoprenaline for both peak and depolarisation midpoint measurements (Figure 4.15 C-E). All data were non-significant. An unusual side effect of the addition of isoprenaline to iPSC-CMs was for the cells to stop contracting making obtaining data for the cells difficult.

Taken together, these data show initial validation of the use of our setup to observe pharmacologically induced changes in the electrophysiological behaviour of iPSC-CMs. However, the detrimental effect of isoprenaline in several experiments requires further investigation.

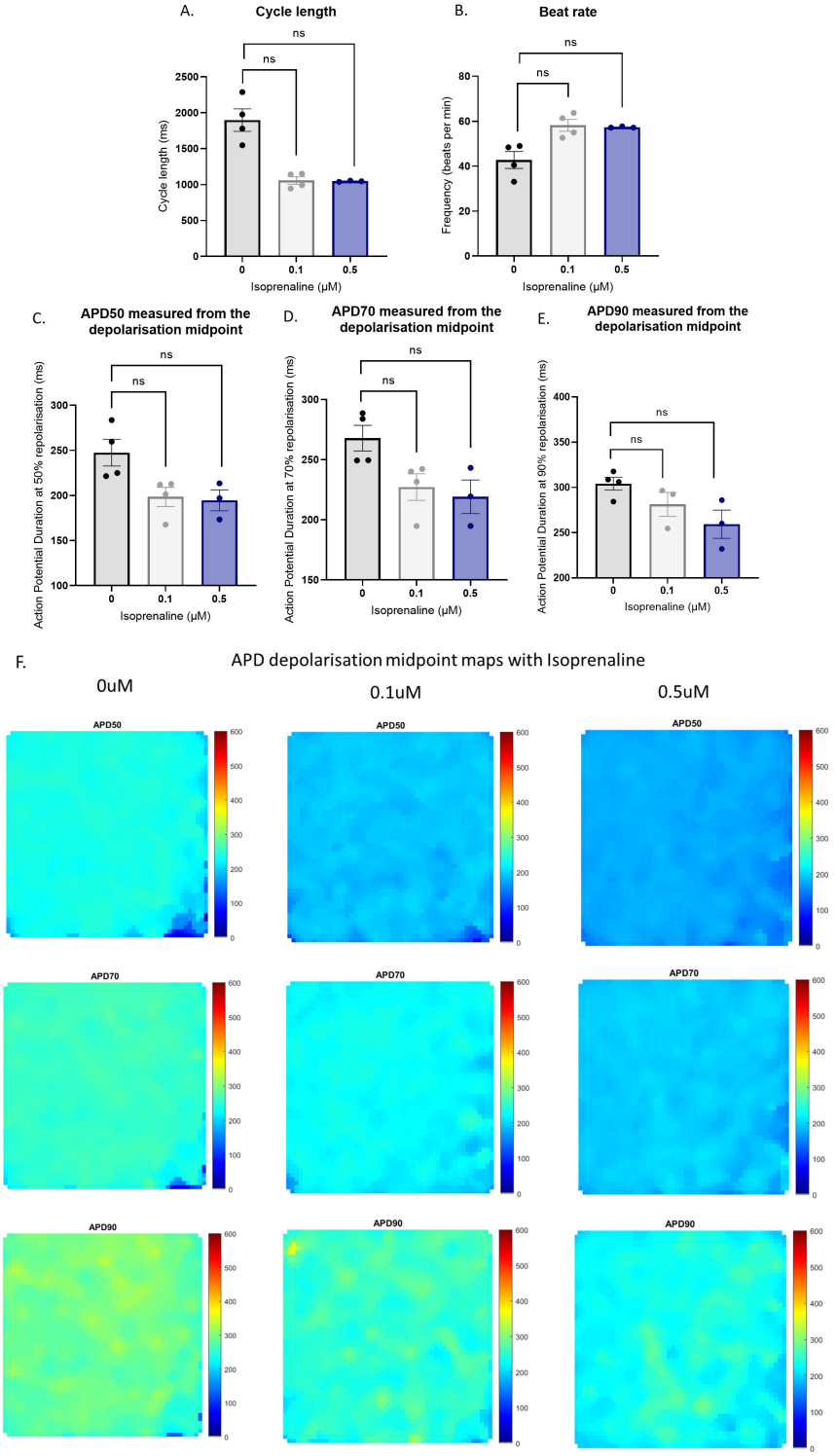


Figure 4.15: **iPSC-CMs were incubated with 0.1, 0.5 µM isoprenaline for 5 minutes before action potential duration measurements were recorded at 50, 70 and 90% repolarisation.** A-B - Cycle length and beat rate at different isoprenaline concentrations. C-E - APD50, 70 and 90 depolarisation midpoint measurements at different isoprenaline concentrations. F. Representative APD50, 70 and 90 depolarisation midpoint maps at different concentrations of isoprenaline. Data presented as mean ± S.E.M. N = 1-2

4.7 Discussion

Optical mapping is an important technique for studying cardiac electrophysiology that provides higher spatial resolution than standard electrode techniques [144]. In this chapter, a new optical mapping system was optimised for use with iPSC-CM monolayers. Analysis of multiple different imaging parameters found that 1.7ms exposure and a pixel size of 8 μm was optimal for imaging of 2D iPSC-CM monolayers. Successful validation of the system was achieved through a demonstration of the appropriate dose response in the presence of isoprenaline.

4.7.1 Selecting the appropriate imaging parameters

The rapid propagation of the cardiac action potential requires high acquisition rates but this can lead to low signal-to-noise ratios [144, 148]. In order to image electrophysiology in cardiomyocytes, the general requirements are a temporal resolution of greater than 500 Hz and a spatial resolution of less than 100 μm [149]. Inappropriate image acquisition can lead to misinterpretation of optical signals and their physiological relevance [144, 148]. This dictates the importance of optimizing optical mapping systems prior to use.

It was observed that there was no significant difference at any of the pixel sizes tested for both calcium and voltage, however, there was an obvious distortion of the optical signal at 51.2 μm during calcium loading. iPSC-CMs are smaller than adult CMs, ranging from 20-70 μm, and calcium release throughout the cell is not uniform, meaning that such a large bin size is likely averaging asynchronous signals [150]. Similar studies using iPSC-CMs for optical mapping have used smaller

pixel sizes of 4 and 6.9 μm but no significant differences were observed between 4 and 8 μm [151, 152]. Therefore, to provide a more manageable dataset (in terms of computer storage), 8 μm was used.

It was also observed that there was no significant difference at any of the exposure times tested for both calcium and voltage. However, the calcium upstroke and the depolarisation phase of an action potential both occur on a millisecond scale. The observation of a more action potential like morphology at the lowest exposure time led us to choose a 1.7ms exposure time for imaging. This reflects a frame rate of 588 fps (frames per second). Heinson *et al* (2023) used a similar rate of 525 fps for imaging of iPSC-CMs [152]. Others have used both higher (992 fps) and lower (130fps) frame rates but obtained similar results, dictating the importance of choosing the right parameters for the individual camera and set up [141, 153].

4.7.2 Blebbistatin

Blebbistatin is often used in optical mapping studies in order to stop contraction [141, 129]. It acts to inhibit myosin II to prevent motion artefacts without having any effects on electrophysiology [154, 129]. However, as discussed at the beginning of this chapter, there are newer reports that blebbistatin does in fact have some effects on electrophysiology, depending on the model used [132, 133, 155]. In this chapter, it was observed that using up to 10 μM blebbistatin had no effect on the electrophysiology of iPSC-CMs. However, interestingly, blebbistatin also had no effect on contraction in the iPSC-CMs. To our knowledge, this is the first

observation of this kind to be reported. In the work presented here, the issue of contraction artefacts was largely circumvented by using a lower magnification. This managed to allow us to avoid contraction artefacts while still being able to obtain a clear signal.

Issues such as these have led more people towards the use of computational approaches to avoid contraction artefacts. A new study by Woodhams *et al* (2023) has demonstrated that blebbistatin may, in fact, have some small but significant effects on iPSC-CM sarcomeres and electrophysiology. They instead describe the use of computer processing to remove motion without pharmacological inhibition [155]. As computational methods such as these become more widespread, it may remove the need for a contraction uncoupler altogether allowing more accurate and representative data to be collected.

4.7.3 Pacing

It is common practice to pace cells when recording electrophysiology. This allows us to account for any variability in beat rate, and the effects beat rate will have on cardiac electrophysiology. iPSC-CMs are generally paced at 1 Hz to reflect the average human heart rate of 60 beats per minute [141, 150]. Pacing can be achieved via point stimulation or field stimulation. The benefits of point stimulation are that it allows for the recording of conduction velocity as well as action potential dynamics.

Unfortunately, the iPSC-CMs used in this study were unresponsive to both field and point stimulation allowing only the recording of spontaneous activity. One of

the main limitations of this is an increase in variability in part due to the heterogeneity of iPSC-derived CMs. Wei *et al* (2020) demonstrated how pacing can significantly reduce plate-to-plate variability as well as reduce the variability in drug response [156]. This ultimately allows for more precise identification of authentic physiological responses.

The spontaneous beating of iPSC-CMs is also indicative of their immature phenotype. There is evidence that pacing can provide a form of electrical maturation [157, 158, 159]. Use of electrical stimulation has led to increases in expression of maturation-related genes such as α-MHC, cTnT, and RYR2, as well as, more structured sarcomeres [159, 160]. Pacing is also something that happens *in vivo*, starting at the sinoatrial node [1, 2]. Without it, our iPSC-CM model is less physiologically relevant.

Moving forward, it will be important to work towards a paceable iPSC-CM model and system in order to provide more reproducible and physiologically relevant results.

4.7.4 Conclusion

Set up and validation of this optical mapping system has not only allowed me to interrogate fibroblast and CM dynamics (results chapter 3) but has provided a methodology for other groups to use. Since completion, it has been used by the Gehmlich group to interrogate the effects of Titin mutations on iPSC-CM electrophysiology (paper in preparation), as well as the effects of culturing iPSC-CMs on

varying substrate stiffness.

Chapter 5

Effects of co-culture with cardiac fibroblasts on electrophysiology and contraction of iPSC-cardiomyocytes

Cardiac fibroblasts are one of the most abundant cell types in the heart. They provide structural support for cardiomyocytes and have an important role following cardiac injury. In recent years, cardiac fibroblasts have been found to have both direct and indirect effects on cardiomyocyte electrophysiology [42, 50, 161]. In this chapter, the effects of co-culture with quiescent cardiac fibroblasts and activated MyoFbs on cardiomyocyte electrophysiology are examined using iPSC-derived cells and optical mapping. This has previously predominantly been done using animal models [42, 50, 123, 161].

5.1 Culture of iPSC-CMs with SB431542 for 2 days has no effect on contraction or electrophysiology

iPSCs were differentiated into cardiac fibroblasts and cardiomyocytes using established protocols [126, 99]. iPSC-cFbs are maintained as quiescent in culture by using TGF-β receptor 1 inhibitor SB431542 (see section 3.4). Research suggests that in the human heart cardiomyocytes make up roughly 75$\%$ by volume

but that cardiomyocytes and cardiac fibroblasts are roughly 50-50 in terms of cell number, about 30-40$\%$ each [4, 6] (see section 1.1). When optimising co-cultures it is important to acknowledge that cardiac fibroblasts are proliferative, whereas cardiomyocytes are not. Therefore, these two cell types cannot be kept in co-culture indefinitely as the cardiac fibroblasts will run out of space to grow and potentially take over the culture. It is also important when thinking about physiological cell numbers to consider that iPSC-CMs are generally smaller than adult cardiomyocytes.

As mentioned in section 3.4, iPSC-cFbs must be cultured in the presence of a TGF-β receptor inhibitor (SB) to prevent activation to MyoFbs [126]. iPSC-CMs were therefore assessed in the presence and absence of SB to ensure possible effects were down to the co-cultures themselves and not the presence of the inhibitor.

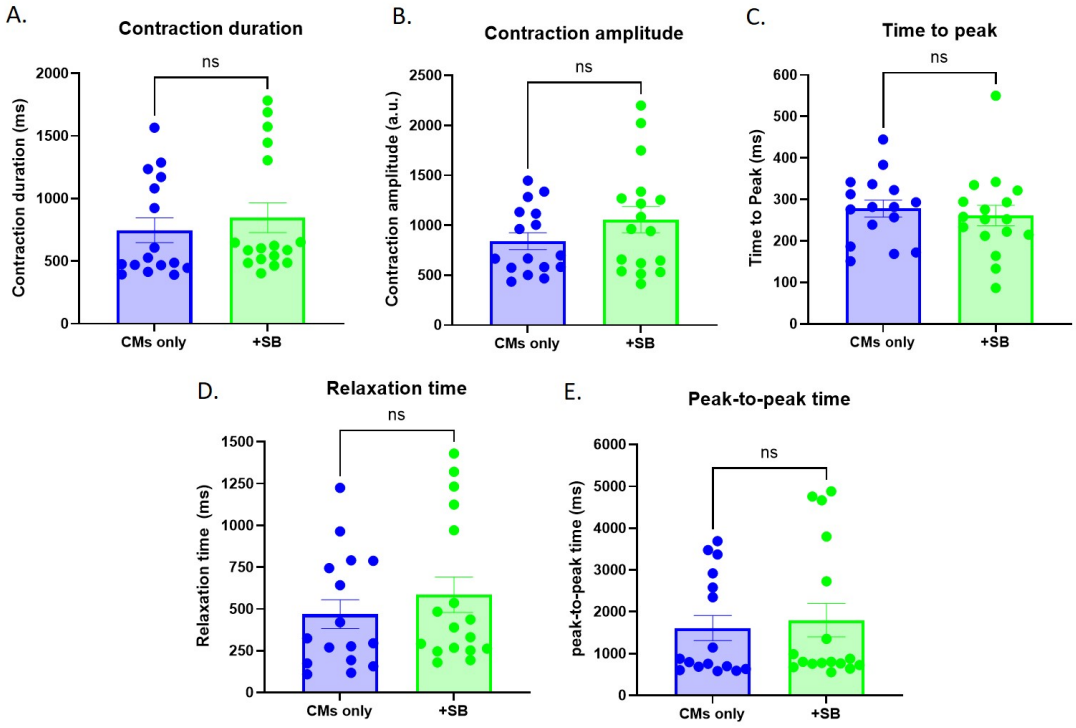


Figure 5.1: **Contraction of iPSC-CMs in the presence or absence of a TGF-β receptor inhibitor.** iPSC-CMs were cultured in the presence or absence of 10 μM SB431542 for 2 days and contraction was assessed using MUSCLEMOTION. A - Contraction duration in the presence or absence of SB. B - Contraction amplitude in the presence or absence of SB. C - Time to peak in the presence or absence of SB. D - Relaxation time in the presence or absence of SB. E - Peak-to-peak time in the presence or absence of SB. Data presented as mean $\pm$ S.E.M. N = 10 batches of iPSC-CMs, n = 1-2 dishes

Contraction was measured using MUSCLEMOTION [162]. Contraction duration and relaxation time are the time it takes for the cells to contract and relax. Contraction amplitude refers to the force of contraction, time to peak refers to the speed of contraction, and peak-to-peak time refers to cycle length (inverse to beat rate). Figure 5.1 shows that there is no significant difference between the SB-treated cells and the untreated controls for any of the contraction parameters measured.

Following contraction measurements, iPSC-CMs were then loaded with Fura-2, AM or Fluovolt. When loaded with Fura-2, AM, similarly there was no significant

effect on cycle length of beat rate in SB-treated versus untreated controls (Figure 5.2 A and B). There was also no significant difference in CTD_{50} measurements of SB-treated iPSC-CMs either measured from the maximum rise upstroke or the peak when compared to the untreated controls, suggesting no changes in calcium inward current, release, extrusion or reuptake caused by SB. (Figure 5.2 C and D).

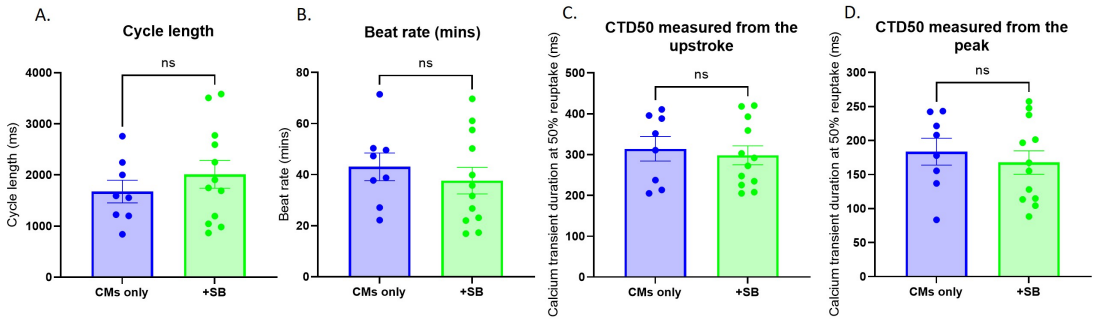


Figure 5.2: **Calcium handling of iPSC-CMs in the presence or absence of a TGF-β receptor inhibitor.** iPSC-CMs were cultured in the presence or absence of 10 μM SB431542 for 2 days and loaded with 10 μM Fura-2, AM for optical mapping. A - Cycle length in the presence or absence of SB. B - Beat rate in the presence or absence of SB. C - CTD_{50} measured from the maximum rise upstroke in the presence or absence of SB. D - CTD_{50} measured from the peak in the presence or absence of SB. Data presented as mean $\pm$ S.E.M. N = 5 batches of iPSC-CMs, n = 1-2 dishes.

When iPSC-CMs were loaded with Fluovolt, there was no significant difference observed in cycle length or beat rate in the SB-treated iPSC-CMs when compared to the untreated controls (Figure 5.3 A and B). There was also no significant difference in APD50, 70 or 90 (Figure 5.3 C-E).

This data demonstrates that the presence of TGF-β receptor inhibitor SB for 2 days has no significant effect on the contraction or electrophysiology of iPSC-CMs.

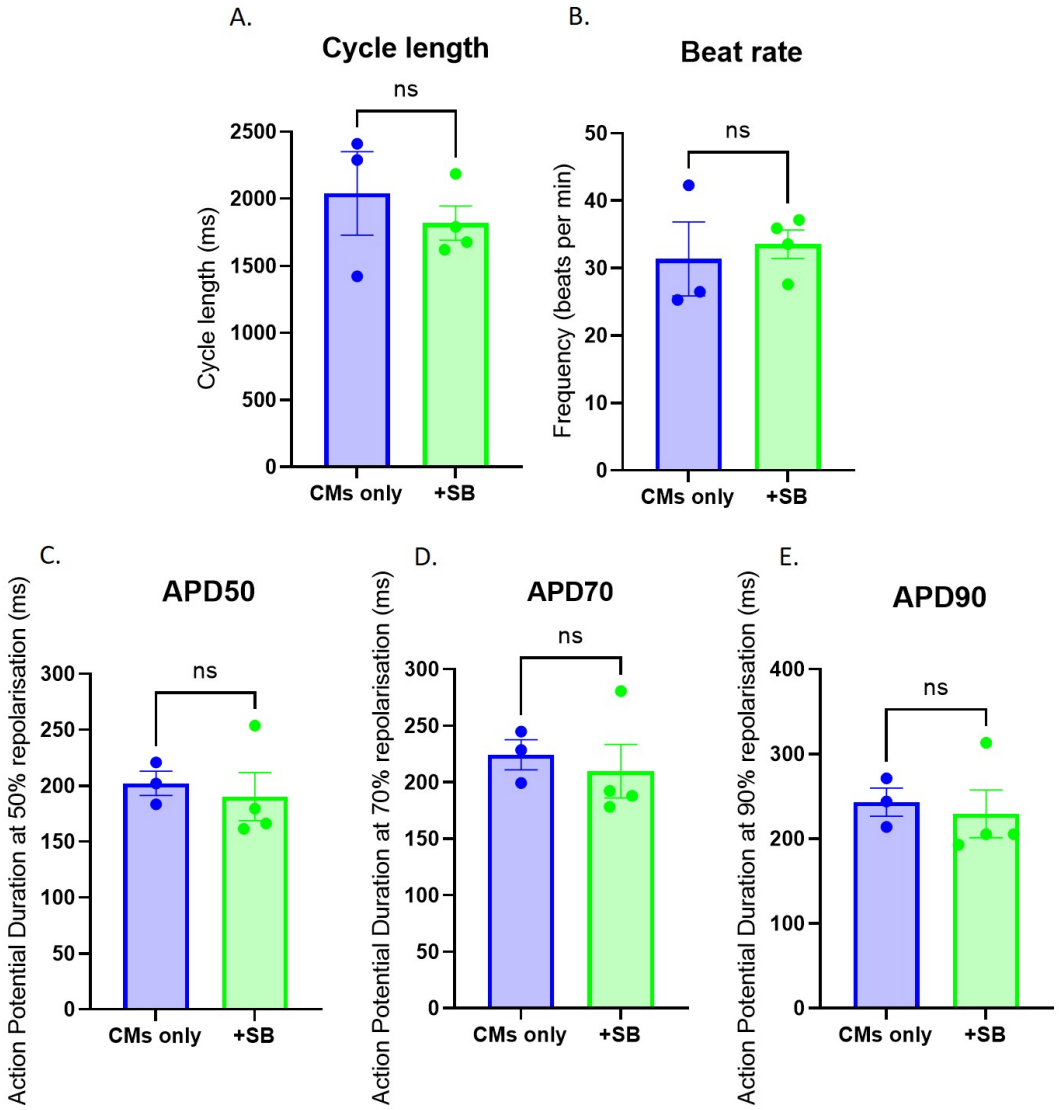


Figure 5.3: **Voltage handling of iPSC-CMs in the presence of absence of a TGF-β receptor inhibitor.** iPSC-CMs were cultured in the presence or absence of 10 μM SB431542 for 2 days and loaded with 10 μM Fluovolt for optical mapping. A - Cycle length in the presence or absence of SB. B - Beat rate in the presence or absence of SB. C-E - APD measurements in the presence or absence of SB. Data presented as mean $\pm$ S.E.M. N = 3 batches of iPSC-CMs, n = 1-2 dishes.

5.2 Co-culture of cardiomyocytes with cardiac fibroblasts for 2 days has no effect on contraction or electrophysiology

For initial co-culture experiments, three ratios of cardiomyocyte to cardiac fibroblast were tested - 2:1 (33% fibroblasts), 5:1 (16% fibroblasts) and 10:1 (11% fi-

broblasts) (Figure 5.4). 2:1 is considered the most physiological in terms of cell numbers in the adult human heart, however, with iPSC-CMs being smaller than adult cardiomyocytes, 5:1 or 10:1 is considered to be more physiological in terms of direct fibroblast to cardiomyocyte connections. Both contraction and electrophysiology of the co-cultures were assessed after 2 days.

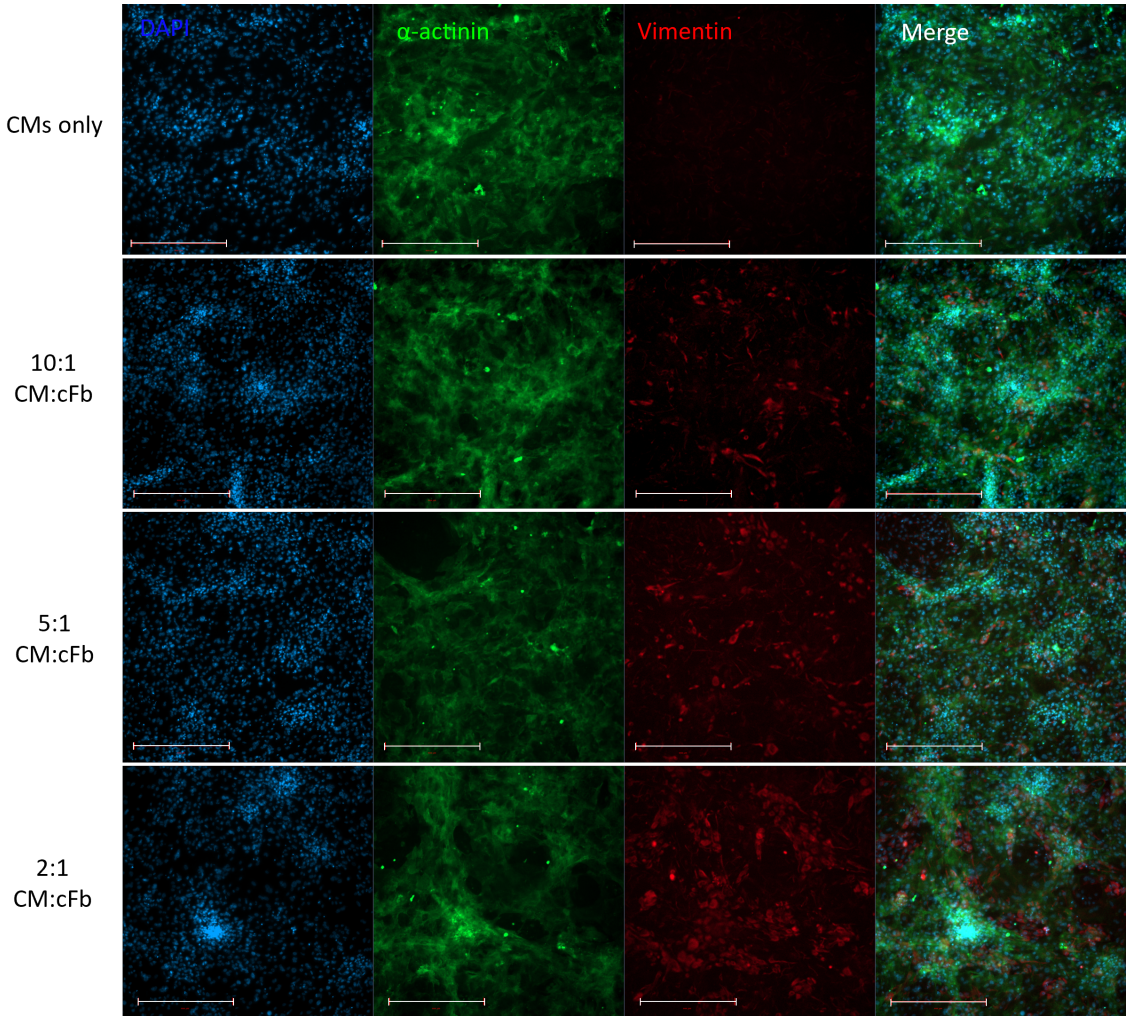


Figure 5.4: **Immunofluorescent staining of iPSC-CM-iPSC-cFb co-cultures.** iPSC-cFbs were seeded ontop of iPSC-CMs at three different ratios - 2:1 (33% fibroblasts), 5:1 (16% fibroblasts) and 10:1 (11% fibroblasts). Cells were fixed after 2 days of culture following optical mapping. DAPI is in blue for nuclear staining. α-actinin is in green as a marker for cardiomyocytes. Vimentin is in red as a marker for cardiac fibroblasts. Scale bar is 500 μm.

When iPSC-CMs were cultured with quiescent iPSC-cFbs (+SB) for 2 days,

there was no significant change in any of the contraction parameters measured with any of the three different ratios tested.

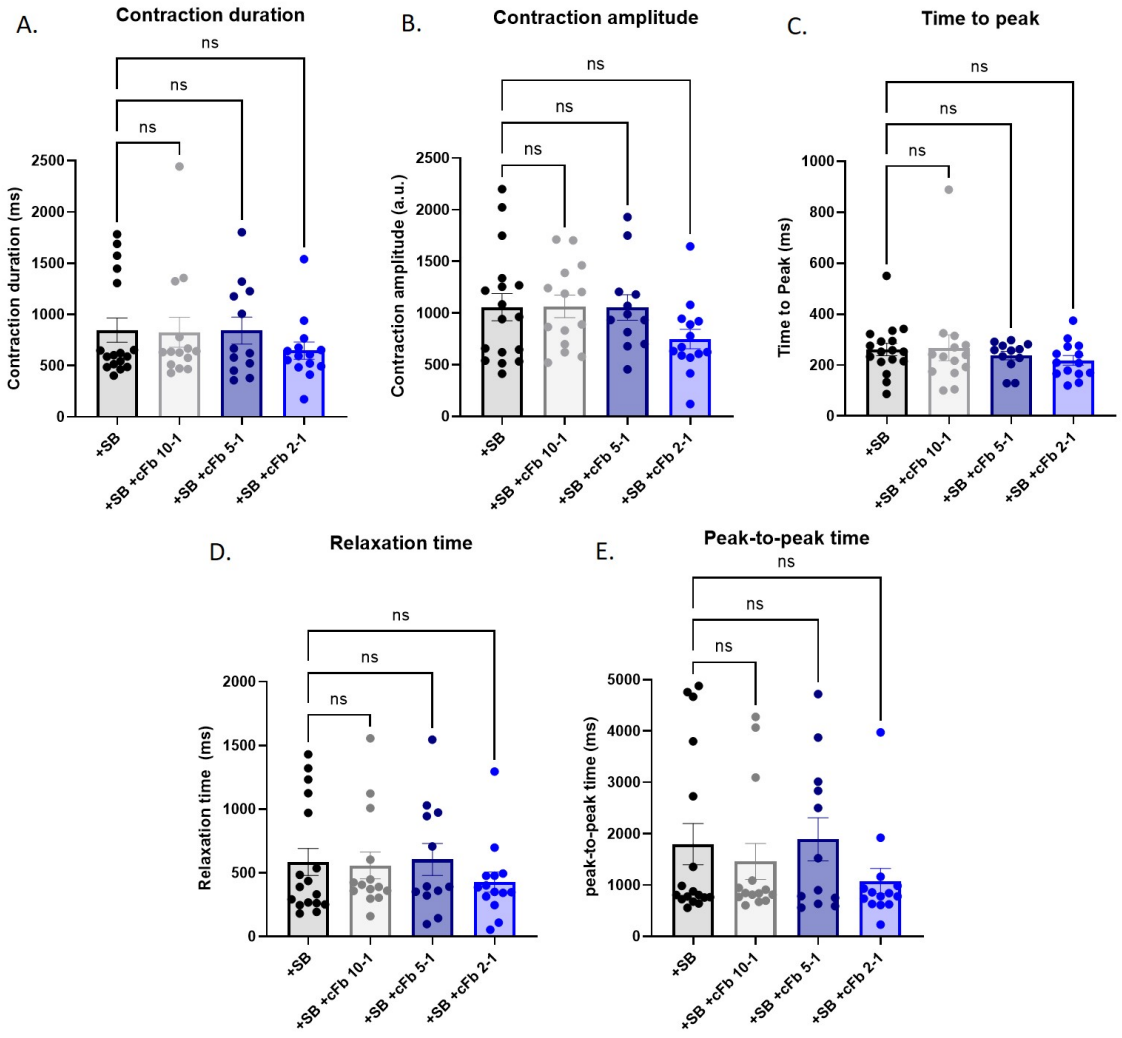


Figure 5.5: **Contraction of iPSC-CMs in the presence of different ratios of quiescent iPSC-cFbs.** iPSC-CMs were cultured with 3 different ratios of quiescent iPSC-cFbs for 2 days and contraction was measured using MUSCLEMOTION. A - Contraction duration in the presence of 11% (10:1), 16% (5:1) or 33% (2:1) iPSC-cFbs. B - Contraction amplitude in the presence of 11% (10:1), 16% (5:1) or 33% (2:1) iPSC-cFbs. C - Time to peak in the presence of 11% (10:1), 16% (5:1) or 33% (2:1) iPSC-cFbs. D - Relaxation time in the presence of 11% (10:1), 16% (5:1) or 33% (2:1) iPSC-cFbs. E - Peak-to-peak time in the presence of 11% (10:1), 16% (5:1) or 33% (2:1) iPSC-cFbs. Data presented as mean ± S.E.M. N = 10 batches of iPSC-CMs, n = 1-2 dishes

When loaded with Fura-2, AM, iPSC-CM-cFb co-cultures at all three ratios

showed no significant difference in cycle length or beat rate when compared to the iPSC-CMs alone (Figure 5.6 A and B). Although there was a trend towards decreased CTD_{50} at a co-culture ratio of 2:1, there were low n numbers so we cannot say whether this would be significant or not (Figure 5.6 C and D). The higher the concentration of fibroblasts, the less well tolerated the calcium dye was. These co-cultures often stopped beating following the dye loading process, with only 2 dishes surviving (Figure5.6). This was also seen when using Fluovolt, where none of the 2:1 co-cultures survived (Figure 5.7). Similarly, when loaded with Fluovolt, iPSC-CM-cFb co-cultures showed no significant differences in cycle length or beat rate when compared to iPSC-CMs alone (Figure 5.7 A and B). There was also no significant differences in APD50, 70 or 90 (Figure 5.7 C-E).

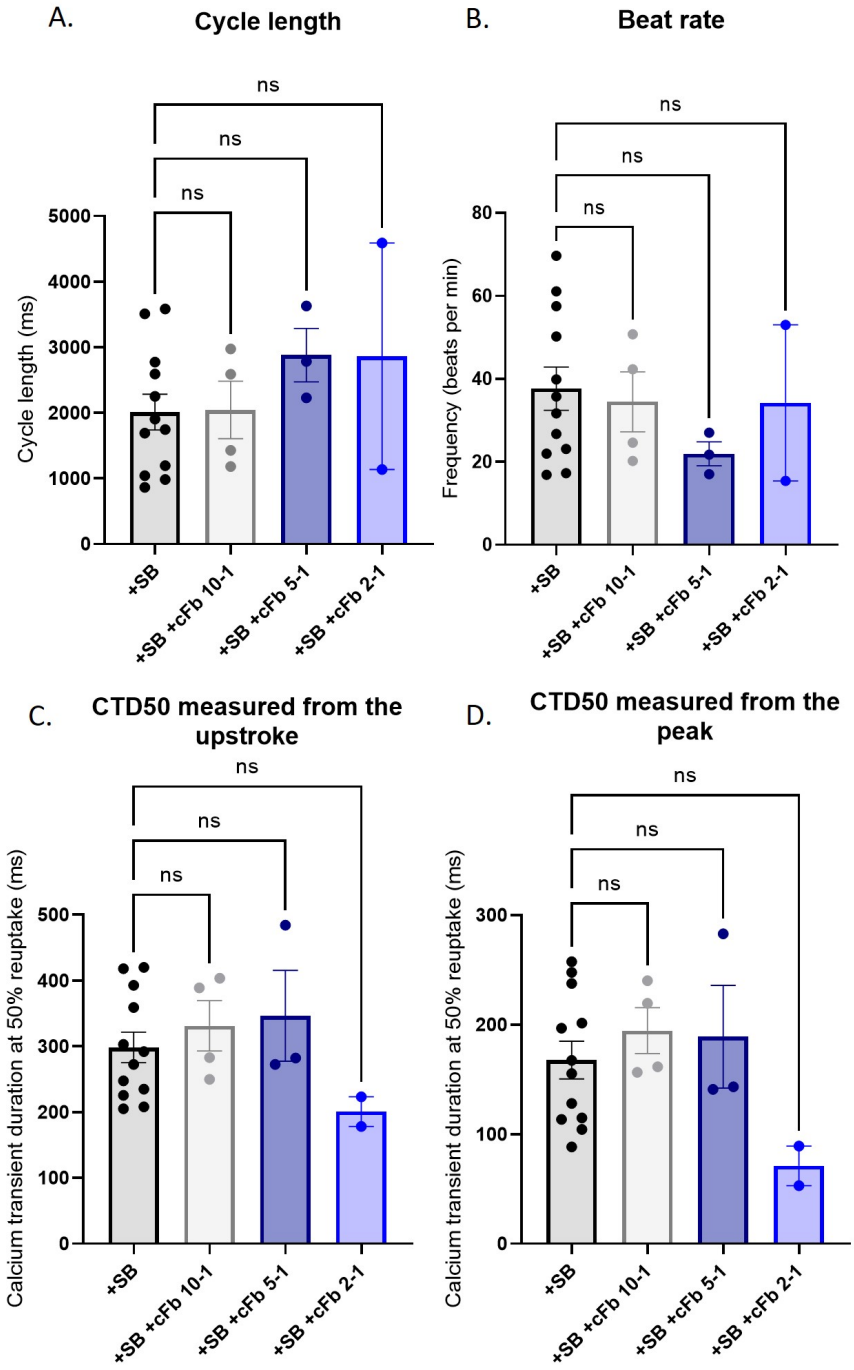


Figure 5.6: **Calcium handling of iPSC-CMs in the presence of different ratios of quiescent iPSC-cFbs.** iPSC-CMs were cultured with 3 different ratios of quiescent iPSC-cFbs for 2 days and then loaded with 10 μM Fura-2, AM. A - Cycle length. A - Cycle length in the presence of 11% (10:1), 16% (5:1) or 33% (2:1) iPSC-cFbs. B - Beat rate in the presence of 11% (10:1), 16% (5:1) or 33% (2:1) iPSC-cFbs. C - CTD_{50} measured from the maximum rise uptstroke in the presence of 11% (10:1), 16% (5:1) or 33% (2:1) iPSC-cFbs. D - CTD_{50} measured from the peak in the presence of 11% (10:1), 16% (5:1) or 33% (2:1) iPSC-cFbs. Data presented as mean $\pm$ S.E.M. N = 2-12 dishes.

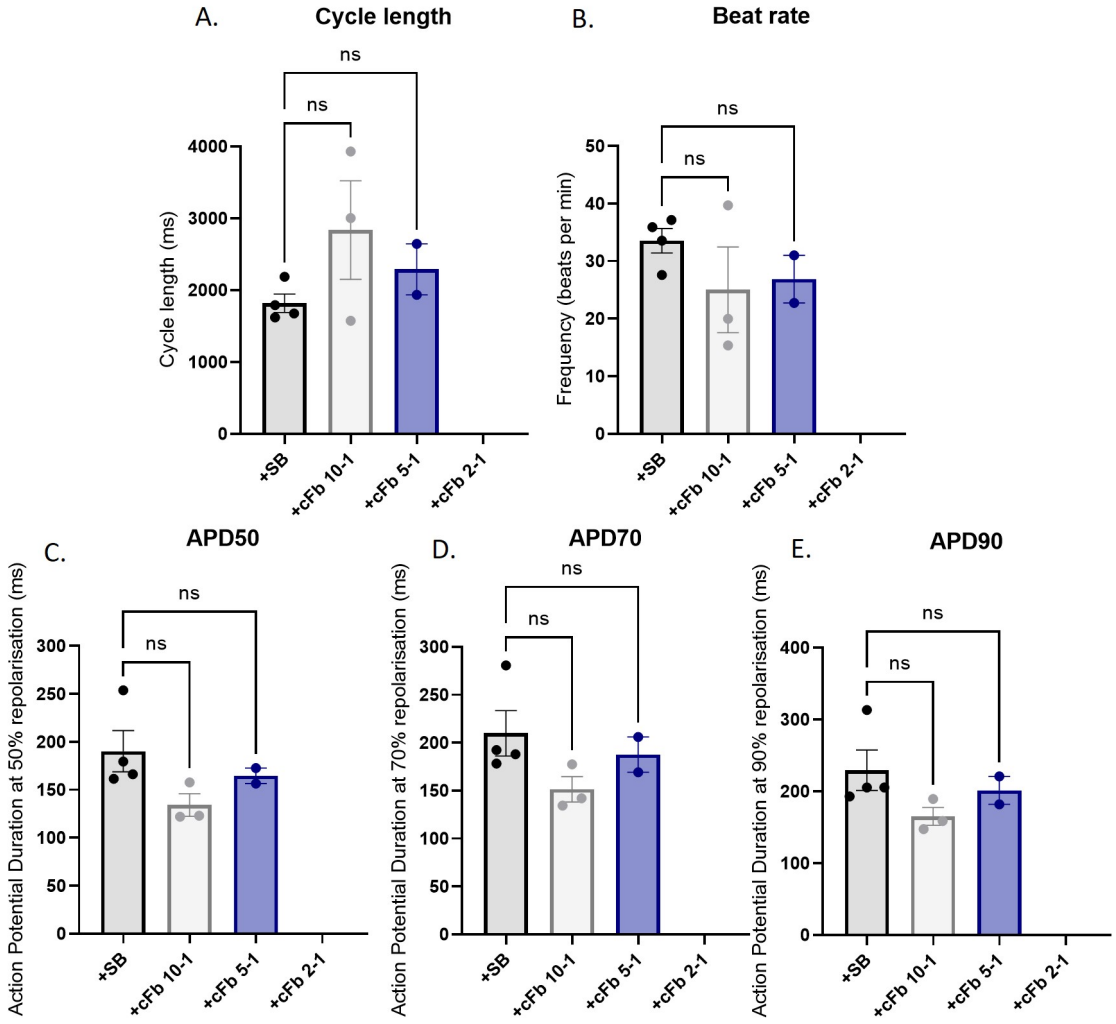


Figure 5.7: **Voltage handling of iPSC-CMs in the presence of different ratios of quiescent iPSC-cFbs.** iPSC-CMs were cultured with 3 different ratios of quiescent iPSC-cFbs for 2 days and then loaded with 0.5x Fluovolt. A - Cycle length. A - Cycle length in the presence of 11% (10:1), 16% (5:1) or 33% (2:1) iPSC-cFbs. B - Beat rate in the presence of 11% (10:1), 16% (5:1) or 33% (2:1) iPSC-cFbs. C - CTD_{50} measured from the maximum rise uptstroke in the presence of 11% (10:1), 16% (5:1) or 33% (2:1) iPSC-cFbs. D - CTD_{50} measured from the peak in the presence of 11% (10:1), 16% (5:1) or 33% (2:1) iPSC-cFbs. Data presented as mean ± S.E.M. N = 2-4 dishes.

This data demonstrates that co-culture of iPSC-CMs with between 11 and 33% iPSC-cFbs for 2 days has no significant effect on contraction. It also suggests there is no effect on electrophysiology, however, this needs further confirmation. Interestingly, a higher number of fibroblasts caused a decrease in dye tolerance for both Fura-2, AM and Fluovolt. Why these cells are more susceptible

to cytotoxicity compared to the iPSC-CMs warrants further investigation.

5.3 Co-culture of cardiomyocytes with cardiac fibroblasts for 5 days has no effect on contraction and electrophysiology

Having seen no effects after 2 days of co-culture, longer culture times of 5 days were investigated. The concentration of 10:1 iPSC-CM to iPSC-cFb (11$\%$ fibroblasts) was used moving forwards due to the lack of success and low viability of the higher concentrations (Section 5.2). The effects of activated versus quiescent fibroblast were also investigated. This was achieved through culture in the presence of SB or TGF-β. The activation time course (Section 3.4.2) helped to inform the 5-day culture time used here as peak α-SMA was seen around 96 hours, past which we begin to enter chronic activation of MyoFbs. Representative images can be seen in figure 5.8.

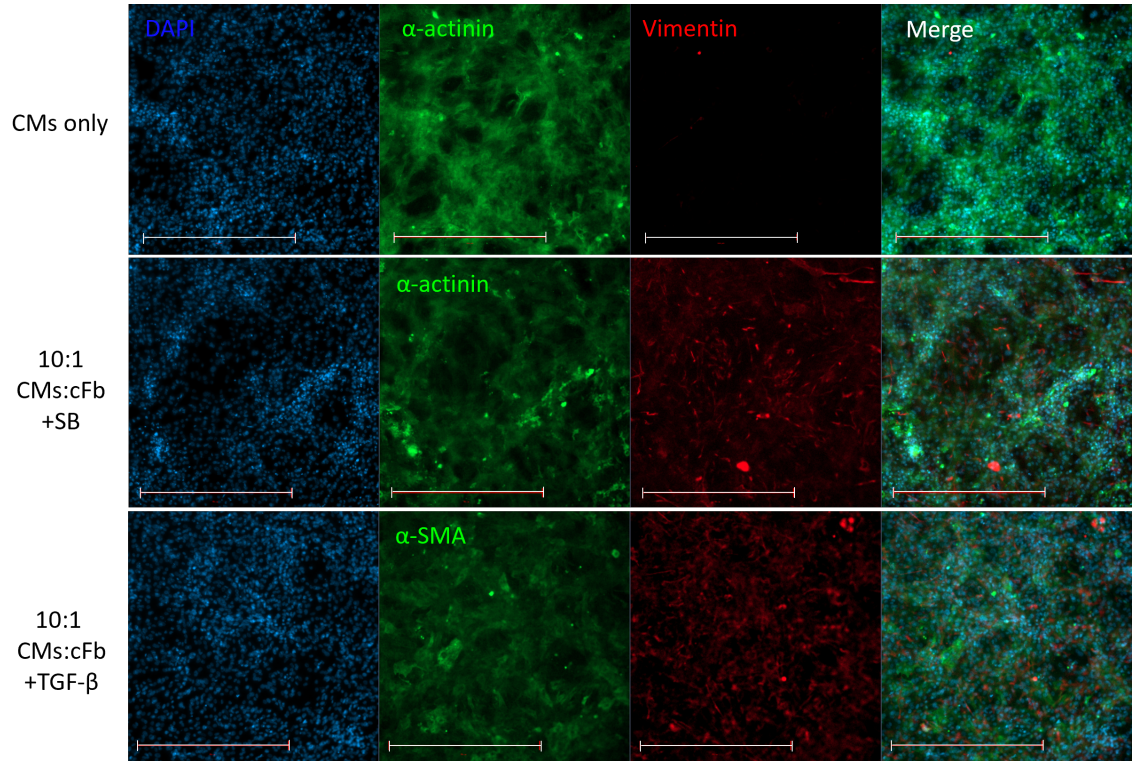


Figure 5.8: **Immunofluorescent staining of iPSC-CM-iPSC-cFb co-cultures.** iPSC-cFbs were seeded ontop of iPSC-CMs at a ratio of 10:1 (11% fibroblasts) in the presence of SB or TGF-β. Cells were fixed after 5 days of culture following optical mapping. DAPI is in blue for nuclear staining. α-actinin is in green as a marker for cardiomyocytes. Vimentin is in red as a marker for cardiac fibroblasts. Scale bar is 500 μm.

The majority of the contraction parameters recorded showed no significant difference between iPSC-CMs alone, with SB or TGF-β, or with quiescent or activated iPSC-cFbs (Figure 5.9 A, B, D and E). However, time to peak, i.e. speed of contraction, was significantly slower in the presence of SB, whether fibroblasts were present or not (Figure 5.9 C). Addition of TGF-β led to no significant differences when compared to iPSC-CMs alone but was signficantly increased when compared to SB treated cells. Again this increase occurred regardless of the presence of fibroblasts (Figure 5.9 C). The effect of SB on contraction was not observed after 2 days. Why culture with SB for 5 days causes a slowing of contraction needs further investigation.

Following contraction measurements, iPSC-CM-iPSC-cFb co-cultures were either loaded with Fura-2, AM or Fluovolt to investigate calcium and voltage handling. Cycle length and beat rate were unchanged by treatment with SB or TGF-β and were unchanged by the addition of quiescent or activated fibroblasts (Figure 5.10 A and D). Though there was a trend toward increased CTD_{50} and CTD_{80} in the presence of TGF-β this was non-significant. There was also no significant change in CTD_{50} or 80 in the presence of SB or fibroblasts.

Cycle length and beat rate were similarly unchanged when using Fluovolt regardless of drug treatment or the presence of fibroblasts (Figure 5.11 A and B). However, when looking at APD measurements there were trends towards shorter APDs in the presence of SB and quiescent fibroblasts (Figure 5.11 C-E). Though this was non-significant when compared to iPSC-CMs alone, the decrease led to significant differences between APDs when compared to SB treated cells (with and without fibroblasts) (Figure 5.11 C-E).

A final assessment of the heterogeneity of the co-cultures was conducted (Figure 5.12). By assessing the standard deviation of the optical mapping data we can determine whether co-culture with quiescent or activated iPSC-cFbs increases heterogeneity and thereby susceptibility to arrhythmias. Standard deviation of CTD_{50} and CTD_{80} values was unchanged by culture with SB or TGF-β or with quiescent or activated iPSC-cFbs (Figure 5.12 A and B). Similarly, the standard

deviation of APD50, 70 and 90 values was not statistically different in any of the tested conditions, with drug or iPSC-cFbs.

In all measures of contraction and electrophysiology, there were no significant differences between iPSC-CMs in the presence of fibroblasts and iPSC-CMs alone regardless of whether quiescent or activated. Any differences seen in contraction and voltage handling seem to be related to the presence of the drug SB alone. Though higher expression of TGF-β is linked to cardiac fibrosis and hypertrophy, there is no current evidence that TGF-β itself has any effects on cardiac electrophysiology [50, 161]. This data concurs, only showing differences between cells cultured in SB and not compared to iPSC-CMs alone. The effects of SB on iPSC-CMs should be further investigated.

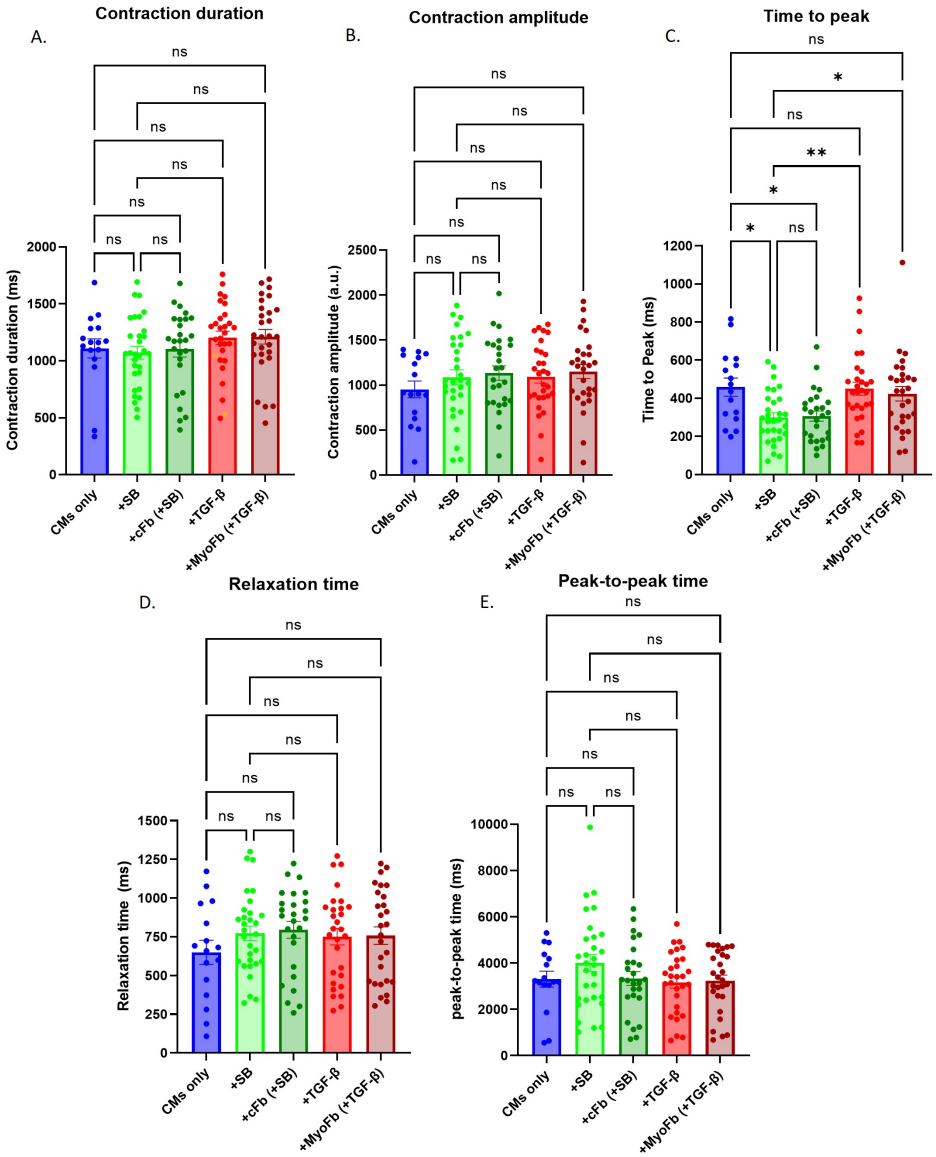


Figure 5.9: **Contraction of iPSC-CMs cultured with quiescent or activated iPSC-cFbs for 5 days.** iPSC-CMs were cultured with iPSC-cFbs for 5 days in the presence of SB or TGF-β to generate quiescent (+SB) cFbs or activated (+TGF-β) MyoFbs. Contraction was measured using MUSCLEMOTION. A - Contraction duration of iPSC-CMs alone or with SB, TGF-β, quiescent or activated iPSC-cFbs. B - Contraction amplitude of iPSC-CMs alone or with SB, TGF-β, quiescent or activated iPSC-cFbs. C - Time to peak of iPSC-CMs alone or with SB, TGF-β, quiescent or activated iPSC-cFbs. D - Relaxation time of iPSC-CMs alone or with SB, TGF-β, quiescent or activated iPSC-cFbs. E - Peak-to-peak time of iPSC-CMs alone or with SB, TGF-β, quiescent or activated iPSC-cFbs. Data presented as mean $\pm$ S.E.M. N = 16-30 dishes.

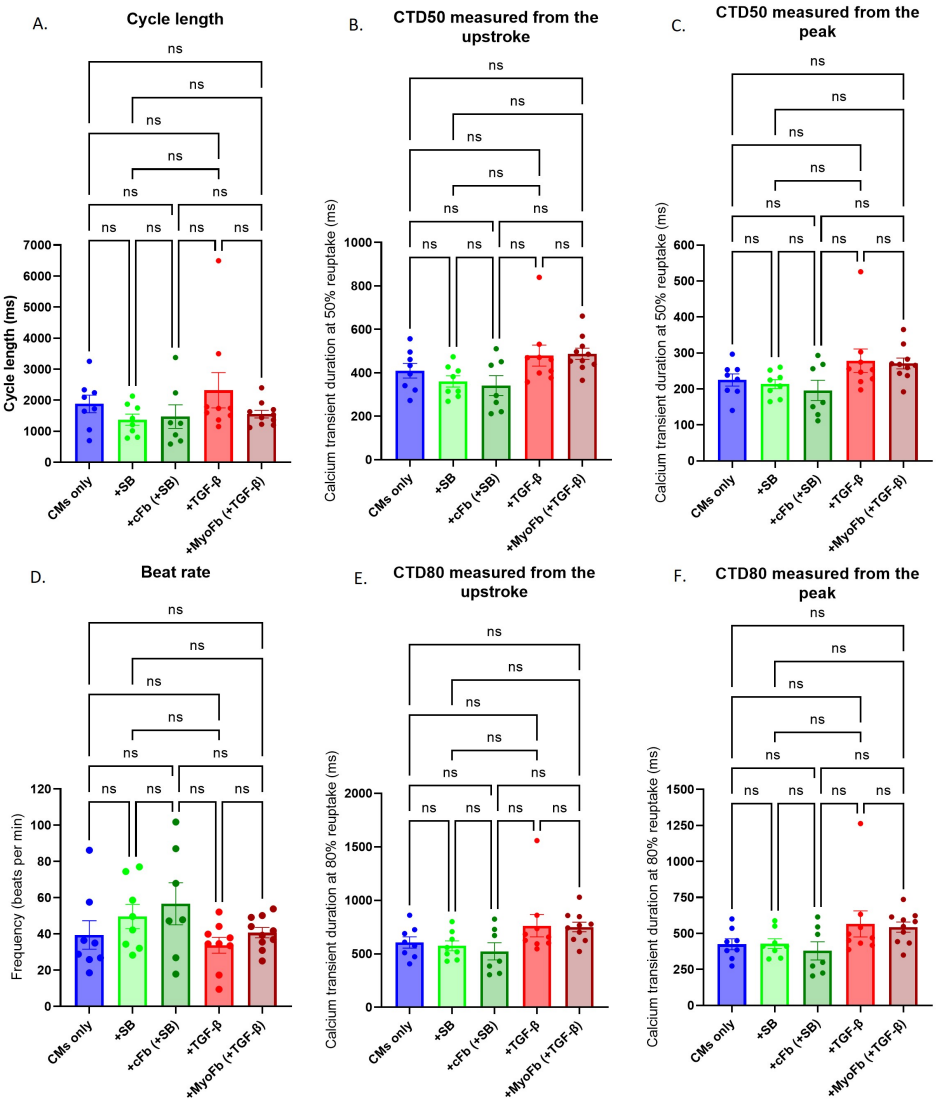


Figure 5.10: **Calcium handling of iPSC-CMs cultured with quiescent (+SB) or activated (+TGF-β) iPSC-cFbs for 5 days.** iPSC-CMs were cultured with iPSC-cFbs for 5 days in the presence of SB or TGF-β to generate quiescent (+SB) cFbs or activated (+TGF-β) MyoFbs. Co-cultures were then loaded with 10 μM Fura-2, AM for optical mapping. A - Cycle length of iPSC-CMs alone or with SB, TGF-β, quiescent or activated iPSC-cFbs. B - CTD_{50} measured from the upstroke of iPSC-CMs alone or with SB, TGF-β, quiescent or activated iPSC-cFbs. C - CTD_{50} measured from the peak of iPSC-CMs alone or with SB, TGF-β, quiescent or activated iPSC-cFbs. D - Beat rate of iPSC-CMs alone or with SB, TGF-β, quiescent or activated iPSC-cFbs. E - CTD_{80} measured from the upstroke of iPSC-CMs alone or with SB, TGF-β, quiescent or activated iPSC-cFbs. F - CTD_{80} measured from the peak of iPSC-CMs alone or with SB, TGF-β, quiescent or activated iPSC-cFbs. Data presented as mean $\pm$ S.E.M. N = 7-10 dishes.

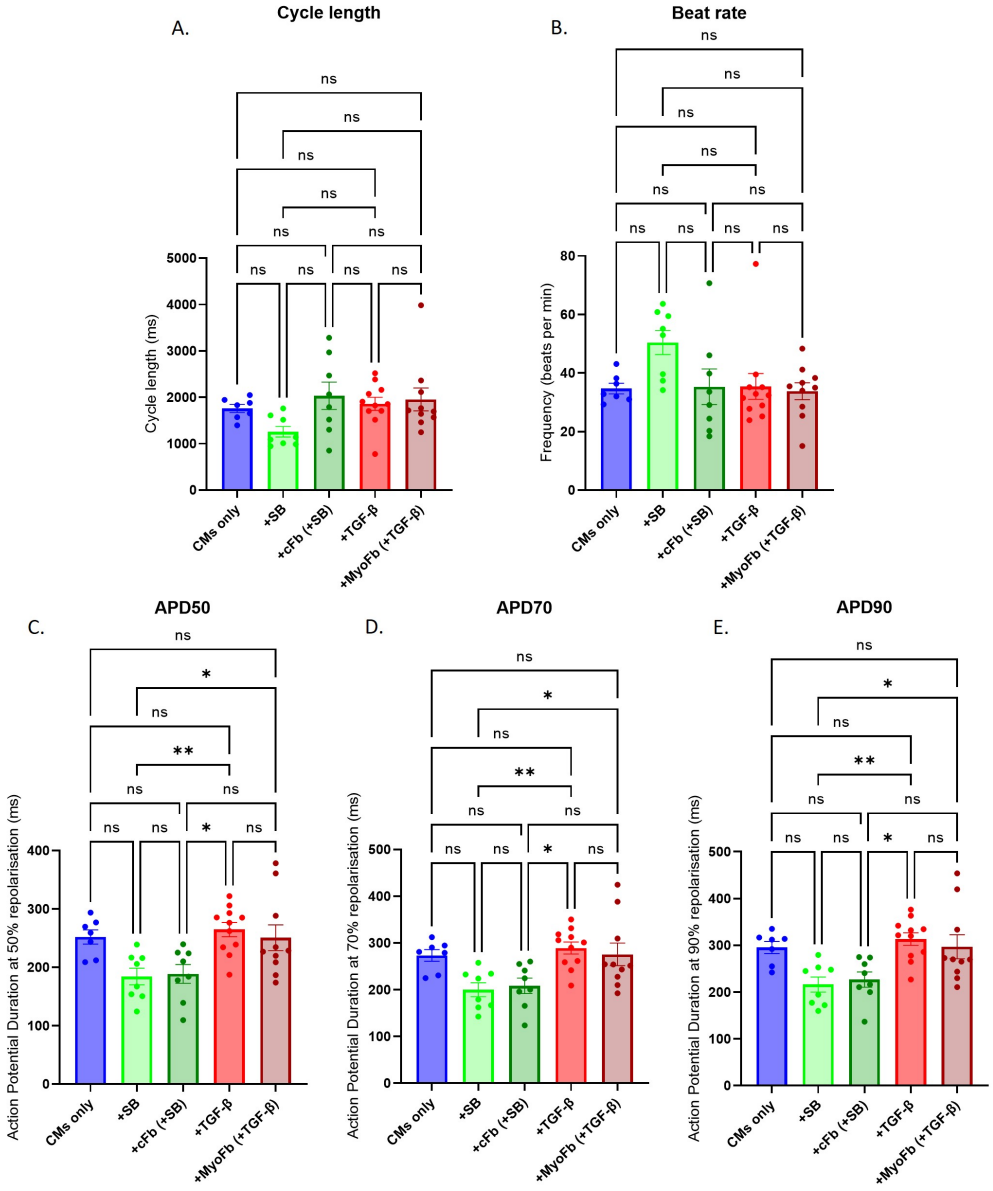


Figure 5.11: **Voltage handling of iPSC-CMs cultured with quiescent (+SB) or activated (+TGF-β) iPSC-cFbs for 5 days.** iPSC-CMs were cultured with iPSC-cFbs for 5 days in the presence of SB or TGF-β to generate quiescent (+SB) cFbs or activated (+TGF-β) MyoFbs. Co-cultures were then loaded with 0.5x Fluovolt for optical mapping. A - Cycle length of iPSC-CMs alone or with SB, TGF-β, quiescent or activated iPSC-cFbs. B - Beat rate of iPSC-CMs alone or with SB, TGF-β, quiescent or activated iPSC-cFbs. C - APD50 of iPSC-CMs alone or with SB, TGF-β, quiescent or activated iPSC-cFbs. D - APD70 of iPSC-CMs alone or with SB, TGF-β, quiescent or activated iPSC-cFbs. E - APD90 measured from the upstroke of iPSC-CMs alone or with SB, TGF-β, quiescent or activated iPSC-cFbs. Data presented as mean $\pm$ S.E.M. N = 7-11 dishes.

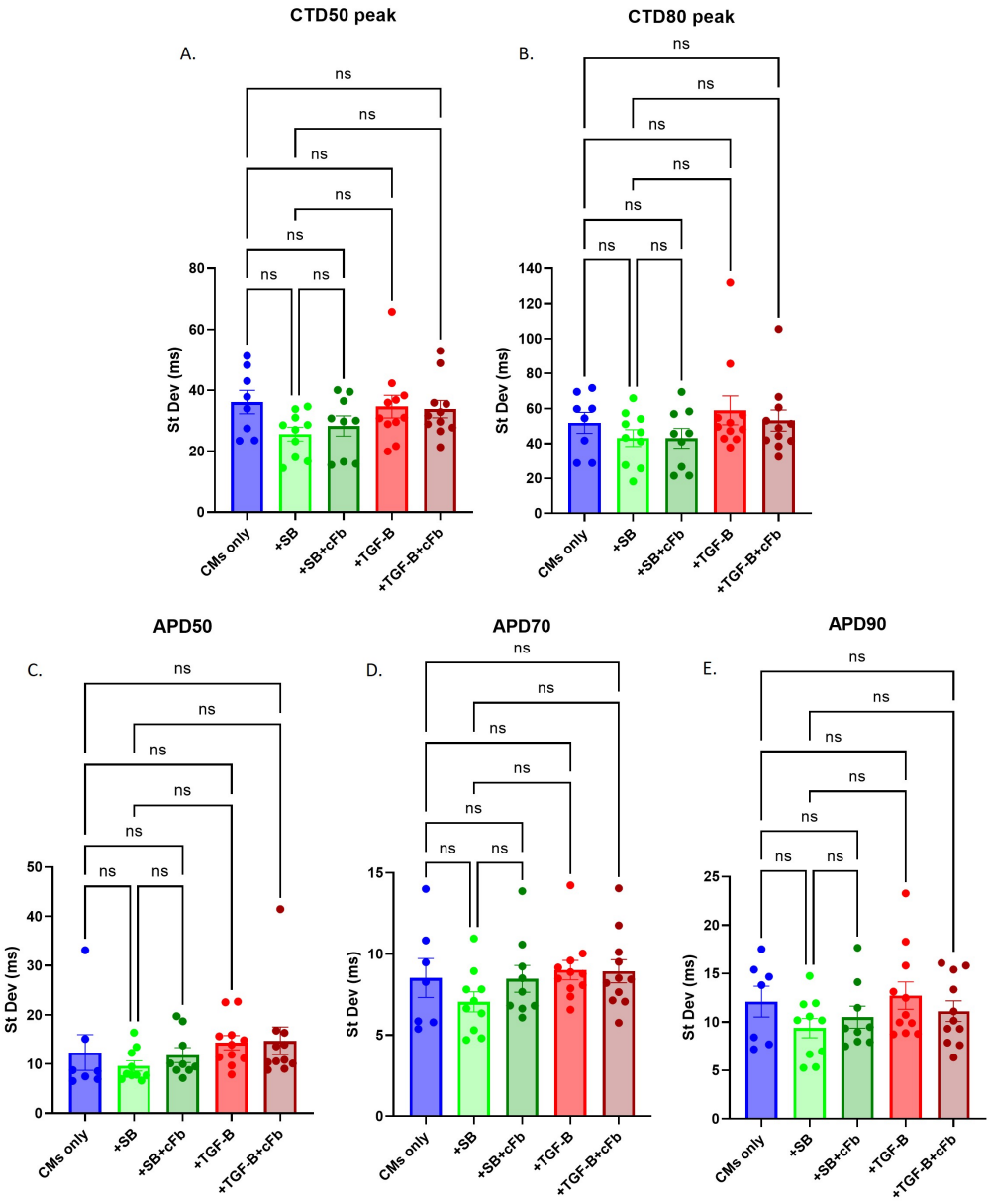


Figure 5.12: **Heterogeneity of iPSC-CM-iPSC-cFb co-cultures.** iPSC-CM-iPSC-cFb co-cultures were optically mapped using Fura-2,AM or Fluovolt. The heterogeneity of the cultures was assessed using the standard deviation of CTD and APD measurements. A - Standard deviation of CTD_{50} values measured from the peak. B - Standard deviation of CTD_{80} values measured from the peak. C - Standard deviation of APD50 values measured from the depolarisation midpoint. D - Standard deviation of APD70 values measured from the depolarisation midpoint. E - Standard deviation of APD90 values measured from the depolarisation midpoint. Data presented as mean $\pm$ S.E.M. N = 8-11 (A,B), 7-11 (C-E)

5.4 Discussion

Several studies over the last 20 years have begun to dissect the importance of the cardiac fibroblast in the electrical remodelling of the myocardium as well as structural remodelling. However, many experiments are conducted using murine CMs and cFbs, despite significant differences in electrophysiology when compared to humans. In this chapter, the aim was to investigate whether direct co-culture with cardiac fibroblasts has any effect on cardiomyocyte electrophysiology and contraction using human iPSCs. Also, how the activation status of cardiac fibroblasts affects cardiomyocyte electrophysiology and contraction. It was observed that quiescent cardiac fibroblasts had no effect on contraction at multiple different ratios after 2 days of co-culture, and that quiescent or activated fibroblasts also had no effect on contraction after 5 days. After 5 days of co-culture, only time to peak was affected by the presence of SB. Investigations of electrophysiology found no significant changes in calcium or voltage with quiescent or activated CM-fibroblast co-cultures when compared to CMs alone. The culture of iPSC-CMs with SB led to a decrease in APD when compared to TGF-β treated cells but not CMs alone.

The presence of electrotonic coupling between cardiac fibroblasts and cardiomyocytes has been confirmed *in vitro* in several animal models of disease [41, 48, 125, 163]. Experiments conducted using direct co-culture models have demonstrated that fibroblasts directly affect cardiomyocyte electrophysiology. Many of these *in vitro* studies have used neonatal rat ventricular cardiomyocytes and fibroblasts [41, 48, 164, 165]. Gaudesius *et al* (2003) demonstrated that while the

presence of a large number of fibroblasts creates a conduction block, as during scar formation, smaller numbers of fibroblasts allow conductivity and simply delay activation times [166]. Others demonstrated that this conductivity occurs in a Cx43-dependent manner [41, 164]. Vasquez *et al* (2010) observed that co-culture with increasing numbers of fibroblasts leads to a slowing of conduction velocity and prolongation of APD70 and Rother *et al* (2015) showed that increasing numbers of fibroblasts leads to a decrease in beat rate [48, 167]. However, several studies that investigated direct co-culture using human cells (iPSCs and primary cells) demonstrated that the presence of fibroblasts improves contraction and is necessary for the formation of 3D EHTs or microtissues [168, 169, 170]. The results obtained in this chapter suggest that it is not just the presence of fibroblasts that is required for electrotonic communication but a specific number of cells and the length of time in contact with cardiomyocytes.

As mentioned in the introduction (section 1.2.1), the exact number of fibroblasts in the heart is under disagreement and is reported to change during health and disease. The amount of cFbs used in *in vitro* studies varies from 5% up to 80% and ratios of CM:cFb reported vary from 2.5:1 up to 1:2. A few studies have investigated how the different numbers of fibroblasts present affect cardiomyocyte behaviour. Using neonatal rat myocytes, Vasquez *et al* (2010) demonstrated that conduction slowing was dependent on fibroblast density. The more fibroblasts there were, the more conduction velocity was slowed [48]. Rother *et al* (2015) also demonstrated that the beat rate was decreased further the more fibroblasts

were added to the co-cultures [167]. The length of time in culture also seems to vary greatly from less than 24 hours up to 8 days. The immunofluorescence staining seen after 5 days (Figure 5.8) suggests confluencies of roughly 40% which is proposed to be physiological, however, in this chapter, no effects were seen after 48 hours or 5 days of direct co-culture.

In the work conducted here, cardiac fibroblasts were plated on top of cardiomyocytes, in part due to the sensitivity of iPSC-CMs. This creates an even distribution of fibroblasts in direct contact with cardiomyocytes. However, there is little evidence that these direct contacts exist *in vivo* [125]. Due to the difficulties of plating iPSC-CMs on glass, I was unable to do Cx43 staining to confirm whether iPSC-derived cells exhibit these direct contacts.

Whether cardiac fibroblasts have an effect on electrophysiology is still being investigated but the question also exists as to whether activated MyoFbs have a differential effect to their quiescent counterparts. Miragoli *et al* (2006) demonstrated using neonatal rat cardiomyocytes that direct co-culture with MyoFbs led to a slowing of conduction however they did not have a quiescent fibroblast control [41]. Vasquez *et al* (2010) similarly showed a decrease in conduction velocity but that this was not significantly different to quiescent cFb co-cultures. They also showed a prolongation of APD70 that occurred similarly in both co-cultures [48]. However, when using primary cells isolated from pigs, Nagaraju *et al* (2019) found no significant difference in APD90 with co-culture of quiescent cFbs but a significant decrease in APD90 with MyoFb co-culture compared to cardiomyocytes

alone [42]. When using human cells Rupert *et al* (2020) compared EHTs made with quiescent and activated fibroblasts and found that the addition of MyoFbs led to a decreased contraction force when compared with both quiescent and cardiomyocytes alone [165]. Blyszczuk *et al* (2020) found that MyoFbs increased the beat rate and decreased relaxation time in cardiac microtissues compared with quiescent cFbs but found no difference in APD [169]. These results differ from the ones found here and perhaps dictate the importance of selecting the right model for experimentation whether that be human cells or 2D versus 3D (See section 6.2.3).

TGF-β receptor inhibition is currently used with cardiac fibroblasts to maintain quiescence and in an attempt to prevent or reverse the MyoFb phenotype in culture. However, results shown here, and by Shen *et al* show that the use of SB decreases time-to-peak [171]. The long-term use of pharmacological inhibition may also have additional unknown side effects and should be investigated further. The use of soft substrates in culture may avoid the necessity for SB and has been demonstrated to decrease activation of MyoFbs in culture [81, 82, 88].

Taken together, all this data re-iterates the importance of selecting the right model for experimentation, not only animal versus human but the specifics of the model, in this example, the co-culture model. The results produced will vary depending on the number of cells used and whether you are using activated or quiescent fibroblasts, all of which will affect the ability to extrapolate data into the clinic.

Cardiac fibroblasts and cardiomyocytes also do not exist in isolation but are constantly surrounded by an ECM support structure which also interacts with the cells. This has not been taken into account for a lot of these published co-culture models, here included. There are difficulties applying this to 2D monolayer cultures as the ECM components are secreted into the media. However, recent developments in biofabrication, such as bioprinting, have allowed for the inclusion of ECM biology into models [172].

5.4.1 Conclusion

Several studies have shown that MyoFbs have an increased expression of Cx43 when compared to quiescent cardiac fibroblasts which you would expect to aid in maintaining conduction and contraction following cardiomyocyte death [41, 42]. However, existing research doesn't agree with the exact outcome of this electrotonic coupling or whether it exists *in vivo*. More work needs to be done using human cells to determine whether electronic coupling does indeed happen in humans and to determine the correct conditions for *in vitro* testing. The development of spatial transcriptomics along with the integration of single-cell sequencing may be able to help elucidate whether these interactions do indeed exist in humans [173].

Chapter 6

Conclusions

6.1 Thesis outcomes

There were three main aims of this thesis:

- To investigate the reversibility of the myofibroblast phenotype (Chapter 3)
- To optimise an optical mapping setup for use with 2D iPSC-CM monolayers (Chapter 4)
- To characterise the effects of quiescent and activated cardiac fibroblasts on iPSC-CM electrophysiology and contraction (Chapter 5)

In carrying out these aims, I have successfully published 2 first-author papers, one review (PMID: 33586463), and one primary research paper (PMID: 37495732). The optical mapping system is now being used by other Ph.D. students to investigate different dilated cardiomyopathy mutations (manuscript in preparation), different substrates for the improved culture and maturation of iPSC-CMs, and other disease phenotypes.

6.2 Discussion

The current standard model for cardiac research is that of the mouse or rat. We know that there are undeniable differences in electrophysiology between these species and humans that make the results of these studies less translatable [89, 90]. The advent of human iPSC technology is circumventing some of these issues however, these models have their own disadvantages. The primary disadvantage is that of electrical and structural immaturity but methods are being developed constantly to aid in this department [94, 95, 96]. Despite this, there are many benefits to using *in vitro* studies in that they are higher throughput and less expensive [100]. However, defining the correct culture conditions are important to improve reproducibility and physiological relevance. This is includes, but is not limited to, culture surface (i.e. stiffness) and cell type.

6.2.1 Stiffness and tissue culture surfaces

In this thesis, it was observed that standard tissue culture plastic activates cardiac fibroblasts to MyoFbs and transitions them into an irreversible chronically activated phenotype that is unresponsive to TGF-β activation (Chapter 3). However, the effects of tissue culture plastic on cardiomyocytes must also be considered. It was discovered by Jacot *et al* (2008) that culturing neonatal rat myocytes on varying stiffnesses (1-50 kPa) led to variations in intracellular calcium levels and calcium transients. Increasing substrate stiffness up to 10 kPa increased calcium-induced calcium release but increasing further up to 50 kPa led to a decrease in calcium release. This was reflected by the greatest transient size being

observed at 10 kPa compared to higher and lower stiffnesses. They also observed maximum force generation on 10 kPa substrates, nearest the stiffness of the native myocardium [174]. Two seperate studies found that with increasing substrate stiffness came an increase in contraction stress for both neonatal rat and hPSC derived CMs [79, 175]. However, Hazeltine *et al* (2012) found no significant change in beat rate across any of the different substrates [175]. It has also been observed that the use of substrates more closely resembling that of the native myocardium leads to better sarcomere alignment that is often associated with maturation, although this differs for different species [79, 174, **?**]. Körner *et al* (2021) further demonstrated how the use of different substrates can affect ion channel expression and structural remodelling, with the lowest alignment of $Ca_v1.2$ and Ryanodine receptor seen on the stiffest substrate, glass [176].

When conducting future studies, the substrate for culture should be considered carefully. The future use of soft substrates may be able to keep cardiac fibroblasts inactivated but also provide a more physiological surface for cardiomyocytes thereby improving future *in vitro* models.

6.2.2 Multicellular models

The heart is an organ made up of several different cell types. This dictates the importance of using co-culture or multicellular systems in research as cardiomyocytes do not exist in isolation. A good example of this is that the use of fibroblasts in EHTs has shown better contractility [168, 169]. Work here investigates the impact of quiescent and activated cardiac fibroblasts on cardiomyocyte behaviour

but other cell types have a role in cardiac homeostasis too. Direct co-culture with macrophages has been shown to increase calcium release and induce higher calcium transient amplitudes [177]. Macrophages also induce MyoFb activation through expression of IL-6 [35]. Co-culture of cardiomyocytes with macrophages or with endothelial cells has also been shown to promote cardiomyocyte maturation through up-regulation of sarcomeric genes or changes in morphology [178, 179].

More recently, tri- and quad-culture systems have begun to be experimented with, including not only fibroblasts but endothelial cells and smooth muscle cells alongside cardiomyocytes. These models show enhanced maturation and vascularisation that create more representative physiological models of human health and disease [180, 181, 182].

6.2.3 2D versus 3D

One of the major limitations of this work is the use of a 2D co-culture model instead of 3D. There are many benefits to 2D cell culture. They allow us to examine rudimentary details on cell structure, cell-cell communications and can inform on cytotoxicity [183, 184]. However, 2D systems cannot be fully translated into clinical trials as they do not mimic the structure, microenvironment, or cell-matrix interactions, and cannot easily be used to examine off-target effects of pharmaceuticals [185]. 3D systems for cardiac research include cardiac spheroids and EHTs. It has been demonstrated that these are superior in relation to drug development [103, 124]. Saleem *et al* (2020) compared drug response of 2D

and 3D human iPSC-cardiomyocytes to animal models and found human iPSC-cardiomyocytes were better predictors of adverse cardiac effects and that 3D models were better still [103]. Beauchamp *et al* (2020) not only showed CM maturation in 3D spheroids but a decreased activation of cardiac fibroblasts when using 3D techniques. They demonstrated that 3D iPSC-cardiomyocytes had a more physiological action potential than their 2D counterparts [124].

Future work has begun with the aim of using optical mapping with multi-cell type EHTs.

6.2.4 Future work

There are a few questions still outstanding following the completion of this thesis. The first involves other methods of reversal for the MyoFb phenotype. With the complexity of the cardiac fibroblast activation pathway, there are many possible targets to investigate. Another target explored within the context of cardiac fibrosis are MicroRNAs (miRNAs). Several studies have implicated miRNA-21 in cardiac fibrosis [186, 187, 188]. Zhou *et al* (2018) observed an up-regulation of miRNA-21 in rat cardiac fibroblasts in response to TGF-β that correlated with MyoFb activation and, that use of a miRNA sponge prevented this MyoFb activation [187]. It was observed that the use of a miRNA-21 inhibitor prevented MyoFb activation and attenuated cardiac fibrosis [186, 187]. Inhibition of miRNA-223 has also been shown to decrease cardiac fibrosis and the related cardiac deterioration [189].

MBNL1 (muscleblind-like1 protein) has recently been identified with a potentially

important role in MyoFb activation [25, 190]. MBNL1 has been shown to be up-regulated in MyoFbs and overexpression of MBNL1 leads to MyoFb activation [25]. Use of a knockout model has demonstrated that a loss of MBNL1 also prevents MyoFb activation [25, 190]. This could be a promising target for reversal studies.

There are also targets that have shown promise using pulmonary or liver MyoFbs that might be worth exploring in cardiac MyoFbs. The transcription factor MyoD has been shown to regulate pulmonary MyoFb differentiation with some potential for reversibility [86]. Prostaglandin E_2 has also been used in reversal studies using pulmonary MyoFbs [191].

Another question surrounds the co-culture model itself. As mentioned at the end of Chapter 5, studies using higher numbers of fibroblasts have observed electrical changes in the presence of cardiac fibroblasts [192]. More specifically, Johnson *et al* (2023) demonstrated significant changes in electrophysiology with co-culture of human cardiomyocytes and MyoFbs. However, this study used significantly higher numbers of fibroblasts than would be found in native tissue (1:2, CM:cFb) [192]. This study also had no quiescent fibroblast control. With more time, perhaps more than one ratio, with higher numbers of fibroblasts, could have been tested for the 5-day experiments conducted in this thesis. In conjunction with Johnson *et al*s (2023) work, it could have shed more light on the CM-cFb interactions within the human context.

Lastly, the use of spontaneous data, rather than paced, brings variability to the data that may have masked any subtle effects the cardiac fibroblasts may have had. Working towards a functioning pacing system for our optical mapping system will be hugely beneficial to future work (as mentioned in Section 4.6.1).

6.3 Conclusions

Cardiac fibroblasts are undoubtedly important in cardiac disease due to their role in cardiac fibrosis. Their role in electrical remodelling is still being investigated and will be important in fully elucidating their roles in arrhythmogenesis. iPSC-derived cells will be a beneficial tool in determining this in a human model however, there is much work that needs to be done to improve this model with regards to maturity. The limitations of culturing fibroblasts combined with the immaturity of hiPSC-CM models, demonstrates the importance of working towards better and more representative models To advance the work further, it will require the full range of model systems available, while acknowledging the particular strengths and weaknesses each possesses.

Bibliography

[1] Rehman I, Rehman A. In: Anatomy, Thorax, Heart. Treasure Island (FL); 2023. Available from: https://www.ncbi.nlm.nih.gov/pubmed/29262022.

[2] Bowdridge EC, DeVallance E, Garner KL, Griffith JA, Stapleton PA, Hussain S, et al. Cardiovascular system. Elsevier; 2023.

[3] Anto Michel N, Ljubojevic-Holzer S, Bugger H, Zirlik A. Cellular Heterogeneity of the Heart [Journal Article]. Front Cardiovasc Med. 2022;9:868466. Available from: https://www.ncbi.nlm.nih.gov/pubmed/35548426.

[4] Litvinukova M, Talavera-Lopez C, Maatz H, Reichart D, Worth CL, Lindberg EL, et al. Cells of the adult human heart [Journal Article]. Nature. 2020;588(7838):466-72. Available from: https://www.ncbi.nlm.nih.gov/pubmed/32971526.

[5] Ivey MJ, Tallquist MD. Defining the Cardiac Fibroblast [Journal Article]. Circ J. 2016;80(11):2269-76. Available from: https://www.ncbi.nlm.nih.gov/pubmed/27746422.

[6] Tucker NR, Chaffin M, Fleming SJ, Hall AW, Parsons VA, Bedi J K C, et al. Transcriptional and Cellular Diversity of the Human Heart [Journal Article]. Circulation. 2020;142(5):466-82. Available from: https://www.ncbi.nlm.nih.gov/pubmed/32403949.

[7] Chaffin M, Papangeli I, Simonson B, Akkad AD, Hill MC, Arduini A, et al. Single-nucleus profiling of human dilated and hypertrophic cardiomyopathy [Journal Article]. Nature. 2022;608(7921):174-80. Available from: https://www.ncbi.nlm.nih.gov/pubmed/35732739.

[8] Amini M, Zayeri F, Salehi M. Trend analysis of cardiovascular disease mortality, incidence, and mortality-to-incidence ratio: results from global burden of disease study 2017 [Journal Article]. BMC Public Health. 2021;21(1):401. Available from: https://www.ncbi.nlm.nih.gov/pubmed/33632204.

[9] Mensah GA, Roth GA, Fuster V. The Global Burden of Cardiovascular Diseases and Risk Factors: 2020 and Beyond [Journal Article]. J Am Coll Cardiol. 2019;74(20):2529-32. Available from: https://www.ncbi.nlm.nih.gov/pubmed/31727292.

[10] Gulati A, Japp AG, Raza S, Halliday BP, Jones DA, Newsome S, et al. Absence of Myocardial Fibrosis Predicts Favorable Long-Term Survival in New-Onset Heart Failure [Journal Article]. Circ Cardiovasc Imaging. 2018;11(9):e007722. Available from: https://www.ncbi.nlm.nih.gov/pubmed/30354674.

[11] Gulati A, Jabbour A, Ismail TF, Guha K, Khwaja J, Raza S, et al. Association of fibrosis with mortality and sudden cardiac death in patients with nonischemic dilated cardiomyopathy [Journal Article]. JAMA. 2013;309(9):896-908. Available from: https://www.ncbi.nlm.nih.gov/pubmed/23462786.

[12] Hall C, Gehmlich K, Denning C, Pavlovic D. Complex Relationship Between Cardiac Fibroblasts and Cardiomyocytes in Health and Disease [Journal Article]. J Am Heart Assoc. 2021;10(5):e019338. Available from: https://www.ncbi.nlm.nih.gov/pubmed/33586463.

[13] Mewton N, Liu CY, Croisille P, Bluemke D, Lima JA. Assessment of myocardial fibrosis with cardiovascular magnetic resonance [Journal Article]. J Am Coll Cardiol. 2011;57(8):891-903. Available from: https://www.ncbi.nlm.nih.gov/pubmed/21329834.

[14] Eijgenraam TR, Sillje HHW, de Boer RA. Current understanding of fibrosis in genetic cardiomyopathies [Journal Article]. Trends Cardiovasc Med. 2020;30(6):353-61. Available from: https://www.ncbi.nlm.nih.gov/pubmed/31585768.

[15] Ten Tusscher KH, Panfilov AV. Influence of diffuse fibrosis on wave propagation in human ventricular tissue [Journal Article]. Europace. 2007;9 Suppl 6:vi38-45. Available from: https://www.ncbi.nlm.nih.gov/pubmed/17959692.

[16] Wu TJ, Ong JJ, Hwang C, Lee JJ, Fishbein MC, Czer L, et al. Characteristics of wave fronts during ventricular fibrillation in human hearts with dilated cardiomyopathy: role of increased fibrosis in the generation of reentry [Journal Article]. J Am Coll Cardiol. 1998;32(1):187-96. Available from: https://www.ncbi.nlm.nih.gov/pubmed/9669269.

[17] Fu X, Khalil H, Kanisicak O, Boyer JG, Vagnozzi RJ, Maliken BD, et al. Specialized fibroblast differentiated states underlie scar formation in the infarcted mouse heart [Journal Article]. J Clin Invest. 2018;128(5):2127-43. Available from: https://www.ncbi.nlm.nih.gov/pubmed/29664017.

[18] Pinto AR, Ilinykh A, Ivey MJ, Kuwabara JT, D'Antoni ML, Debuque R, et al. Revisiting Cardiac Cellular Composition [Journal Article]. Circ Res. 2016;118(3):400-9. Available from: https://www.ncbi.nlm.nih.gov/pubmed/26635390.

[19] Wang L, Yu P, Zhou B, Song J, Li Z, Zhang M, et al. Single-cell reconstruction of the adult human heart during heart failure and recovery reveals the cellular landscape underlying cardiac function [Journal Article]. Nat Cell Biol. 2020;22(1):108-19. Available from: https://www.ncbi.nlm.nih.gov/pubmed/31915373.

[20] Nagaraju CK, Robinson EL, Abdesselem M, Trenson S, Dries E, Gilbert G, et al. Myofibroblast Phenotype and Reversibility of Fibrosis in Patients With End-Stage Heart Failure [Journal Article]. J Am Coll Cardiol. 2019;73(18):2267-82. Available from: https://www.ncbi.nlm.nih.gov/pubmed/31072570.

[21] Sridhar S, Vandersickel N, Panfilov AV. Effect of myocyte-fibroblast coupling on the onset of pathological dynamics in a model of ventricular tissue [Journal Article]. Sci Rep. 2017;7:40985. Available from: https://www.ncbi.nlm.nih.gov/pubmed/28106124.

[22] Ali SR, Ranjbarvaziri S, Talkhabi M, Zhao P, Subat A, Hojjat A, et al. Developmental heterogeneity of cardiac fibroblasts does not predict pathological proliferation and activation [Journal Article]. Circ Res. 2014;115(7):625-35. Available from: https://www.ncbi.nlm.nih.gov/pubmed/25037571.

[23] Daseke n M J, Tenkorang MAA, Chalise U, Konfrst SR, Lindsey ML. Cardiac fibroblast activation during myocardial infarction wound healing: Fibroblast polarization after MI [Journal Article]. Matrix Biol. 2020;91-92:109-16. Available from: https://www.ncbi.nlm.nih.gov/pubmed/32446909.

[24] van den Borne SW, Diez J, Blankesteijn WM, Verjans J, Hofstra L, Narula J. Myocardial remodeling after infarction: the role of myofibroblasts [Journal Article]. Nat Rev Cardiol. 2010;7(1):30-7. Available from: https://www.ncbi.nlm.nih.gov/pubmed/19949426.

[25] Bugg D, Bailey LRJ, Bretherton RC, Beach KE, Reichardt IM, Robeson KZ, et al. MBNL1 drives dynamic transitions between fibroblasts and myofibroblasts in cardiac wound healing [Journal Article]. Cell Stem Cell. 2022;29(3):419-33 e10. Available from: https://www.ncbi.nlm.nih.gov/pubmed/35176223.

[26] Hall C, Law JP, Reyat JS, Cumberland MJ, Hang S, Vo NTN, et al. Chronic activation of human cardiac fibroblasts in vitro attenuates the reversibility of the myofibroblast phenotype [Journal Article]. Sci Rep. 2023;13(1):12137. Available from: https://www.ncbi.nlm.nih.gov/pubmed/37495732.

[27] Eghbali M, Czaja MJ, Zeydel M, Weiner FR, Zern MA, Seifter S, et al. Collagen chain mRNAs in isolated heart cells from young and adult rats [Journal Article]. J Mol Cell Cardiol. 1988;20(3):267-76. Available from: https://www.ncbi.nlm.nih.gov/pubmed/3398057.

[28] Li J, Philip JL, Xu X, Theccanat T, Abdur Razzaque M, Akhter SA. beta-Arrestins regulate human cardiac fibroblast transformation and collagen synthesis in adverse ventricular remodeling [Journal Article]. J Mol Cell Cardiol. 2014;76:73-83. Available from: https://www.ncbi.nlm.nih.gov/pubmed/25134464.

[29] Nguyen DT, Nagarajan N, Zorlutuna P. Effect of Substrate Stiffness on Mechanical Coupling and Force Propagation at the Infarct Boundary [Journal Article]. Biophys J. 2018;115(10):1966-80. Available from: https://www.ncbi.nlm.nih.gov/pubmed/30473015.

[30] Penke LR, Peters-Golden M. Molecular determinants of mesenchymal cell activation in fibroproliferative diseases [Journal Article]. Cell Mol Life Sci. 2019;76(21):4179-201. Available from: https://www.ncbi.nlm.nih.gov/pubmed/31563998.

[31] Khalil H, Kanisicak O, Prasad V, Correll RN, Fu X, Schips T, et al. Fibroblast-specific TGF-beta-Smad2/3 signaling underlies cardiac fibrosis [Journal Article]. J Clin Invest. 2017;127(10):3770-83. Available from: https://www.ncbi.nlm.nih.gov/pubmed/28891814.

[32] Vaughan MB, Howard EW, Tomasek JJ. Transforming growth factor-beta1 promotes the morphological and functional differentiation of the myofibroblast [Journal Article]. Exp Cell Res. 2000;257(1):180-9. Available from: https://www.ncbi.nlm.nih.gov/pubmed/10854066.

[33] Lijnen P, Petrov V, Rumilla K, Fagard R. Transforming growth factor-beta 1 promotes contraction of collagen gel by cardiac fibroblasts through their differentiation into myofibroblasts [Journal Article]. Methods Find Exp Clin Pharmacol. 2003;25(2):79-86. Available from: https://www.ncbi.nlm.nih.gov/pubmed/12731452.

[34] Cao L, Chen Y, Lu L, Liu Y, Wang Y, Fan J, et al. Angiotensin II upregulates fibroblast-myofibroblast transition through Cx43-dependent CaMKII and TGF-beta1 signaling in neonatal rat cardiac fibroblasts [Journal Article]. Acta Biochim Biophys Sin (Shanghai). 2018;50(9):843-52. Available from: https://www.ncbi.nlm.nih.gov/pubmed/30060053.

[35] Ma F, Li Y, Jia L, Han Y, Cheng J, Li H, et al. Macrophage-stimulated cardiac fibroblast production of IL-6 is essential for TGF beta/Smad activation and cardiac fibrosis induced by angiotensin II [Journal Article]. PLoS One. 2012;7(5):e35144. Available from: https://www.ncbi.nlm.nih.gov/pubmed/22574112.

[36] Herum KM, Choppe J, Kumar A, Engler AJ, McCulloch AD. Mechanical regulation of cardiac fibroblast profibrotic phenotypes [Journal Article]. Mol Biol Cell. 2017;28(14):1871-82. Available from: https://www.ncbi.nlm.nih.gov/pubmed/28468977.

[37] Suzuki T, Tsuruda A, Katoh S, Kubodera A, Mitsui Y. Purification of endothelin from a conditioned medium of cardiac fibroblastic cells using beating rate assay of myocytes cultured in a serum-free medium [Journal Article]. J Mol Cell Cardiol. 1997;29(8):2087-93. Available from: https://www.ncbi.nlm.nih.gov/pubmed/9281441.

[38] Schroedl NA, Hartzell CR. Myocytes and fibroblasts exhibit functional synergism in mixed cultures of neonatal rat heart cells [Journal Article]. J Cell Physiol. 1983;117(3):326-32. Available from: https://www.ncbi.nlm.nih.gov/pubmed/6361043.

[39] Kamkin A, Kiseleva I, Lozinsky I, Scholz H. Electrical interaction of mechanosensitive fibroblasts and myocytes in the heart [Journal Article]. Basic Res Cardiol. 2005;100(4):337-45. Available from: https://www.ncbi.nlm.nih.gov/pubmed/15822004.

[40] Maleckar MM, Greenstein JL, Giles WR, Trayanova NA. Electrotonic coupling between human atrial myocytes and fibroblasts alters myocyte ex-

citability and repolarization [Journal Article]. Biophys J. 2009;97(8):2179-90. Available from: https://www.ncbi.nlm.nih.gov/pubmed/19843450.

[41] Miragoli M, Gaudesius G, Rohr S. Electrotonic modulation of cardiac impulse conduction by myofibroblasts [Journal Article]. Circ Res. 2006;98(6):801-10. Available from: https://www.ncbi.nlm.nih.gov/pubmed/16484613.

[42] Nagaraju CK, Dries E, Gilbert G, Abdesselem M, Wang N, Amoni M, et al. Myofibroblast modulation of cardiac myocyte structure and function [Journal Article]. Sci Rep. 2019;9(1):8879. Available from: https://www.ncbi.nlm.nih.gov/pubmed/31222006.

[43] Vozzi C, Dupont E, Coppen SR, Yeh HI, Severs NJ. Chamber-related differences in connexin expression in the human heart [Journal Article]. J Mol Cell Cardiol. 1999;31(5):991-1003. Available from: https://www.ncbi.nlm.nih.gov/pubmed/10336839.

[44] McArthur L, Chilton L, Smith GL, Nicklin SA. Electrical consequences of cardiac myocyte: fibroblast coupling [Journal Article]. Biochem Soc Trans. 2015;43(3):513-8. Available from: https://www.ncbi.nlm.nih.gov/pubmed/26009200.

[45] Rackauskas M, Verselis VK, Bukauskas FF. Permeability of homotypic and heterotypic gap junction channels formed of cardiac connexins mCx30.2, Cx40, Cx43, and Cx45 [Journal Article]. Am J Physiol Heart Circ Physiol. 2007;293(3):H1729-36. Available from: https://www.ncbi.nlm.nih.gov/pubmed/17557922.

[46] Nagibin V, Egan Benova T, Viczenczova C, Szeiffova Bacova B, Dovinova I, Barancik M, et al. Ageing related down-regulation of myocardial connexin-43 and up-regulation of MMP-2 may predict propensity to atrial fibrillation in experimental animals [Journal Article]. Physiol Res. 2016;65 Suppl 1:S91-S100. Available from: https://www.ncbi.nlm.nih.gov/pubmed/27643943.

[47] Watanabe M, Ichinose S, Sunamori M. Age-related changes in gap junctional protein of the rat heart [Journal Article]. Exp Clin Cardiol. 2004;9(2):130-2. Available from: https://www.ncbi.nlm.nih.gov/pubmed/19641700.

[48] Vasquez C, Mohandas P, Louie KL, Benamer N, Bapat AC, Morley GE. Enhanced fibroblast-myocyte interactions in response to cardiac injury [Jour-

nal Article]. Circ Res. 2010;107(8):1011-20. Available from: https://www.ncbi.nlm.nih.gov/pubmed/20705922.

[49] Zhang Y, Kanter EM, Yamada KA. Remodeling of cardiac fibroblasts following myocardial infarction results in increased gap junction intercellular communication [Journal Article]. Cardiovasc Pathol. 2010;19(6):e233-40. Available from: https://www.ncbi.nlm.nih.gov/pubmed/20093048.

[50] Cartledge JE, Kane C, Dias P, Tesfom M, Clarke L, McKee B, et al. Functional crosstalk between cardiac fibroblasts and adult cardiomyocytes by soluble mediators [Journal Article]. Cardiovasc Res. 2015;105(3):260-70. Available from: https://www.ncbi.nlm.nih.gov/pubmed/25560320.

[51] Kaur K, Zarzoso M, Ponce-Balbuena D, Guerrero-Serna G, Hou L, Musa H, et al. TGF-beta1, released by myofibroblasts, differentially regulates transcription and function of sodium and potassium channels in adult rat ventricular myocytes [Journal Article]. PLoS One. 2013;8(2):e55391. Available from: https://www.ncbi.nlm.nih.gov/pubmed/23393573.

[52] LaFramboise WA, Scalise D, Stoodley P, Graner SR, Guthrie RD, Magovern JA, et al. Cardiac fibroblasts influence cardiomyocyte phenotype in vitro [Journal Article]. Am J Physiol Cell Physiol. 2007;292(5):C1799-808. Available from: https://www.ncbi.nlm.nih.gov/pubmed/17229813.

[53] Tzavlaki K, Moustakas A. TGF-beta Signaling [Journal Article]. Biomolecules. 2020;10(3). Available from: https://www.ncbi.nlm.nih.gov/pubmed/32210029.

[54] Teekakirikul P, Eminaga S, Toka O, Alcalai R, Wang L, Wakimoto H, et al. Cardiac fibrosis in mice with hypertrophic cardiomyopathy is mediated by non-myocyte proliferation and requires Tgf-beta [Journal Article]. J Clin Invest. 2010;120(10):3520-9. Available from: https://www.ncbi.nlm.nih.gov/pubmed/20811150.

[55] Thompson NL, Bazoberry F, Speir EH, Casscells W, Ferrans VJ, Flanders KC, et al. Transforming growth factor beta-1 in acute myocardial infarction in rats [Journal Article]. Growth Factors. 1988;1(1):91-9. Available from: https://www.ncbi.nlm.nih.gov/pubmed/3078566.

[56] Rahmutula D, Marcus GM, Wilson EE, Ding CH, Xiao Y, Paquet AC, et al. Molecular basis of selective atrial fibrosis due to overexpression of transforming growth factor-beta1 [Journal Article]. Cardiovasc

Res. 2013;99(4):769-79. Available from: https://www.ncbi.nlm.nih.gov/pubmed/23612580.

[57] Nakajima H, Nakajima HO, Salcher O, Dittie AS, Dembowsky K, Jing S, et al. Atrial but not ventricular fibrosis in mice expressing a mutant transforming growth factor-beta(1) transgene in the heart [Journal Article]. Circ Res. 2000;86(5):571-9. Available from: https://www.ncbi.nlm.nih.gov/pubmed/10720419.

[58] Kuwahara F, Kai H, Tokuda K, Kai M, Takeshita A, Egashira K, et al. Transforming growth factor-beta function blocking prevents myocardial fibrosis and diastolic dysfunction in pressure-overloaded rats [Journal Article]. Circulation. 2002;106(1):130-5. Available from: https://www.ncbi.nlm.nih.gov/pubmed/12093782.

[59] Driesen RB, Nagaraju CK, Abi-Char J, Coenen T, Lijnen PJ, Fagard RH, et al. Reversible and irreversible differentiation of cardiac fibroblasts [Journal Article]. Cardiovasc Res. 2014;101(3):411-22. Available from: https://www.ncbi.nlm.nih.gov/pubmed/24368833.

[60] Zeigler AC, Richardson WJ, Holmes JW, Saucerman JJ. A computational model of cardiac fibroblast signaling predicts context-dependent drivers of myofibroblast differentiation [Journal Article]. J Mol Cell Cardiol. 2016;94:72-81. Available from: https://www.ncbi.nlm.nih.gov/pubmed/27017945.

[61] Ceccato TL, Starbuck RB, Hall JK, Walker CJ, Brown TE, Killgore JP, et al. Defining the Cardiac Fibroblast Secretome in a Fibrotic Microenvironment [Journal Article]. J Am Heart Assoc. 2020;9(19):e017025. Available from: https://www.ncbi.nlm.nih.gov/pubmed/32924724.

[62] McLellan MA, Skelly DA, Dona MSI, Squiers GT, Farrugia GE, Gaynor TL, et al. High-Resolution Transcriptomic Profiling of the Heart During Chronic Stress Reveals Cellular Drivers of Cardiac Fibrosis and Hypertrophy [Journal Article]. Circulation. 2020;142(15):1448-63. Available from: https://www.ncbi.nlm.nih.gov/pubmed/32795101.

[63] Fukamizu A, Takahashi S, Seo MS, Tada M, Tanimoto K, Uehara S, et al. Structure and expression of the human angiotensinogen gene. Identification of a unique and highly active promoter [Journal Article]. J Biol Chem. 1990;265(13):7576-82. Available from: https://www.ncbi.nlm.nih.gov/pubmed/1692023.

[64] Yang G, Merrill DC, Thompson MW, Robillard JE, Sigmund CD. Functional expression of the human angiotensinogen gene in transgenic mice [Journal Article]. J Biol Chem. 1994;269(51):32497-502. Available from: https://www.ncbi.nlm.nih.gov/pubmed/7798251.

[65] Toto RD, Rinner S, Ram CV. ACE inhibitors and target organ protection. An expanded role for these antihypertensive agents? [Journal Article]. Postgrad Med. 2004;116(2):11-6, 19-22, 48. Available from: https://www.ncbi.nlm.nih.gov/pubmed/15323151.

[66] Schieffer B, Wirger A, Meybrunn M, Seitz S, Holtz J, Riede UN, et al. Comparative effects of chronic angiotensin-converting enzyme inhibition and angiotensin II type 1 receptor blockade on cardiac remodeling after myocardial infarction in the rat [Journal Article]. Circulation. 1994;89(5):2273-82. Available from: https://www.ncbi.nlm.nih.gov/pubmed/8181153.

[67] Sun Y, Zhang JQ, Zhang J, Ramires FJ. Angiotensin II, transforming growth factor-beta1 and repair in the infarcted heart [Journal Article]. J Mol Cell Cardiol. 1998;30(8):1559-69. Available from: https://www.ncbi.nlm.nih.gov/pubmed/9737942.

[68] Sadoshima J, Izumo S. Molecular characterization of angiotensin II–induced hypertrophy of cardiac myocytes and hyperplasia of cardiac fibroblasts. Critical role of the AT1 receptor subtype [Journal Article]. Circ Res. 1993;73(3):413-23. Available from: https://www.ncbi.nlm.nih.gov/pubmed/8348686.

[69] Fredj S, Bescond J, Louault C, Delwail A, Lecron JC, Potreau D. Role of interleukin-6 in cardiomyocyte/cardiac fibroblast interactions during myocyte hypertrophy and fibroblast proliferation [Journal Article]. J Cell Physiol. 2005;204(2):428-36. Available from: https://www.ncbi.nlm.nih.gov/pubmed/15717324.

[70] Brilla CG, Funck RC, Rupp H. Lisinopril-mediated regression of myocardial fibrosis in patients with hypertensive heart disease [Journal Article]. Circulation. 2000;102(12):1388-93. Available from: https://www.ncbi.nlm.nih.gov/pubmed/10993857.

[71] Arcone R, Pucci P, Zappacosta F, Fontaine V, Malorni A, Marino G, et al. Single-step purification and structural characterization of human

interleukin-6 produced in Escherichia coli from a T7 RNA polymerase expression vector [Journal Article]. Eur J Biochem. 1991;198(3):541-7. Available from: https://www.ncbi.nlm.nih.gov/pubmed/2050135.

[72] Banerjee I, Fuseler JW, Intwala AR, Baudino TA. IL-6 loss causes ventricular dysfunction, fibrosis, reduced capillary density, and dramatically alters the cell populations of the developing and adult heart [Journal Article]. Am J Physiol Heart Circ Physiol. 2009;296(5):H1694-704. Available from: https://www.ncbi.nlm.nih.gov/pubmed/19234091.

[73] Fontes JA, Rose NR, Cihakova D. The varying faces of IL-6: From cardiac protection to cardiac failure [Journal Article]. Cytokine. 2015;74(1):62-8. Available from: https://www.ncbi.nlm.nih.gov/pubmed/25649043.

[74] Melendez GC, McLarty JL, Levick SP, Du Y, Janicki JS, Brower GL. Interleukin 6 mediates myocardial fibrosis, concentric hypertrophy, and diastolic dysfunction in rats [Journal Article]. Hypertension. 2010;56(2):225-31. Available from: https://www.ncbi.nlm.nih.gov/pubmed/20606113.

[75] Ancey C, Corbi P, Froger J, Delwail A, Wijdenes J, Gascan H, et al. Secretion of IL-6, IL-11 and LIF by human cardiomyocytes in primary culture [Journal Article]. Cytokine. 2002;18(4):199-205. Available from: https://www.ncbi.nlm.nih.gov/pubmed/12126642.

[76] Hirota H, Yoshida K, Kishimoto T, Taga T. Continuous activation of gp130, a signal-transducing receptor component for interleukin 6-related cytokines, causes myocardial hypertrophy in mice [Journal Article]. Proc Natl Acad Sci U S A. 1995;92(11):4862-6. Available from: https://www.ncbi.nlm.nih.gov/pubmed/7539136.

[77] Jastrzebski ZD. Nature and properties of engineering materials. Wiley international editons.. New York: Wiley; 1959.

[78] Hinz B. Matrix mechanics and regulation of the fibroblast phenotype [Journal Article]. Periodontology 2000. 2013;63(1):14-28. Available from: <GotoISI>://WOS:000322916100002.

[79] Bhana B, Iyer RK, Chen WL, Zhao R, Sider KL, Likhitpanichkul M, et al. Influence of substrate stiffness on the phenotype of heart cells [Journal Article]. Biotechnol Bioeng. 2010;105(6):1148-60. Available from: https://www.ncbi.nlm.nih.gov/pubmed/20014437.

[80] Wang H, Haeger SM, Kloxin AM, Leinwand LA, Anseth KS. Redirecting valvular myofibroblasts into dormant fibroblasts through light-mediated reduction in substrate modulus [Journal Article]. PLoS One. 2012;7(7):e39969. Available from: https://www.ncbi.nlm.nih.gov/pubmed/22808079.

[81] Wang J, Chen H, Seth A, McCulloch CA. Mechanical force regulation of myofibroblast differentiation in cardiac fibroblasts [Journal Article]. Am J Physiol Heart Circ Physiol. 2003;285(5):H1871-81. Available from: https://www.ncbi.nlm.nih.gov/pubmed/12842814.

[82] Landry NM, Rattan SG, Dixon IMC. An Improved Method of Maintaining Primary Murine Cardiac Fibroblasts in Two-Dimensional Cell Culture [Journal Article]. Sci Rep. 2019;9(1):12889. Available from: https://www.ncbi.nlm.nih.gov/pubmed/31501457.

[83] Kamkin A, Kiseleva I, Wagner KD, Scholz H. In: Kamkin A, Kiseleva I, editors. Mechano-Electric Feedback in the Heart: Evidence from Intracellular Microelectrode Recordings on Multicellular Preparations and Single Cells from Healthy and Diseased Tissue. Moscow; 2005. Available from: https://www.ncbi.nlm.nih.gov/pubmed/21290768.

[84] Zhuang J, Yamada KA, Saffitz JE, Kleber AG. Pulsatile stretch remodels cell-to-cell communication in cultured myocytes [Journal Article]. Circ Res. 2000;87(4):316-22. Available from: https://www.ncbi.nlm.nih.gov/pubmed/10948066.

[85] Thompson SA, Copeland CR, Reich DH, Tung L. Mechanical coupling between myofibroblasts and cardiomyocytes slows electric conduction in fibrotic cell monolayers [Journal Article]. Circulation. 2011;123(19):2083-93. Available from: https://www.ncbi.nlm.nih.gov/pubmed/21537003.

[86] Hecker L, Jagirdar R, Jin T, Thannickal VJ. Reversible differentiation of myofibroblasts by MyoD [Journal Article]. Exp Cell Res. 2011;317(13):1914-21. Available from: https://www.ncbi.nlm.nih.gov/pubmed/21440539.

[87] Derangeon M, Montnach J, Cerpa CO, Jagu B, Patin J, Toumaniantz G, et al. Transforming growth factor beta receptor inhibition prevents ventricular fibrosis in a mouse model of progressive cardiac conduction disease [Journal Article]. Cardiovasc Res. 2017;113(5):464-74. Available from: https://www.ncbi.nlm.nih.gov/pubmed/28339646.

[88] Gilles G, McCulloch AD, Brakebusch CH, Herum KM. Maintaining resting cardiac fibroblasts in vitro by disrupting mechanotransduction [Journal Article]. PLoS One. 2020;15(10):e0241390. Available from: https://www.ncbi.nlm.nih.gov/pubmed/33104742.

[89] Zaragoza C, Gomez-Guerrero C, Martin-Ventura JL, Blanco-Colio L, Lavin B, Mallavia B, et al. Animal models of cardiovascular diseases [Journal Article]. J Biomed Biotechnol. 2011;2011:497841. Available from: https://www.ncbi.nlm.nih.gov/pubmed/21403831.

[90] Ding Y, Wang Y, Jia Q, Wang X, Lu Y, Zhang A, et al. Morphological and Functional Characteristics of Animal Models of Myocardial Fibrosis Induced by Pressure Overload [Journal Article]. Int J Hypertens. 2020;2020:3014693. Available from: https://www.ncbi.nlm.nih.gov/pubmed/32099670.

[91] Leong XF, Ng CY, Jaarin K. Animal Models in Cardiovascular Research: Hypertension and Atherosclerosis [Journal Article]. Biomed Res Int. 2015;2015:528757. Available from: https://www.ncbi.nlm.nih.gov/pubmed/26064920.

[92] Wang Y, Wang M, Samuel CS, Widdop RE. Preclinical rodent models of cardiac fibrosis [Journal Article]. Br J Pharmacol. 2022;179(5):882-99. Available from: https://www.ncbi.nlm.nih.gov/pubmed/33973236.

[93] Hearse DJ, Sutherland FJ. Experimental models for the study of cardiovascular function and disease [Journal Article]. Pharmacol Res. 2000;41(6):597-603. Available from: https://www.ncbi.nlm.nih.gov/pubmed/10816328.

[94] Lin B, Li Y, Han L, Kaplan AD, Ao Y, Kalra S, et al. Modeling and study of the mechanism of dilated cardiomyopathy using induced pluripotent stem cells derived from individuals with Duchenne muscular dystrophy [Journal Article]. Dis Model Mech. 2015;8(5):457-66. Available from: https://www.ncbi.nlm.nih.gov/pubmed/25791035.

[95] Matsa E, Rajamohan D, Dick E, Young L, Mellor I, Staniforth A, et al. Drug evaluation in cardiomyocytes derived from human induced pluripotent stem cells carrying a long QT syndrome type 2 mutation [Journal Article]. Eur Heart J. 2011;32(8):952-62. Available from: https://www.ncbi.nlm.nih.gov/pubmed/21367833.

[96] Mummery CL, Zhang J, Ng ES, Elliott DA, Elefanty AG, Kamp TJ. Differentiation of human embryonic stem cells and induced pluripotent stem cells to cardiomyocytes: a methods overview [Journal Article]. Circ Res. 2012;111(3):344-58. Available from: https://www.ncbi.nlm.nih.gov/pubmed/22821908.

[97] Funakoshi S, Yoshida Y. Recent progress of iPSC technology in cardiac diseases [Journal Article]. Arch Toxicol. 2021;95(12):3633-50. Available from: https://www.ncbi.nlm.nih.gov/pubmed/34657219.

[98] Burridge PW, Matsa E, Shukla P, Lin ZC, Churko JM, Ebert AD, et al. Chemically defined generation of human cardiomyocytes [Journal Article]. Nat Methods. 2014;11(8):855-60. Available from: https://www.ncbi.nlm.nih.gov/pubmed/24930130.

[99] Mosqueira D, Mannhardt I, Bhagwan JR, Lis-Slimak K, Katili P, Scott E, et al. CRISPR/Cas9 editing in human pluripotent stem cell-cardiomyocytes highlights arrhythmias, hypocontractility, and energy depletion as potential therapeutic targets for hypertrophic cardiomyopathy [Journal Article]. Eur Heart J. 2018;39(43):3879-92. Available from: https://www.ncbi.nlm.nih.gov/pubmed/29741611.

[100] Ebert AD, Liang P, Wu JC. Induced pluripotent stem cells as a disease modeling and drug screening platform [Journal Article]. J Cardiovasc Pharmacol. 2012;60(4):408-16. Available from: https://www.ncbi.nlm.nih.gov/pubmed/22240913.

[101] Moretti A, Bellin M, Welling A, Jung CB, Lam JT, Bott-Flugel L, et al. Patient-specific induced pluripotent stem-cell models for long-QT syndrome [Journal Article]. N Engl J Med. 2010;363(15):1397-409. Available from: https://www.ncbi.nlm.nih.gov/pubmed/20660394.

[102] Wang Y, Liang P, Lan F, Wu H, Lisowski L, Gu M, et al. Genome editing of isogenic human induced pluripotent stem cells recapitulates long QT phenotype for drug testing [Journal Article]. J Am Coll Cardiol. 2014;64(5):451-9. Available from: https://www.ncbi.nlm.nih.gov/pubmed/25082577.

[103] Saleem U, van Meer BJ, Katili PA, Mohd Yusof NAN, Mannhardt I, Garcia AK, et al. Blinded, Multicenter Evaluation of Drug-induced Changes in Contractility Using Human-induced Pluripotent Stem Cell-derived Cardiomyocytes [Journal Article]. Toxicol Sci. 2020;176(1):103-23. Available from: https://www.ncbi.nlm.nih.gov/pubmed/32421822.

[104] Pointon A, Pilling J, Dorval T, Wang Y, Archer C, Pollard C. From the Cover: High-Throughput Imaging of Cardiac Microtissues for the Assessment of Cardiac Contraction during Drug Discovery [Journal Article]. Toxicol Sci. 2017;155(2):444-57. Available from: https://www.ncbi.nlm.nih.gov/pubmed/28069985.

[105] Burridge PW, Li YF, Matsa E, Wu H, Ong SG, Sharma A, et al. Human induced pluripotent stem cell-derived cardiomyocytes recapitulate the predilection of breast cancer patients to doxorubicin-induced cardiotoxicity [Journal Article]. Nat Med. 2016;22(5):547-56. Available from: https://www.ncbi.nlm.nih.gov/pubmed/27089514.

[106] Stillitano F, Hansen J, Kong CW, Karakikes I, Funck-Brentano C, Geng L, et al. Modeling susceptibility to drug-induced long QT with a panel of subject-specific induced pluripotent stem cells [Journal Article]. Elife. 2017;6. Available from: https://www.ncbi.nlm.nih.gov/pubmed/28134617.

[107] Chong JJ, Yang X, Don CW, Minami E, Liu YW, Weyers JJ, et al. Human embryonic-stem-cell-derived cardiomyocytes regenerate non-human primate hearts [Journal Article]. Nature. 2014;510(7504):273-7. Available from: https://www.ncbi.nlm.nih.gov/pubmed/24776797.

[108] Shiba Y, Gomibuchi T, Seto T, Wada Y, Ichimura H, Tanaka Y, et al. Allogeneic transplantation of iPS cell-derived cardiomyocytes regenerates primate hearts [Journal Article]. Nature. 2016;538(7625):388-91. Available from: https://www.ncbi.nlm.nih.gov/pubmed/27723741.

[109] Goversen B, van der Heyden MAG, van Veen TAB, de Boer TP. The immature electrophysiological phenotype of iPSC-CMs still hampers in vitro drug screening: Special focus on IK1 [Journal Article]. Pharmacol Ther. 2018;183:127-36. Available from: https://www.ncbi.nlm.nih.gov/pubmed/28986101.

[110] Feric NT, Radisic M. Maturing human pluripotent stem cell-derived cardiomyocytes in human engineered cardiac tissues [Journal Article]. Adv Drug Deliv Rev. 2016;96:110-34. Available from: https://www.ncbi.nlm.nih.gov/pubmed/25956564.

[111] Yang X, Rodriguez ML, Leonard A, Sun L, Fischer KA, Wang Y, et al. Fatty Acids Enhance the Maturation of Cardiomyocytes Derived from Human Pluripotent Stem Cells [Journal Article]. Stem Cell Reports.

2019;13(4):657-68. Available from: https://www.ncbi.nlm.nih.gov/pubmed/31564645.

[112] Drawnel FM, Boccardo S, Prummer M, Delobel F, Graff A, Weber M, et al. Disease modeling and phenotypic drug screening for diabetic cardiomyopathy using human induced pluripotent stem cells [Journal Article]. Cell Rep. 2014;9(3):810-21. Available from: https://www.ncbi.nlm.nih.gov/pubmed/25437537.

[113] Machiraju P, Greenway SC. Current methods for the maturation of induced pluripotent stem cell-derived cardiomyocytes [Journal Article]. World J Stem Cells. 2019;11(1):33-43. Available from: https://www.ncbi.nlm.nih.gov/pubmed/30705713.

[114] Lundy SD, Zhu WZ, Regnier M, Laflamme MA. Structural and functional maturation of cardiomyocytes derived from human pluripotent stem cells [Journal Article]. Stem Cells Dev. 2013;22(14):1991-2002. Available from: https://www.ncbi.nlm.nih.gov/pubmed/23461462.

[115] Sartiani L, Bettiol E, Stillitano F, Mugelli A, Cerbai E, Jaconi ME. Developmental changes in cardiomyocytes differentiated from human embryonic stem cells: a molecular and electrophysiological approach [Journal Article]. Stem Cells. 2007;25(5):1136-44. Available from: https://www.ncbi.nlm.nih.gov/pubmed/17255522.

[116] Feaster TK, Cadar AG, Wang L, Williams CH, Chun YW, Hempel JE, et al. Matrigel Mattress: A Method for the Generation of Single Contracting Human-Induced Pluripotent Stem Cell-Derived Cardiomyocytes [Journal Article]. Circ Res. 2015;117(12):995-1000. Available from: https://www.ncbi.nlm.nih.gov/pubmed/26429802.

[117] Jimenez-Vazquez EN, Jain A, Jones DK. Enhancing iPSC-CM Maturation Using a Matrigel-Coated Micropatterned PDMS Substrate [Journal Article]. Curr Protoc. 2022;2(11):e601. Available from: https://www.ncbi.nlm.nih.gov/pubmed/36383047.

[118] McDevitt TC, Angello JC, Whitney ML, Reinecke H, Hauschka SD, Murry CE, et al. In vitro generation of differentiated cardiac myofibers on micropatterned laminin surfaces [Journal Article]. J Biomed Mater Res. 2002;60(3):472-9. Available from: https://www.ncbi.nlm.nih.gov/pubmed/11920672.

[119] Motlagh D, Hartman TJ, Desai TA, Russell B. Microfabricated grooves recapitulate neonatal myocyte connexin43 and N-cadherin expression and localization [Journal Article]. J Biomed Mater Res A. 2003;67(1):148-57. Available from: https://www.ncbi.nlm.nih.gov/pubmed/14517872.

[120] Correia C, Koshkin A, Duarte P, Hu D, Carido M, Sebastiao MJ, et al. 3D aggregate culture improves metabolic maturation of human pluripotent stem cell derived cardiomyocytes [Journal Article]. Biotechnol Bioeng. 2018;115(3):630-44. Available from: https://www.ncbi.nlm.nih.gov/pubmed/29178315.

[121] Lemoine MD, Mannhardt I, Breckwoldt K, Prondzynski M, Flenner F, Ulmer B, et al. Human iPSC-derived cardiomyocytes cultured in 3D engineered heart tissue show physiological upstroke velocity and sodium current density [Journal Article]. Sci Rep. 2017;7(1):5464. Available from: https://www.ncbi.nlm.nih.gov/pubmed/28710467.

[122] Zhang D, Shadrin IY, Lam J, Xian HQ, Snodgrass HR, Bursac N. Tissue-engineered cardiac patch for advanced functional maturation of human ESC-derived cardiomyocytes [Journal Article]. Biomaterials. 2013;34(23):5813-20. Available from: https://www.ncbi.nlm.nih.gov/pubmed/23642535.

[123] Baudino TA, McFadden A, Fix C, Hastings J, Price R, Borg TK. Cell patterning: interaction of cardiac myocytes and fibroblasts in three-dimensional culture [Journal Article]. Microsc Microanal. 2008;14(2):117-25. Available from: https://www.ncbi.nlm.nih.gov/pubmed/18312716.

[124] Beauchamp P, Jackson CB, Ozhathil LC, Agarkova I, Galindo CL, Sawyer DB, et al. 3D Co-culture of hiPSC-Derived Cardiomyocytes With Cardiac Fibroblasts Improves Tissue-Like Features of Cardiac Spheroids [Journal Article]. Front Mol Biosci. 2020;7:14. Available from: https://www.ncbi.nlm.nih.gov/pubmed/32118040.

[125] Camelliti P, Green CR, LeGrice I, Kohl P. Fibroblast network in rabbit sinoatrial node: structural and functional identification of homogeneous and heterogeneous cell coupling [Journal Article]. Circ Res. 2004;94(6):828-35. Available from: https://www.ncbi.nlm.nih.gov/pubmed/14976125.

[126] Zhang H, Tian L, Shen M, Tu C, Wu H, Gu M, et al. Generation of Quiescent Cardiac Fibroblasts From Human Induced Pluripotent Stem Cells for In Vitro Modeling of Cardiac Fibrosis [Journal Article]. Circ Res.

2019;125(5):552-66. Available from: https://www.ncbi.nlm.nih.gov/pubmed/31288631.

[127] Santiago JJ, Dangerfield AL, Rattan SG, Bathe KL, Cunnington RH, Raizman JE, et al. Cardiac fibroblast to myofibroblast differentiation in vivo and in vitro: expression of focal adhesion components in neonatal and adult rat ventricular myofibroblasts [Journal Article]. Dev Dyn. 2010;239(6):1573-84. Available from: https://www.ncbi.nlm.nih.gov/pubmed/20503355.

[128] Tomasek JJ, Gabbiani G, Hinz B, Chaponnier C, Brown RA. Myofibroblasts and mechano-regulation of connective tissue remodelling [Journal Article]. Nat Rev Mol Cell Biol. 2002;3(5):349-63. Available from: https://www.ncbi.nlm.nih.gov/pubmed/11988769.

[129] Attin M, Clusin WT. Basic concepts of optical mapping techniques in cardiac electrophysiology [Journal Article]. Biol Res Nurs. 2009;11(2):195-207. Available from: https://www.ncbi.nlm.nih.gov/pubmed/19617237.

[130] Cumberland MJ, Riebel LL, Roy A, O'Shea C, Holmes AP, Denning C, et al. Basic Research Approaches to Evaluate Cardiac Arrhythmia in Heart Failure and Beyond [Journal Article]. Front Physiol. 2022;13:806366. Available from: https://www.ncbi.nlm.nih.gov/pubmed/35197863.

[131] O'Shea C, Kabir SN, Holmes AP, Lei M, Fabritz L, Rajpoot K, et al. Cardiac optical mapping - State-of-the-art and future challenges [Journal Article]. Int J Biochem Cell Biol. 2020;126:105804. Available from: https://www.ncbi.nlm.nih.gov/pubmed/32681973.

[132] Brack KE, Narang R, Winter J, Ng GA. The mechanical uncoupler blebbistatin is associated with significant electrophysiological effects in the isolated rabbit heart [Journal Article]. Exp Physiol. 2013;98(5):1009-27. Available from: https://www.ncbi.nlm.nih.gov/pubmed/23291912.

[133] Kappadan V, Telele S, Uzelac I, Fenton F, Parlitz U, Luther S, et al. High-Resolution Optical Measurement of Cardiac Restitution, Contraction, and Fibrillation Dynamics in Beating vs. Blebbistatin-Uncoupled Isolated Rabbit Hearts [Journal Article]. Front Physiol. 2020;11:464. Available from: https://www.ncbi.nlm.nih.gov/pubmed/32528304.

[134] Fedorov VV, Lozinsky IT, Sosunov EA, Anyukhovsky EP, Rosen MR, Balke CW, et al. Application of blebbistatin as an excitation-contraction uncoupler for electrophysiologic study of rat and rabbit hearts [Journal Article]. Heart

Rhythm. 2007;4(5):619-26. Available from: https://www.ncbi.nlm.nih.gov/pubmed/17467631.

[135] Marchant James L, Smith Frank M, Farrell Anthony P. The effective use of blebbistatin to study the action potential of cardiac pacemaker cells of zebrafish (Danio rerio) during incremental warming [Journal Article]. Curr Res Physiol. 2022;5:48-54. Available from: https://www.ncbi.nlm.nih.gov/pubmed/35128467.

[136] Dou Y, Arlock P, Arner A. Blebbistatin specifically inhibits actin-myosin interaction in mouse cardiac muscle [Journal Article]. Am J Physiol Cell Physiol. 2007;293(3):C1148-53. Available from: https://www.ncbi.nlm.nih.gov/pubmed/17615158.

[137] Hu Z, Yu L, Yu Z. Theoretical analysis on ratiometric fluorescent indicators caused biased estimates of intracellular free calcium concentrations [Journal Article]. J Photochem Photobiol B. 2005;78(3):179-87. Available from: https://www.ncbi.nlm.nih.gov/pubmed/15708514.

[138] Knisley SB, Justice RK, Kong W, Johnson PL. Ratiometry of transmembrane voltage-sensitive fluorescent dye emission in hearts [Journal Article]. Am J Physiol Heart Circ Physiol. 2000;279(3):H1421-33. Available from: https://www.ncbi.nlm.nih.gov/pubmed/10993810.

[139] Lee P, Quintanilla JG, Alfonso-Almazan JM, Galan-Arriola C, Yan P, Sanchez-Gonzalez J, et al. In vivo ratiometric optical mapping enables high-resolution cardiac electrophysiology in pig models [Journal Article]. Cardiovasc Res. 2019;115(11):1659-71. Available from: https://www.ncbi.nlm.nih.gov/pubmed/30753358.

[140] Salama G, Morad M. Merocyanine 540 as an optical probe of transmembrane electrical activity in the heart [Journal Article]. Science. 1976;191(4226):485-7. Available from: https://www.ncbi.nlm.nih.gov/pubmed/1082169.

[141] Lee P, Klos M, Bollensdorff C, Hou L, Ewart P, Kamp TJ, et al. Simultaneous voltage and calcium mapping of genetically purified human induced pluripotent stem cell-derived cardiac myocyte monolayers [Journal Article]. Circ Res. 2012;110(12):1556-63. Available from: https://www.ncbi.nlm.nih.gov/pubmed/22570367.

[142] Denning C, Borgdorff V, Crutchley J, Firth KS, George V, Kalra S, et al. Cardiomyocytes from human pluripotent stem cells: From laboratory curiosity

to industrial biomedical platform [Journal Article]. Biochim Biophys Acta. 2016;1863(7 Pt B):1728-48. Available from: https://www.ncbi.nlm.nih.gov/pubmed/26524115.

[143] Louch WE, Koivumaki JT, Tavi P. Calcium signalling in developing cardiomyocytes: implications for model systems and disease [Journal Article]. J Physiol. 2015;593(5):1047-63. Available from: https://www.ncbi.nlm.nih.gov/pubmed/25641733.

[144] Laughner JI, Ng FS, Sulkin MS, Arthur RM, Efimov IR. Processing and analysis of cardiac optical mapping data obtained with potentiometric dyes [Journal Article]. Am J Physiol Heart Circ Physiol. 2012;303(7):H753-65. Available from: https://www.ncbi.nlm.nih.gov/pubmed/22821993.

[145] Banville I, Chattipakorn N, Gray RA. Restitution dynamics during pacing and arrhythmias in isolated pig hearts [Journal Article]. J Cardiovasc Electrophysiol. 2004;15(4):455-63. Available from: https://www.ncbi.nlm.nih.gov/pubmed/15089996.

[146] Koller ML, Riccio ML, Gilmour J R F. Dynamic restitution of action potential duration during electrical alternans and ventricular fibrillation [Journal Article]. Am J Physiol. 1998;275(5):H1635-42. Available from: https://www.ncbi.nlm.nih.gov/pubmed/9815071.

[147] Mehta A, Chung YY, Ng A, Iskandar F, Atan S, Wei H, et al. Pharmacological response of human cardiomyocytes derived from virus-free induced pluripotent stem cells [Journal Article]. Cardiovasc Res. 2011;91(4):577-86. Available from: https://www.ncbi.nlm.nih.gov/pubmed/21565833.

[148] Mironov SF, Vetter FJ, Pertsov AM. Fluorescence imaging of cardiac propagation: spectral properties and filtering of optical action potentials [Journal Article]. Am J Physiol Heart Circ Physiol. 2006;291(1):H327-35. Available from: https://www.ncbi.nlm.nih.gov/pubmed/16428336.

[149] Djemai M, Cupelli M, Boutjdir M, Chahine M. Optical Mapping of Cardiomyocytes in Monolayer Derived from Induced Pluripotent Stem Cells [Journal Article]. Cells. 2023;12(17). Available from: https://www.ncbi.nlm.nih.gov/pubmed/37681899.

[150] Liu W, Han JL, Tomek J, Bub G, Entcheva E. Simultaneous Widefield Voltage and Dye-Free Optical Mapping Quantifies Electromechanical Waves

in Human Induced Pluripotent Stem Cell-Derived Cardiomyocytes [Journal Article]. ACS Photonics. 2023;10(4):1070-83. Available from: https://www.ncbi.nlm.nih.gov/pubmed/37096210.

[151] Burridge PW, Thompson S, Millrod MA, Weinberg S, Yuan X, Peters A, et al. A universal system for highly efficient cardiac differentiation of human induced pluripotent stem cells that eliminates interline variability [Journal Article]. PLoS One. 2011;6(4):e18293. Available from: https://www.ncbi.nlm.nih.gov/pubmed/21494607.

[152] Heinson YW, Han JL, Entcheva E. Portable low-cost macroscopic mapping system for all-optical cardiac electrophysiology [Journal Article]. J Biomed Opt. 2023;28(1):016001. Available from: https://www.ncbi.nlm.nih.gov/pubmed/36636698.

[153] Podgurskaya AD, Tsvelaya VA, Slotvitsky MM, Dementyeva EV, Valetdinova KR, Agladze KI. The Use of iPSC-Derived Cardiomyocytes and Optical Mapping for Erythromycin Arrhythmogenicity Testing [Journal Article]. Cardiovasc Toxicol. 2019;19(6):518-28. Available from: https://www.ncbi.nlm.nih.gov/pubmed/31165980.

[154] Herron TJ, Lee P, Jalife J. Optical imaging of voltage and calcium in cardiac cells tissues [Journal Article]. Circ Res. 2012;110(4):609-23. Available from: https://www.ncbi.nlm.nih.gov/pubmed/22343556.

[155] Woodhams LG, Guo J, Schuftan D, Boyle JJ, Pryse KM, Elson EL, et al. Virtual blebbistatin: A robust and rapid software approach to motion artifact removal in optical mapping of cardiomyocytes [Journal Article]. Proc Natl Acad Sci U S A. 2023;120(38):e2212949120. Available from: https://www.ncbi.nlm.nih.gov/pubmed/37695908.

[156] Wei F, Pourrier M, Strauss DG, Stockbridge N, Pang L. Effects of Electrical Stimulation on hiPSC-CM Responses to Classic Ion Channel Blockers [Journal Article]. Toxicol Sci. 2020;174(2):254-65. Available from: https://www.ncbi.nlm.nih.gov/pubmed/32040191.

[157] Kroll K, Chabria M, Wang K, Hausermann F, Schuler F, Polonchuk L. Electro-mechanical conditioning of human iPSC-derived cardiomyocytes for translational research [Journal Article]. Prog Biophys Mol Biol. 2017;130(Pt B):212-22. Available from: https://www.ncbi.nlm.nih.gov/pubmed/28688751.

[158] Crestani T, Steichen C, Neri E, Rodrigues M, Fonseca-Alaniz MH, Ormrod B, et al. Electrical stimulation applied during differentiation drives the hiPSC-CMs towards a mature cardiac conduction-like cells [Journal Article]. Biochem Biophys Res Commun. 2020;533(3):376-82. Available from: https://www.ncbi.nlm.nih.gov/pubmed/32962862.

[159] Wu P, Deng G, Sai X, Guo H, Huang H, Zhu P. Maturation strategies and limitations of induced pluripotent stem cell-derived cardiomyocytes [Journal Article]. Biosci Rep. 2021;41(6). Available from: https://www.ncbi.nlm.nih.gov/pubmed/33057659.

[160] Ma R, Liang J, Huang W, Guo L, Cai W, Wang L, et al. Electrical Stimulation Enhances Cardiac Differentiation of Human Induced Pluripotent Stem Cells for Myocardial Infarction Therapy [Journal Article]. Antioxid Redox Signal. 2018;28(5):371-84. Available from: https://www.ncbi.nlm.nih.gov/pubmed/27903111.

[161] Salvarani N, Maguy A, De Simone SA, Miragoli M, Jousset F, Rohr S. TGF-beta(1) (Transforming Growth Factor-beta(1)) Plays a Pivotal Role in Cardiac Myofibroblast Arrhythmogenicity [Journal Article]. Circ Arrhythm Electrophysiol. 2017;10(5):e004567. Available from: https://www.ncbi.nlm.nih.gov/pubmed/28500173.

[162] Sala L, van Meer BJ, Tertoolen LGJ, Bakkers J, Bellin M, Davis RP, et al. MUSCLEMOTION: A Versatile Open Software Tool to Quantify Cardiomyocyte and Cardiac Muscle Contraction In Vitro and In Vivo [Journal Article]. Circ Res. 2018;122(3):e5-e16. Available from: https://www.ncbi.nlm.nih.gov/pubmed/29282212.

[163] Quinn TA, Camelliti P, Rog-Zielinska EA, Siedlecka U, Poggioli T, O'Toole ET, et al. Electrotonic coupling of excitable and nonexcitable cells in the heart revealed by optogenetics [Journal Article]. Proc Natl Acad Sci U S A. 2016;113(51):14852-7. Available from: https://www.ncbi.nlm.nih.gov/pubmed/27930302.

[164] Kizana E, Ginn SL, Smyth CM, Boyd A, Thomas SP, Allen DG, et al. Fibroblasts modulate cardiomyocyte excitability: implications for cardiac gene therapy [Journal Article]. Gene Ther. 2006;13(22):1611-5. Available from: https://www.ncbi.nlm.nih.gov/pubmed/16838030.

[165] Kostecki GM, Shi Y, Chen CS, Reich DH, Entcheva E, Tung L. Optogenetic current in myofibroblasts acutely alters electrophysiology and conduction

of co-cultured cardiomyocytes [Journal Article]. Sci Rep. 2021;11(1):4430. Available from: https://www.ncbi.nlm.nih.gov/pubmed/33627695.

[166] Gaudesius G, Miragoli M, Thomas SP, Rohr S. Coupling of cardiac electrical activity over extended distances by fibroblasts of cardiac origin [Journal Article]. Circ Res. 2003;93(5):421-8. Available from: https://www.ncbi.nlm.nih.gov/pubmed/12893743.

[167] Rother J, Richter C, Turco L, Knoch F, Mey I, Luther S, et al. Crosstalk of cardiomyocytes and fibroblasts in co-cultures [Journal Article]. Open Biol. 2015;5(6):150038. Available from: https://www.ncbi.nlm.nih.gov/pubmed/26085516.

[168] Rupert CE, Kim TY, Choi BR, Coulombe KLK. Human Cardiac Fibroblast Number and Activation State Modulate Electromechanical Function of hiPSC-Cardiomyocytes in Engineered Myocardium [Journal Article]. Stem Cells Int. 2020;2020:9363809. Available from: https://www.ncbi.nlm.nih.gov/pubmed/32724316.

[169] Blyszczuk P, Zuppinger C, Costa A, Nurzynska D, Di Meglio FD, Stellato M, et al. Activated Cardiac Fibroblasts Control Contraction of Human Fibrotic Cardiac Microtissues by a beta-Adrenoreceptor-Dependent Mechanism [Journal Article]. Cells. 2020;9(5). Available from: https://www.ncbi.nlm.nih.gov/pubmed/32443848.

[170] Mainardi A, Carminati F, Ugolini GS, Occhetta P, Isu G, Robles Diaz D, et al. A dynamic microscale mid-throughput fibrosis model to investigate the effects of different ratios of cardiomyocytes and fibroblasts [Journal Article]. Lab Chip. 2021;21(21):4177-95. Available from: https://www.ncbi.nlm.nih.gov/pubmed/34545378.

[171] Shen S, Sewanan LR, Campbell SG. Evidence for synergy between sarcomeres and fibroblasts in an in vitro model of myocardial reverse remodeling [Journal Article]. J Mol Cell Cardiol. 2021;158:11-25. Available from: https://www.ncbi.nlm.nih.gov/pubmed/33992697.

[172] Aazmi A, Zhang D, Mazzaglia C, Yu M, Wang Z, Yang H, et al. Biofabrication methods for reconstructing extracellular matrix mimetics [Journal Article]. Bioact Mater. 2024;31:475-96. Available from: https://www.ncbi.nlm.nih.gov/pubmed/37719085.

[173] Longo SK, Guo MG, Ji AL, Khavari PA. Integrating single-cell and spatial transcriptomics to elucidate intercellular tissue dynamics [Journal Article].

Nat Rev Genet. 2021;22(10):627-44. Available from: https://www.ncbi.nlm.nih.gov/pubmed/34145435.

[174] Jacot JG, McCulloch AD, Omens JH. Substrate stiffness affects the functional maturation of neonatal rat ventricular myocytes [Journal Article]. Biophys J. 2008;95(7):3479-87. Available from: https://www.ncbi.nlm.nih.gov/pubmed/18586852.

[175] Hazeltine LB, Simmons CS, Salick MR, Lian X, Badur MG, Han W, et al. Effects of substrate mechanics on contractility of cardiomyocytes generated from human pluripotent stem cells [Journal Article]. Int J Cell Biol. 2012;2012:508294. Available from: https://www.ncbi.nlm.nih.gov/pubmed/22649451.

[176] Korner A, Mosqueira M, Hecker M, Ullrich ND. Substrate Stiffness Influences Structural and Functional Remodeling in Induced Pluripotent Stem Cell-Derived Cardiomyocytes [Journal Article]. Front Physiol. 2021;12:710619. Available from: https://www.ncbi.nlm.nih.gov/pubmed/34489730.

[177] Hitscherich PG, Xie LH, Del Re D, Lee EJ. The effects of macrophages on cardiomyocyte calcium-handling function using in vitro culture models [Journal Article]. Physiol Rep. 2019;7(13):e14137. Available from: https://www.ncbi.nlm.nih.gov/pubmed/31301118.

[178] Long C, Guo R, Han R, Li K, Wan Y, Xu J, et al. Effects of macrophages on the proliferation and cardiac differentiation of human induced pluripotent stem cells [Journal Article]. Cell Commun Signal. 2022;20(1):108. Available from: https://www.ncbi.nlm.nih.gov/pubmed/35850719.

[179] Dunn KK, Reichardt IM, Simmons AD, Jin G, Floy ME, Hoon KM, et al. Coculture of Endothelial Cells with Human Pluripotent Stem Cell-Derived Cardiac Progenitors Reveals a Differentiation Stage-Specific Enhancement of Cardiomyocyte Maturation [Journal Article]. Biotechnol J. 2019;14(8):e1800725. Available from: https://www.ncbi.nlm.nih.gov/pubmed/30927511.

[180] Lesman A, Gepstein L, Levenberg S. Cell tri-culture for cardiac vascularization [Journal Article]. Methods Mol Biol. 2014;1181:131-7. Available from: https://www.ncbi.nlm.nih.gov/pubmed/25070333.

[181] Giacomelli E, Meraviglia V, Campostrini G, Cochrane A, Cao X, van Helden RWJ, et al. Human-iPSC-Derived Cardiac Stromal Cells Enhance Maturation in 3D Cardiac Microtissues and Reveal Non-cardiomyocyte Contributions to Heart Disease [Journal Article]. Cell Stem Cell. 2020;26(6):862-79 e11. Available from: https://www.ncbi.nlm.nih.gov/pubmed/32459996.

[182] Kahn-Krell A, Pretorius D, Guragain B, Lou X, Wei Y, Zhang J, et al. A three-dimensional culture system for generating cardiac spheroids composed of cardiomyocytes, endothelial cells, smooth-muscle cells, and cardiac fibroblasts derived from human induced-pluripotent stem cells [Journal Article]. Front Bioeng Biotechnol. 2022;10:908848. Available from: https://www.ncbi.nlm.nih.gov/pubmed/35957645.

[183] Amelian A, Wasilewska K, Megias D, Winnicka K. Application of standard cell cultures and 3D in vitro tissue models as an effective tool in drug design and development [Journal Article]. Pharmacol Rep. 2017;69(5):861-70. Available from: https://www.ncbi.nlm.nih.gov/pubmed/28623710.

[184] Duval K, Grover H, Han LH, Mou Y, Pegoraro AF, Fredberg J, et al. Modeling Physiological Events in 2D vs. 3D Cell Culture [Journal Article]. Physiology (Bethesda). 2017;32(4):266-77. Available from: https://www.ncbi.nlm.nih.gov/pubmed/28615311.

[185] Habanjar O, Diab-Assaf M, Caldefie-Chezet F, Delort L. 3D Cell Culture Systems: Tumor Application, Advantages, and Disadvantages [Journal Article]. Int J Mol Sci. 2021;22(22). Available from: https://www.ncbi.nlm.nih.gov/pubmed/34830082.

[186] Yuan J, Chen H, Ge D, Xu Y, Xu H, Yang Y, et al. Mir-21 Promotes Cardiac Fibrosis After Myocardial Infarction Via Targeting Smad7 [Journal Article]. Cell Physiol Biochem. 2017;42(6):2207-19. Available from: https://www.ncbi.nlm.nih.gov/pubmed/28817807.

[187] Zhou XL, Xu H, Liu ZB, Wu QC, Zhu RR, Liu JC. miR-21 promotes cardiac fibroblast-to-myofibroblast transformation and myocardial fibrosis by targeting Jagged1 [Journal Article]. J Cell Mol Med. 2018;22(8):3816-24. Available from: https://www.ncbi.nlm.nih.gov/pubmed/29808534.

[188] He X, Zhang K, Gao X, Li L, Tan H, Chen J, et al. Rapid atrial pacing induces myocardial fibrosis by down-regulating Smad7 via microRNA-21 in rabbit [Journal Article]. Heart Vessels. 2016;31(10):1696-708. Available from: https://www.ncbi.nlm.nih.gov/pubmed/26968995.

[189] Liu X, Xu Y, Deng Y, Li H. MicroRNA-223 Regulates Cardiac Fibrosis After Myocardial Infarction by Targeting RASA1 [Journal Article]. Cell Physiol Biochem. 2018;46(4):1439-54. Available from: https://www.ncbi.nlm.nih.gov/pubmed/29689569.

[190] Davis J, Salomonis N, Ghearing N, Lin SC, Kwong JQ, Mohan A, et al. MBNL1-mediated regulation of differentiation RNAs promotes myofibroblast transformation and the fibrotic response [Journal Article]. Nat Commun. 2015;6:10084. Available from: https://www.ncbi.nlm.nih.gov/pubmed/26670661.

[191] Garrison G, Huang SK, Okunishi K, Scott JP, Kumar Penke LR, Scruggs AM, et al. Reversal of myofibroblast differentiation by prostaglandin E(2) [Journal Article]. Am J Respir Cell Mol Biol. 2013;48(5):550-8. Available from: https://www.ncbi.nlm.nih.gov/pubmed/23470625.

[192] Johnson RD, Lei M, McVey JH, Camelliti P. Human myofibroblasts increase the arrhythmogenic potential of human induced pluripotent stem cell-derived cardiomyocytes [Journal Article]. Cell Mol Life Sci. 2023;80(9):276. Available from: https://www.ncbi.nlm.nih.gov/pubmed/37668685.